Thermalization in Pure States and Black Holes

A Thesis

Submitted to the

Tata Institute of Fundamental Research, Mumbai

for the Degree of Doctor of Philosophy

in Physics

by

Ritam Sinha

Department of Theoretical Physics

Tata Institute of Fundamental Research

Mumbai - 400 005, India

August 2018

Final version submitted in **November 2018**

Declaration

This thesis is a presentation of my original research work. Wherever contributions of others are involved, every effort is made to indicate this clearly, with due reference to the literature, and acknowledgement of collaborative research and discussions. The work was done under the guidance of Professor Gautam Mandal, at the Tata Institute of Fundamental Research, Mumbai.

[**Ritam Sinha**]

In my capacity as supervisor of the candidates thesis, I certify that the above statements are true to the best of my knowledge.

[**Prof. Gautam Mandal**]

Date: 02 August, 2018

To Ma, Baba and Jethu

Acknowledgements

When I was young, my parents used to subscribe to a Bengali daily newspaper which, on every Sunday, used to feature a column titled *"Haal Chhero Na!"*, or *"Do not give up!"* in Bengali. It featured a story about an influential personality from one the fields of Music, Science, Mathematics, Arts or Literature, who had faced various odds in their personal lives and had despite made great contributions in their respective fields. It was this column that had introduced me to the likes of Ramanujan, Beethoven and many more. If nothing more, the snippets from the life of these great men is what I reminisce very fondly and often they have acted like a magic potion, pulling me up whenever I felt low in life. This thesis is a culmination of many such moments of struggle, that easily outnumber the times I have truly felt triumphant and in control of my work. However, working towards this thesis has been a life lesson for me, teaching me to move on no matter how rugged the terrains appear. The satisfaction and joy that I feel at having reached the goal is beyond words. However, I would certainly not have made it thus far, had it not been for help and support of numerous people, only a handful of whom I will manage to thank here.

It is said that the gift of knowledge is the greatest gift in the world. The most important people I have to thank for this gift are my parents. *Ma*, for spending countless hours toiling after me trying to teach me the virtues of life. It is you who make me what I am today. *Baba*, for making me see the world through your eyes and in the process, opening new worlds for me. For inculcating in me the love for literature, sports, politics and music. These are some of the things I cherish the most in the world. To the both of you, for teaching me how to love and care selflessly.

To Mr. PK Chatterjee and Mr. Ashok Bangabash, two exceptional teachers and wonderful gentlemen who opened my eyes to the beauty of Physics. I shall forever be indebted to you. To the best physics teacher I have had in college, Dr. Dhruba Banerjee. Your amazing quality to simplify the most complicated concepts still mesmerises me.

To the person I adore the most at TIFR, my advisor, Prof. Gautam Mandal. You are an amazing mentor and an exceptional human being. All the reasons why I can call myself a physicist, I owe to you. I have immensely enjoyed all our academic and non-academic discussions. I would forever be indebted to you for introducing me to black holes and ethanol, both of which I enjoy tremendously. Most importantly, thank you for being a friend and a guardian to me all through these years.

I would like to thank Shiraz and Sandeep, for being the brilliant mentors that they are, and creating a fantastic atmosphere for learning and research at TIFR, especially for young physicists. I have learnt some of my most valuable lessons about physics and research during my discussions and conversations with you. To some of my most wonderful seniors, Nilay, Umesh, Tarun, Shiroman and Shouvik, for being great friends and equally good teachers that any young student would hope for in this field. I have always learnt a lot from all of you.

To all the DTP Members in C338, for being an extremely hard working and fun-loving team, working together with the goal of understanding the mysteries of the universe a bit more, a bit better. Being a part of you will be one of the most cherished phases of my life.

What is life without friends, and by all means I made plenty at TIFR. With these people I have shared the best of times and the worst of times. Here are a few who deserve to be mentioned. Chitrak, for the one year you were at TIFR, it was the best year I had. You are my brother from another mother. Nairit, for sponsoring my TIFR life, literally. I would always remain indebted to you for the things I learnt from you, about life and the world at large. Atreyee, for all the fights I had (and still have) with you, that make us understand each other better. I hope to fight harder and travel farther with you over many more years to come. To all the three of you, for making me a better person and for all the evenings we spent together reflecting upon the wonders of the universe. Soureek, Debjyoti, Khadiza, Subhadeep, Gourab, for all the wonderful moments we have spent together, at and outside TIFR. I especially cherished the times we shared during the festive occasions, like Durga pujo

and Diwali. I will always miss the gossips we shared and the late night chit-chats (except Debbie's pj's) and canteen trips. Geet, for being my partner in crime and my daily dose of entertainment in an otherwise monotonous life. I feel we share a special bond since we grew up together as physicists and as individuals. With Rahul and Nikhil, we had the most awesome (and untidy) row that C338 has ever seen or will ever do in the near future.

To Nilakash, for being a wonderful friend and a delightful colleague. I learnt a lot of physics from you and I thoroughly enjoyed our collaborations. I really admired your capacity for original thought. It has had a great impact on me and this thesis.

A special mention must be made of the 100+ restaurants that I visited with various subsets of these people, during my stay at TIFR and the wonderful people working there, sharing and serving joy each day in the form of their wonderful cuisines.

Finally, Ayesha, for making me the sociable person I am today, for putting up with my oddities and for the sacrifices you made. I am already a much better person because of you. Your smile has always been the cure for all my worries. This journey would be incomplete without you. This thesis is as much yours as it is mine.

Ritam Sinha

Date: 3rd July, 2018

List of Publications

Publications by the author summarised in this thesis

1. *"Dynamical Entanglement Entropy with Angular Momentum and U(1) charge"*,
   Pawel Caputa, Gautam Mandal, **Ritam Sinha**,
   JHEP 1311 (2013) 052, arXiv:1306.4974[hep-th]

2. *"The* inside outs *of AdS_3/CFT_2: exact AdS wormholes with entangled CFT duals"*,
   Gautam Mandal, **Ritam Sinha**, Nilakash Sorokhaibam,
   JHEP 1501 (2015) 036, arXiv:1405.6695v1[hep-th]

3. *"Thermalisation with Chemical Potentials, and Higher Spin Black Holes"*,
   Gautam Mandal, **Ritam Sinha**, Nilakash Sorokhaibam,
   JHEP 1508 (2015) 013, arXiv:1501.04580 [hep-th]

4. *"Higher Point Conformal Blocks and Entanglement Entropy in Heavy States"*,
   Pinaki Banerjee, Shouvik Datta, **Ritam Sinha**,
   JHEP 1605 (2016) 127, arXiv:1601.06794 [hep-th]

5. *"Finite Size Effect on Dynamical Entanglement Entropy: CFT and Holography"*,
   Gautam Mandal, **Ritam Sinha**, Tomonori Ugajin,
   arXiv:1604.07830 [hep-th], Prepared for submission to JHEP

The second and third paper are based on a joint work with Sorokhaibam Nilakash Singh and have partial overlap with his thesis. The contents of the first, fourth and fifth paper are exclusive to this thesis.

Other Publications by the author during the course of graduate studies at TIFR

1. *"Spectral Form Factor in Non-Gaussian Random Matrix Theories"*,
   Adwait Gaikwad, **Ritam Sinha**,
   arXiv:1706.07439 [hep-th], Prepared for submission to PRD

2. *"A Complex Fermionic Tensor Model in d Dimensions"*,
   Shiroman Prakash, **Ritam Sinha**,
   JHEP 1802 (2016) 086, arXiv:1710.09357 [hep-th]

3. *"Dual Superconformal Symmetry of N=2 Chern-Simons theory with Fundamental Matter and Non-Renormalization at Large N"*,
   Sachin Jain, **Ritam Sinha**, et.al.,
   arXiv:1711.02672 [hep-th], Submitted to PRL

Contents

Chapter 1

Introduction

1.1 Thermalization

A BRIEF HISTORY OF QUANTUM STATISTICAL MECHANICS

By the end of the 19th century, the field of classical statistical mechanics was extremely well developed. It owed most of its tremendous success to having provided a microscopic understanding of some of the very fundamental ideas in classical thermodynamics, namely temperature and entropy. The framework of classical statistical mechanics is very general, in that it can accommodate a description of not just systems that are *in* equilibrium, but also systems that are far away from it. So much so, that in the year 1894, the famous experimental physicist Albert A. Michelson[1] remarked that, *"The more important fundamental laws and facts of physical science have all been discovered, and these are so firmly established that the possibility of their ever being supplanted in consequence of new discoveries is exceedingly remote."*[2]. His statement, however, turned out to be far from the truth.

The dawn of the 20th century marked the discovery of two immensely profound ideas in the history of mankind, Quantum Mechanics and General Relativity. Although developments

[1] Of the Michelson-Morley experiment fame, who also won a Nobel Prize in physics in 1907
[2] Fun fact: This quote is often misattributed to Lord Kelvin

in General Relativity took a backseat during the first half of the century, Quantum Mechanics was being developed at a break-neck speed during the 1920's. In fact it required less than a decade for the stalwarts of the time to lay out a complete and consistent mathematical framework for this *New Mechanics*! Quantum mechanics turned out to be an extremely important tool for understanding the physics at the small scale. With its staggering success in explaining phenomena such as the Zeeman effect and the spectrum of Hydrogen, there remained no doubt, whatsoever, that *this* was indeed the correct theory for describing the physics of atoms and molecules.

This immediately inspired the pursuit for trying to understand how ideas in classical statistical mechanics could be applied to quantum many body systems. Leading this endeavour was the famous theoretical physics *John von Neumann* who, in 1929 and thereafter, put forward some brilliant ideas. Using the newly developed language of operators and Hilbert spaces, he proposed the idea of *entropy maximisation* to address the issue of thermalisation in *many-body, out-of-equilibrium* quantum systems. These efforts led to the very beginning of an entirely new disciple called *Quantum Statistical Mechanics*. The amalgamation of the two ideas, however, had very deep-rooted problems, precisely concerning the issue of how closed, isolated, quantum many-body systems thermalise. It is, therefore, extremely important to understand how to define thermalisation in such quantum systems that are described by *pure states*. It is important to mention that a comprehensive list of *necessary* conditions for the thermalisation of such out-of-equilibrium quantum systems, is still an *open* question, that has eluded a complete and satisfactory answer for almost a century now. What has been formulated, however, is a list of *sufficient* conditions, which when satisfied, lead to the thermalisation of the quantum system. We shall discuss some of these ideas and conditions in detail.

WHAT IS THERMALIZATION?

Systems in thermal equilibrium are very well understood, both classically and quantum mechanically, as being characterised by a set of *mutually commuting, conserved, macroscopic*

observables that label the final (Gibbs) density matrix of the system. The trouble occurs when quantum many-body systems are driven out-of-equilibrium. Starting from a pure state, that describes the many-body system, one unitarily evolves it using the Schroedinger's equation. From the tenets of quantum mechanics, one knows that unitary evolution will never allow for a pure state to transition over to a mixed state. Since thermalisation requires the appearance of a mixed state, it is, therefore, not clear whether and how such states would ever attain thermal equilibrium. At this point then, it seems impossible that such states would ever thermalise! However, what saves the day here are a special class of pure states that are called *typical*. A typical state is such that the expectation value of any observable in this state, integrated over a Haar measure of similar states chosen from a uniform random distribution, is very close to its micro-canonical average. If in addition, the state has a small variance, then one can further say that the expectation value in a *single* micro-state is well approximated by the micro-canonical expectation value. In case the state describes a large system, one can use the *equivalence of ensembles* to approximate the expectation values with there canonical average values. In such an ensemble, all the thermodynamic notions of macroscopic observables are very well defined. This realisation is extremely important, since it tells us at least one way in which we understand how pure states can resemble thermal states. Having said that, one must remember that such a definition is merely indicative. It does not tell us about how generic pure states can dynamically achieve thermality (or typicality). There are, in fact, quite a few other conditions that such states need to fulfil in order to thermalise under a unitary time evolution. Motivated by this observation, we shall, henceforth, describe and try to look for thermalising pure states in the two following ways, 1. in terms of complete pure states that show the requisite microscopic properties (for the equivalence of ensembles to hold), via ETH; 2. in terms of subsystems of pure excited states that are mixed and hence allow for a description by a canonical ensemble under time evolution. We shall deal with both these kinds of states in this thesis. However, we shall postpone the discussion of ETH for the time being and focus only on the sufficiency

conditions for thermalisation of subsystems (which is what we would mean by a system henceforth). We shall define a number of these sufficient conditions that have been found to apply to a wide class of systems (including conformal field theories, that are the focus of this thesis).

WHAT IS EQUILIBRATION?

One of the most important sufficiency conditions for understanding thermalisation is *equilibration*. An out-of-equilibrium quantum system is said to have equilibrated, if correlation functions of the system display tiny fluctuations around some fixed value for a sufficiently large amount of time. If the fixed value is the long time average of the correlation functions themselves, then the process is referred to as *equilibration on average*[3]. If the operators, in this case belong to only a particular sub-system, then the above statement would refer to the equilibration of such subsystems alone. This process is then referred to as *subsystem equilibration*. One must mention that while considering subsystems, there is an additional class of observables that can be used to display equilibration of the system, namely the reduced density matrix of the subsystem itself[4]. It is important to note that not all initial states equilibrate. This condition of equilibration rather singles out a very specific class of initial states, by imposing constraints on the amplitudes of individual energy eigenstates that comprise it. In other words, as mentioned above, if a pure state describing a large enough quantum system approaches a typical state, then any of its sub-systems will equilibrate under time evolution. This class is seemingly larger than the class which requires the full state of the system approach an equilibrium configuration.

OTHER SUFFICIENCY CONDITIONS

One of the other very important sufficiency conditions is that the final equilibrium state of the system be completely independent of any microscopic details of the initial state. This is the property that is often referred to as *coarse-gaining* and is what results in the

[3]There is another sense in which systems may equilibrate, namely *equilibration over intervals*. However, for the purpose of this thesis, by equilibration we shall always mean equilibration on average.

[4]In fact, we shall make exclusive use of this tool in chapter 4 of this thesis.

loss-of-information about the initial state of the system. This implies that a large class of initial states, with a given set of conserved macroscopic observables, would all correspond to the same final equilibrium state as an end result of a unitary evolution. One needs to be more careful for the case of sub-systems, since there might be some locally exact conserved quantities that do not characterise the full system, but are important to describe the final equilibrium state of the sub-system[5]. This also inherently implies that the final state of the sub-system is in a way, completely independent of state of the rest of the system. There are numerous reasons why such a loss of information corresponding to the microscopic details of the system might happen. Intuitively, one may think of this information loss as happening due to the rest of the system acting as a bath for the subsystem under consideration. Such a process generally includes various mechanisms via which higher corrections to the leading thermal behaviour are suppressed. Since this is a dynamic scenario, the corrections generally involves functions of time that get smaller the longer we wait (indicating dissipative behaviour). The suppression could also be facilitated due to the presence of a large number of degrees of freedom of the quantum system. Another possibility is to look at only a specific class of observables that very naturally coarse grain over the microscopic degrees of freedom of the system. It is one of the goals of this thesis to explain some of these mechanisms in the case of time evolving CFTs and even otherwise.

In the process of approaching thermal equilibrium, coarse-graining over the initial micro-state generally requires the final density matrix to asymptotically approach a diagonal form. This subsequently makes the off-diagonal elements of the density matrix of the subsystem approach a vanishingly small value, while making the state more mixed. The ETH employs this idea at the operator level in a very efficient way which we shall explain shortly. For the subsystems, the density matrix can be shown to dynamically become more diagonal. We shall show this for a special class of initial states in Chapter 4. It is suggested that this

[5]Some examples of this include many-body localisation, discrete symmetries arising from broken ergodicity, local magnetic fields, etc.

happens mostly because of interactions between the subsystem and the bath, as stated above. The vanishing of the off-diagonal elements is sometimes also referred to as *decoherence*.

Finally, fulfilling all the above conditions may still not be enough for the system to thermalise. One ultimate requirement is for the density matrix of the sub-system to be very close (in the sense of distances on the Hilbert space) to a Gibbs' ensemble. Whether it is a canonical or a grand canonical or a generalised Gibbs' ensemble (GGE) will depends on how many local exactly conserved quantities the subsystem has. We shall show how this idea is realised for observables in the system in Chapters 2 and 3 and for the density matrix in Chapter 4.

We are finally in a position to define what we mean by *thermalization*, at least in the context of this thesis.

An out-of-equilibrium, many-body, quantum system undergoing unitary time evolution is said to have thermalised, if the observables in the system equilibrate to a fixed value, where the reduced density matrix of any sub-region admits a description in terms of a Gibbs and other Generalised Gibbs ensembles.

Since, most of these conditions have been formulated for subsystems, we shall refer to this phenomena as *subsystem thermalisation*. As has been emphasised throughout, these are only the sufficient and not the necessary conditions for thermalisation. Also, there are no rigorous proofs for most of these conditions, but only general observations that have been accumulated through a case by case study of numerous quantum systems. Nevertheless, this definition of thermalisation is exactly what is relevant in the context of this thesis, as we shall see in the chapters to follow.

ISSUES WITH (SUBSYSTEM) THERMALIZATION

Having defined thermalisation, what now remains to be understood are the problems one faces with these definitions. In a recent review, Cardy [72] listed some of the important problems in the field that need to be addressed, accompanied by the answers to some others that have already been solved. We shall paraphrase the problems here in a manner suited

to the style of this thesis. The reason being, many of the problems listed shall be dealt with in this thesis. The following is a list of some of the important questions:

1. To quantify how close the reduced density matrix (RDM) of a subsystem can approach a thermal density matrix.

   This problem was first dealt with in a paper by Cardy [71] himself, where he suggested a particular measure (a variant of the trace distance in quantum information theory) to study the overlap of the RDM with the thermal density matrix. In Chapter 4, we shall study this problem in detail where we not only perform the explicit calculation for the Candy-Calabrese state, but in fact generalise it to the generalised CC (gCC) state to include an arbitrary number of higher spin conserved quantities. In general, this is a difficult question and a proof of the statement for any arbitrary quantum many-body system is still lacking.

2. To understand how additional conserved quantities affect the final thermal state of the system described by a CFT.

   Unlike the previous case, this phenomenon is much better understood in a plethora of integrable models where the final state appears to be the Generalised Gibbs' ensemble. Again, Cardy [72] himself has tried to answer this question by generalising the CC state to include various higher power and derivatives of the stress tensor. In Chapter 4, we too shall work with a more generalised CC state that include a different set of higher spin conserved currents and show precisely how the density matrix of the CFT approaches the GGE.

3. To understand the effects of relaxing the CC ansatz on the thermalisation of the system[6].

[6]This should be understood in conjunction with the section on Quantum Quenches where the CC ansatz is explained in detail.

The answer to this question is somewhat related to which final state the system reaches, in the manner in which it is dealt with in this thesis. This is because one way to relax the CC state is to use conserved charges to perturb away from the CC state. However, one could use non-conserved operators to deform the CC state. The understanding then is that all such perturbations are microscopic details of the initial CC state that should be lost in the unitary time evolution to obtain a truly thermal state. So, the nature of perturbations should play an important role in understanding the effects it has on the thermalization of the system.

4. To understand how thermalization is affected by the presence of spatial boundaries in the system.

   In [71], Cardy introduced a measure called the revival function that basically measures the overlap of the CC state with its time-evolved version. If the overlap is low at all times, it implies that the states are far away from each other and there is no revival at any point. If, however, the overlap function is close to one after a sufficient amount of time has lapsed, then that implies a revival of the full system to its initial state. He showed that revival occurs in the presence of boundaries. We dedicate the entirety of Chapter 5 to the study of revivals, where we try to understand the effect of boundaries on correlation functions of operators and the entanglement entropy of subsystems.

So to summarise, the important problems in the current literature, with respect to the dynamics of quenches and thermalisation thereafter, deal entirely with the issue of how systems approach thermal equilibrium. Many of them have been addressed in the Chapters 4 and 5 of this thesis. However, the proofs mostly remain within the confines of conformal field theory. Nonetheless, any analytical result plays a key role in understanding the underlying mechanism for the thermalisation of pure states. Especially since they are very hard problems to be addressed in complete generality. In fact, most of these problems have been around since the very inception of quantum statistical mechanics . The reason they have re-appeared

in the recent literature is two-fold. The first reason is due to the tremendous advances that have been made in the realms of experimental physics, in particular in the field of cold-atom physics. The invention of ion-traps has made it possible to simulate 1-D lattices with the trapped cold-atoms playing the role of the degrees of freedom on the lattice. They have, therefore, formed a testing ground for a huge array of theoretical ideas pertaining to low dimensional statistical mechanical and condensed matter systems. The second reason (more relevant to the subject of this thesis) is the advent of the AdS/CFT correspondence, which has been used to map the physics of strongly coupled gauge theories to that of weakly coupled gravity. The CFT part of the correspondence implies that every statement that we made in field theory should find a corresponding analogue on the gravitational side. The correspondence has therefore given us a hope to relate problems in black hole physics to that of table-top experiments, which is an extremely exciting idea in itself! We shall hereby embark upon a more detailed discussion of the gravitational problems addressed in this thesis in lieu of the aforementioned correspondence.

WHAT IS THE ADS/CFT CORRESPONDENCE?

There are many versions of the AdS/CFT correspondence that appear in the current literature. We shall start by providing a precise statement for the version of the correspondence that shall be of most concern to this thesis. The AdS/CFT correspondence is originally a duality between string theory and superconformal gauge theory that was proposed in [176, 238]. Since the Einstein theory of gravity emerges in the low-energy limit of string theory, and the correspondence has been generalised to various dimensions, the AdS/CFT correspondence in its modern avatar is essentially a duality between conformal field theories (CFTs) in d-dimensions and theories of Einstein gravity in d+1 dimensions in asymptotically AdS (AAdS) spaces. Owing to the time-like structure of the asymptotic boundary in AAdS spacetimes, the CFTs can be thought of as living at the asymptotic boundary of the d+1 dimensional gravitational theory (thereby, being described in one lower dimension). There is a version of the duality involving higher spin theories of gravity

in 2+1 dimensions and higher spin fields in the CFT in 2 dimensions describing a non-supersymmetric set-up. This understanding is key to the realisation that supersymmetry is not an essential ingredient for holography [7]. As is true with any standard duality, the AdS/CFT correspondence provides a map for the interpretation of all quantities on the CFT side with corresponding quantities on the gravity side. It is a non-perturbative duality that is true at the level of the partition function (and therefore, the Hilbert space) of the theory. Namely,

$$Z_{AdS_{d+1}}[M] = Z_{CFT_d}[\partial M = \Sigma] \tag{1.1}$$

Where ∂M is the boundary of the manifold ∂M. The gravitational picture emerges at the large N limit of the CFT, where N corresponds to the $SU(N)$ in a gauge theory or to the number of degrees of freedom for a more general CFT. At the operator level, the AdS/CFT dictionary suggests that *single trace operators* in the CFT must correspond to *single particle states* in the bulk AdS. One way to see this is to consider a scalar field in the bulk, and solve for its equations of motion with a negative cosmological constant. There are two possible asymptotic solutions that appear: one solution (the normalisable mode), dies off at infinity and is associated with the expectation value of the spin zero single trace primary operator in the CFT; the other solution (the non-normalisable mode) grows at infinity and acts as a source in the boundary CFT for generating correlations of the same scalar primary. For higher spin fields, the normalisable mode is associated with the corresponding higher spin s current in the CFT. The non-normalisable mode, again sources the correlation functions of the higher spin currents in the CFT. Of course there is a lot more to the duality, but this is as much as we would be required to know to discuss the problems that concern us. Any additional details shall be provided as we require them along the course of this thesis.

[7] The same, however, cannot be said for conformal symmetry with absolute certainty yet.

HAWKING'S INFORMATION PUZZLE

One of the most intriguing objects in general relativity is a black hole. A black hole is a solution to Einstein's equations that has a horizon which divides the spacetime into interior and exterior regions. In the language of mathematics, the horizon is a null surface which hides the singularity from the outside world. Having said that, in classical general relativity, the horizon is not a special place. This is because an observer falling into the black hole, never senses the presence of a horizon. This fact becomes evident in an appropriate co-ordinate system used to parametrise the black hole solution. For instance, consider the case of a black hole whose metric is described in Schwarzschild co-ordinates. The metric displays a singularity at the position of the horizon, which is just a co-ordinate singularity[8]. However, if we go to the Eddington-Finkelstein (EF) co-ordinates (or the Kruskal co-ordinates), the singularity disappears. One simple physical reason for that is, at least in the EF co-ordinate system, we move to the frame of the in-falling observer, where we can cross the horizon without any trouble. However, owing to the property of null surfaces, it is easy to see that the nothing can escape from the interior of a black hole due to the presence of the horizon. In this sense, the horizon somewhat safeguards the interior of a black hole. Thereby, the ultimate fate of any in-falling observer would be to plunge to its death by falling into the black hole singularity!

Based on this observation, in the year 1972, Jacob Bekenstein suggested an intriguing thought experiment [35]. He suggested throwing buckets of hot water into a black hole! His motive was very simple, to bring to light a contradiction. He argued that the hot water has a finite amount of entropy. When thrown into the black hole, this entropy gets completely lost to the outside world, thereby decreasing the entropy of the Universe! That, however, cannot happen simply because it would violate the second law of thermodynamics, which suggests that the entropy of any system can only increase. The second law is one of the most fundamental laws of nature, much like the conservation of energy, and hence would lead to

[8]This is because the Ricci scalar and all other quantities related to curvature are regular at the horizon

devastating consequences, if violated by physical systems. The only way out of this puzzle, without dismissing the existence of black holes, was to associate some amount of entropy to them. This way, when objects with finite entropy fall into the black hole, the entropy of the black hole would increase by more than the amount falling in, thereby preserving the second law. This simple suggestion had remarkable consequences for black hole physics. That is because once you associate an entropy with a system, you usually also have to associate a temperature with it. This observation then suggested that black holes must also have a finite temperature. In fact, one could view a black hole as a complete thermodynamic object [32,36,37]. In [139], Hawking famously calculated the temperature of a black hole using semi-classical approximations. An important consequence of this realisation was that, as a finite temperature thermodynamic object, the black hole could now emit thermal radiation and evaporate away completely! This phenomena led to the formulation of Hawking's famous *Black Hole Information Paradox*!

Before we state the Black Hole information paradox, it is important to mention that there exist numerous versions of the paradox in the literature that have been formulated over the last 40 years. Some of them have been solved for, most still remain unsolved. One way or the other, the paradox has exposed the grave shortcomings in our understanding of the quantum structure of spacetime, besides underlining the approach to a viable and acceptable candidate for the theory of quantum gravity. The older versions of the paradox are too numerous, including a case by case discussion of the associated problems in spacetimes with positive, negative and a zero value of the cosmological constant, and are way beyond the scope of this thesis[9]. A relatively newer version of the paradox was formulated in the context of the AdS/CFT correspondence and is much more in line with the topics discussed in this thesis. That version goes by the name of the *Firewall Paradox* [14,15].

[9]For a discussion, one should see [153,177,184,186,230] and references therein

THE PROBLEM WITH BLACK HOLE FORMATION

Before the advent of the AdS/CFT correspondence, the information paradox was formulated by Hawking in the following language. Suppose we consider an in-falling shell of matter, which is collapsing under its own gravitational pull. This matter maybe characterised by its mass, charge and various other parameters, all of which form the initial state. Once the collapse starts and a sufficient amount of matter enters its Schwarzschild radius, an apparent horizon begins to form which now no more allows anything inside of it to escape. This apparent horizon gives way to the event horizon at the end of the collapse process. However, once the black hole has formed, it is characterised by only its mass, charge and angular momentum, all of which are macroscopic observables. These specify the thermal Gibbs' ensemble used to describe the state of the black hole. The information about the specific initial state (all the microscopic details), which caused the black hole to form in the first place, is no longer retained in the final state. This is the *first version of the information problem* that we shall address in this thesis. This paradox becomes much sharper in the context of AdS/CFT. The entire process can be viewed in the CFT independently owing to the correspondence. We start by defining a pure state that contains not just the macroscopic variables, but also the microscopic details of the specific initial state dual to the pure shell of in-falling matter in the bulk. The CFT hamiltonian then unitarily evolves this state, causing the matter to collapse in the bulk. After evolving the state for a sufficiently long amount of time, a black hole appears in the bulk, although the CFT state remains pure due to the constraints of unitarity! As one can observe, this is precisely the problem we faced while defining the process of thermalisation entirely from the field theory point of view above. So, the AdS/CFT correspondence makes the information paradox much sharper by equating it with the problem of thermalisation in the CFT. It is then a viable approach to start looking for a solution in the field theory itself. At this point, it must be mentioned that in the Chapters 4 and 5 of this thesis, we shall address the black

hole formation problem in conjunction with the thermalisation problem in field theory by trying to understand how pure states correspond to black holes.

THE PROBLEM WITH BLACK HOLE EVAPORATION

The *second version of the information problem*, involves the evaporation of an already formed black hole and problems therein. This version, therefore, mostly concerns the smaller black holes that evaporate in all spacetimes (including AdS)[10]. Soon after Hawking's paper, outlining the evaporation of a Black Hole by emitting Hawking quanta, Page realised a very peculiar feature of this process. His observation can be best stated from the point of view of an observer at asymptotic infinity who wants to collect all the Hawking quanta coming out of an evaporating black hole. We also suppose that such a black hole has been created by the collapse of some pure shell of matter. Then, owing to the unitarity of quantum mechanics, the observer at infinity must have a bunch of Hawking quanta, at the end of the black hole evaporation process, all of which are described by a pure state. Having understood what to expect at the beginning and in the end of the process of evaporation, let us ask what happens at the intermediate time-scales. The quantity that the observer at infinity is measuring as a function of time is the entanglement between the quanta it collects and the quanta that are still to be radiated. According to Hawking, the quanta emitted by the black hole are a result of the process of pair production happening very close to the horizon, where one particle falls in while the other escapes to infinity. Needless to say, the pair of particles are entangled amongst themselves[11]. Each such quanta that is collected at infinity results in an increase in the entanglement. One might naively think that the profile of entanglement would keep rising linearly till all the quanta have been radiated out. However, the end result of evaporation should have been a pure state with zero entropy and not a finite value. So, effectively, the profile of entanglement (also called the Page Curve), must have a dip at some point in time

[10] Large Black Holes evaporate in flat spacetimes but in AdS, they may be in stable equilibrium due to the timelike nature of its asymptotic boundary

[11] This pair is almost in a pure state and the entanglement between this pair is essential for the smoothness of the horizon.

and return to zero in the end. A possible resolution to the problem could come from taking into account the entanglement between the early quanta (A) that was emitted a long time ago, and the quanta that is recently produced via pair production near the horizon (B)[12]. However, very recent arguments from strong-suadditivity of entanglement have suggested that the entanglement between A and B (the early and late quanta) as a system with C (the quanta inside the BH) is greater than the entanglement of A with the rest of the quanta. This, however, is the paradox! Since, adding an additional quanta B to the additional radiation A must decrease the the entropy of the observer beyond Page time[13]. Stated in another way, the paradox brings to light an underlying tension between the unitary nature of quantum mechanics (entanglement between A and B) and the monogamy of entanglement (B and C). One way to resolve the paradox might be to modify the entanglement structure between the various quanta. Trying to preserve unitarity and modifying the assumptions regarding the entanglement between B and C, [13, 16, 187, 188] realised that the expectation value of the stress-energy tensor increases drastically near the horizon, allowing for a *firewall* to open up. By a firewall, they implied a very high number of highly energetic photons that reside somewhere near the horizon, and were simply a result of severing the entanglement between the outgoing quanta and the quanta inside the black hole. This implies that any in-falling observer would instantly burn and perish at the horizon! However, what is more noticeable is that the in-falling observer would in-fact perceive the horizon as a special place, which (as we had discussed above), it should not! So, then trying to preserve unitarity and resolve the information paradox, we would have compromised the diffeomorphism invariance of the bulk. After a lot of heated debates going back and forth, the most satisfactory resolution we have till date is the work of Pappadodimas and Raju [204, 205]. However, in Chapters 2 and 3 of this thesis, we would like to partially address this issue (based on the works [138, 175], by showing that at least in the eternal black hole case dual to the TFD state, the spacetime

[12] We shall denote the quanta inside the black hole as C

[13] The time when half of the total quanta have been emitted by the black hole and the Page Curve has started to dip.

behind the horizon is smooth and can be probed by space-like geodesics that run between the two boundaries through the black hole interior. Had there been a firewall, such a thing would not have been possible.

ABOUT THE THESIS

In the above discussion, we have tried to present a general flow of ideas that have inspired the works in this thesis. There are five different projects that have been presented in the form of five different chapters. The context for each of these works has been introduced wherever possible, in the discussion above. Nonetheless, it is necessary to once again highlight the underlying theme of this thesis. In all of these works, we have tried to explore how to understand thermalization in pure states. Owing to the AdS/CFT correspondence, we have been able to apply these ideas to the physics of black holes in the bulk and answer some questions with regard to their formation and evaporation. Below, we present a summary of the thesis.

In Chapter 2 of this thesis, we add additional charges to the TFD state and study the behaviour of time dependent entanglement entropy in it. The eternal black hole in the dual bulk theory geometries this entanglement in the form of geodesics that pass through the black hole interior, thereby suggesting the presence of a smooth geometry (and simultaneously, the absence of a firewall). The growth of the EE in the CFT suggests a growth in the length of the geodesics passing through the interior of the black hole, which in turn implies a growth in the volume of the black hole interior. In Chapter 3, we try explore a bit further by starting from the Fefferman-Graham metric describing the exterior geometry of a black hole in and AAdS space, and constructing a set of co-ordinates, analogous to the Eddington-Finkelstein co-ordinates, that allows us to go inside the black hole. The metric in these co-ordinates is smooth beyond the horizon. In fact, we invoke four different sets of the metric covering four different patches of the eternal black hole and smoothly transforming into each other in the regions of overlap, which happen to the the interiors. A fifth patch smoothly patches up the bifurcate horizon with the other metrics. This metric is special since it also describes

perturbed black hole geometries obtained by applying unitary (Virasoro) transformations independently on either boundary. In Chapter 4, we revisit the discussion of thermalisation in the context of quantum quenches in 1+1 dimensional conformal field theories. Using the aide of one-point functions of quasi-primary operators as well as the reduced density matrix pertaining to a sub-system, we show how thermalization occurs in the case of a quench from a gapped to a gapless phase; the ground state of the gapped phase being viewed as a Cardy-Calabrese (CC) state. We then generalise the CC state to include a number of higher spin conserved charges, pertaining to the currents in the W_∞ algebra, to try and understand its effects on thermalisation. We discover that the rate of decay gets modified by a term proportional to the charges of the primary operators under the additional conserved currents. Interestingly, we are able to match the rate of decay with the quasi-normal modes of a black hole in AdS, with and without a higher spin charge, indicating at a connection between the time-dependent CFT and the black hole geometry. In Chapter 5 of this thesis, we try to understand the effect of finite size on thermalization in the previous quench set-up. We discover that quantities such as the one-point function of quasi-primaries, including the stress tensor, and entanglement entropy, which intially thermalised in the infinite system, now display a revival at time scales proportional to the system size. The same can be seen on the gravitational side, where we discover a geometry oscillating between a black hole and a thermal AdS. However, there are many open questions which are discussed further in detail. In Chapter 6, we move to the regime of a large central charge CFT where we consider the vacuum state perturbed by a heavy primary operator. We show the way such heavy states are perceived as thermal states by the light primaries, presenting them as examples of thermal eigenstates. These states can be understood as being dual to a black hole. This is one instance where the sub-leading corrections, that render the state pure, are all suppressed by $1/c$. The crux of this chapter, however, is to show that the thermal behaviour persists even if we consider higher point correlation functions. Such correlators are extremely useful

in the present context to calculate quantities like, mutual information, out-of-time-ordered correlators, etc. We end with the conclusion and a discussion of possible open problems.

Before we proceed further, we would like to introduce some very important concepts that shall be extensively used throughout this thesis.

1.2 Pure States

1.2.1 The Thermofield Double State

The Thermo-field double (TFD) state was introduced in the 1970's in the field of statistical mechanics to facilitate the calculation of correlation functions in thermal systems. Usually calculating the expectation value of an observable, $\hat{A}$ say, in a thermal state involves performing a sum over the energy levels of the systems, each associated with a particular weight. Performing this sum can, however, be a daunting task. Instead, an easier way is to introduce an exact second copy of the system and create a very particular pure state out of it. This state is what is referred to as the TFD state, and mathematically it is defined as,

$$|\psi\rangle = \sum_n e^{-\beta E_n/2} |n\rangle_1 \otimes |n\rangle_2 \tag{1.2}$$

where $|n\rangle$ is an energy eigenstate with energy E_n. The subscripts denote the system to which the eigenstates belongs. This state has the curious feature that if one of its constituent systems is traced over, we recover the thermal density matrix corresponding to the other system. So the construction of a pure state like (1.2) is what is fittingly called *purification*. This is a very general feature, where any mixed state can be made pure by adding additional d.o.f. and entangling them in a specific way to the d.o.f. of the original system. More often than not, the system and it's complement do not even have the same size (or d.o.f.). The TFD state is, therefore, very special since it is constructed out of two copies of the exact same system.

Coming back to the issue of calculating expectation values of observables, an operator on either one of the systems acts as a very effective coarse-grainer, since its expectation value in the TFD state doesn't care about the presence of the other system. Thus,

$$\langle\psi|\hat{A}_1|\psi\rangle = \mathrm{Tr}_1(\rho_1\beta_1\hat{A}_1) \tag{1.3}$$

All calculations involving traces reduce to that of expectation values in the TFD state. Since calculating expectation values is seemingly simpler, this serves the original motivation for introducing this state.

The TFD state was, however, re-introduced in its recent context of the AdS/CFT correspondence, in a paper by Maldacena [177] in 2001. In this paper, he conjectured that the TFD state describing entangled CFTs in d-dimensions, was dual to an eternal black hole in d+1 dimensional asymptotically AdS spacetime. Such a black hole has a common interior, two horizons, two exteriors and two asymptotically AdS boundaries where the CFTs live. The system has two Hamiltonians, namely,

$$H_+ = H_R + H_L, \;\; H_- = H_R - H_L \tag{1.4}$$

It is easy to check that the TFD state is an eigenstate of the H_- Hamiltonian, while it undergoes a non-trivial time evolution under the H_+ Hamiltonian.

The TFD state prepares an initial entangled state for the boundary CFTs, while simultaneously inducing a Hartle Hawking state for the bulk gravitational theory, at the $t = 0$ slice. Thereafter, evolving the state with the H_+ Hamiltonian, creates a black hole in the bulk with two exteriors and a common interior. In the bulk theory, one can reflect about the $t = 0$ slice to get the entire eternal BH geometry, while always remembering that the two boundaries and hence the two exteriors are entangled.

For the two exterior regions , each of which is hidden from the other by its own horizon, the other exterior is just part of the spacetime forming the interior of the black hole. Living at the asymptotic infinity of these exterior regions, each of the two CFTs are also oblivious to the presence of each other. Hence,

$$\langle\psi|[\mathcal{O}_L, \mathcal{O}_R]|\psi\rangle = 0 \tag{1.5}$$

where $(\mathcal{O}_L, \mathcal{O}_R)$ are generic operators on either CFT. This implies that the two CFTs are completely causally disconnected. However, a very intriguing feature of this construction, despite the causal dissociation of the CFTs, is that the two sided correlation functions, *in this state*, are non-zero! It is very important to emphasise that this is a property of the state in which this expectation value is evaluated.

Ideally, the two CFTs belong to two different Hilbert spaces $\mathcal{H}_L$ and $\mathcal{H}_R$ respectively. So, operators in these two disjoint CFTs do not allow for any OPE between them, and hence their correlation function is zero. However, if we consider a state in the enlarged Hilbert space $\mathcal{H}_L \otimes \mathcal{H}_R$, which entangles the two CFTs, then the correlation function between the operators of the two CFTs becomes non-zero, when evaluated in this state. This happens because the state induces a map between the operators in the two CFTs which then allows for them to have a non-zero OPE and therefore a non-zero correlation. The TFD is one such realisation of an entangled state in the enlarged Hilbert space that induces a map between two CFTs. For the TFD, this map can be better understood as an analog of the KMS condition, which is stated as,

$$\mathrm{Tr}(\hat{\rho}^{1/2}A_L(t)\hat{\rho}^{1/2}B_R(0)) = \mathrm{Tr}(\hat{\rho}B_R(0)A_R(t-i\beta/2)) = \mathrm{Tr}(\hat{\rho}^{1/2}B_L(-I\beta/2)\hat{\rho}^{1/2}A_R(t-i\beta/2)) \tag{1.6}$$

This relation just emphasises that within correlation functions in the TFD state, operators on the left CFT can be understood as operators on the right CFT with a shift of $-i\beta/2$ along the Euclidean time circle.

This short description makes clear the importance of the TFD state as a unique state with very interesting properties. The most interesting of these is the fact that it is the only kind of purification that has a holographic dual. This raises the question as to whether it is really fine-tuned for the purposes of holography or whether there are other generalisations of it that allow for a holographic dual[14]. It is also important to ask how stable it is to perturbations. That would tell us how stable its dual gravitational theory is[15].

An important physical idea, that came about more recently [138, 175], is the way the entanglement between the CFTs is realised in the dual bulk theory. It was suggested that a physical realisation of the entanglement comes about by realising that there are space-like pathways, also called *wormholes*, that run between the left and right boundaries through the black hole interior. In fact, there had been speculations, since the discovery of the Ryu-Takayanagi surfaces [149, 220], about space-time being completely made out of entanglement in the underlying quantum theory. This physical realisation of the CFT entanglement has been suggested to give rise to the geometry of the interior of the eternal BH. Further still, this seems to be a very efficient set-up (and currently, the only one) that allows access to the interior of the black hole using non-local boundary operators. We shall elaborate on this further. More immediately, we shall elaborate on some other ways to understand the TFD setup and how it induces a Hartle-Hawking wave function in the bulk.

[14] As far as we know, with a factor of $\beta/2$ separation along the thermal circle, this is the only state with a holographic dual. Whether there are other kinds of holographic duals possible for arbitrary separations between the CFTs is not known.

[15] A lot of work has been done recently in trying to understand perturbations of the TFD state and its consequences for holography. We will not cover this question in detail in this thesis. However, some of the recent works in this direction include [225, 226]

1.2.2 The Pair-Production Representation

On the CFT side, the path integral that prepares the TFD state, is over an interval of length $\beta/2$ times a sphere. In other words,

$$\Sigma = I_{\beta/2} \times S^{d-1} \tag{1.7}$$

To get a pictorial understanding of the geometry, let us confine ourselves to $d = 2$, where Σ is just a cylinder of length $\beta/2$. The two ends of the cylinder are the two boundaries that specify the initial state of the two CFTs. The cylinder itself is a geometric realisation of the entanglement between the CFTs. In order to check if this manifold really produces the TFD state, one should be able to reproduce the matrix elements of the TFD state starting from the transition amplitude of the state on the left CFT ($|\phi_L\rangle$) to the state on the right CFT ($|\phi_R\rangle$) along Σ. Thus,

$$\begin{aligned}
\langle\tilde{\phi}_L|\exp(-\beta H/2)|\phi_R\rangle &= \sum_n \exp(-\beta E_n/2)\langle\tilde{\phi}_L|n\rangle\langle n|\phi_R\rangle \\
&= \sum_n \exp(-\beta E_n/2)\langle n|\phi_L\rangle\langle n|\phi_R\rangle \\
&= \langle\psi|(|\phi_L\rangle \otimes |\phi_R\rangle)
\end{aligned} \tag{1.8}$$

This proves that the TFD state is indeed equivalent to doing the path integral over Σ. A similar statement carries forth in higher dimensions, where instead of a circle we would have a $d-1$ dimensional sphere. Now, the bulk dual of this state should be a Euclidean gravity solution, on a manifold M, that has the surface $\partial M = \Sigma$ as its boundary. Next, we shall discuss one such possible solution in gravity.

1.2.3 The Hartle-Hawking Representation

Euclidean geometries necessarily use the imaginary time prescription, which has been very successfully understood and applied to various problems relating to quantum gravity by Hawking and collaborators since the 1970's. One such solution is simply the Euclidean version of the Schwarzchild solution in AdS space, given by

$$ds^2 = (r - r_0)^2 d\tau^2 + \frac{dr^2}{(r - r_0)^2} + r^2 d\Omega_{d-1}^2 \tag{1.9}$$

As is understandable from the above metric, it describes a Euclidean black hole with $r > r_0$, where r_0 is the black hole radius. Interesting properties of the geometry are revealed in a set of near -horizon co-ordinates, defined in terms of (ρ, τ). The first simplification happens in the form of a factorisation of the 2-sphere from the rest of the geometry. In the (ρ, τ) co-ordinates, the geometry resembles a cylinder, a little far away from the horizon. At this point, $\tau \sim \tau + \beta$. Near the horizon, however, one must carefully define the boundary conditions so as not to get a singularity at $\rho = \rho_0$. This regulated solution happens to be disc near the horizon. The entire geometry is sometimes referred to as the *cigar* solution, owing to its appearance. Choosing the correct periodicity defines for us the Hawking temperature, which is related to the inverse of β. One can now imagine the surface Σ appearing as the boundary of this geometry, if we only let $\tau \in [0, \beta/2]$. This is exactly the geometry in the Euclidean section of the eternal BH and hence appears to be the dual of our solution above. This, of course, does not prove the uniqueness of the solution[16].

The Schwinger-Keldysh Representation

The Schwinger-Keldysh formalism, also called the *in-in* formalism, was introduced independently by Schwinger [222] and Keldysh [155] to study specific out-of-equilibrium

[16]For more details one must look at the comprehensive lecture notes by T. Hartman, and the original paper of Maldacena [177]

quantum systems. It was later generalised to study many-body out-of-equilibrium quantum systems, by Feynman and Vernon [109]. Since then it has found applications in numerous areas such as cosmology, hydrodynamics and various other open quantum systems[17].

The basic idea of the SK formalism is to understand how the density matrix can be used to study physical observables such as expectation values and correlation functions, in an out-of-equilibrium quantum system. The difficulty in performing such calculations, in a time-dependent system, lies in the fact that the final state, as an end-result of the evolution, is not always known [18]. To remedy this problem, the SK formalism completely by-passes the final state by introducing a second copy of the original system which evolves in exactly the same way, but in the opposite time-direction. The two copies do not interact in any physical way, except at the boundaries where the (right-most) fields on either contour are identified. As for the initial state, it is assumed to be the same for both the systems, since they are exact replicas of each other. In fact the initial density matrix determines the exact entanglement pattern between the two systems.[19].

To understand the mathematical set-up better, let us define the time-evolved density matrix as:

$$\hat{\rho}(t) = U(t,T)\hat{\rho}(T)U^{\dagger}(t,T) = U(t,T)\hat{\rho}(T)U(T,t)$$

where $U(t,T)$ is just the unitary evolution matrix from t to T. The generating functional can then be defined as,

$$\mathcal{Z}_{SK}(\mathcal{J}_L,\mathcal{J}_R) = \mathrm{Tr}(U(\mathcal{J}_R)\hat{\rho}U(\mathcal{J}_L)^{\dagger}) \tag{1.10}$$

where $(\mathcal{J}_L,\mathcal{J}_R)$ are the sources for the operators on the left and right contour, respectively. This generating functional can be used to compute all possible correlation functions of operators placed on either boundary. It is easy to see that all possible combinations would

[17] See [132, 133] for a recent review.

[18] This is in contrast with an equilibrium system, where the final state for an interacting theory differs from the initial state by just an overall phase factor.

[19] If the initial density matrix is thermal, then there are additional analytic properties that arise, such as the KMS condition, which can be visualised by considering the Euclidean time direction to be a circle.

calculate the advanced, retarded, Feynman and anti-Feynman correlators. Putting the left and right sources to be equal projects us onto a sector of the theory that has an additional $U(1)_T$ topological symmetry[20].

The reason for introducing the SK formalism is that the TFD state can actually be viewed as an SK contour, with equal sources, but now with the two time contours separated over a distance of $\beta/2$ along the imaginary time direction. For calculating correlation functions of operators in the TFD set-up, one can consider the initial density matrix to be the TFD density matrix and view the real time contours as containing the left and right CFT operators. This implies that each of the two copies of the Hilbert space, $\mathcal{H}_R \otimes \mathcal{H}_L^*$, belong to one of the two time contours. The TFD calculates the same out-of-equilibrium quantities as the original SK contour. This is because, as in the case of a thermal state, the TFD state also has a time circle. This gives rise to certain additional analytic properties (related to the KMS condition). From (1.10), we can derive the analogous generating functional for the TFD system as,

$$\mathcal{Z}_{TFD}(\mathcal{J}_L = \mathcal{J}_R) = \mathrm{Tr}(\hat{\rho}^{\frac{1}{2}} U(\mathcal{J}) \hat{\rho}^{\frac{1}{2}} U(\mathcal{J})^\dagger) \tag{1.11}$$

Although not obvious how this calculates the same correlation functions as the SK contour, the circle along the imaginary time direction gives rise to additional analyticity properties (1.6), and the condition,

$$U(\mathcal{J}) = \hat{\rho}^{-\frac{1}{2}} U(\mathcal{J}) \hat{\rho}^{\frac{1}{2}} \tag{1.12}$$

Which makes clear how they are the same. The most important application that this property has found is in the recent developments of discussions on chaos and scrambling in many body systems, where it has been used extensively to calculate out-of-time-ordered correlation functions [172].

[20] See [132, 133] for a recent review for the consequences of such an additional symmetry

1.2.4 CC states

One often hears about quenching in the context of metallurgy, where certain metals, mostly iron, is heated to extremely high temperatures and then cooled suddenly, mostly to obtain certain desirable properties. On a broader context, the word quenching refers to the process of a *rapidly* changing environment around a system to drive it out-of-equilibrium. In the context of theoretical and experimental physics, the word quenching has now come to refer to both rapid and not-so-rapid processes to drive quantum systems (including relativistic QFTs) out-of-equilibrium.

The way it is achieved in theoretical systems is very simple. To begin with, the system is prepared in an eigenstate of a given Hamiltonian $H_0(\{\lambda_i\})$. Thereafter, a certain parameter (could even be more than one) of $H_0(\{\lambda_i\})$ is changed suddenly to a new value. Let us call the new Hamiltonian $H(\{\lambda_f\})$. It is important that the change of the parameter(s) happens over a time-scale which is smaller than the relaxation time of the system. This then does not allow for the system to relax and adjust to the change in the parameter, thereby driving it out-of-equilibrium. This process is what has come to be know as a *quantum quench*. The old eigenstate now evolves non-trivially under the new Hamiltonian, since it is not an eigenstate of $H(\{\lambda_f\})$.

There is a huge literature dealing with how to compute correlation functions of operators following a quantum quench in various statistical mechanical models[21]. Of much interest are states that describe closed, isolated quantum systems undergoing a quantum quench. The interest in such systems stems from trying to understand whether such states reach an equilibrium following a quench, and if so, via what underlying mechanism. It is a separate question altogether to understand if the equilibrium values can be described by some Gibbs' ensemble. In case it is so, the system will be understood to have thermalised.

[21] See [56–58, 209] for a comprehensive review and list of references.

Usually, calculating physical observables, such as correlation functions and entanglement entropy, analytically, in time-dependent systems is very difficult. One can still make considerable progress by considering integrable systems or resorting to numerical computations. However, in recent years, performing analytic computations has received a tremendous boost due to the insights of Cardy and Calabrese [55,59,61,65] who suggested that one could gain a lot of mileage by carefully choosing the final values of the parameters in a quench. They suggested that at least in case of the simplest 1+1 dimensional quantum systems, we could choose the final values of the parameters to be the values defining a critical point of the system. The critical point is a point in the phase space which is scale invariant and often allows for a description by a conformal field theory (CFT). Thus, all correlation functions in the time-evolving, post-quench phase of the system could be evaluated using symmetries of the CFT. This makes it possible to obtain analytic results for any quench achieved via any protocol, as long as the end result of the quench puts the system in a gapped phase. It is of course true that these ideas apply to only a very small class of quenches. In fact, one might consider more exotic quenches across critical points [84–87,158,192,247], or quenches from an ungapped to an ungapped phase through a gapped phase (which maybe useful in holography), or even fermionic quenches [206,215]. There has been a significant amount of progress made in performing analytical calculations along all these directions. However, in this thesis, we shall only concern ourselves with gapped to gapless quenches.

Let us outline the proposal of Cardy and Calabrese for the simplest case of a 1+1 dimensional free massive bosonic QFT, undergoing a mass quench. We begin by preparing the system in an eigenstate $|\psi\rangle$ of the initial Hamiltonian $H_0(m_0)$ and subsequently tuning the mass to zero ($m_0 \to 0$) over a time scale much smaller than m_0^{-1} (which is the typical relaxation time scale in this case). The final Hamiltonian, of course, describes a Gaussian fixed point, which is scale invariant. Since the change is very *sudden*, the state $|\psi\rangle$ remains oblivious to the change in the Hamiltonian and hence, is no longer an eigenstate. It thereby undergoes non-trivial time-evolution when evolved with the new Hamiltonian. The insight

of Cardy and Calabrese was to suggest an ansatz for the form of this eigenstate in terms of a conformal boundary state $|B\rangle$ which is perturbed away from its fixed point by a relevant (or marginal) operator. In the case of the mass quench, their ansatz reads,

$$|\psi\rangle \propto \exp(-\tau H_{CFT})|B\rangle \tag{1.13}$$

Here, H_{CFT} refers to the final Hamiltonian at the Gaussian fixed point. However, for more general Hamiltonians, it could be any other fixed point of the system. In 1+1 D, the Hamiltonian is a relevant operator, being obtained from the spatial integration of the stress tensor. The factor of τ_0 is related to the initial mass of system in the gapped phase. This factor is fixed by requiring that the expectation value of H_{CFT} in $|\psi\rangle$ is the same as in the deformed boundary state. This also fixes the proportionality constant to 1. This ansatz raises a lot of questions and we shall dedicate Chapters 4 and 5 of this thesis discussing various generalisations and subtleties of this ansatz alone. For the time-being, we shall try to motivate this ansatz further along the lines of [59, 65].

Although (1.13) has been presented in the context of a massive quench in a 1+1 D bosonic QFT, it describes a much larger class of systems. To begin with, the initial state must be translationally invariant and must correspond to a system with short-range correlations. Ideally, the ground state of a gapped Hamiltonian displays such properties, although other excited eigenstates may also be considered. The conformal boundary state $|B\rangle$ usually appears as the boundary conditions of a CFT (for eg. the Ising model at its fixed point), so as not to break the conformal invariance of the bulk. The reason why it makes an appearance here can be explained in two ways,

1. In the quench from a massive to a massless phase, all possible modes of the final system are excited. This leads to a non-renormalizable state which is the state $|B\rangle$. However, to describe subsequent time evolution of the system, such a state is useless and must be supplied with a UV cut-off. The factor of $\exp(-\tau H_{CFT})$ serves exactly that purpose

to make the state normalizable. The normalised state describes only long wavelength (low-energy) modes with the pre-factor correlating it over scales of τ. This way the cut-off parameter also gets related to the energy pumped into (or taken out-of) the system. In the simple case of the mass quench, $\tau = \beta/4 = 1/(4m_0)$[22].

2. Every bulk CFT has its own set of allowed conformal boundary states that sit at a fixed point of the boundary RG flow. Each such state has its own basin of attraction that contains the ground states of all possible gapped Hamiltonians. Hence, starting from the ground-state of a gapped Hamiltonian, one can reach the conformal boundary state by acting on it with relevant deformations. This is exactly what is expressed in (1.13).

Having argued for the use of (1.13) as an ansatz, it is important to state what simplifications it brings about in the calculations. Confining our attention only to CC states, we can't help but notice the intriguing geometrical picture that it reveals. We can imagine the state $|B\rangle$ to be defined along the imaginary time slice $\tau = 0$. Then the deformation can be thought of as an evolution along the imaginary time direction for a duration of $\tau = \beta/4$. This gives us a strip geometry of width $\beta/4$. Similarly, we can consider the ket state as another strip geometry of the same width. Together then the normalised state $\langle\psi|\psi\rangle$ corresponds to a strip of width $\beta/2$. Note that the width is not β, which would correspond to a cylinder geometry representing a thermal state. Instead, this is the geometrical representation of a state following a quench to a gapless phase. For convenience, we can re-label the state as running between $\tau \in [-\beta/4, \beta/4]$. The simplification comes

[22] In the original work of CC, they suggested that starting from the ground state of a free massive scalar theory, and quenching the mass parameter to zero, gives rise to (1.13). This was pointed out to be an erroneous conclusion in [180], in which they suggested that starting from the ground state in such a quench, one can never discard the other irrelevant operators that may arise in a generalisation of (1.13) and whose conjugate variables are higher inverse powers of the mass. The argument was based on the absence of a second scale in the system, with respect to which the mass could be taken to zero. One instance of such a general state has been discussed in Chapter 4 of this thesis. The authors of [180], however, also suggested that the CC state could be produced if one instead started with an excited state of the gapped Hamiltonian. In such a case, the excitation scale provides for the second scale factor with respect to which the coefficient of the higher irrelevant operators could be taken to zero.

about from realising that the states along the boundaries of the strip are conformally invariant, as the bulk itself. Thereafter one can calculate all correlation functions in the time-evolving, post-quench state as operator insertions on the strip along the $\tau = 0$ slice, analytically continued along the real time-direction and using conformal symmetries to map them to suitable manifolds (the upper-half plane or the full plane) for evaluation. We shall discuss more about such calculations in Chapters 4 and 5.

It is intriguing to understand how robust this ansatz is and what are the possible generalisations of this state that one might consider. One very obvious generalisation is to add more irrelevant terms in the exponent in (1.13) and understand the consequences within correlation functions. Cardy has already considered a generalisation of the state by adding higher powers and derivatives of the stress tensor, integrated over space, in the exponent [72]. Another possible generalisation is to perturb the state by adding the higher spin conserved charges, $\mathcal{W}_n$, of a 2D CFT. This analysis has been carried out in [182] and is the subject of discussion in Chapter 3.

These states also have the property that correlators of quasi-primary operators in a CFT, thermalise in them [72, 182]. This property has necessitated the use of such states in studies of thermalisation of closed, isolated, out-of-equilibrium quantum systems. However, they have also been shown to display non-thermal behaviour in case the system has finite boundaries [71, 73, 163, 183]. A detailed discussion of this issue and possible ways to re-approach thermalisation shall form the subject matter of Chapter 5.

1.2.5 Heavy states

Heavy states are the simplest of the pure states that we consider in this thesis. They are created by acting upon the vacuum with a "heavy" primary operator in a two-dimensional

CFT. Thus[23],

$$|\mathcal{O}_H\rangle = \mathcal{O}_H(0)|vac\rangle \tag{1.14}$$

By heavy, we mean here an operator whose conformal dimension scales with the central charge with (at least) an order one coefficient. Thus, $h_H/c \sim \mathcal{O}(1)$ in the $c \to \infty$ limit. These operators were used for the first time in the context of Liouville theories [223], and have been recently revived in the context of 2D CFTs [20, 31, 135] to understand black holes. This part is owing to a novel property of such heavy states: when viewed from a low-energy theory, they appear to be thermal. This was shown to be the case, in the context of calculating correlators of "light" quasi-primary operators in these states. By "light" again, we mean here operators that scale with the central charge with a coefficient much smaller than one, however. Thus, $h_L/c \ll h_H/c$, in the $c \to \infty$ limit. In this sense, these heavy states are like micro states of a black hole. The one point function of a light primary in this state (calculated on a cylinder with a compact spatial direction) is,

$$\frac{\langle \mathcal{O}_H|\mathcal{O}_L(x)|\mathcal{O}_H\rangle}{\langle \mathcal{O}_H|\mathcal{O}_H\rangle} \simeq C_{HHL}\exp(-h_L t) \tag{1.15}$$

The decay of a primary operator is the characteristic signature of its expectation value in a thermal state. This, therefore, proves the statement regarding the thermal behaviour of the pure heavy state. The two point function can be similarly shown to be thermal, but requires a bit more work. A two-point function of light operators in the heavy state becomes a four point function in the vacuum and starts receiving contributions from the conformal blocks of all primary operators in the theory. The interesting part of the large central charge limit is then that, 1. conformal blocks corresponding to all primary operators can be exponentiated as $\exp -cf(z_i, h_i/c)$, 2. the conformal block corresponding to the identity operator contributes the most, thereby dominating the sum, in this limit. So, the two point function of light operators in the heavy states is given by the exchange of the identity

[23] The conjugate state is $\langle \mathcal{O}_H| = \langle vac|\mathcal{O}_H^\dagger(\infty)$.

operator and its descendants [135]. The exponentiated vacuum (and even the non-vacuum) conformal block can be computed using certain monodromy methods that shall be outlined in detail in Chapter 6 of this thesis. The result then is a thermal two point function that decays at large times. The interesting and extremely educational part about this calculation is how leaving out the $1/c$ corrections in a vacuum correlator gives us a thermal result! This is also one of the ways in which we would want to understand pure states as describing black holes. In Chapter 6, we shall show how to calculate higher point correlations in these heavy states and whether and how, they too appear to be in a thermal background. Finally, we should mention that inserting a heavy operator in the vacuum backreacts on the geometry non-trivially, providing it with a description in terms of a stress-tensor. In [20, 31, 135], it was shown how to write down a metric corresponding to this perturbed geometry in the Fefferman-Graham co-ordinates. The two point functions and entanglement entropy results were matched between the bulk and the CFT providing evidence for the validity of this conjecture. In Chapter 6, we shall provide further evidence by providing a match at the level of higher-point functions.

1.3 General Notions

1.3.1 Entanglement Entropy

In Conformal Field Theory

Entanglement provides a way to understand and quantify correlations between the degrees of freedom (d.o.f.) in quantum systems. One possible measure of such entanglement is the entanglement entropy (EE), which is defined along the lines of von Neumann entropy, but now for reduced density matrices describing the d.o.f. in spatial sub-regions ($A = \cup_i A_i$). It is defined as,

$$S_A = -Tr(\rho_A \log \rho_A) \text{ with } \rho_A = Tr_{A^c} \rho_{tot} \tag{1.16}$$

For most states (including the ground state of simple models), the reduced density matrices are horribly complicated objects. This makes EE a hard quantity to compute. In 2-d CFTs, however, this calculation was performed analytically using the replica method in [61, 64]. The idea is to first calculate an auxilliary quantity, called the Rényi entropy and obtain the EE from an analytic continuation of that. The calculation of the Rényi entropy relies on considering n replicas of the original CFT and sewing them along the intervals A_i using twist and anti-twist operators. With appropriate conformal transformations to a single sheet, one can reduce the calculation to that of a two-point function of n-th order twist operators (σ_{pm}) on the appropriate geometry. The mathematical expression for the Rényi entropy of a single interval A is,

$$S_A^{(n)} = \frac{1}{1-n} \log(\mathrm{Tr}\rho_A^n) = \langle \sigma_+(z_1, \bar{z}_1)\sigma_-(z_2, \bar{z}_2)\rangle_{\mathcal{M}} \tag{1.17}$$

The EE is then obtained from the above quantity by analytically continuing $n \to 1$. An extension of this calculation to very specific time-dependent states was done in [59] where the EE also becomes time-dependent. We shall use these ideas explicitly in Chapters 2 and 3, and again in Chapters 5 and 6 to obtain various results with interesting physical interpretations.

In AdS Gravity

Due to the AdS/CFT correspondence, one might expect an extension of the idea of EE into the bulk as well. The first prescription for calculating EE in the AdS bulk was outlined by Ryu and Takayanagi in [220] (also called the RT prescription). For every region A in a d-dimensional CFT, the prescription requires one to construct a minimal surface Σ in the $d+1$-dimensional AdS bulk, such that the boundary of the surface $\partial\Sigma$ intersects ∂A at the asymptotic infinity. The EE is then given in terms of the area of the d-dimensional minimal surface in the following way,

$$S_A = \frac{Area(\Sigma)}{4G_N} \tag{1.18}$$

where G_N is the Newton's constant in $d+1$-dimensions. Since, we know how to analytically obtain the EE in a 2-d CFT, we would be interested in the analogous 3-d gravity calculation. In 3-dimensions, the area of the minimal surface corresponds to the length of the geodesic that joins the two end-points of the interval in the CFT, through the bulk. The single interval EE in the vacuum and the thermal state of the CFT were shown to match the corresponding calculations in a Global AdS and a BTZ black hole background, respectively [220].

The prescription was extended to include time-dependent geometries in the bulk (dual to time-dependent CFT states) in [149]. The EE is also time-dependent in such states. The new prescription in the bulk is now to compute the area of the extremal (instead of the minimal) surface that intersects the boundary of the entangling region at asymptotic infinity. We shall use these ideas related to time-dependent pure states and their bulk duals extensively (in Chapters 2 and 5) to explore a great deal about universal behaviour during approach to thermalization in both field theories and their gravitational counterparts.

1.3.2 Eigenstate Thermalization Hypothesis (ETH)

The eigenstate thermalisation hypothesis was first proposed my Srednicki, as a condition that systems should display in order they thermalize. Details about the ETH can be found in the original paper [229] and a number of recent reviews [83, 124]. Here we wish to just provide the statement for what we mean by the ETH.

The ETH is a very general statement made at the level of a class of operators in any system. The statement begins by supposing that we have a pure state $|\psi\rangle$ that can be written in the energy eigen-basis $|n\rangle$, with the support of $n \in [E, E + \Delta E]$ and $\Delta E \ll E$. This implies that $|\psi\rangle$ is a micro state with support on a certain band of the spectrum. Now suppose we have a class of operators $\{A\}$, whose expectation values we wish to calculate in the above state. For that, we consider the time dependent expectation value of an operator

$\hat{A}$ belonging to the above class,

$$\langle\psi(t)|\hat{A}|\psi(t)\rangle = \sum_n |c_n|^2 A_{nn} + \sum_{n\neq m} c_m^* c_n A_{mn} \exp(-i(E_n - E_m)t) \tag{1.19}$$

In the above expression, we have taken the liberty to separate out the diagonal and the off-diagonal components of the matrix corresponding to the operator. Usually, while calculating *long time averages*, one simply integrates over a sufficiently long time interval. That is good enough to kill all the oscillating time phases and provide one with a fixed value for the one-point functions. The idea of ETH instead is to get rid of the time dependent phases in the off-diagonal sector by putting certain assumptions on the off-diagonal matrix elements of the operator in the energy eigenbasis, namely the A_{nm}'s. The *first condition* of ETH is to assume that the off-diagonal elements A_{nm}, are exponentially small in the no. of d.o.f. of the system, namely $A_{nm} \sim \exp(-\mathcal{O}(N))$ with $n \neq m$. The idea behind this is the following: at $t = 0$, all phases in the system are aligned and the second term (a sum over $\mathcal{O}(N^2)$ terms) is comparable to (or probably even larger than) the first term in (1.19). However, soon after the beginning of time-evolution of the system, the phases corresponding to various energy intervals begin to *decohere*, leading to a fall in the amplitude of the term. However, if the A_{nm} are not considered to be small, there is a possibility that these terms would still be comparable to the first term. Thus, at long times, only the first term survives. This is indeed the phenomenon of *equilibration*, as discussed in the introduction. Now, although the first term appears to be diagonal, it is still not thermal since it does not admit a description in terms of an ensemble. This can however, be achieved by making a *second assumption* on the diagonal matrix elements, as dictated by ETH. This assumption says that the diagonal matrix elements A_{nn} are the same over all the basis states, while being an $\mathcal{O}(1)$ quantity. This in a way implies that the operator "coarse-grains"[24] over the energy levels in the energy band ΔE around E. This allows for A_{nn} to be taken out of the sum. The sum

[24]By "coarse-graining" we mean the mechanism via which the operator forgets about the initial state.

then just evaluates to one, owing to the normalisability of the coefficients c_n. Thermalisation is, hence, achieved where the time-dependent one-point function of the operator equals its micro-canonical ensemble average value. Thus,

$$\langle\psi(t)|\hat{A}|\psi(t)\rangle \simeq A_{nn} \tag{1.20}$$

For sufficient degrees of freedom in the system, this value can be equated with the canonical and grand canonical ensemble average values, via the *equivalence of ensemles* thereby introducing the notion of temperature and chemical potentials in the system.

Chapter 2

Dynamical Entanglement Entropy with Angular Momentum and a U(1) charge

2.1 Introduction and Summary

Entanglement entropy (EE) of a quantum system has turned out be a useful observable in many areas of physics; see reviews [61, 62, 99, 198]. In this chapter, we will primarily use EE as a dynamical tool, especially to describe equilibration in 1+1 dimensional quantum field theories. Time-dependent EE in 1+1 dimensional CFT has been studied in detail in [59, 61]. Let us consider a CFT with an infinite spatial direction; the EE for a single interval of length l, is found to saturate, according to the formula [1]

$$S_{\text{ent}}(t, l|\psi) \xrightarrow{t\gg l} l\, s_{\text{eqm}}(E), \quad s_{\text{eqm}}(E) = \sqrt{2\pi c E/3} \tag{2.1}$$

[1] In [59, 61], the entropy density is given by $s_{\text{eqm}} = c\pi/(3\beta)$, where β is the inverse temperature of a canonical ensemble equivalent to a microcanonical ensemble at energy E, given by $\beta = \sqrt{\pi c/6E}$. With this, we recover the RHS of 2.1.

In the above equation, the LHS is the EE of an interval of length l, computed in the state $|\psi\rangle$ at time t; we will denote the energy density of the state as E. $s_{\rm eqm}(E)$ is the equilibrium entropy density in the microcanonical ensemble as a function of energy density E. It is assumed here that length of the interval l is greater than the characteristic length scale $1/\sqrt{E}$ associated with the state $|\psi\rangle$ (this condition will play an important role in Section 2.8). [138] showed that the time-development in 2.1 can be interpreted holographically in terms of a BTZ black hole, and derived 2.1 using the Ryu-Takayanagi definition of holographic EE [220] (see [2, 7, 25, 168] for other recent works on holographic thermalization using dynamic EE). The linear growth in time was given an intuitive explanation in terms of oppositely moving entangled pair of excitations [59]; one of the objectives of this chapter is to explain the saturation value in terms of quantum ergodicity. An important point to note about 2.1 is the *information loss* aspect of this equation: on the RHS of 2.1, all information about the specific state $|\psi\rangle$ appears to be lost, other than energy E of the state. We will elaborate on this further in Section 2.2.3. Indeed, the above statement of equilibration is similar in spirit to the following statement of quantum ergodicity (see [209], Section III-A)

$$\mathrm{Tr}\left(\rho_{\rm pure} O\right) \xrightarrow{t\to\infty} \mathrm{Tr}\left(\rho_{\rm mc} O\right), \quad \rho_{\rm pure} = |\psi\rangle\langle\psi|, \quad \rho_{\rm mc} = \frac{1}{\mathbf{\Omega}(E)} \sum_{i\in\mathcal{H}_E} |i\rangle\langle i|, \tag{2.2}$$

which is believed to be true for a class of "macroscopic" observables O. Here, $\rho_{\rm mc}$ defines a microcanonical ensemble at energy E; $\mathcal{H}_E$ denotes the subspace of states with this energy, and $\mathbf{\Omega}(E)$ is the dimension of $\mathcal{H}_E$. We will, in fact, derive 2.1 from 2.2, modulo some assumptions, in Section 2.7. Thus, in the time-development described in 2.1 not only is the memory of the initial state lost, the RHS is given in terms of a mixed state. It is worth noting that in 2.2 no mention is made about the time scale of change; thus, the time-development in 2.1 provides a time scale for equilibration. In this chapter, we will show that the above statement of equilibration also holds in the presence of additional conserved charges, besides the energy E. In particular, we will show that if the initial state $|\psi\rangle$ has a non-zero angular

momentum J [2] and a U(1) charge Q, we have [3]

$$S_{ent}(t, l|\psi) \xrightarrow{t\gg l} l\, s_{eqm}(E, J, Q) \tag{2.3}$$

Here $s_{\rm eqm}(E, J, Q)$ equals the equilibrium entropy density in a microcanonical ensemble, described in Eqs.2.23 and 2.49, which give the detailed form of the time-dependence. Eq. 2.3 is the main result of this chapter; it is presented here in the limit in which the excitation energy of the initial state is much higher than $1/t, 1/l$. The precise version of this statement as well as the exact expression for the LHS without this restriction is given in Sections 2.2 and 2.4). We derive 2.3 also from a holographic set-up (Sections 2.3 and 2.5). The holographic dual consists of a spinning BTZ black hole plus a U(1) gauge field described by a CS theory.

Eq. 2.3 leads us to the following natural conjecture for an integrable 1+1 dimensional CFT. Suppose the initial state $|\psi\rangle$ has an infinite number of non-zero conserved charges $Q_i, i = 1, ..., \infty$ (including energy). We conjecture that the long time behaviour of the EE in this case is given by

$$\begin{aligned} &S_{\rm ent}(t, L|\psi) \xrightarrow{t\gg l} l\, s_{\rm eqm}(\{Q_i\}) \\ &s_{\rm eqm}(\{Q_i\}) = s_{\rm GGE}(\{\mu_i\}) \end{aligned} \tag{2.4}$$

where μ_i are values of chemical potentials conjugate to the infinite number of charges Q_i carried by the quantum state $|\psi\rangle$. In the second line, we have used the equivalence between the microcanonical ensemble (with infinite number of charges) and the generalized Gibbs ensemble (GGE). The corresponding generalization of 2.2 to 2-dimensional integrable systems

[2] In this paper, we will mostly be concerned with a non-compact spatial direction, so J is actually a linear momentum. However, we regard this non-compact direction as arising in the limit of a large circle (the bulk dual is a BTZ black string which can be regarded as the limit of a BTZ black hole), and will continue to call J an 'angular momentum'.

[3] The divergent piece $S_{\rm div}$ is the same as in the previous literature, including in [59, 138]. We do not have anything new to add regarding this term; for a recent discussion, see [167].

has already been proved [57, 179, 216]. A natural speculation about a holographic dual of the above involves higher spin black holes [18] (see Section 2.5.2 for a brief discussion).

A few remarks are in order:

1. We reproduce the CFT results In this chapter from AdS in two ways: (a) by an explicit evaluation of the Ryu-Takayanagi (RT) formula for holographic EE and matching with CFT, and (b) showing that the RT formula follows from a conventional AdS/CFT dual of the CFT correlators of twist fields in a double scaling limit. Method (b) constitutes a 'proof' of the RT prescription for 1+1 dimensional CFT (see Section 2.3.1 for details).

2. We encounter a puzzle in applying the RT prescription for holographic EE in the presence of the U(1) charge. The U(1) charge we consider is implemented in the AdS dual by a U(1) Chern-Simons (CS) theory, and addition of a U(1) charge does not change the metric. Therefore the RT holographic EE is independent of the U(1) charge, which seems to be in conflict with the CFT expressions which clearly depend on this charge. We resolve this puzzle in Section 2.5.1.

2.2 Entanglement Entropies with spin: CFT

2.2.1 Thermofield double

Let us consider a 2D CFT at a finite temperature, which is represented by a thermofield double consisting of two identical copies of the CFT [231]. Consider the following initial (pure) state, belonging to the thermofield double, on the time slice $t = 0$:

$$|\psi\rangle = C \sum_i \exp[-\beta(E_i + \mathbf{\Omega} J_i)/2] \, |i\rangle \otimes |i\rangle \tag{2.5}$$

The normalization constant C is given in terms of the partition function

$$|C|^{-2} \equiv Z(\beta, \mathbf{\Omega}) \equiv \mathrm{Tr}\, e^{-\beta(H+\mathbf{\Omega}J)} = \mathrm{Tr} \exp[-\beta_+ L_0 - \beta_- \bar{L}_0], \tag{2.6}$$

and we use the following identifications

$$H = L_0 + \bar{L}_0, \qquad J = L_0 - \bar{L}_0, \qquad \beta_\pm = \beta(1 \pm \mathbf{\Omega}) \tag{2.7}$$

The index i of the sums goes over a complete set of states of H_1 (equivalently H_2). The definition implies that the expectation values $\langle E \rangle, \langle J \rangle$ in this state are non-zero, and are related to the inverse temperature β and the 'angular velocity' $\mathbf{\Omega}$ (which is essentially a chemical potential for the conserved angular momentum).[4] In a Euclidean spacetime, $\mathbf{\Omega}$ must be chosen to be purely imaginary:

$$\mathbf{\Omega} = i\mathbf{\Omega}_E \tag{2.8}$$

Now, consider two identical entangling regions $A \subset \mathbb{R}$ in both copies of the field theory and compute the time evolution of the EE. First, we take A to be a semi-infinite line. Following the prescription in [64] (see review [61]) the entanglement Renyi entropy (ERE) is given by the CFT functional integral over a Riemann surface obtained by gluing n copies of a cylinder [5] along two semi-infinite cuts from $z_1 = \bar{z}_1 = 0$ and from $z_2 = i\beta_+/2$, $\bar{z}_2 = -i\beta_-/2$, both running off to infinity (see Figure 1). Such a partition function, in turn, boils down to the two-point function of twist fields $\phi_\pm$ [64] at the two branch points. Thus, the ERE is given by

$$S^{(n)} = \frac{1}{1-n} \log\langle \phi^+(z_1, \bar{z}_1)\phi^-(z_2, \bar{z}_2)\rangle \tag{2.9}$$

[4] As mentioned in footnote 2, for a non-compact spatial direction, J is actually a linear momentum; $\mathbf{\Omega}$ is the corresponding chemical potential.

[5] We will use complex coordinates $(z, \bar{z}) = \sigma_1 \pm i\sigma_2$ on the cylinder, with $-H$ and iP as the generator of translation along σ_2 and σ_1. The formula 2.6 implies the following twisted identification $(\sigma_1, \sigma_2) \equiv (\sigma_1 - \beta\mathbf{\Omega}_E, \sigma_2 + \beta)$; in terms of the complex coordinates $z \equiv z + i\beta_+$,$\bar{z} \equiv \bar{z} - i\beta_-$, where we have used 2.7 and 2.8.

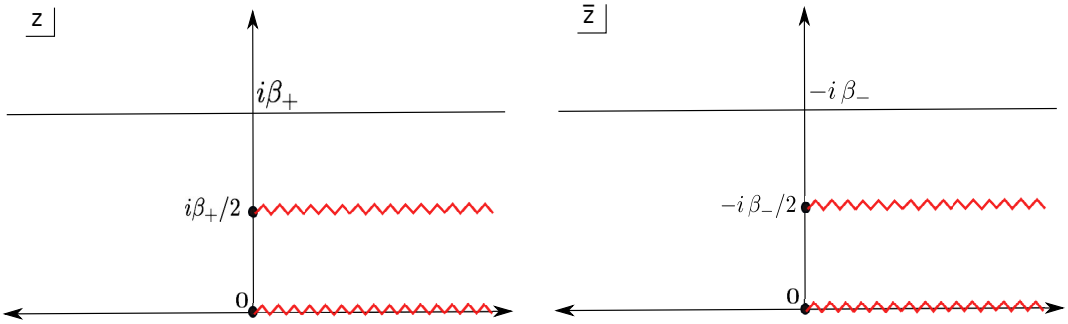

Figure 2.1: The lower branch cuts on left and right represent the (holomorphic and antiholomorphic coordinates) of the entangling interval in the first copy of the CFT. The upper branch cuts represent the second CFT.

To obtain this two-point function we first map the cylinder to the plane with coordinates given by

$$w(z) = \exp\left(\frac{2\pi\, z}{\beta_+}\right), \qquad \bar{w}(\bar{z}) = \exp\left(\frac{2\pi\, \bar{z}}{\beta_-}\right) \tag{2.10}$$

The two-point function on the plane of an operator O with conformal dimensions $(h, \bar{h})$ is given by

$$\langle O(w_1, \bar{w}_1) O(w_2, \bar{w}_2)\rangle = \frac{1}{(w_2 - w_1)^{2h} (\bar{w}_2 - \bar{w}_1)^{2\bar{h}}} \tag{2.11}$$

Now, under a conformal mapping $(w, \bar{w}) \to (z, \bar{z})$, correlators transform as

$$\langle O(z_1, \bar{z}_1) O(z_2, \bar{z}_2)...\rangle = \prod_i \left(\frac{dw_i}{dz_i}\right)^h \left(\frac{d\bar{w}_i}{d\bar{z}_i}\right)^{\bar{h}} \langle O(w_1, \bar{w}_1) O(w_2, \bar{w}_2)...\rangle \tag{2.12}$$

The ERE 2.9 can be obtained by using these results and the fact that for the twist fields $\phi_\pm$ of order n

$$\beta = \frac{1}{T}, \qquad \beta_\pm = \beta(1 \pm \Omega), \qquad h = \bar{h} = \frac{c}{24}\left(n - \frac{1}{n}\right) \tag{2.13}$$

As explained in [64], the EE is obtained by taking the $n \to 1$ limit. This gives

$$S_{EE} = S^{(1)} = \frac{c}{6} \log\left(\frac{\beta_+ \beta_-}{\pi^2 \epsilon^2} \sinh\frac{\pi(z_2 - z_1)}{\beta_+} \sinh\frac{\pi(\bar{z}_2 - \bar{z}_1)}{\beta_-}\right) \tag{2.14}$$

The cut-off ϵ is used to regularize the expression, as in [64]. [6] To explicitly evaluate 2.14 we substitute the values of $(z_{1,2}, \bar{z}_{1,2})$ mentioned above 2.9, and obtain the divergent value

$$S_{EE} = S_{EE,0} = \frac{c}{6} \log \left(\frac{\beta_+ \beta_-}{\pi^2 \epsilon^2} \right) \tag{2.15}$$

Here the subscript zero indicates that the EE is computed at $t = 0$.

Time-dependent EE

We will now consider the (Lorentzian) time-evolution of the thermofield state 2.5:

$$|\psi(t)\rangle = \exp[-iHt]|\psi\rangle = C \sum_i \exp[-\beta(E_i + \mathbf{\Omega} J_i)/2 - i2E_i t] \, |i\rangle \otimes |i\rangle \tag{2.16}$$

and will compute the time-dependent ERE and EE based on this time-dependent state. In the notation of footnote 5, the total evolution operator in 2.16 translates $(\sigma_1, \sigma_2) = (0, 0) \to (\sigma_1, \sigma_2) = (-\beta \mathbf{\Omega}_E/2, \beta/2 + 2it)$. This implies the following analytically continued location of the two branch points

$$z_1 = \bar{z}_1 = 0, \quad z_2 = -2t + i\,\beta_+/2, \quad \bar{z}_2 = 2t - i\,\beta_-/2 \tag{2.17}$$

Note that $\bar{z}_2 \neq z_2^*$; this happens because σ_2 is now complex. By using the new locations of the branch points in 2.14

$$S_{EE} = \frac{c}{6} \log \left(\frac{\beta_+ \beta_-}{\pi^2 \epsilon^2} \cosh \frac{2\pi t}{\beta_+} \cosh \frac{2\pi t}{\beta_-} \right) \tag{2.18}$$

[6] This equation appears in Ref. [149], where it signifies the equilibrium EE of a finite interval of length $|z_2 - z_1|$.

Clearly at large $t \gg \beta, \beta\mathbf{\Omega}_E$, the cosh terms can be replaced by exponentials, which show that the finite part grows linearly with time:

$$S_{EE}(t) = S_{EE,0} + t\,(2s_{\rm eqm}), \quad s_{\rm eqm} = \frac{\pi c}{3\beta(1-\Omega^2)} \qquad t \gg \beta, \beta\mathbf{\Omega}_E \tag{2.19}$$

where $s_{\rm eqm}$ is the equilibrium entropy density, further elaborated below 2.23. $S_{EE,0}$ is already defined in 2.15.

Finite interval

Now, take A be a finite interval of length l. In this case, we need to consider a functional integral over the cylinder with two *finite* cuts. The locations of the branch points $(z_i, \bar{z}_i)$ are

$$\begin{aligned} &z_1 = \bar{z}_1 = 0,\ z_2 = \bar{z}_2 = l, \\ &z_3 = l - 2t + i\frac{\beta_+}{2},\ \bar{z}_3 = l + 2t - i\frac{\beta_-}{2}, \quad z_4 = -2t + i\frac{\beta_+}{2},\ \bar{z}_4 = 2t - i\frac{\beta_-}{2} \end{aligned} \tag{2.20}$$

As described in [59,138], the entanglement Renyi entropy is given by the four-point correlator of the twist fields

$$S_n = \frac{1}{1-n}\log\langle\phi^+(z_1,\bar{z}_1)\phi^-(z_2,\bar{z}_2)\phi^+(z_3,\bar{z}_3)\phi^-(z_4,\bar{z}_4)\rangle \tag{2.21}$$

As before, a way to compute this would be by mapping the points to the plane using (2.10), computing the correlator there and transforming back to the cylinder by using 2.12. The details of this calculation are similar to the $\mathbf{\Omega} = 0$ case discussed in [138]. The 4-point function on the plane depends on the cross-ratio

$$x = \frac{w_{12}w_{34}}{w_{13}w_{24}} = \frac{2\sinh^2\frac{\pi l}{\beta_+}}{\cosh\frac{2\pi l}{\beta_+} + \cosh\frac{4\pi\, t}{\beta_+}}, \qquad \bar{x} = \frac{\bar{w}_{12}\bar{w}_{34}}{\bar{w}_{13}\bar{w}_{24}} = \frac{2\sinh^2\frac{\pi l}{\beta_-}}{\cosh\frac{2\pi l}{\beta_-} + \cosh\frac{4\pi\, t}{\beta_-}} \tag{2.22}$$

where $w_{ij} = w(z_i) - w(z_j)$ and similarly for $\bar{w}$. Let us assume that $l, t \gg \beta, \beta\mathbf{\Omega}_E$. We then have: $x \sim (1 + \exp[\frac{4\pi}{\beta_+}(t - l/2)])^{-1}$ up to $O(\exp[-t/\beta_+], \exp[-l/\beta_+])$.

Case (i): For $t < l/2$ [7], we then have $x \to 1$, which, in terms of the original coordinates, implies $z_2 \to z_3$ and hence a factorization $\langle 1\ 4\rangle\langle 2\ 3\rangle$. Once we realize this, we can go back to 2.21 and evaluate the four-point function as

$$\langle \phi^+(z_1, \bar{z}_1)\phi^-(z_4, \bar{z}_4)\rangle\langle \phi^-(z_2, \bar{z}_2)\phi^+(z_3, \bar{z}_3)\rangle$$

Case (ii): For $t > l/2$ [8], by similar reasonings, we have $x \to 0$, which implies the other factorization for the 4-point function

$$\langle \phi^+(z_1, \bar{z}_1)\phi^-(z_2, \bar{z}_2)\rangle\langle \phi^+(z_3, \bar{z}_3)\phi^-(z_4, \bar{z}_4)\rangle$$

Using our results from the previous subsections about the two-point function, we find the following behaviour of the EE:

$$S_{EE} = \begin{cases} 2t\,(2s_{\text{eqm}}) + S_{\text{div}} & t \leq l/2 \\ \\ l\,(2s_{\text{eqm}}) + S_{\text{div}} & t \geq l/2 \end{cases}$$
$$s_{\text{eqm}} = \frac{\pi c}{3\beta(1-\Omega^2)} = \sqrt{\frac{\pi c}{6}(E+J)} + \sqrt{\frac{\pi c}{6}(E-J)} \tag{2.23}$$

Clearly the EE saturates after time $t = l/2$. Here s_{eqm} is the equilibrium entropy density of (either copy of) the CFT; the first expression on the second line gives its value in the canonical ensemble and the second expression gives the microcanonical value (see Section 2.9.1 for the relation between the two ensembles). For $\mathbf{\Omega} = 0$ the results of this section

[7] Strictly speaking, we need here $(l/2 - t) \gg \beta_\pm$, to ensure $x \to 1$.
[8] We actually need $(t - l/2) \gg \beta_\pm$. See footnote 7.

correctly reduce to those derived in [138]. [9] The divergent part S_{div} is the same as $S_{EE,0}$ is 2.15 and 2.19.

We have thus proved 2.3 starting from a rather special pure state of the form 2.5. We will now present a more general derivation starting from an *arbitrary* initial state.

2.2.2 Single CFT, arbitrary state

Let us now consider a single CFT, defined on a cylinder (with coordinates described in footnote 5). We start with a pure state $|B\rangle$ at time $\sigma_2 = 0$, and evolve it by (i) translating in σ_2 by $\beta/4$ (as in [138]) and (ii) in σ_1 by $-\beta\mathbf{\Omega}_E$; this leads to another pure state

$$|\psi\rangle = \exp[-\beta(H + \mathbf{\Omega}J)/4]|B\rangle, \tag{2.24}$$

We will regard this as the initial state for further, Lorentzian, time evolution, and compute the time-dependent EE for a single interval in the state

$$|\psi(t)\rangle = \exp[-iHt]|\psi\rangle = \exp[-(\beta/4 + it)H - \beta\mathbf{\Omega}J/4]|B\rangle. \tag{2.25}$$

By choosing $|B\rangle$ arbitrarily, we can obtain an arbitrary initial state $|\psi\rangle$. We will comment in Section 2.2.3 on the independence of the EE with respect to the choice of this initial state.

Let us first consider the case where the interval is a half-line. Suppose at $\sigma_2 = 0$, the half-line ends at $\sigma_1 = 0$. Then after the evolution, this point is translated to $\sigma_1 = -\beta\mathbf{\Omega}_E/4, \sigma_2 = \beta/4 + it$ [10], or, in terms of the $z, \bar{z}$ coordinates (see footnote 5), to the point

$$z_1 = t + i\beta_+/4, \qquad \bar{z}_1 = -(t + i\beta_-/4) \tag{2.26}$$

[9] The expression for the time-dependent entanglement entropy for the finite interval, in 2.23, is twice that for the half-line 2.19, as observed in [138] for $\mathbf{\Omega} = 0$. We will encounter the same feature for a single CFT, as well as for the bulk duals.

[10] Recall that in 2.25, $-H, iJ$ are, respectively, the translation operators in σ_2, σ_1, and $\mathbf{\Omega} = i\mathbf{\Omega}_E$. See below 2.16.

The computation of the time-dependent EE, in part similar to that described above, involves a generalization of the techniques in [59, 138]. The entanglement Renyi entropy involves computing the one-point function of the twist fields $\phi^+(z_1, \bar{z}_1)$ (of 2.9) on an (analytically extended) strip ($\sigma_1 \in R, 0 \leq \text{Re}(\sigma_2) \leq \beta/2, \text{Im}(\sigma_2) = t > 0$) with boundary conditions specified by the state $|B\rangle$. As before, we will map this geometry to the (upper half) plane by using 2.10, where the boundary condition now applies to the boundary of the UHP. As discussed in [74], as long as the state $|B\rangle$ represents a conformally invariant condition (more on this in Section 2.2.3), the one-point function $\langle \phi^+(w_1, \bar{w}_1)\rangle$ in the UHP is given by

$$\langle \phi^+(w_1, \bar{w}_1)\rangle|_{UHP} = (w_1 - \bar{w}_1)^{-h-\bar{h}} \tag{2.27}$$

which equals the two-point function of ϕ^+ at w_1 with its image ϕ^- at $\bar{w}_1$ in the full plane. The original one-point function on the strip is now obtained by 2.10

$$\langle \phi^+(z_1, \bar{z}_1)\rangle = \left(\frac{\beta_+}{\pi\,\epsilon}\sinh\left(\frac{\pi\, z_1}{\beta_+} - \frac{\pi\,\bar{z}_1}{\beta_-}\right)\right)^{-h}\left(\frac{\beta_-}{\pi\,\epsilon}\sinh\left(\frac{\pi\, z_1}{\beta_+} - \frac{\pi\,\bar{z}_1}{\beta_-}\right)\right)^{-\bar{h}} \tag{2.28}$$

By putting the values 2.26, we can compute the Renyi entropy. Taking the $n \to 1$ limit, we obtain the EE

$$S_{EE} = \frac{c}{6}\log\left(\cosh\left(\frac{2\pi\, t}{\beta(1-\Omega^2)}\right)\right) + \frac{c}{12}\log\frac{\beta^2(1-\Omega^2)}{\pi^2\epsilon^2} \tag{2.29}$$

For large $t \gg \beta, \beta\mathbf{\Omega}$, the EE evolves linearly with a coefficient equal to half of the one for the thermofield double. For $\Omega = 0$ we recover the result of [138].

In the case of finite interval, let us suppose that the interval stretches from $\sigma_1 = -l/2$ and $\sigma_1 = l/2$ at $\sigma_2 = 0$. At time t these end-points are translated to $(z_1, \bar{z}_1)$ and $(z_2, \bar{z}_2)$, where

$$z_1 = -\frac{l}{2} + i\frac{\beta_+}{4} - t, \quad \bar{z}_1 = -\frac{l}{2} - i\frac{\beta_-}{4} + t, \qquad z_2 = \frac{l}{2} + i\frac{\beta_+}{4} - t, \quad \bar{z}_2 = \frac{l}{2} - i\frac{\beta_-}{4} + t$$

The computation of the EE follows by using a slight modification of [59, 138]. The Renyi entropy is given in terms of a two-point function on the above-mentioned strip which can be obtained, from the UHP result

$$\langle \phi_+(w_1)\phi_-(w_2)\rangle \sim \left(\frac{|w_1-\bar{w}_2||w_2-\bar{w}_1|}{|w_1-w_2||\bar{w}_1-\bar{w}_2||w_1-\bar{w}_1||w_2-\bar{w}_2|}\right)^{h+\bar{h}} \tag{2.30}$$

using the conformal transformation (2.10). The EE turns out to be

$$S_{EE} = \frac{c}{6}\log\left(\frac{\beta_+\beta_-}{\pi^2\epsilon^2}\frac{(\cosh\frac{2\pi\Omega\, l}{\beta(1-\Omega^2)}+\cosh\frac{4\pi\, t}{\beta(1-\Omega^2)})\sinh\frac{\pi l}{\beta(1+\Omega)}\sinh\frac{\pi l}{\beta(1-\Omega)}}{\cosh\frac{2\pi\, l}{\beta(1-\Omega^2)}+\cosh\frac{4\pi\, t}{\beta(1-\Omega^2)}}\right) \tag{2.31}$$

As in case of the thermo-field double, we again have, for large t/β and l/β, two cases (depending on the relative magnitude of t and $l/2$), that clearly illustrate the saturation of the entanglement entropy (see Fig 2.2)

$$S_{EE} = \begin{cases} 2t\, s_{\rm eqm} + S_{\rm div} & t \le l/2 \\ \\ l\, s_{\rm eqm} + S_{\rm div} & t \ge l/2 \end{cases} \tag{2.32}$$

where $s_{\rm eqm}$ is the equilibrium entropy density given in 2.23. Note that the saturation value of the entanglement entropy for the single CFT is expectedly half of that in the case of the thermofield double given by 2.23. Also note that the saturation value depends on the angular momentum (see Fig 2.2).

The above equation 2.32 is again of the form of 2.3. Thus, we have now proved this equation starting from an arbitrary initial state 2.24.

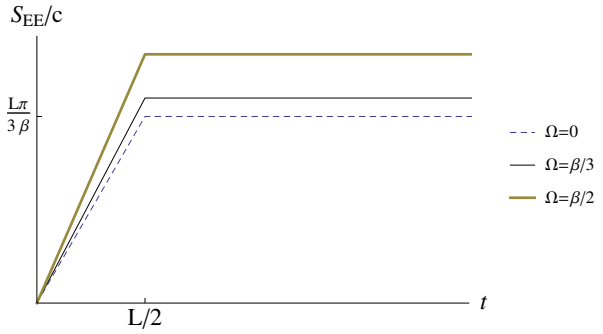

Figure 2.2: *Saturation of the Entanglement Entropy for different values of* Ω

2.2.3 Information loss

We wish to mention a rather remarkable feature of the EE described in this subsection. By choosing the state $|B\rangle$ in 2.24 appropriately, we can make the initial state $|\psi\rangle$ completely arbitrary (contrast this with the state 2.5 which is fixed by the choice of $\beta, \mathbf{\Omega}$); however, the entanglement entropy of an interval in any such state is independent of the choice of the state (this statement is even true for EE at any finite time). The feature of the calculation that makes this happen is the following. Recall that the choice of $|\psi\rangle$ corresponds to the choice of a boundary condition for the two-dimensional CFT (in an appropriate coordinate system, the state specifies a boundary condition on the boundary of the upper half plane (UHP)). As has been shown in [59], as long as the state $|\psi\rangle$ is a conformally invariant boundary state, the correlation function of twist fields in the UHP, involved in computing the Reny entropy boils down to correlators on the plane involving the original twist fields and their images in the lower half plane. This result is universal and is independent of the choice of the specific conformal boundary state, of which there is an infinite tower (the so-called Ishibashi states). Furthermore, as emphasized in [59], even if our initial state is not one of the conformally invariant boundary states, RG flow takes it to the nearby Ishibashi state; thus, for sufficiently large length scales/time scales the result becomes completely universal. From the holographic viewpoint, the universality is encapsulated by the fact that the bulk is given by a BTZ black hole geometry. These features have already appeared in the work

of [138]. Such universalities with respect to the initial state have also been remarked upon in [25, 168].

2.3 EE with spin: holographic calculation

As shown in [151, 177] (see also [54, 138, 149]) the above CFT calculations find natural duals in BTZ geometries. For non-zero angular momentum J, the holographic dual of the thermofield double involves (a Euclidean continuation of) the eternal (2+1)-dimensional BTZ black hole [23], given by

$$ds^2 = -\frac{(r^2-r_+^2)(r^2-r_-^2)}{r^2}dt^2 + \frac{r^2}{(r^2-r_+^2)(r^2-r_-^2)}dr^2 + r^2\left(d\phi - \frac{r_+ r_-}{2\,r^2}dt\right)^2 \tag{2.33}$$

Here $\phi \sim \phi + 2\pi$ for the BTZ black hole, and $\phi \in \mathbb{R}$ for the BTZ black string. [11] The mass M, angular momentum J, temperature T and angular velocity $\mathbf{\Omega}$ are determined by the inner (r_-) and outer (r_+) horizons, as follows:

$$M = r_+^2 + r_-^2, \quad J = 2\,r_+ r_-, \quad T = 1/\beta = \frac{2\pi r_+}{r_+^2 - r_-^2}, \quad \mathbf{\Omega} = \frac{r_-}{r_+} \tag{2.34}$$

The BTZ metric can be mapped into the Poincare patch of Euclidean AdS_3 ($ds^2 = (dy^2 + dw_+ dw_-)/y^2$) via

$$w_\pm = \sqrt{\frac{r^2-r_+^2}{r^2-r_-^2}}\, e^{2\pi u_\pm/\beta_\pm}, \quad y = \sqrt{\frac{r_+^2-r_-^2}{r^2-r_-^2}}\, e^{\pi(u_+/\beta_+ + u_-/\beta_-)} \tag{2.35}$$

where $u_\pm = \phi \pm t$, and $\beta_\pm = \beta(1 \pm \mathbf{\Omega})$ (see, e.g., [157], Eq. (21)). The Euclidean continuation of the above geometry 2.33 is given by $t \to it$, $u_\pm \to (z, \bar{z})$, $w_\pm \to (w, \bar{w})$, $\mathbf{\Omega} \to i\mathbf{\Omega}_E$. Note

[11] The BTZ string can be obtained from the BTZ black hole by scaling $(r, r_\pm, t, \phi)$ with a parameter λ such that, as $\lambda \to \infty$, $\lambda r, \lambda r_\pm, t/\lambda, \phi/\lambda$ are held fixed. In this chapter, we will mostly be concerned with the black string, since the dual CFT has non-compact space. For the black string, the angular momentum J actually becomes the linear momentum; however, as declared in footnote 2, we continue using the notation J and the misnomer 'angular momentum'.

that in the limit $r >> r_+$, the (Euclidean continuation of the) map 4.16 precisely reduces to the transformation (2.10) in the CFT, as it must for consistency with holography.

We will now compute the holographic EE (hEE) for an interval A by using the Ryu-Takayanagi (RT) proposal [220], or more precisely the generalization in [149] for computing covariant EE, according to which the hEE is given by the length of the extremal [12] geodesic(s) that connects the boundary of A. The precise formula reads

$$S_{hEE} = \frac{\mathcal{L}(\gamma)}{4G_N} \tag{2.36}$$

where, in our case, $\mathcal{L}(\gamma)$ is the length computed with the metric (2.33) and G_N is the Newton constant in 3 dimensions. Following along the lines of [138], it is easy to verify that 2.36 indeed reproduces the CFT results 2.23 and 2.32. We will skip the explicit expressions since they are a straightforward generalization of [138] (we will make some more remarks on the geodesic lengths below in Section 2.3.2), and prefer to include an alternative 'derivation', which is more closely related to standard AdS/CFT arguments.

2.3.1 A 'proof' of Ryu-Takayanagi formula for 1+1 dimensional CFT

Recall that, in CFT, Entanglement Renyi Entropy (ERE) of a single interval $[u, v]$ is computed by the two-point function of the twist fields $\langle \Phi_+(u)\Phi_-(v)\rangle$ with dimension[13]

$$h = \frac{c}{24}\left(n - \frac{1}{n}\right) = \frac{1}{16G_N}\left(n - \frac{1}{n}\right) \tag{2.37}$$

[12] The original RT prescription faces a subtlety for Lorentzian backgrounds. Namely, in general, geodesics that connect the boundaries do not lie on fixed time slices. In these cases EE is given by the area of the extremal surface given by the saddle point of the area action [149].

[13] In the second equality we inserted the Brown-Henneaux relation $R_{AdS}/G_N = 2c/3$. In our formulas $R_{AdS} = 1$.

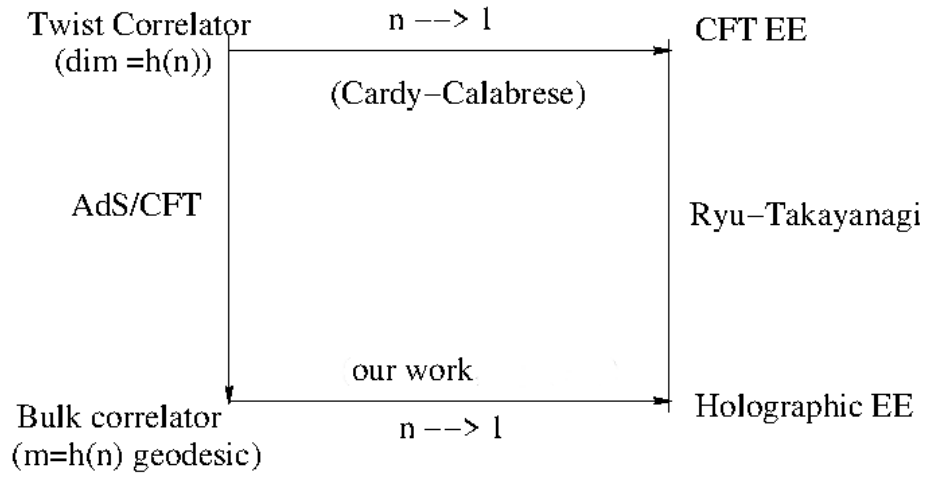

Figure 2.3: A sketch of the 'proof' of the Ryu-Takayanagi formula. The use of AdS/CFT map in the left vertical arrow is justified in the limit of $n = 1 + \epsilon$ (see text).

More precisely the ERE, from CFT, is given by

$$S^{(n)}_{[u,v]} = \frac{1}{1-n} \log\langle \phi_+(u)\phi_-(v)\rangle \tag{2.38}$$

We will now show how in a double scaling limit fixed, the expression 2.38 reduces to the Ryu-Takayanagi expression 2.36 through more or less standard AdS/CFT arguments.

Our strategy of computing 2.38 would be to compute the CFT two-point function holographically. We need to take the limit $c \to \infty$ to ensure semiclassical gravity. The CFT two-point function will be given in terms of a bulk propagator of a dual scalar field whose mass m (see the paragraph around 2.41 for subtle assumptions involved in the existence of such dual scalar fields), by the standard mass-dimension formula for large c, will be $m = h$. The bulk propagator between two points, on the other hand, is given in terms of the geodesic length of a particle of mass m connecting the two points. Using these results, the CFT two-point function in 2.38 boils down to

$$\lim_{c\to\infty} \langle \phi_+(u)\phi_-(v)\rangle \xrightarrow{AdS_3/CFT_2} e^{-2h\,\mathcal{L}(\gamma_{[u,v]})} \tag{2.39}$$

where $\mathcal{L}(\gamma_{[u,v]})$ is the length of the geodesic, in the BTZ geometry, connecting the two boundary points u and v. Using this and 2.37, the holographic entanglement Renyi entropy 2.38 reduces to

$$S^{(n)}_{[u,v]} = \frac{2h\,\mathcal{L}(\gamma_{[u,v]})}{n-1} = \frac{\mathcal{L}(\gamma_{[u,v]})}{8G_N}\,(1+1/n) \tag{2.40}$$

Taking the $n \to 1$ limit, we recover the formula prescribed by Ryu and Takayanagi (2.36).

The steps mentioned in the above 'proof' are symbolically represented in the 'commutative diagram' in Fig 2.3.

The importance of double scaling: In order to have a semiclassical gravity dual, we must take the limit $c \to \infty$. Now, the conventional relation between two-point functions of CFT primary fields and two-point functions of the corresponding bulk duals assumes that dimensions of the CFT fields do not scale with the central charge (this ensures the use of linear response under deformation of the CFT by these fields). This assumption appears to be, *a priori*, violated by the twist operators with scaling dimensions 2.37. However, we should recall that eventually we are interested in the entanglement entropy which involves taking the limit $n \to 1$. What we propose here is that we should take a judicious combination of the $c \to \infty$ and $n \to 1$ limits; to be precise, let us define the following double scaling limit

$$c \to \infty, n \to 1, c(n-1) = \text{fixed} \tag{2.41}$$

It is easy to see that in this limit the dimension h of the twist operator remains finite; hence computation of its two-point function by the method described above should be justified. In terms of the commutative diagram Fig. 2.3, the above remarks justify the use of AdS/CFT in the left vertical arrow for $n = 1 + \epsilon$.

A remark: it would be interesting to understand the connection of the above argument with that of Lewkowycz and Maldacena in [165]. If one took the $c \to \infty$ limit without the concurrent $n \to 1$, the bottom left of the commutative diagram in Fig. 2.3 would

be represented by the back-reacted conical geometry sourced by the world-line of the very massive quantum of the scalar field described above [94]; this is, at least qualitatively, similar to the picture of [165]. However, in view of the above discussion, it appears that in the double scaling limit described above, the bulk partition function with the conical geometry is given in terms of a propagator of the scalar particle in the undeformed geometry. We hope to come back to this interesting issue in the future.

2.3.2 Conclusion of this section

In the light of our arguments above, the holographic computation and its agreement with results of Section 2.2 become very transparent. In fact, to reproduce the CFT results now, we only need to know the length of a massive geodesic (with mass equal to h) between two points at the boundary of the spinning BTZ background. This length was found in [157] (formula (34))[14]. Using it in our algorithm precisely reproduces the CFT two point function from bulk:

$$\langle \phi^+(z_1,\bar{z}_1)\phi^-(z_2,\bar{z}_2)\rangle = \left(\frac{\beta_+}{\pi\,\epsilon}\sinh\frac{\pi\,l}{\beta_+}\right)^{-2h}\left(\frac{\beta_-}{\pi\,\epsilon}\sinh\frac{\pi\,\bar{l}}{\beta_-}\right)^{-2\bar{h}} \tag{2.42}$$

Since the CFT two-point function itself is reproduced, we get the same entanglement entropy as in the CFT.

For two finite intervals (which appear here for the thermofield double) we use the same arguments since the four point correlator factorizes into a product of two-point functions (see also [135]), which are then computed using the bulk propagator, as above. Similarly, the holographic EE for the pure B-state is just the half of the full space answer, as found earlier in the $\mathbf{\Omega} = 0$ case in [138]).

We have thus holographically derived 2.23 and 2.32 and hence holographically proved 2.3 for the case with non-zero angular momentum.

[14] see also [169] for more discussion on the geodesic length and AdS/CFT correlators

2.4 EE for a charged state: CFT

In this section, we will suppose that the CFT has a global $U(1)$ charge, and that the initial state has a non-zero value of this charge. For simplicity, we will first consider the case of zero angular momentum. In this case, the counterpart of 2.5 will be given by

$$|\psi\rangle = C \sum_i \exp[-\beta(E_i - \mu Q_i)/2] \, |i\rangle \otimes |i\rangle \tag{2.43}$$

The $U(1)$ symmetry implies that the CFT has a $U(1)$ Kac-Moody algebra

$$J(z)J(0) = k/(2z^2) + \text{regular terms} \tag{2.44}$$

plus its antiholomorphic counterpart. The Kac-Moody currents have the usual OPE with the stress tensor $T_{zz}, \bar{T}_{\bar{z}\bar{z}}$.

It is well-known, e.g. in the context of $\mathcal{N} = 2$ superconformal field theories, that the Kac-Moody and Virasoro algebras admit an automorphism called "spectral flow". By choosing a flow parameter $\eta = \mu/2$, (using the conventions of [161], Eq. (2.7)) we find the following expression for the automorphism

$$L_0 \to L_0^{(\mu)} = L_0 - \frac{\mu}{k} Q/2 + \frac{\mu^2}{4k}, \; Q \to Q^{(\mu)} = Q - \mu/k \tag{2.45}$$

where k is the level of the U(1) Kac-Moody algebra, defined in 2.44. Although it is perhaps best studied in the context of $\mathcal{N} = 2$ superconformal theories, the phenomenon of spectral flow is very generic; it exists for simple systems such as free massless charged fermions (see Section 2.9.1) for which half-integral spectral flows connect the NS and R sectors; indeed in [120] arguments have been presented for its appearance under rather general circumstances.

With this proviso, we will assume that the charged models we have possess a spectral flow. It is easy, then, to see that the CFT calculations in previous sections can be simply

generalized by using the unitary transformation implementing the spectral flow. For example, consider the Renyi entropy for the CFT on the plane which has the generic form

$$S^{(n)}_{Renyi} = Z_n/Z_1^n \tag{2.46}$$

where Z_n is a partition function of an appropriate n-sheeted surface and Z_1 is the partition function on the plane. Now note that, by spectral flow (using $H = 2L_0$ for $J = 0$),

$$\mathrm{Tr}\exp[-\beta(H - \mu Q + k\mu^2/2)] = \mathrm{Tr}\exp[-\beta H], \tag{2.47}$$

which trivially leads to

$$\mathrm{Tr}\exp[-\beta(H - \mu Q)] = \mathrm{Tr}\exp[-\beta(H - \mu^2/4k)] \tag{2.48}$$

Thus, the effect of adding the μQ term is equivalent, in the partition function and hence in 5.27, to the universal shift 2.48 to the Hamiltonian. Using this line of reasoning, it is easy to show that the time-dependent EE is given by applying this shift to the energy E in the expression for s_{eqm}. The generalization to non-zero J is straightforward, in that the same shift again applies to the energy E. Using this shift to 2.23, and the relation between μ and Q as in Section 2.9.1 (this relation is also discussed in [120, 161]), we now get the general result for the dynamical EE for non-zero E, J and Q

$$\begin{aligned} S_{\mathrm{ent}}(t, l|\psi) &= \begin{cases} \frac{t}{2}\, s_{\mathrm{eqm}}(E, J, Q) + S_{\mathrm{div}}, & t \le l/2 \\ l\, s_{\mathrm{eqm}}(E, J, Q) + S_{\mathrm{div}}, & t > l/2 \end{cases} \\ s_{\mathrm{eqm}} &= \sqrt{\frac{\pi c}{6}(E + J - \frac{\pi}{2k}Q^2)} + \sqrt{\frac{\pi c}{6}(E - J - \frac{\pi}{2k}Q^2)} \end{aligned} \tag{2.49}$$

The dynamical EE for the pure state and single CFT with non-zero Q follows similarly and it is given by half of the above result for the thermofield double.

We have thus derived the form of the dynamical EE, 2.3, for arbitrary E, J, Q.

2.5 Holographic EE with charge: BTZ plus CS U(1)

The bulk dual of the above CFT has been described in various places; in particular, we will follow the account given in [161]. The bulk dual consists of AdS gravity plus a bulk $U(1)$ CS gauge field. The metric is given, as in Sec 2.3, by a spinning black hole 2.33; in addition, there is a bulk gauge field solution given by the flat connection

$$A = \frac{\mu}{k}(dz + d\bar{z}) \tag{2.50}$$

Before proceeding, we now encounter an obvious puzzle.

2.5.1 A puzzle

In the previous section (Section 2.4) we found that the entropy density clearly depends on the charge Q. The grand canonical expression of such an entropy density is, therefore, expected to be of the form $s(\beta, \mathbf{\Omega}, \mu)$. In the bulk dual, as we just mentioned, μ appears only in the gauge field solution 2.50 and not in the metric which retains the $\mu = 0$ form, 2.33. The Ryu-Takayanagi prescription, therefore, will give the time-dependent EE as in the uncharged case. In particular, we will again obtain 2.23 and 2.32. This clearly appears to contradict 2.49 which we derived in the CFT.

Indeed, rather than for the EE, one could ask the same question about the BH entropy. By the black hole area law,

$$s = s(\beta) = \pi c/(3\beta(1 - \mathbf{\Omega}^2)) \tag{2.51}$$

which is clearly independent of the chemical potential μ for the charge. Indeed, in terms of the microcanonical ensemble, the above entropy density precisely agrees with 2.23. The puzzle is, how can we get the entropy density in 2.49 from gravity?

The resolution of this puzzle can be described in two equivalent ways, one in the language of the microcanonical ensemble and the second in the language of the (equivalent) grand canonical ensemble.

- 'Microcanonical' resolution:

  Although the U(1) CS action in the bulk is topological and hence does not couple to the metric, it has a boundary term of the form A^2 (see, e.g. [161]). This leads to an additional contribution to T_{zz} at the boundary, resulting in the following shift

  $$L_0 = L_{0,\text{bulk}} + Q^2/(4k),\ \bar{L}_0 = \bar{L}_{0,\text{bulk}} + Q^2/(4k), \tag{2.52}$$

  This shift, in fact, is the bulk equivalent of 2.48. See also Sec 2.6 for another application of this shift.

- 'Grand Canonical' resolution:

  The microcanonical expression for the entropy density in 2.49 can be converted into the grand canonical form using the formulae in Section 2.9.1. Surprisingly, from that expression, the μ-dependence drops out, leaving the expression 2.51! The temperature and the two 'chemical potentials' $\mathbf{\Omega}, \mu$ are of course the same in the CFT and in the AdS dual; hence we get agreement between the bulk and boundary expressions.

Summary We have thus proved 2.3 holographically in the presence of both angular momentum and charge.

2.5.2 Higher Spin

It is natural to speculate how to extend the above calculations to the case of further additional charges. A natural setting for this is to consider higher spin black hole backgrounds whose CFT dual corresponds to coset models [119] (this speculation was made earlier in [179]). There exist limits of the parameter space of this duality, which are described by free fermions which describe a particularly simple form of an integrable CFT. A similar integrable system of free fermions was recently discussed in [179] where a version of 2.2 was found to be true in the framework of the generalized Gibbs ensemble, and it was speculated there that the equilibrium configuration of the Gaberdiel-Gopakumar free fermions could be given by the higher spin black holes. This makes it rather natural to conjecture that 2.4 should be true in this case, where the bulk dual geometry should be that of a higher spin black hole. See the most recent progress in this direction [17, 93].

2.6 Universal limits

By now, there is a lot of evidence that in the limit of a small entangling region[15] A, EE obeys the analogue of the first law of thermodynamics [9, 42, 200, 240]

$$\Delta E_A = T_{ent}\, \Delta S_A \tag{2.53}$$

Here, the increase of energy in an interval $A = l$ is computed by integrating the holographic energy-momentum tensor T_{tt} over the entangling interval, ΔS_A is a leading-l difference between the EE computed in an excited state and that in the vacuum, and T_{ent} is a universal constant that depends on the number of dimensions. More explicitly

$$\Delta E_A = \int_{A=l} dx\, T_{tt} = \frac{MRl}{16\pi G_N} \tag{2.54}$$

[15] Or in the limit of $\beta \to \infty$

where R is the radius of asymptotically AdS_3 background with time component of the metric given by $f(z)^{-1} \sim 1 + Mz^2$.

For spinning BTZ solution (2.33), the increase EE of a single interval of length l [149] is given by

$$\Delta S_l = \frac{c}{6} \log \left(\frac{\beta_+ \beta_-}{\pi^2 \epsilon^2} \sinh \frac{\pi l}{\beta_+} \sinh \frac{\pi l}{\beta_-} \right) - \frac{c}{3} \log \frac{l}{\epsilon} \sim \frac{c\pi^2 (1+\Omega^2) T^2 \, l^2}{18(1-\Omega^2)^2} \tag{2.55}$$

Using the relation between the mass and the temperature

$$M = (2\pi T)^2 \frac{1+\Omega^2}{(1-\Omega^2)^2} \tag{2.56}$$

the first law relation for EE becomes

$$\Delta E_l = \frac{3}{\pi l} \Delta S_l \tag{2.57}$$

in agreement with [42].

On the other hand, in the limit of large l or large temperature T, the EE reaches the extensive form given by the thermal entropy of the system (see the review [61])

$$S_l \approx l \, s_{\text{eqm}}(\beta) \tag{2.58}$$

For spinning BTZ, s_{eqm} can be read off from 2.23. Thus,

$$S_l \approx \frac{c\pi \, l}{3\beta(1-\Omega^2)} \tag{2.59}$$

The result depends only on the central charge of the CFT and on β and $\mathbf{\Omega}$, and is, therefore, a universal limiting value.

Let us now look how the universal limits incorporate the presence of the U(1) CS fields. As explained in the previous section, U(1) gauge fields give an additional boundary contribution to the energy-momentum tensor

$$T_{tt} = T_{tt}^{\text{grav}} + T_{tt}^{\text{gauge}} = \frac{MR}{16\pi G_N} + \frac{\mu^2}{2\pi} = \frac{\pi c}{6\beta^2} + \frac{\mu^2}{4\pi k} \equiv E_{\text{bulk}} + \frac{\mu^2}{4\pi k} \tag{2.60}$$

This is consistent with (5.4) noting $T_{tt} = L_0/\pi$. This way, using the spectral flow argument, we have, as in 2.52

$$E_{\text{bulk}} = E_{\text{bdry}} - \frac{\mu^2}{4\pi k} \tag{2.61}$$

and the first law-like relation remains the same.

The value of the thermal entropy at which EE saturates can be expressed in terms of microcanonical energy density E and potential μ. However, in the grand canonical ensemble it is only a function of β that matches the holographic prescription that is"blind" to the gauge fields, as we noted in the previous section.

2.7 Relation with quantum ergodicity

The idea of ergodicity is that given sufficient time, the "time average of various properties of a system", evolving from some initial state $\mathcal{S}_0$ can be equated to an "ensemble average of those properties", where the ensemble is constructed out of all possible states $\mathcal{S}$ of the system which have the same conserved charges as $\mathcal{S}_0$. In the classical version, the initial state is a point in the phase space; ergodicity says that under dynamical evolution the point moves "democratically" in the submanifold M of the phase space, allowed by conservation laws, so that the time average of a phase space function $f(q,p)$ can be equated to an average of f taken over M with uniform weight. In quantum mechanics, under the usual conservation

law of energy, the statement boils down to (see, e.g., the review in [209])

$$(1/T)\int_0^T dt\ \mathrm{Tr}\ \left(\rho_{\rm pure}(t)\ O\right) \xrightarrow{T\to\infty} \mathrm{Tr}\left(\rho_{\rm micro}\ O\right), \quad \rho_{\rm pure} = |\psi\rangle\langle\psi|,$$
$$\rho_{\rm micro} = \frac{1}{N}\sum_{i=1}^{N} |i\rangle\langle i| \approx \rho_{\rm thermal} = \frac{1}{Z}\exp[-\beta H] \tag{2.62}$$

Sometimes an alternative statement (Eq. 2.2) is made [209]

$$\mathrm{Tr}\left(\rho_{\rm pure}\ O\right) \xrightarrow{t\to\infty} \mathrm{Tr}\left(\rho_{\rm thermal}\ O\right) \tag{2.63}$$

with respect to a certain class of "macroscopic" observables, for which the time averaging in 2.62 is not necessary. Let us now consider a partition $A \cup B$ of space, say for quantum field theory, or for spins on a lattice. Consider a basis of states $|i_A\rangle|n_B\rangle$ where the states $|i_A\rangle$ are supported entirely on A, and the states $|n_B\rangle$ are supported entirely on B (it could consist of spins in A and B. Let us consider the projection operator $P_B = \sum_n |n_B\rangle\langle n_B|$ onto the states of B. To make connection with the discussion above, we choose $O = P_B\ |i_A\rangle\langle j_A|$ in 2.2, assuming that this is an appropriate "macroscopic" operator. Eq. 2.2 then gives us the following limiting value of the matrix element of the reduced density matrix $\rho_A = \mathrm{Tr}(P_B\ \rho_{\rm pure})$

$$\langle i_A|\rho_A|j_A\rangle \xrightarrow{t\to\infty} \langle i_A|\rho_{A,\beta}|j_A\rangle, \qquad \rho_{A,\beta} \equiv \mathrm{Tr}\left(P_B\ \exp[-\beta H]/Z\right) \tag{2.64}$$

The asymptotic value of the time-dependent EE, then would be

$$S_{\rm EE} \xrightarrow{t\to\infty} S[\rho_{A,\beta}] \equiv -\mathrm{Tr}\left(\rho_{A,\beta}\log\rho_{A,\beta}\right) \tag{2.65}$$

The latter entropy measures the von Neumann entropy of the reduced density matrix *in an overall mixed state*. Now we expect that for a large enough $l = l_A$

$$S[\rho_{A,\beta}]/l = s(\beta) \tag{2.66}$$

where $s(\beta)$ is the thermal entropy density at an inverse temperature β. In Section 2.9.2 we present a proof of this statement using a discrete system and assuming the equivalence between microcanonical and grand canonical ensembles. Additionally, in Section 2.8 we explicitly verify 2.66 in the case of a massive, charged scalar field.

We have therefore proved

$$S_{\text{EE}} \xrightarrow{t\to\infty} l\, s \tag{2.67}$$

This is the same as 2.1, where a time scale of saturation is set by l.

The proof of saturation outlined above holds in principle for any field theory and in any number of dimensions. Hence, we expect the behaviour 2.67 to be valid quite generally.

For integrable systems and the generalized Gibbs ensemble, the story of quantum ergodicity is less developed, although we still expect an equation of the form 2.63 to hold for a suitable class of "macroscopic" observables (see [209]). [16]

2.8 Non-CFT: EE for charged, massive scalar field

In this section, we consider an *a priori* calculation of EE for a charged, massive scalar field. The motivation for this calculation is to have an additional evidence for 2.66. Our CFT calculations for the saturation value of the time-dependent EE already provide indirect evidence for this formula. However, in this section we consider a non-conformal system and perform a direct computation of the EE using the methods of [144].

[16] These observables typically display some non-locality; however, see [76] for the behaviour of local observables.

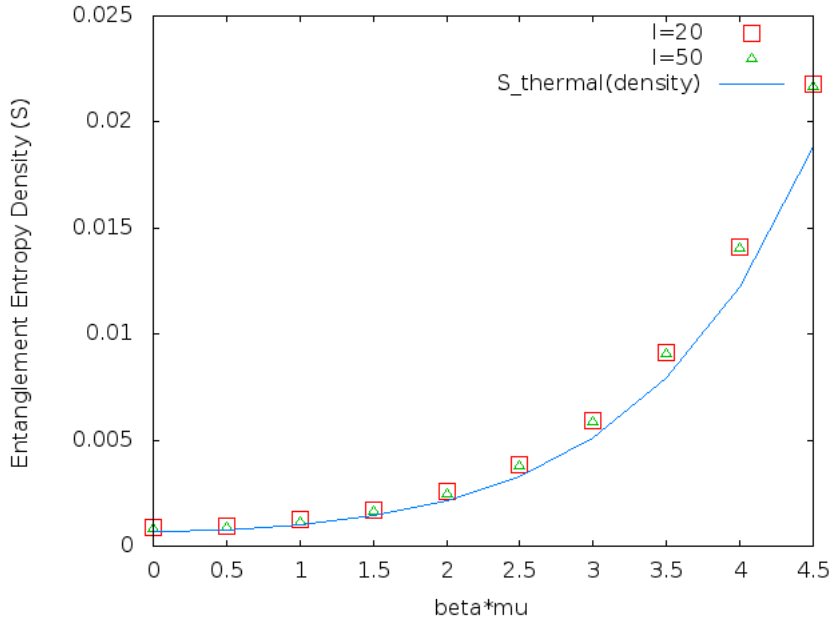

Figure 2.4: Plot of $S[\rho_{A,\beta}]/l$ (the LHS of 2.66 vs $\beta\mu$, for $\beta m = 10$. The plot marked with squares has $l/\beta = 10$; the plot marked with triangles has $l/\beta = 25$. The solid line corresponds to the RHS of 2.66, viz. the thermal entropy density, which is obtained using standard formulae, and Mathematica. It is clear that 2.66 holds to a good accuracy. The agreement is better for small $\beta\mu$ than for large $\beta\mu$; however, this could be due to some numerical instability.

The charged scalar field is described by a Hamiltonian

$$H = \int dx \left(\pi^\dagger \pi + (\nabla\phi)^\dagger(\nabla\phi) + m^2\phi^\dagger\phi\right) \tag{2.68}$$

and a conserved U(1) charge

$$Q = i\int dx(\pi^\dagger\phi - \phi^\dagger\pi) \tag{2.69}$$

We will suppose that the full system (with spatial partition A and its complement B) is in a grand canonical ensemble

$$\rho_{\text{total}} = \frac{\exp[-\beta(H-\mu Q)]}{\text{Tr}[\exp[-\beta(H-\mu Q)]]} \tag{2.70}$$

We are interested in computing the reduced density matrix $\rho_A = \mathrm{Tr}_B \rho_{\text{total}}$, and the EE $S_A = -\mathrm{Tr}\rho_A \log \rho_A$. We will proceed using a generalization of the formalism described in [144], and describe only the essentially new features. Note that formalism in [144] permits a straightforward generalization from the case of a single scalar ϕ to multiple flavours $\phi_a, a = 1, 2, ..., N_f$, with the C-matrix generalized to

$$(C^2)^{ab}_{ij} = \sum_{k=1}^{n} < \phi^a_i \phi^c_k >< \pi^c_k \pi^b_j > \tag{2.71}$$

The EE is given by (using the notation from 2.65)

$$S[\rho_{A,\beta}] = \mathrm{Tr}[(C + 1/2)\log(C + 1/2) - (C - 1/2)\log(C - 1/2)] \tag{2.72}$$

where the trace is now over both the $\{i, j\}$ and $\{a, b\}$ indices. For the free complex scalar at hand, $N_f = 2$, and $C^{ab}_{ij} = C_{ij}\delta^{ab}$. We compute C^2 using 2.71 and the following ingredients:

$$\begin{aligned}
< \phi_j \phi^\dagger_k > &= \frac{1}{2N} \sum_{a=0}^{N-1} \frac{1}{2\epsilon\omega_i} [\coth(\frac{\omega_i + \mu}{2T}) + \coth(\frac{\omega_i - \mu}{2T})] \cos[\frac{2\pi}{N} a(j-k)] \\
< \pi_j \pi^\dagger_k > &= \frac{1}{2N} \sum_{a=0}^{N-1} \frac{\epsilon\omega_i}{2} [\coth(\frac{\omega_i + \mu}{2T}) + \coth(\frac{\omega_i - \mu}{2T})] \cos[\frac{2\pi}{N} a(j-k)] \\
< \pi_j \pi^\dagger_k > &=< \pi^\dagger_j \pi_k >, \quad < \phi_j \phi^\dagger_k > =< \phi^\dagger_j \phi_k >
\end{aligned} \tag{2.73}$$

The computation of 2.72 is performed numerically. We reproduce a representative plot in Fig. 2.4.

2.9 Appendix

2.9.1 Microcanonical vs grand canonical quantities

Consider a grand canonical ensemble given by the following density matrix and partition function

$$\rho = (1/Z)\exp[-\beta(H + \mathbf{\Omega}P - \mu Q)],\ Z = \mathrm{T}r\exp[-\beta(H + \mathbf{\Omega}P - \mu Q)] \tag{2.74}$$

The partition function can be written as

$$Z \equiv \exp[-\beta G] = \sum_{E,J,Q} \exp[S(E,Q,J) - \beta(E + \mathbf{\Omega}P - \mu Q)] \tag{2.75}$$

If the summand in the last function has a single sharp maximum around a unique set of values E, P, Q, the distribution essentially becomes equivalent to that of a microcanonical ensemble, where we have

$$\partial S/\partial E = \beta, \qquad \partial S/\partial J = -\beta\mathbf{\Omega}, \qquad \partial S/\partial Q = -\beta\mu \tag{2.76}$$

This gives us the grand canonical parameters in terms of the microcanonical ones. The converse relations are also easy to derive:

$$\partial(\beta G)/\partial\beta = E - \mathbf{\Omega}J - \mu Q,\ \ -1/\beta\ \partial(\beta G)/\partial\mathbf{\Omega} = J,\ \ -1/\beta\ \partial(\beta G)/\partial\mu = Q \tag{2.77}$$

This gives us the following relation

$$S = \beta^2 \partial G/\partial\beta \tag{2.78}$$

Using the above relations, we can prove that if the microcanonical entropy density is given by

$$S = \sqrt{aE + bJ - dQ^2} + \sqrt{aE - bJ - dQ^2} \tag{2.79}$$

the grand canonical expression for the entropy is

$$s = \frac{2a}{\beta(1 - a^2\mathbf{\Omega}^2/b^2)} \tag{2.80}$$

Surprisingly, $S(\beta, \mathbf{\Omega}, \mu) = S(\beta, \mathbf{\Omega})$, which is independent of β.

Notation: In the body of the chapter, we have used the notations E, J, Q as the energy *density*, J as the angular momentum *density* and Q as the charge *density* whereas s denotes the entropy density. Equations (2.79) and (2.80) hold for the densities with trivial modifications.

Free massless charged fermion in 1+1

We consider free massless charged fermions in 1+1 dimension, at a temperature $1/\beta$ and chemical potential μ. Explicit calculation gives the following Gibbs free energy

$$g(\beta, \mu) = -\left(\frac{\pi}{6\beta^2} + \frac{\mu^2}{2\pi}\right) \tag{2.81}$$

The energy density e and the charge density q are given by

$$e = \frac{\pi}{6\beta^2} + \frac{\mu^2}{2\pi}, \; q = \frac{\mu}{\pi} \tag{2.82}$$

For this system the grand canonical entropy density is given by

$$s(\beta, \mu) = s(\beta) = \frac{\pi}{3\beta} \tag{2.83}$$

and the microcanonical entropy density is given by

$$s(e,q) = \sqrt{\frac{2\pi}{3}(e - \frac{\pi}{2}q^2)} \tag{2.84}$$

2.9.2 Proof of 2.66

Consider a basis of the Hilbert space $\{|i,A\rangle, |k,B\rangle\}, i = 1, ..., N_A; k = 1, ...N_B$, where N_A, N_B denote the number of independent states $|i,A\rangle$ belonging to the partition A, and similarly for N_B. A microcanonical density matrix $\rho_{\rm mc}$ is given by

$$\rho_{\rm mc} = \frac{1}{N_A N_B} \sum_{i,A;k,B} |i,A\rangle|k,B\rangle\langle i,A|\langle k,B\rangle \tag{2.85}$$

By tracing over the B states, we get

$$\rho_{A,mc} \equiv {\rm Tr}_B \rho_{\rm mc} = \frac{1}{N_A} \sum_{i,A} |i,A\rangle\langle i,A|$$

The von Neumann entropy of this density matrix is given by

$$S_A = \log N_A$$

Now imagine that our system is a lattice of n-level 'spins' ($n = 2$ is Ising), and that there are l_A spins in the partition A; then

$$S_A = l_A \log n$$

Now we can easily show that the von Neumann entropy of 2.85 is

$$S = (l_A + l_B) \log n$$

Hence the entropy density is

$$s = \log n$$

Now by denoting l_A as l, and assuming the equivalence between the microcanonical ensemble in 2.85 and the canonical ensemble as in 2.64 we obtain 2.66.

Chapter 3

The inside/outs of AdS_3/CFT_2 [1]

3.1 Introduction and Summary

It has been a matter of lively debate whether the standard description of a large black hole with a smooth horizon is quantum mechanically consistent, and is, in fact, consistent with AdS/CFT. While the firewall hypothesis [13, 16] [2] argues against the validity of the standard description, Maldacena and Susskind [175] have suggested that the region inside the horizon is a geometric representation of quantum mechanical entanglement. Both the above proposals, and related issues, are discussed in a number of papers; for a partial list, related to the discussion in this chapter, see [13, 16, 22, 27, 185, 204, 205, 225, 226, 235]. The proposal of [175], summarized by the symbolic equation ER = EPR, [3] is illustrated by the eternal black hole geometry which is dual to the thermofield state [177]. [4] It has been argued in several papers (see, e.g., [27, 185]) that although the proposal holds for this illustrative

[1] The contents of this chapter have partial overlap with the thesis work of Sorokhaibam Nilakash Singh. The conclusions arrived at are results of joint effort.

[2] See also [48].

[3] Einstein-Rosen (wormhole) = Einstein-Podolsky-Rosen (entangled state).

[4] See [138] for an AdS/CFT check on the dynamical entanglement entropy which involves the wormhole region, and [67] for generalization to include angular momentum and charge.

case, it does not hold in general. One of the objectives of the present work is to explicitly construct a general class of two-sided geometries [5] which represent entangled CFT's.

A useful approach to construct the geometric dual to a CFT state is by using a Fefferman-Graham (FG) expansion, with boundary data provided by the CFT state. To begin with, let us consider the case of a single CFT. Since we are primarily interested in the metric, let us focus, for simplicity, on states in which only the stress tensor is excited. The dual geometry would then be given by the solution to the appropriate Einstein equations subject to the boundary data provided by the stress tensor. This approach has been particularly fruitful in the context of the AdS_3/CFT_2 duality where the Fefferman-Graham expansion has been shown, for pure gravity, to terminate [30] , yielding the following exact metric [6]

$$ds^2 = \frac{dz^2}{z^2} - dx_+ dx_- \left(\frac{1}{z^2} + z^2 \frac{L(x_+)\bar{L}(x_-)}{16}\right) + \frac{1}{4}\left(L(x_+)dx_+^2 + \bar{L}(x_-)dx_-^2\right) \tag{3.1}$$

The boundary data ($z \to 0$) is represented by the following holographic stress tensors (we choose $-\Lambda = 1/\ell^2 = 1$)

$$8\pi G_3 T_{++}(x_+) = \frac{L(x_+)}{4},\ 8\pi G_3 T_{--}(x_-) = \frac{\bar{L}(x_-)}{4} \tag{3.2}$$

The above metric becomes singular at the horizon

$$z = z_0 \equiv 2\left(L(x_+)\bar{L}(x_-)\right)^{-1/4}, \tag{3.3}$$

and therefore the metric 5.57, describes only an exterior geometry. [7]

How does one carry out such a construction with two boundaries, with two sets of boundary data? Indeed, it is not even clear, *a priori*, whether simultaneously specifying

[5] By *two-sided*, we mean geometries which have two asymptotically AdS regions.

[6] In 5.57, $x_\pm = t \pm x$, with $x \in \mathbb{R}$. For $L, \bar{L}$ constant, this corresponds to the BTZ black string.

[7] The inverse metric g^{MN} blows up at the horizon, as in case of Schwarzschild geometry. However, unlike there, here the other region $z > z_0$ does *not* represent the region behind the horizon; rather it gives a second coordinatization of the exterior region again. In this chapter, we will use a different set of coordinate systems to probe the interior and a second exterior region.

two independent pieces of boundary data can always lead to a consistent solution in the bulk (this question has been raised in several recent papers, e.g. see [235]). A possible approach to this problem is suggested by the fact that the eternal BTZ solution, which contains 5.57 with constant stress tensors, admits a maximal extension with two exteriors, which are joined to an interior region across a smooth horizon. The maximal extension is constructed by transforming, e.g., to various Eddington-Finkelstein (EF) coordinate patches (described in Appendix 3.9.1). A naive generalization of such a procedure in case of variable $L, \bar{L}$, of transforming the metric 5.57 to EF type coordinates, does not seem to work since it leads to a complex metric in the interior region [8]. A second approach could be to solve Einstein's equations, by using the constant $L, \bar{L}$ (eternal BTZ) solution as a starting point and, incorporate the effect of variable $L, \bar{L}$ perturbatively, either in a derivative expansion or an amplitude expansion. While this method may indeed work, at the face of it, it is far from clear how the variation in $L, \bar{L}$ can be chosen to be different at the two boundaries.

In this chapter, we will use the method of solution generating diffeomorphisms (SGD). In gauge theory terms, these are asymptotically nontrivial gauge transformations which correspond to global charge rotations; the use of these objects was introduced in [123, 214, 236], and used crucially by Brown and Henneaux [50] to generate 'Virasoro charges' through asymptotically nontrivial SGDs that reduced at the AdS boundary to conformal transformations. (We discuss these in more detail in Section 3.2). Brown and Henneaux had discussed only the asymptotic form of the SGDs. We apply two independent, exact Brown-Henneaux SGDs [9] to different coordinate patches of the eternal BTZ geometry, yielding a black hole spacetime with two completely general stress tensors on the two boundaries. In other words, our strategy for solving the boundary value problem can be summarized as: given arbitrary boundary data in terms of stress tensors $T_R, \bar{T}_R$, and $T_L, \bar{T}_L$, we (i) find the two specific sets of conformal transformations (which we are going to call G_+, G_- and

[8] Such a coordinate transformation has been discussed in [129] in an asymptotic series near the boundary.

[9] It has been shown by Roberts [218] that the exterior metric 5.57 can be obtained by an exact Brown-Henneaux type diffeomorphism applied to the Poincare metric. See Appendix 5.56 for a discussion on this and a different, new, transformation which is closer to the ones we use in this chapter.

H_+, H_-) which, when acting on a constant stress tensor, gives rise to these stress tensors, (ii) find the SGD's which reduce to these conformal transformations and (iii) apply the SGD's to the eternal BTZ metric.

This solves the boundary value problem we posed above.

The results in this chapter are organized as follows:

(1) The new solutions: In Section 3.2 we describe the explicit *solution generating diffeomorphisms* (SGDs) and construct the resulting two-sided black hole geometries. The diffeomorphisms reduce to conformal transformations at each boundary, parameterized by functions $G_\pm$ on the right and $H_\pm$ on the left. The SGD parameterized by $G_\pm$ is applied to the Eddington-Finkelstein coordinate chart EF1 (which covers the right exterior and the black hole interior, see Figure 3.1) and to EF4 (right exterior + white hole interior), whereas the SGD parameterized by $H_\pm$ is applied to the Eddington-Finkelstein coordinate chart EF2 (left exterior + black hole interior) and to EF3 (left exterior + white hole interior). To cover the entire spacetime we also use a Kruskal chart K5 which covers an open neighbourhood of the bifurcate Killing horizon; here we leave the original Kruskal metric unaltered. The effect of the above SGDs is that we have a description of different metric tensors in different charts. In Section 3.2.3 we show that all these can be pieced together to give a single (pseudo-)Riemannian manifold; we prove this by showing that in the pairwise overlap of any two charts $N_1 \cap N_2$ the different metrics constructed above differ only by a trivial diffeomorphism (see the definition 3.2.5); the full metric, specified with the help of the various charts, is schematically represented in Figure 3.3. An important manifestation of the asymptotic nontriviality of the SGDs is to move and warp the infra-red regulator surface (see Figure 3.2); the change in the boundary properties, as found in later sections, can be directly attributed to this.

The new spacetime so constructed inherits the original causal structure, with the event horizon, the bifurcation surface, and the two exterior and interior regions (see also footnotes 10 and 32). The horizon is, therefore, regular by construction. In the new EF coordinates (the *tilded* coordinates) the horizon consists of smoothly undulating surfaces (see Fig 3.4).

(2) The CFT duals: In section 3.3 we use the observation that the SGDs reduce asymptotically to conformal transformations to assert that the CFT duals to our geometries are given by unitary transformations $U_L \otimes U_R$ to the thermofield double state. Since the unitary transformations implement conformal transformations, AdS/CFT implies that CFT correlators in the transformed state are holographically computed by the new spacetime geometry. We posit this as a test of the proposed AdS/CFT correspondence.

(3) The AdS/CFT checks: In section 3.4 we carry out this test for the stress tensor. We compute the holographic stress tensor [28, 227] in the new geometry and show that it exactly matches with the expectation value of the conformally transformed (including the Schwarzian derivative) stress tensor in the thermofield double state. In section 3.5 we compare AdS and CFT results for both $\langle O_L O_R \rangle$ and $\langle O_R O_R \rangle$ types of correlators. The holographic two-point function is found by computing geodesic lengths in the new geometries and we find that it correctly matches with the two-point function of transformed operators. This can be regarded as an evidence for the ER=EPR relation in the presence of probes.

(4) Entanglement entropy: As a further check, in section 3.6 we apply the above result for two-point functions to show that the entanglement entropy EE in CFT matches the holographic EE [149, 220] including when the Ryu-Takayanagi geodesic passes through the wormhole. This constitutes a direct proof of the ER=EPR conjecture for the entire class of geometries constructed in this chapter. We work out the dynamical entanglement entropy in an example (see fig 3.5).

(5) Holographic entropy from horizon: In section 3.7, we make crucial use of the existence of smooth horizons on both sides to compute a holographic entropy along the lines of [43]. We are able to compute the entropy in the CFT by using the Cardy formula and an

adiabatic limit (which allows the use of the 'instantaneous' energy eigenvalues to compute degeneracies); the holographic entropy agrees with this. The entropy turns out to be divergenceless, reflecting the dissipationless nature of 2D CFT. There is, however, a nontrivial local flow of entropy (see fig 3.6).

(6) ER=EPR: In Section 3.8 we discuss some implications of our solutions *vis-a-vis* the ER=EPR relation of Maldacena and Susskind [175]. Our solutions establish an infinite family of quantum states entangling two CFTs which are represented in the bulk by wormhole geometries. We show, in particular, that out of a given set of quantum states we consider, all characterized by the same energy, there are states with low entanglement entropies, which nevertheless are still represented by wormhole geometries; this is in keeping with the picture of geometric entanglement suggested in [175].

3.2 The solutions

In this section we obtain the new solutions by carrying out the procedure outlined in the Introduction. As explained in Section 3.9.1, for constant $L, \bar{L}$, the metric 5.57 represents a BTZ black hole of constant mass and angular momentum 3.82. In that case, one can construct EF coordinates (see Section 3.9.1) to extend the spacetime to include the region behind the horizon and a second exterior. We will, in fact, use five charts to cover the extended geometry (see Fig 3.1).

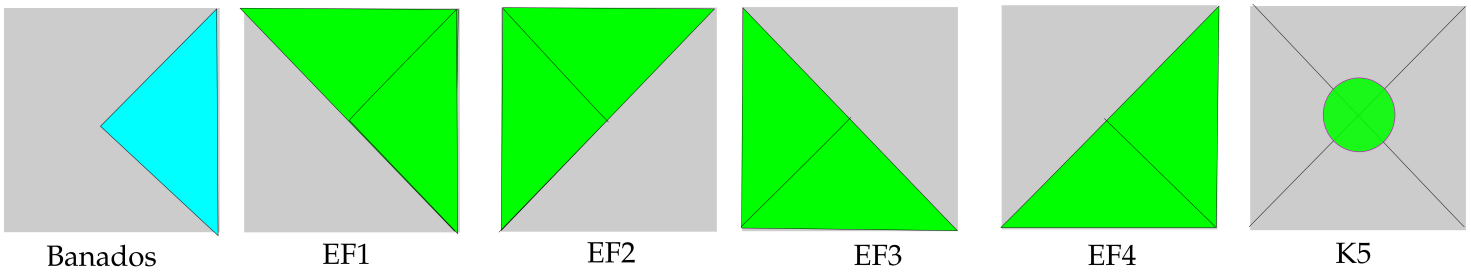

Figure 3.1: The (green parts of) the five figures on the right depict the five coordinate charts used in this chapter to cover the eternal BTZ solution.[10] The coordinate chart K5 is needed to cover the "bifurcation surface" where the past and future horizons meet (it is a point in the Penrose diagram). The leftmost diagram (in blue) represents the coordinate chart used in 5.57. Each of the coordinate charts is shown, for facility of comparison, within a Penrose diagram where the parts not within the chart are shown in gray.

3.2.1 The eternal BTZ geometry

We will now briefly review some properties of the eternal BTZ geometry. The maximal extension of the eternal BTZ geometry, starting from 5.57 is described in detail in Section 3.9.1. We will briefly reproduce some of the formulae relevant to the coordinate system ("EF1") describing the right exterior and the interior. The EF1 coordinates are obtained from the coordinates of 5.57 by the transformations

$$\frac{z}{z_0} = \sqrt{\frac{1}{\lambda_0}\left(\lambda - \sqrt{\lambda^2 - \lambda_0^2}\right)} x_+ \quad = v - \frac{1}{2\sqrt{L}} \log\left(\frac{\lambda - \lambda_0}{\lambda + \lambda_0}\right), \; x_- = w - \frac{1}{2\sqrt{\bar{L}}} \log\left(\frac{\lambda - \lambda_0}{\lambda + \lambda_0}\right)$$

The metric, in these coordinates, becomes

$$ds^2 = \frac{d\lambda^2}{4(\lambda + \lambda_0)^2} + \frac{L}{4} dv^2 + \frac{\bar{L}}{4} dw^2 - \lambda \, dvdw + \frac{\sqrt{L}}{2(\lambda + \lambda_0)} dvd\lambda + \frac{\sqrt{\bar{L}}}{2(\lambda + \lambda_0)} dwd\lambda \qquad (3.4)$$

[10] This is the entire geometry for the non-spinning BTZ; for spinning BTZ solutions, we do not attempt to cover the region beyond the inner horizon, since in this chapter we are interested in the asymptotic properties in the two exteriors mentioned above. See also footnote 32.

The event horizon λ_H, the inner horizon λ_i, and the singularity λ_s are at

$$\lambda_H = \lambda_0 \equiv \frac{\sqrt{L\bar{L}}}{2},\ \lambda_i = -\lambda_0,\ \lambda_s = -\frac{1}{4}(L + \bar{L}) \tag{3.5}$$

Note that for BTZ black holes without angular momentum $\bar{L} = L$ and $\lambda_i = \lambda_s$. The location of the event horizon corresponds to 3.3.

In order to regulate IR divergences coming from $\lambda \to \infty$, we define a cut-off surface Σ_B at a constant large $\lambda = \lambda_{ir}$; the metric 3.4 on Σ_B turns out to be

$$\lambda = \lambda_{ir} = 1/\epsilon^2 \Rightarrow ds^2|_{\Sigma_B} = -(1/\epsilon^2)\ dv\ dw(1 + O(\epsilon^2)) \tag{3.6}$$

By the usual AdS/CFT correspondence the leading term defines the boundary metric (see Section 3.9.3)

$$ds^2_{bdry} = -dv\ dw \tag{3.7}$$

The subleading term in the metric corresponds to the normalizable metric fluctuation, which gives the expectation value of the stress tensor; this is the holographic stress tensor [28], and is given here by

$$8\pi G_3 T_{vv}(x_+) = \frac{L}{4},\ 8\pi G_3 T_{ww}(x_-) = \frac{\bar{L}}{4} \tag{3.8}$$

It is easy to see that we will get the same boundary metric and stress tensor from an analysis of the coordinate chart EF4. It is also straightforward to derive similar results for the left exterior (which represent a state with the same mass and angular momentum) using EF2 and EF3.

3.2.2 Solution generating diffeomorphisms (SGD)

We will now proceed to construct new solutions with arbitrary boundary data at the two boundaries (represented by two arbitrary holographic stress tensors $T_{R,\mu\nu}(x)$ and $T_{L,\mu\nu}(x)$) by applying the method of solution generating diffeomorphisms to the above geometry, as explained in the introduction.

The solution generating diffeomorphisms can be described as follows. Suppose we start with a certain metric $g_{MN}(x)dx^M dx^N$ [11] in a certain coordinate chart $\mathcal{U}_P$ containing a point P. The new metric $\tilde{g}_{MN}$, in this coordinate chart, is given in terms of a diffeomorphism (active coordinate transformation) $f : \tilde{x}^M = \tilde{x}^M(x)$, by the definition

$$g \to \tilde{g} \equiv f^* g : \quad \tilde{g}_{MN}(\tilde{x}) \equiv \frac{\partial x^P}{\partial \tilde{x}^M} \frac{\partial x^Q}{\partial \tilde{x}^N} g_{PQ}(x) \tag{3.9}$$

In the above, f^*g is a standard mathematical notation for the pullback of the metric g under the diffeomorphism f. For diffeomorphisms differing infinitesimally from the identity map: $\tilde{x}^M = x^M - \xi^M(x)$, we, of course, have the familiar relation

$$\delta g_{MN}(x) = D_M \xi_N + D_N \xi_M \tag{3.10}$$

Normally, a diffeomorphism is considered giving rise to a physically indistinguishable solution; this, however, is not true when the diffeomorphism is non-trivial at infinity (this is explained in more detail in Section 3.2.5).

As explained in Section 3.9.1, we use five charts to cover the entire eternal BTZ geometry (see Fig 3.1). These charts are labelled as EF1, EF2, EF3, EF4 and K5. We use a nontrivial diffeomorphism in each of EF1, EF2, EF3 and EF4, which overlap with the boundary and the identity transformation in the Kruskal patch K5.

[11] Notation: $x^M = \{\lambda, x^\mu\}$, $x^\mu = \{v, w\}$.

The metric in the coordinate chart EF1

The diffeomorphism in the EF1 coordinate chart is given by

$$\lambda = \frac{\tilde{\lambda}}{G'_+(\tilde{v})G'_-(\tilde{w})},\ v = G_+(\tilde{v}),\ w = G_-(\tilde{w}) \tag{3.11}$$

The new metric $\tilde{g}_{MN}$, written in terms of $\tilde{x}^M = (\tilde{\lambda}, \tilde{v}, \tilde{w})$, is

$$\begin{aligned}\tilde{g}_{MN}(\tilde{x})d\tilde{x}^M d\tilde{x}^N \equiv ds^2 = \frac{1}{B^2}\Big[&d\tilde{\lambda}^2 + A_+^2 d\tilde{v}^2 + A_-^2 d\tilde{w}^2 + 2A_+ d\tilde{v}d\tilde{\lambda} + 2A_- d\tilde{w}d\tilde{\lambda} \\ &- \tilde{\lambda}\left(B^2 + 2\left(A_+\frac{G''_-(\tilde{w})}{G'_-(\tilde{w})} + A_-\frac{G''_+(\tilde{v})}{G'_+(\tilde{v})} + \tilde{\lambda}\frac{G''_+(\tilde{v})G''_-(\tilde{w})}{G'_+(\tilde{v})G'_-(\tilde{w})}\right)\right)d\tilde{v}d\tilde{w}\Big]\end{aligned} \tag{3.12}$$

where

$$\begin{aligned}A_+ &= \sqrt{L}G'_+(\tilde{v})(\tilde{\lambda} + \tilde{\lambda}_0) - \tilde{\lambda}\frac{G''_+(\tilde{v})}{G'_+(\tilde{v})}, \\ A_- &= \sqrt{\bar{L}}G'_-(\tilde{w})(\tilde{\lambda} + \tilde{\lambda}_0) - \tilde{\lambda}\frac{G''_-(\tilde{w})}{G'_-(\tilde{w})}, \\ B &= 2(\tilde{\lambda} + \tilde{\lambda}_0)\end{aligned}$$

For infinitesimal transformations $G_\pm(x) \equiv x + \epsilon_\pm(x)$, this amounts to an asymptotically nontrivial diffeomorphism ξ^M (see 3.10)[12]

$$\xi_1^v = \epsilon_+(v),\ \xi_1^w = \epsilon_-(w),\ \xi_1^\lambda = -\lambda\left(\epsilon'_+(v) + \epsilon'_-(w)\right) \tag{3.13}$$

The behaviour of the metric 3.12 at a constant large λ surface is given by

$$ds^2 = -\tilde{\lambda}\ d\tilde{v}d\tilde{w}\ (1 + O(1/\tilde{\lambda})) \tag{3.14}$$

[12]The subscript in ξ_1^M refers to the chart EF1.

This, by following arguments similar to the previous case (see Section 3.2.1), identifies the IR cutoff surface as

$$\tilde{\lambda}_{ir} = (1/\epsilon^2) \tag{3.15}$$

and the boundary metric as

$$ds^2_{bdry} = -d\tilde{v}d\tilde{w} \tag{3.16}$$

The subleading term in 3.14, as explored in Section 3.4, gives the holographic stress tensor. We will see there that the subleading term depends on the SGD functions $G_{\pm}$; this feature is what makes the SGD's asymptotically *nontrivial* (see Section 3.2.5 for a more detailed discussion on this).

In terms of the old λ-coordinate, the surface 3.15 is

$$\lambda = 1/(\epsilon^2 G'_+(\tilde{v})G'_-(\tilde{w})) \tag{3.17}$$

Note that this surface is different from 3.6, and is nontrivially warped, as in Figure 3.2. This is another manifestation of the asymptotic non-triviality of the diffeomorphism 3.11, which is responsible for nontrivial transformation of bulk quantities, such as geodesic lengths.

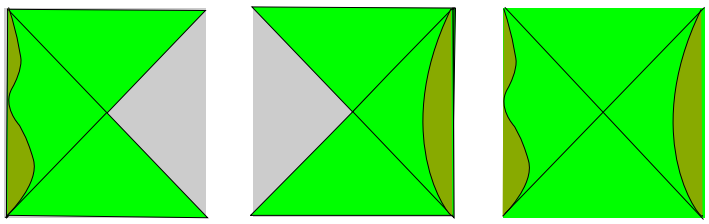

Figure 3.2: This figure shows the IR cut-off 3.15 in the new geometries. The effect of the SGDs, in the old (un-tilded) coordinates, is to deform the IR cut-off surfaces. The surface deformation on the right exterior is given by the change from 3.6 to 3.17; there is a similar surface deformation on the left exterior.

We note that the leading large $\tilde{\lambda}$ behaviour of 3.12 is that of AdS_3

$$ds^2 = \frac{d\tilde{\lambda}^2}{4\tilde{\lambda}^2} - \tilde{\lambda}\ d\tilde{v}\ d\tilde{w} + ... \tag{3.18}$$

As mentioned before, and will be explored in detail in Section 3.4, the subleading terms, represented by the ellipsis ..., are nontrivially different from that of AdS_3.

The metric in the coordinate chart EF2

The diffeomorphism (SGD) used in the coordinate chart EF2 (see Fig 3.1), which is independent of the one above used in EF1, is given by

$$\lambda_1 = \frac{\tilde{\lambda}_1}{H'_+(\tilde{u})H'_-(\tilde{\omega})},\ \ u = H_+(\tilde{u}),\ \ \omega = H_-(\tilde{v}) \tag{3.19}$$

which leads to the metric

$$\begin{aligned} ds^2 = \frac{1}{B^2}\Big[&d\tilde{\lambda}_1^2 + A_+^2 d\tilde{u}^2 + A_-^2 d\tilde{\omega}^2 - 2A_+ d\tilde{u} d\tilde{\lambda}_1 - 2A_- d\tilde{\omega} d\tilde{\lambda}_1 \\ &- \tilde{\lambda}_1\left(B^2 - 2\left(A_+\frac{H''_-(\tilde{\omega})}{H'_-(\tilde{\omega})} + A_-\frac{H''_+(\tilde{u})}{H'_+(\tilde{u})} - \tilde{\lambda}_1\frac{H''_+(\tilde{u})H''_-(\tilde{\omega})}{H'_+(\tilde{u})H'_-(\tilde{\omega})}\right)\right)d\tilde{\omega}d\tilde{u}\Big] \end{aligned} \tag{3.20}$$

where

$$A_+ = \sqrt{L}H'_+(\tilde{u})(\tilde{\lambda}_1 + \tilde{\lambda}_0) + \tilde{\lambda}_1\frac{H''_+(\tilde{u})}{H'_+(\tilde{u})},\ A_- = \sqrt{L}H'_-(\tilde{\omega})(\tilde{\lambda}_1 + \tilde{\lambda}_0) + \tilde{\lambda}_1\frac{H''_-(\tilde{\omega})}{H'_-(\tilde{\omega})},\ B = 2(\tilde{\lambda}_1 + \tilde{\lambda}_0)$$

For infinitesimal transformations $H_\pm(x) = x + \varepsilon_\pm(x)$, this implies a diffeomorphism ξ_2^M where

$$\xi_2^u = -\varepsilon_+(u),\ \xi_2^\omega = -\varepsilon_-(\omega),\ \xi_2^\lambda = -\lambda\left(\varepsilon'_+(u) + \varepsilon'_-(\omega)\right) \tag{3.21}$$

Note, once again, the asymptotic nontriviality of the above diffeomorphism.

3.2.3 The full metric

In a manner similar to the above, we apply the SGD characterized by $G_\pm$ on EF4 (which shares the right exterior with EF1, see Appendix 3.9.1): and the SGD characterized by $H_\pm$ on EF3 (which shares the left exterior with EF2):

$$\begin{aligned}
\text{EF4}: \quad & \lambda = \frac{\tilde{\lambda}}{G'_+(\tilde{u}_1)G'_-(\tilde{\omega}_1)},\ u_1 = G_+(\tilde{u}_1),\ \omega_1 = G_-(\tilde{\omega}_1) \\
& \text{infinitesimally} \quad \left(\xi_4^\lambda, \xi_4^{u_1}, \xi_4^{\omega_1}\right) = \left(-\lambda(\epsilon'_+(u_1) + \epsilon'_-(\omega_1)), \epsilon_+(u_1), \epsilon_-(\omega_1)\right) \\
\text{EF3}: \quad & \lambda = \frac{\tilde{\lambda}_1}{H'_+(\tilde{v}_1)H'_-(\tilde{w}_1)},\ v_1 = H_+(\tilde{v}_1),\ w_1 = H_-(\tilde{w}_1) \\
& \text{infinitesimally} \quad \left(\xi_4^\lambda, \xi_4^{v_1}, \xi_4^{w_1}\right) = \left(-\lambda(\varepsilon'_+(v_1) + \varepsilon'_-(w_1)), \varepsilon_+(v_1), \varepsilon_-(w_1)\right) \qquad (3.22)
\end{aligned}$$

The infinitesimal transformations are similar to those in eqs. 3.13 and 3.21. As mentioned above, we use the identity diffeomorphism of Kruskal patch K5 (with $\xi_5^M = 0$). The expressions for the metric in various coordinate charts are given in 3.12, 3.20, 3.113, 3.114 and 3.103.

We will now show that the five different metrics in the five coordinate charts define a single metric in the entire spacetime. To see this, note that although the SGD's applied on the five charts are different, (equivalently, for infinitesimal transformations, the diffeomorphisms ξ_i^M in the five charts differ from each other), they satisfy the following sufficient criteria:

(i) At both the right (and left) exterior boundary, the diffeomorphisms coincide. For example, in case of the right exterior (see 3.99), as $\lambda \to \infty$, $u_1 \to v$, $\omega_1 \to w$. Hence $\tilde{u}_1 = G_+^{-1}(u_1) \to G_+^{-1}(v) = \tilde{v}$. In other words, for infinitesimal transformations $\xi_4^M(P) \to \xi_1^M(P)$ for a given point P with $\lambda \to \infty$. This implies that the metric 3.12 coincides at the right boundary with the similar metric3.113 obtained by applying the $G_\pm$ transformations on the coordinate chart EF4. Similarly, the metric 3.20 obtained

by the $H_\pm$ transformations in EF2 and the similar metric 3.114 obtained by the $H_\pm$ transformations in EF3 coincide at the left exterior boundary.

(ii) Away from the boundary, the metrics obtained in the various EF coordinate charts differ from each other only by trivial diffeomorphisms which become the identity transformation at infinity. Since the physical content of each of these metrics is represented only by the boundary data, the above point (i) ensures that all the different metrics represent the same single spacetime metric in different charts (see Figure 3.3).

(iii) It is clear that the SGDs lead to a *smooth metric* in each chart, provided $G_\pm(x), H_\pm(x)$ are differentiable and invertible functions. In the rest of the chapter, we will only consider such functions. It can be verified that such a class of functions is sufficiently general to generate (through transformations such as 3.41) any pair of physically sensible holographic stress tensors at both boundaries.

Analogy with the Dirac monopole

It is important to note that our new solutions can only be specified in terms of a different metric in different coordinate charts which are equivalent to each other. This is analogous to case of the Dirac monopole: the gauge field A_μ for a static U(1) magnetic monopole of charge q_m at the origin needs to be specified separately on two separate coordinate charts:

$$F = q_m \sin\theta \; d\theta \; d\phi : \; A_N = q_m(1-\cos\theta) \; d\phi, \; A_S = q_m(-1-\cos\theta) \; d\phi \tag{3.23}$$

Here $\mathbb{R}^3 - \{0\}$ is viewed as $\mathbb{R} \times S^2$ where S^2 is described by two coordinate charts N_N and N_S (such as obtained by a stereographic projection on to the plane) which include all points of S^2 minus the south and north pole respectively. A^θ_N vanishes (and is hence regular) at the north pole $\theta = 0$, but develops a string singularity at the south pole $\theta = \pi$ (for each $r > 0$). Similarly, A_S is regular at the south pole, but has a string singularity at the north pole. The

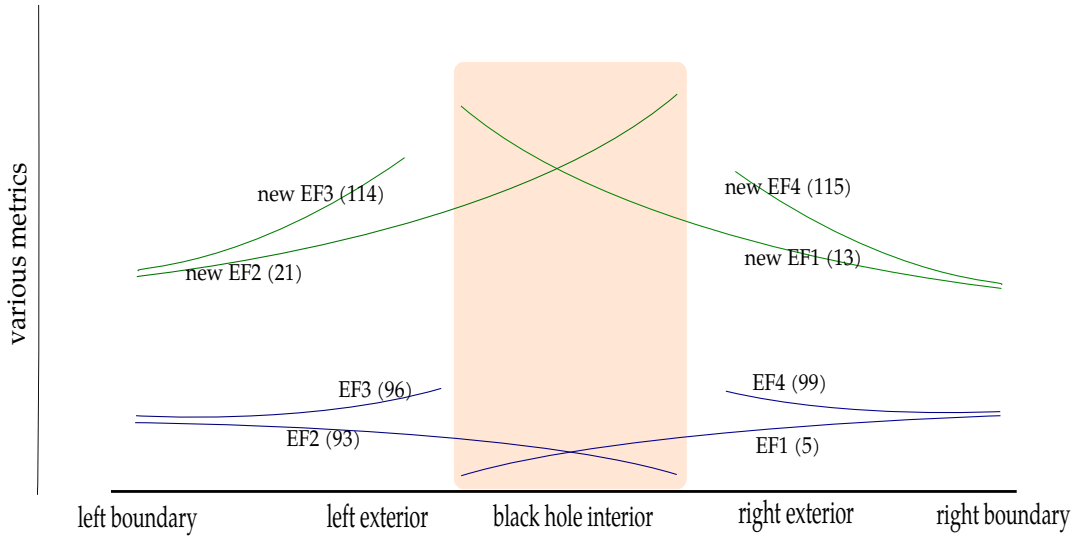

Figure 3.3: A schematic illustration of metrics in this chapter related by trivial and nontrivial diffeomorphisms (see the definition 3.2.5). The metrics 3.4, 3.92, 3.95 and 3.98, represented by the blue lines, define the eternal BTZ geometry; they are all related by trivial diffeomorphisms, which either do not extend to the boundaries or when they do, they become identity asymptotically. The metrics 3.12, 3.20, 3.113 and 3.114, represented by the green lines, define our new solution characterized by the functions $G_\pm, H_\pm$. These are also all related by trivial diffeomorphisms, which satisfy the same criteria as above. The two sets however represent physically different metrics since they are related to each other by nontrivial diffeomorphisms; for instance, 3.4 and 3.12 are related by a diffeomorphism, schematically represented by their separation, which does not vanish (become identity) asymptotically.

important point to note is that in spite of appearances, A_N and A_S describe the same gauge field in the region of overlap $N_N \cap N_S$. This is because in this region, $A_N = A_S + d\chi$ where $\chi = 2q_m d\phi$ represents a pure gauge transformation for appropriately quantized q_m (Dirac quantization condition).

In the present case the metric 3.12 written in EF1, although non-singular on the future horizon, is singular on the past horizon for general $G_\pm$. In order to describe the metric in a neighbourhood of the past horizon, we must switch to the metric in EF4. Similarly, in order to describe the diffeomorphism at the bifurcation surface, we must use the metric 3.103 in the K5 coordinate chart.

Summary of this subsection:

The metrics 3.12, 3.20, 3.113, 3.114 and 3.103, valid in the coordinate charts EF1, EF2, EF3, EF4 and K5 respectively, define a spacetime with a regular metric. The metrics are asymptotically AdS_3 at both the right and left boundaries; the subleading terms in the metric are determined by the solution generating diffeomorphisms $G_\pm, H_\pm$ and can be chosen to fit boundary data specified by arbitrary holographic stress tensors. A schematic representation of our solution is presented in Figure 3.3.

3.2.4 Horizon

In Section 3.2.2 we viewed the SGDs as a coordinate transformation. Alternatively, however, we can also view the diffeomorphism as an active movement of points: $x^M \to \tilde{x}^M = x^M + \xi^M$. In this viewpoint, the future horizon $\lambda = \lambda_H = \lambda_0$ (see 3.5) on the right moves to

$$\tilde{\lambda}_H = G'_+(\tilde{v})\ G'_-(\tilde{w})\lambda_0,\ \tilde{\lambda}_{1,H} = H'_+(\tilde{u})\ H'_-(\tilde{\omega})\lambda_0 \tag{3.24}$$

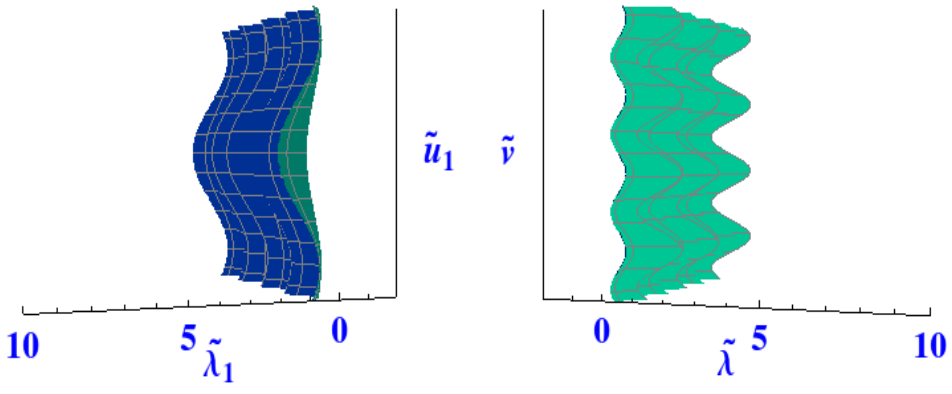

Figure 3.4: The figure on the right shows the location of the horizon on the right in the $\tilde{\lambda}, \tilde{v}, \tilde{w}$ coordinates. The figure on the left shows the location of the horizon on the left in the $\tilde{\lambda}_1, \tilde{u}, \tilde{\omega}$ coordinates. These are described by 3.24. These surfaces are diffeomorphic to the undeformed horizon 3.5 depicted in Figure 3.2. Although the horizon has an undulating shape in our coordinate system, the expansion parameter, measured by the divergence of the area-form, vanishes (see Eq. 3.73).

Similar statements can be made in the other coordinate charts. The horizons represented this way are smooth but undulating (see figure 3.4).

The geometry of warped horizons in [43, 44] was used to yield a holographic prescription for computing local entropy current of a fluid. In Section 3.7 we use a similar technology to compute a holographic entropy in our case.

3.2.5 On the nontriviality of solution generating diffeomorphisms

It is natural to wonder how a metric such as 3.12 provides a new solution since it is obtained by a diffeomorphism from 3.4; however, the fact that the diffeomorphism 3.11 is asymptotically nontrivial makes the new solution physically distinct. Thus, in 3.11 $\tilde{\lambda}$ remains different from λ in the asymptotic region. Indeed, as we will see, the first subleading term in the metric 3.12 carries nontrivial data about a holographic stress tensor 3.41 on the right boundary.

Asymptotically AdS_3 diffeomorphisms were first discussed by Brown and Henneaux [50] who showed that such transformation led to an additional surface contribution to conserved charges of the system. These observations were preceded by a general discussion of such surface charges in the context of gauge theories and gravity in [123, 214, 236]. These authors identified asymptotically non-vanishing pure gauge transformations as global charge rotations.

In the current AdS/CFT context, the surface charges are encapsulated by the holographic stress tensors on the two boundaries. As we will see shortly, they change nontrivially under the solution generating diffeomorphisms (SGD's). In fact, the SGD's reduce to conformal transformations on the boundary. As a result, the 'global charge rotations' mentioned above correspond to a *conformal* transformation of the stress tensor. The important point is that

starting from a given constant stress tensor on each boundary, the two independent SGD's can generate two *independent* and *completely general* stress tensors by this method.

We should note that the diffeomorphisms define a new theory in which the appropriate choice of the IR cutoff surface is 3.15. In this description, the horizon becomes an undulating surface as in Fig 3.4. An equivalent ('active') viewpoint is to describe the new geometry in terms of the old coordinates 3.4, but to change the IR-cutoff surface from 3.6 to 3.15. In either case, the holographic stress tensor changes.

We conclude this section with the following definition of a nontrivial diffeomorphism, which has been implicit in much of the above discussion.

Definition

A local diffeomorphism which does not extend to either boundary (left or right), or a diffeomorphism which extends to a boundary but asymptotically approaches the identity diffeomorphism there, is called a 'trivial' diffeomorphism. Contrarily, a diffeomorphism which extends to a boundary where it does not approach the identity diffeomorphism, is called 'nontrivial'. Quantitatively, a nontrivial diffeomorphism (f) is one under which the holographic stress tensor computed from the existing metric g at the boundary is different from that computed from the pulled back metric f^*g.

3.3 The Dual Conformal Field Theory

As we saw above, the SGD's reduce to conformal transformations at the boundary. We will construct the CFT-dual to the new solutions using the above idea.

Note that the eternal BTZ black hole geometry, described by 3.4 and 3.92, corresponds to the following thermofield double state [67, 138, 149, 177]

$$|\psi_0\rangle = Z(\beta_+, \beta_-)^{-1/2} \sum_n \exp[-\beta_+ E_{+,n}/2 - \beta_- E_{-,n}/2]|n\rangle|n\rangle \tag{3.25}$$

The states $|n\rangle \in \mathcal{H}$ denote all simultaneous eigenstates of $H_\pm = (H \pm J)/2$ with eigenvalues $E_{\pm,n}$. $|\psi_0\rangle$ here is a pure state in $\mathcal{H} \otimes \mathcal{H}$ obtained by the 'purification' of the thermal state 3.26. [13]

$$Z(\beta_+, \beta_-) = \mathrm{Tr}\rho_{\beta_+,\beta_-} \qquad \text{with} \qquad \rho_{\beta_+,\beta_-} = \exp[-\beta_+ H_+ - \beta_- H_-] = \exp[-\beta(H + \Omega J)] \tag{3.26}$$

represents the grand canonical ensemble in $\mathcal{H}$ with inverse temperature β and angular velocity Ω (which can be viewed as the thermodynamic conjugate to the angular momentum J). Also $\beta_\pm = \beta(1 \pm \Omega)$. [14]

Note that $|\psi_0\rangle$ is a pure state in $\mathcal{H} \otimes \mathcal{H}$, and is a 'purification' of the thermal state 3.26.

The non-spinning BTZ: The CFT dual for the more familiar case of non-spinning eternal BTZ black hole ($\Omega = 0 = J$) is the standard thermofield double:

$$|\psi_{0,0}\rangle = Z(\beta)^{-1/2} \sum_n \exp[-\beta E_n/2]|n\rangle|n\rangle \tag{3.27}$$

where $|n\rangle$ now denotes all eigenstates of H. [15]

[13] For definiteness, we will sometimes call the two Hilbert spaces $\mathcal{H}_L$ and $\mathcal{H}_R$, where L, R represent 'left' and 'right', corresponding to the two exterior boundaries of the eternal BTZ. Indeed, L, R also have an alternative meaning. The left/right boundary of the eternal BTZ geometry maps to the left/right Rindler wedge of the boundary of Poincare coordinates, respectively.

[14] The thermal state ρ_{β_+,β_-} (see 3.26) implies a field theory geometry where the light cone directions have periods $\beta_\pm$.

[15] An entanglement entropy for this state was calculated in [138] and matched with a bulk geodesic calculation. This was generalized to the spinning eternal BTZ black hole in [67]

CFT duals of our solutions Following the arguments above 3.25, we claim that the CFT-duals to the new solutions described in Section 3.2.3 are described by the following pure states in $\mathcal{H} \otimes \mathcal{H}$:

$$|\psi\rangle = U_L U_R |\psi_0\rangle = Z(\beta_+, \beta_-)^{-1/2} \sum_n \exp[-\beta_+ E_{+,n}/2 - \beta_- E_{-,n}/2] U_L |n\rangle U_R |n\rangle \tag{3.28}$$

where U_R is the unitary transformation which implements the conformal transformations on the CFT on the right boundary (characterized by $G_\pm$), and U_L is the unitary transformation which implements the conformal transformations on the CFT on the left boundary (characterized by $H_\pm$). See Appendix 3.10.1 for an explicit construction of a unitary transformations U_R.

In the following sections, we will provide many checks for this proposal. However, first we shall discuss how to compute various correlators in the above state 3.28.

3.3.1 Correlators

Let us first consider correlators in the standard thermofield double state 3.25. It is known that correlators of one-sided CFT observables, say O_R, satisfy an AdS/CFT relation of the form [16]

$$\langle \psi_0 | O_R(P_1) O_R(P_2) ... O_R(P_n) | \psi_0 \rangle \equiv \mathrm{Tr} \left(\rho_{\beta_+,\beta_-} O_R(P_1) O_R(P_2) ... O_R(P_n) \right) = G_{\text{bulk}}(\mathbf{P}_1, \mathbf{P}_2, ... \mathbf{P}_n) \tag{3.29}$$

where the bulk correlator G_{bulk} is computed from the (right exterior region of) a dual black hole geometry with temperature $T = 1/\beta$ and angular velocity Ω. Two-sided correlators, similarly, satisfy a relation like

$$\langle \psi_0 | O_R(P_1) O_R(P_2) ... O_R(P_m) O_L(P'_1) ... O_L(P'_n) | \psi_0 \rangle = G_{\text{bulk}}(\mathbf{P}_1, \mathbf{P}_2, ... \mathbf{P}_m; \mathbf{P}'_1, ..., \mathbf{P}'_n) \tag{3.30}$$

[16] We will mostly use unprimed labels, $P_1, P_2, ...$ for points on the spacetime of the 'right' CFT, and primed labels, $P'_1, P'_2, ...$ for the space of the 'left' CFT.

where the bulk correlator on the RHS is computed from the two-sided geometry of the eternal BTZ black hole [67,138,149,177], represented in this chapter by 3.4 and 3.92. The bold-faced label $\mathbf{P}$ above represents an image of the field theory point P on a cut-off surface in the bulk under the usual AdS/CFT map. E.g. in the coordinates of 3.4, the map is given by

$$P \mapsto \mathbf{P} \equiv (\lambda = \lambda_{ir} = 1/\epsilon^2, P) \tag{3.31}$$

where ϵ is the UV cut-off in the CFT, cf. 3.6). There is a similar map for the *left* boundary. In particular, the holographic correspondence for the two point functions of scalar operators can be written simply as [169]:

$$\begin{aligned} \langle\psi_0|O_R(P)O_R(Q)|\psi_0\rangle &= \mathrm{T}r(\rho_{\beta_+,\beta_-}O_R(P)O_R(Q)) = \exp[-2hL(\mathbf{P},\mathbf{Q})] \\ \langle\psi_0|O_R(P)O_L(Q')|\psi_0\rangle &= \exp[-2hL(\mathbf{P},\mathbf{Q}')] \end{aligned} \tag{3.32}$$

where $L(\mathbf{P},\mathbf{Q})$ is the length of the extremal geodesic connecting $\mathbf{P}$ and $\mathbf{Q}$ (similarly with $L(\mathbf{P},\mathbf{Q}')$).

It is easy to see that correlators in the new, transformed, state $|\psi\rangle$ 3.28 can be understood as correlators of transformed operators in the old state $|\psi_0\rangle$, i.e.

$$\langle\psi|O_R(P_1)...O_R(P_m)O_L(P'_1)...O_L(P'_n)|\psi\rangle = \langle\psi_0|\tilde{O}_R(P_1)...\tilde{O}_R(P_m)\tilde{O}_L(P'_1)...\tilde{O}_L(P'_n)|\psi_0\rangle \tag{3.33}$$

where

$$\tilde{O}_R(P) \equiv U_R^\dagger O_R(P) U_R, \qquad \tilde{O}_L(P') \equiv U_L^\dagger O_L(P') U_L \tag{3.34}$$

For a primary field O_R with conformal dimensions $(h, \bar{h})$, the conformally transformed operator satisfies the relation

$$\tilde{O}_R(\tilde{v}, \tilde{w}) = O_R(v, w) \left(\frac{dv}{d\tilde{v}}\right)^h \left(\frac{dw}{d\tilde{w}}\right)^{\bar{h}} \tag{3.35}$$

3.3.2 Strategy for checking AdS/CFT

To check the claim that the states 3.28 are CFT-duals to the new bulk geometries found in Section 3.2.3, we need to show a relation of the form (cf. 3.30)

$$\langle\psi_0|\tilde{O}_R(P_1)...\tilde{O}_R(P_m)\tilde{O}_L(P'_1)...\tilde{O}_L(P'_n)|\psi_0\rangle = \tilde{G}_{\text{bulk}}(\tilde{\mathbf{P}}_1, \tilde{\mathbf{P}}_2, ...\tilde{\mathbf{P}}_m; \tilde{\mathbf{P}}'_1, ..., \tilde{\mathbf{P}}'_n) \tag{3.36}$$

where the RHS is computed in the new geometries. Here $\tilde{\mathbf{P}}$ represents the image of the CFT point P, under AdS/CFT, on the cut-off surface 3.15 in the new geometry. In the language of 3.12, the map is

$$P \mapsto \tilde{\mathbf{P}} = (\tilde{\lambda} = \tilde{\lambda}_{ir} = 1/\epsilon^2, P) \tag{3.37}$$

Two-point correlators: In the particular case of two-point functions

$$\begin{aligned}\langle\psi_0|\tilde{O}_R(P)\tilde{O}_R(Q)|\psi_0\rangle &= \text{Tr}(\rho_{\beta_+,\beta_-}\tilde{O}_R(P)\tilde{O}_R(Q)) = \exp[-2h\tilde{L}(\tilde{\mathbf{P}}, \tilde{\mathbf{Q}})] \\ \langle\psi_0|\tilde{O}_R(P)\tilde{O}_L(Q')|\psi_0\rangle &= \exp[-2h\tilde{L}(\tilde{\mathbf{P}}, \tilde{\mathbf{Q}}')]\end{aligned} \tag{3.38}$$

where $\tilde{L}(\tilde{\mathbf{P}}, \tilde{\mathbf{Q}})$ is the length of the extremal geodesic connecting P and Q in the new geometry (similarly with $\tilde{L}(\tilde{\mathbf{P}}, \tilde{\mathbf{Q}}')$). The discerning reader may justifiably wonder how a geodesic length in the new geometry can be different from that in the original, eternal BTZ black hole geometry, since the former is obtained by a diffeomorphism from the latter; the point is that the bulk points $\tilde{\mathbf{P}}$, given by 3.37 are *not* the same as the bulk points $\mathbf{P}$ given by 3.31. For example, a geodesic with endpoints at a fixed IR cut-off $\tilde{\lambda} = 1/\epsilon^2$ (both on the right exterior) corresponds, in the eternal BTZ black hole, to a geodesic with two end-points at

3.17 $\lambda = 1/(\epsilon^2 G'_+(\tilde{v})G'_-(\tilde{w}))$. As we will see below, it is this shift which ensures the equality in 3.38. This is one more instance of how our geometries are nontrivially different from the original BTZ solution although they are obtained by diffeomorphisms (see Section 3.2.5 for more detail).

3.4 Holographic Stress Tensor

In this section we will discuss our first observable O: the stress tensor. We will first consider the stress tensor of the boundary theory on the right. The generalization to the stress tensor on the left is trivial. The equation 3.36 now implies that we should demand the following equality

$$\langle\psi|T_{vv}(P)|\psi\rangle \equiv \mathrm{Tr}\left(\rho_{\beta_+,\beta_-} U_R^\dagger T_{vv}(P) U_R\right) = \tilde{T}_{\mathrm{bulk},\tilde{v}\tilde{v}}(\tilde{\mathbf{P}}) \tag{3.39}$$

and a similar equation for the right-moving stress tensor $T_{ww}(w)$.

Bulk The RHS of this equation is simply the holographic stress tensor, computed in the new geometry 3.12. We use the definition of holographic stress tensor in [28, 227]:[17]

$$8\pi G_3 T_{\mu\nu} = \lim_{\epsilon\to 0}\left(K_{\mu\nu} - K h_{\mu\nu} - h_{\mu\nu}\right) \tag{3.40}$$

where $h_{\mu\nu}$ is the induced metric on the cut-off surface $\Sigma : \tilde{\lambda} = \tilde{\lambda}_{ir} = 1/\epsilon^2$, chosen in accordance with 3.37 which is the natural one in the new geometry (note that it is different from the cut-off surface implied by 3.31). $K_{\mu\nu}$ and K are respectively the extrinsic curvature

[17] We drop the subscript bulk from the bulk stress tensor, as it should be obvious from the context whether we are talking about the CFT stress tensor or the holographic stress tensor.

and its trace on Σ. It is straightforward to do the explicit calculation; we find that

$$8\pi G_3 T_{\tilde{v}\tilde{v}} = \frac{L}{4} G'_+(\tilde{v})^2 + \frac{3G''_+(\tilde{v})^2 - 2G'_+(\tilde{v})G'''_+(\tilde{v})}{4G'_+(\tilde{v})^2},$$
$$8\pi G_3 T_{\tilde{w}\tilde{w}} = \frac{\bar{L}}{4} G'_-(\tilde{w})^2 + \frac{3G''_-(\tilde{w})^2 - 2G'_-(\tilde{w})G'''_-(\tilde{w})}{4G'_-(\tilde{w})^2} \tag{3.41}$$

This clearly looks like a conformal transformation of the original stress tensor 3.8. We will explicitly verify below that it agrees with the CFT calculation. The generalization to T_{ww} and to the stress tensors of the second CFT is straightforward.This clearly has the form of a conformal transformation of the original stress tensor 3.8. We will explicitly verify below in the CFT that it indeed is precisely a conformal transformation, as demanded by 3.39. The generalization of 3.41 to the stress tensors $T_{\tilde{u}\tilde{u}}, T_{\tilde{\omega}\tilde{\omega}}$ of the second CFT is straightforward.

In this chapter, we will sometimes use the notation $T_R, \bar{T}_R$ for $T_{\tilde{v}\tilde{v}}, T_{\tilde{w},\tilde{w}}$, and $T_L, \bar{T}_L$ [18] for $T_{\tilde{u}\tilde{u}}, T_{\tilde{\omega}\tilde{\omega}}$ respectively. It is clear that by appropriately choosing the functions $G_\pm$ and $H_\pm$, any set of boundary stress tensors $T_{R,L}, \bar{T}_{R,L}$ can be generated. This is how our solutions described in Section 3.2.3 solve the boundary value problem mentioned in the Introduction.

CFT The unitary transformation in the LHS of 3.39, implements, by definition, the following conformal transformation (see Appendix 3.10.1 for more details) on the quantum operator

$$U_R^\dagger T_{vv}(P) U_R = \left(\frac{\partial \tilde{v}}{\partial v}\right)^{-2} [T_{\tilde{v}\tilde{v}}(\tilde{v}) - \frac{c}{12} S(v, \tilde{v})] \tag{3.42}$$

From 3.11, the relevant conformal transformation here is $v = G_+(\tilde{v})$. Using this, the definition 3.121 of the Schwarzian derivative $S(v, \tilde{v})$, and the identification [50]

$$G_3 = 3/(2c), \tag{3.43}$$

we find that 3.42 exactly agrees with 3.41.

[18] $T_R, \bar{T}_R$ represent the left-moving and right-moving stress tensors on the Right CFT; similarly for $T_L, \bar{T}_L$.

This *p*roves the AdS-CFT equality 3.39 for the stress tensor.

3.5 General two-point correlators

In this section we will discuss general two-point correlators, both from the bulk and CFT viewpoints following the steps outlined in Section 3.3.1.

3.5.1 Boundary-to-Boundary Geodesics

As mentioned in 3.32, the holographic calculation of a two-point correlator reduces to computing the geodesic length between the corresponding boundary points. We will first calculate correlators in the thermofield double state 3.25, which involves computing geodesics in the eternal BTZ geometry 3.4.

In the eternal BTZ geometry

RL geodesic: Let us consider a geodesic running from a point $\mathbf{P}(1/\epsilon_R^2, v, w)$ on the right boundary to a point $\mathbf{Q}' = (1/\epsilon_L^2, u, \omega)$ on the left boundary.[19] As shown in Section 3.9.1 (see [138]) both the right exterior ($\subset$ EF1) and the left exterior ($\subset$ EF2) can be mapped to a single coordinate chart in Poincare coordinates. Let the Poincare coordinates for $\mathbf{P}$ and $\mathbf{Q}'$, be $(X_{+R}, X_{-R}, \zeta_R)$ and $(X_{+L}, X_{-L}, \zeta_L)$ respectively. By using the coordinate transformations given in (3.111) and (3.112), we find, upto the first subleading order in ϵ_R and ϵ_L,

$$\begin{aligned} X_{+R} &= e^{\sqrt{L}v}, \quad X_{-R} = -e^{-\sqrt{L}w} + L\epsilon_R^2 e^{-\sqrt{L}w}, \quad \zeta_R^2 = L\epsilon_R^2\, e^{\sqrt{L}(v-w)} \\ X_{+L} &= -e^{\sqrt{L}u} + L\epsilon_L^2 e^{\sqrt{L}u}, \quad X_{-L} = e^{-\sqrt{L}\omega}, \quad \zeta_L^2 = L\epsilon_L^2\, e^{\sqrt{L}(u-\omega)} \end{aligned} \tag{3.44}$$

[19] For the calculation at hand we need to put $\epsilon_L = \epsilon_R = \epsilon$; however, we keep the two cutoffs independent for later convenience.

with $L = \bar{L}$.[20] The geodesic in Poincare coordinates is given by

$$X_+ = A\tanh\tau + C, \quad X_- = B\tanh\tau + D, \quad \zeta = \frac{\sqrt{-AB}}{\cosh\tau}$$

where τ is the affine parameter, which takes the values τ_R and τ_L at $\mathbf{P}$ and $\mathbf{Q}'$ respectively. The constants A, B, C, D, τ_L and τ_R are fixed by the endpoint coordinates given above. In the limit $\epsilon_R, \epsilon_L \to 0$, we obtain

$$\begin{aligned}
\tau_R &= \log\left[\frac{e^{-(\sqrt{L}v+\sqrt{L}\omega)/2}}{\sqrt{2}}\sqrt{\frac{(e^{\sqrt{L}v}+e^{\sqrt{L}u})(e^{\sqrt{L}w}+e^{\sqrt{L}\omega})}{\lambda_0\epsilon_R^2}}\right] \\
\tau_L &= -\log\left[\frac{e^{-\sqrt{L}(u+w)/2}}{\sqrt{2}}\sqrt{\frac{(e^{\sqrt{L}v}+e^{\sqrt{L}u})(e^{\sqrt{L}w}+e^{\sqrt{L}\omega})}{\lambda_0\epsilon_L^2}}\right]
\end{aligned}$$

where $\lambda_0 = L/2$ (see 3.5). The geodesic length is now simply given by the affine parameter length

$$L(\mathbf{P}, \mathbf{Q}') = \tau_R - \tau_L = \log\left[\frac{4\cosh[\sqrt{L}(v-u)/2]\cosh[\sqrt{L}(w-\omega)/2]}{L\epsilon_R\epsilon_L}\right] \tag{3.45}$$

For comparison with CFT correlators in the thermofield double, we will put, in the above expression, $\epsilon_L = \epsilon_R = \epsilon$, where ϵ is the (real space) UV cut-off in the CFT.

RR geodesic: If we take the two boundary points on the same exterior region, say on the right, $\mathbf{P_1}(1/\epsilon_1^2, v_1, w_1)$ and $\mathbf{P_2}(1/\epsilon_2^2, v_2, w_2)$, then the corresponding Poincare coordinates are (using (3.111))

$$\begin{aligned}
X_{+1} &= e^{\sqrt{L}v_1}, \qquad X_{-1} = -e^{-\sqrt{L}w_1} + L\epsilon_1^2 e^{-\sqrt{L}w_1}, \quad \zeta_1^2 = L\epsilon_1^2\, e^{\sqrt{L}(v_1-w_1)} \\
X_{+2} &= e^{\sqrt{L}v_2}, \qquad X_{-2} = -e^{-\sqrt{L}w_2} + L\epsilon_2^2 e^{-\sqrt{L}w_2}, \quad \zeta_2^2 = L\epsilon_2^2\, e^{\sqrt{L}(v_2-w_2)}
\end{aligned} \tag{3.46}$$

[20] For simplicity, we present the calculation here for $L = \bar{L}$; the generalization to the spinning BTZ is straightforward.

Following steps similar to above, we have, in the $\epsilon_1, \epsilon_2 \to 0$ limit,

$$\begin{aligned}\tau_1 &= \log\Big[\frac{e^{-(v_1+w_2)/2}}{\sqrt{2}}\sqrt{\frac{(e^{v_1}-e^{v_2})(-e^{w_1}+e^{w_2})}{\lambda_0\epsilon_1^2}}\Big]\\ \tau_2 &= -\log\Big[\frac{e^{-(v_1+w_1)/2}}{\sqrt{2}}\sqrt{\frac{(-e^{v_1}+e^{v_2})(e^{w_1}-e^{w_2})}{\lambda_0\epsilon_2^2}}\Big]\end{aligned}$$

The geodesic length is then

$$L(\mathbf{P_1},\mathbf{P_2}) = \tau_{+1} - \tau_{+2} = \log\left[\frac{4\,\sinh[(v_1-v_2)/2]\sinh[(w_1-w_2)/2]}{L\epsilon_1\epsilon_2}\right] \tag{3.47}$$

For comparison with CFT, we will put $\epsilon_1 = \epsilon_2 = \epsilon$.

In the new geometries

As explained in Section 3.2, the IR boundary in the new solutions, obtained by the SGDs, is given by the equation 3.15 or equivalently by 3.17, and analogous equations on the left. This is encapsulated by the CFT-to-bulk map 3.37. In case of the *RL geodesic*, the CFT endpoints (P, Q') now translate to new boundary points $(\tilde{\mathbf{P}}, \tilde{\mathbf{Q}}')$ with the following new values of the old $(\lambda,\, \lambda_1)$ coordinates:

$$\lambda \equiv \frac{1}{\epsilon_R^2} = \frac{1}{\epsilon^2 G'_+(\tilde{v})G'_-(\tilde{w})}, \qquad \lambda_1 \equiv \frac{1}{\epsilon_L^2} = \frac{1}{\epsilon^2 H'_+(\tilde{u})H'_-(\tilde{\omega})} \tag{3.48}$$

which just has the effect of conformally transforming the boundary coordinates// $\epsilon_R = \epsilon \to \epsilon_R = \epsilon\sqrt{G'_+(\tilde{v})G'_-(\tilde{w})}$, $\epsilon_L = \epsilon \to \epsilon_L = \epsilon\sqrt{H'_+(\tilde{u})H'_-(\tilde{\omega})}$. Using these new values of $\epsilon_{L,R}$, we get

$$L(\tilde{\mathbf{P}},\tilde{\mathbf{Q}}') = \log\left[\frac{4\cosh[\sqrt{L}(G_+(\tilde{v})-H_+(\tilde{u}))/2]}{\sqrt{L}\epsilon\sqrt{G'_+(\tilde{v})H'_+(\tilde{u})}}\frac{\cosh[\sqrt{L}(G_-(\tilde{w})-H_-(\tilde{\omega}))/2]}{\sqrt{L}\epsilon\sqrt{G'_-(\tilde{w})H'_-(\tilde{\omega})}}\right] \tag{3.49}$$

Similarly,

$$L(\tilde{\mathbf{P}}_{\mathbf{1}}, \tilde{\mathbf{P}}_{\mathbf{2}}) = \log\left[\frac{4\sinh[\sqrt{L}(G_+(\tilde{v}_1)-G_+(\tilde{v}_2))/2]}{\sqrt{L}\epsilon\sqrt{G'_+(\tilde{v}_1)G'_+(\tilde{v}_2)}}\frac{\sinh[\sqrt{L}(G_-(\tilde{w}_1)-G_-(\tilde{w}_2))/2]}{\sqrt{L}\epsilon\sqrt{G'_-(\tilde{w}_1)G'_-(\tilde{w}_2)}}\right] \tag{3.50}$$

3.5.2 General two-point correlators from CFT

In the thermofield double state

RL correlator: For the eternal BTZ string, the coordinate transformations from the EF to Poincare (see Appendix 3.9.1) reduce, at the boundary, to a conformal transformation from the Rindler to Minkowski coordinates, so that the boundary of the right (left) exterior maps to the right (left) Rindler wedge [138]. It is expedient to compute the CFT correlations first in the Minkowski plane, and then conformally transform the result to Rindler coordinates. Using this method of [138], we get the following result

$$\begin{aligned}\langle\psi_0|O(X_{+R},X_{-R})\,O(X_{+L},X_{-L})|\psi_0\rangle &= \frac{(\sqrt{L}e^{\sqrt{L}v})^h(\sqrt{L}e^{-\sqrt{L}w})^{\bar{h}}(-\sqrt{L}e^{\sqrt{L}u})^h(-\sqrt{L}e^{-\sqrt{L}\omega})^{\bar{h}}}{(\frac{e^{\sqrt{L}v}+e^{\sqrt{L}u}}{\epsilon})^{2h}(\frac{-e^{-\sqrt{L}w}-e^{-\sqrt{L}\omega}}{\epsilon})^{2\bar{h}}}\\ &= \Big(\frac{4\cosh\left[\sqrt{L}(v-u)/2\right]\,\cosh\left[\sqrt{L}(w-\omega)/2\right]}{L\epsilon^2}\Big)^{-2h}\end{aligned}$$

where the operator O is assumed to have dimensions $(h,\bar{h})$ and we have used a real space field theory cut-off ϵ. We have related the temperature of the CFT to $L(=\bar{L})$ by the equation $\sqrt{L}=2\pi/\beta$. // It is easy to see that this correlator satisfies the relation 3.32

$$\langle\psi_0|O(X_{+R},X_{-R})\,O(X_{+L},X_{-L})|\psi_0\rangle = e^{-2hL(\mathbf{P},\mathbf{Q})} \tag{3.51}$$

where in the expression on the right hand side for the geodesic length (3.45), we use $\epsilon_R = \epsilon_L = \epsilon$ as explained before.

RR correlator: By following steps similar to the above, the two-point correlator between the points (3.46) is given by

$$\begin{aligned}\langle\psi_0|\mathcal{O}(X_{+1},X_{-1})\,\mathcal{O}(X_{+2},X_{-2})|\psi_0\rangle &= \frac{(\sqrt{L}e^{\sqrt{L}v_1})^h(\sqrt{L}e^{-\sqrt{L}w_1})^{\bar{h}}(\sqrt{L}e^{\sqrt{L}v_2})^h(\sqrt{L}e^{-\sqrt{L}w_2})^{\bar{h}}}{(\frac{e^{\sqrt{L}v_1}-e^{\sqrt{L}v_2}}{\epsilon})^{2h}(\frac{-e^{-\sqrt{L}w_1}+e^{-\sqrt{L}w_2}}{\epsilon})^{2\bar{h}}} \\ &= \Big(\frac{4\sinh\left[\sqrt{L}(v_1-v_2)/2\right]\,\sinh\left[\sqrt{L}(w_1-w_2)/2\right]}{L\epsilon^2}\Big)^{-2h}\end{aligned}$$

It follows, therefore, that

$$\langle\psi_0|\mathcal{O}(X_{+1},X_{-1})\,\mathcal{O}(X_{+2},X_{-2})|\psi_0\rangle = e^{-2hL(\mathbf{P_1},\mathbf{P_2})} \tag{3.52}$$

where, again, the geodesic length on the right hand side is read off from 3.49 with $\epsilon_1=\epsilon_2=\epsilon$.

In the new states

As explained in 3.33, correlators in the state $|\psi\rangle$ 3.28 can be computed by using a conformal transformation 3.35 of the operators. The new correlator is, therefore, found from the old one 3.51 by a conformal transformation of the boundary coordinates and an inclusion of the Jacobian factors. The latter has, in fact, the effect of the replacement $\epsilon^2\to\epsilon^2\sqrt{G'_+(\tilde{v})G'_-(\tilde{w})H'_+(\tilde{u})H'_-(\tilde{\omega})}$. With these ingredients, it is straightforward to verify that 3.38 is satisfied. Similar arguments apply to RR and LL correlators.

3.6 Entanglement entropy

We define an entangling region $A=A_R\cup A_L$, where A_R is a half line $(v-w)/2>x_R$ on the right boundary at 'time' $(v+w)/2=t_R$ and A_L is a half line $(u-\omega)/2>x_L$ of the left boundary at 'time' $(u+\omega)/2=t_L$. The boundary of the region A consists of a point

$P(v_{\partial A}, w_{\partial A})$ on the right and a point $Q'(u_{\partial A}, \omega_{\partial A})$ on the left, with coordinates

$$\begin{aligned} P: \quad v_{\partial A} &= t_R + x_R, \quad w_{\partial A} = t_R - x_R \\ Q': \quad u_{\partial A} &= t_L + x_L, \quad \omega_{\partial A} = t_L - x_L \end{aligned} \tag{3.53}$$

Bulk calculations

In the BTZ geometry

We calculate the entanglement entropy S_A of the region A using the holographic entanglement formula of [149, 220]. The HEE is given in terms of the geodesic length $L(\mathbf{P}, \mathbf{Q}')$. The geodesic length, as calculated in (3.45), is

$$L(\mathbf{P}, \mathbf{Q}') = \log \left[\frac{4 \cosh[\sqrt{L}(v_{\partial A} - u_{\partial A})/2] \cosh[\sqrt{L}(w_{\partial A} - \omega_{\partial A})/2]}{M\epsilon^2} \right] \tag{3.54}$$

The HEE is then given by $S_A = L(\mathbf{P}, \mathbf{Q}')/4G_3$. Using 5.60, we get

$$S_A = \frac{c}{6} \log \left[\frac{4 \cosh[\sqrt{L}((t_R + x_R) - (t_L + x_L))/2] \cosh[\sqrt{L}((t_R - x_R) - (t_L - x_L))/2]}{M\epsilon^2} \right] \tag{3.55}$$

Note that for $x_R = x_L = 0$ and $t = t_R = -t_L$ (which correspond to a non-trivial time evolution in the geometry) the HEE 3.55 reduces to

$$S_A = \frac{c}{3} \log \left[\cosh \frac{2\pi t}{\beta} \right] + \frac{c}{3} \log \left[\frac{\beta/\pi}{\epsilon} \right] \tag{3.56}$$

which reproduces the result for the HEE in [138].[21]

[21] The UV cutoff in [138] is half of the cutoff, ϵ used here.

In the new geometries

The HEE corresponding to the conformally transformed state 3.28 is given by the length $L(\tilde{\mathbf{P}}, \tilde{\mathbf{Q}}')$ connecting the end-points P and Q' in the new geometries described in Section 3.2.3. Working on lines similar to the derivation of 3.47, the HEE is given by

$$\begin{aligned} S_A &= \frac{c}{6}\log\Big[\frac{4\cosh[\sqrt{L}(G_+(\tilde{t}_R+\tilde{x}_R)-H_+(\tilde{t}_L+\tilde{x}_L))/2]}{\sqrt{L}\epsilon\sqrt{G'_+(\tilde{t}_R+\tilde{x}_R)H'_+(\tilde{t}_L+\tilde{x}_L)}} \\ &\qquad \frac{\cosh[\sqrt{L}(G_-(\tilde{t}_R-\tilde{x}_R)-H_-(\tilde{t}_L-\tilde{x}_L))/2]}{\sqrt{L}\epsilon\sqrt{G'_-(\tilde{t}_R-\tilde{x}_R)H'_-(\tilde{t}_L-\tilde{x}_L)}}\Big] \end{aligned} \tag{3.57}$$

CFT calculations

In the thermofield double state

The technique of calculating the entanglement entropy in the thermofield double state is well-known [75]. The Renyi entanglement entropy $S_A^{(n)}$ of the region A (3.53) is given by the trace of the n^{th} power of the reduced density matrix ρ_A^n. The latter can be shown to be a Euclidean path integral on an n-sheeted Riemann cylinder. This can then be calculated in terms of the two point correlator, on a complex plane, of certain twist fields $\mathcal{O}$, with conformal dimensions

$$h = \frac{c}{24}(n-1/n), \quad \bar{h} = \frac{c}{24}(n-1/n) \tag{3.58}$$

inserted at the end-points (P, Q') of A. The two-point correlator is given by a calculation similar to that in the previous section. Thus,

$$\begin{aligned} S_A^{(n)} &= \langle \mathcal{O}_R(v_{\partial A}, w_{\partial A})\, \mathcal{O}_L(u_{\partial A}, \omega_{\partial A})\rangle \\ &= \frac{(\sqrt{L})^{2h+2\bar{h}}}{(4\cosh[\sqrt{L}((t_R+x_R)-(t_L+x_L))/2]/\epsilon)^{2h}(\cosh[\sqrt{L}((t_R-x_R)-(t_L-x_L))/2]/\epsilon)^{2\bar{h}}} \end{aligned}$$

The entanglement entropy $S_A = -\partial_n S_A^{(n)}|_{n=1}$ is

$$S_A = \frac{c}{6}\log\left[\frac{4\cosh[\sqrt{L}((t_R+x_R)-(t_L+x_L))/2]\cosh[\sqrt{L}((t_R-x_R)-(t_L-x_L))/2]}{L\epsilon^2}\right] \quad (3.59)$$

This proves that the CFT entanglement entropy and holographic entanglement entropy(3.55) are equal.

In the new states

The EE of the region A, computed in the new state 3.28, is given in terms of the conformally transformed two-point function described in 3.33. The conformally transformed points are given by

$$v_{\partial A} = G_+(\tilde{v}_{\partial A}) = G_+(\tilde{t}_R + \tilde{x}_R), \qquad w = G_-(\tilde{w}_{\partial A}) = G_-(\tilde{t}_R - \tilde{x}_R)$$
$$u_{\partial A} = H_+(\tilde{u}_{\partial A}) = H_+(\tilde{t}_L + \tilde{x}_L), \qquad \omega = H_-(\tilde{\omega}_{\partial A}) = H_-(\tilde{t}_L - \tilde{x}_L)$$

It follows that the entanglement entropy is

$$S_{A,CFT} = \frac{c}{6}\log\Bigg[\frac{4\cosh[\sqrt{L}(G_+(\tilde{t}_R+\tilde{x}_R)-H_+(\tilde{t}_L+\tilde{x}_L))/2]}{\epsilon\sqrt{L}\sqrt{G'_+(\tilde{t}_R+\tilde{x}_R)H'_+(\tilde{t}_L+\tilde{x}_L)}} \frac{\cosh[\sqrt{L}(G_-(\tilde{t}_R-\tilde{x}_R)-H_-(\tilde{t}_L-\tilde{x}_L))/2]}{\epsilon\sqrt{L}\sqrt{G'_-(\tilde{t}_R-\tilde{x}_R)H'_-(\tilde{t}_L-\tilde{x}_L)}}\Bigg] \quad (3.60)$$

which matches with the HEE (3.57).

3.6.1 Dynamical entanglement entropy in a specific new geometry

We now compute the entanglement entropy in an illustrative geometry specified by a particular choice of the functions $G_\pm$ and $H_\pm$. In this example, we take

$$x_R = 0, \quad t_R = t, \quad x_L = 0, \quad t_L = -t$$

For simplicity, we consider $G_\pm$ and $H_\pm$ which satisfy

$$G_+(x) \equiv G_-(x) \equiv G(x), \quad H_+(x) \equiv H_-(x) \equiv H(x)$$

With the transformations given above, we have

$$\tilde{x}_R = 0, \quad \tilde{v}_{\partial A} = \tilde{w}_{\partial A} = \tilde{t}_R = \tilde{t}, \qquad \tilde{x}_L = 0, \quad \tilde{u}_{\partial A} = \tilde{\omega}_{\partial A} = \tilde{t}_L = -\tilde{t} \tag{3.61}$$

The expression for the HEE (3.57) then reduces to

$$S_A = \frac{c}{3} \log \left[\frac{2\cosh[\sqrt{L}(G(\tilde{t}) + H_1(\tilde{t}))/2]}{\epsilon \sqrt{L} \sqrt{G'(\tilde{t}) H_1'(\tilde{t})}} \right] \tag{3.62}$$

where we have defined the notation $-H(-\tilde{t}) = H_1(\tilde{t})$.

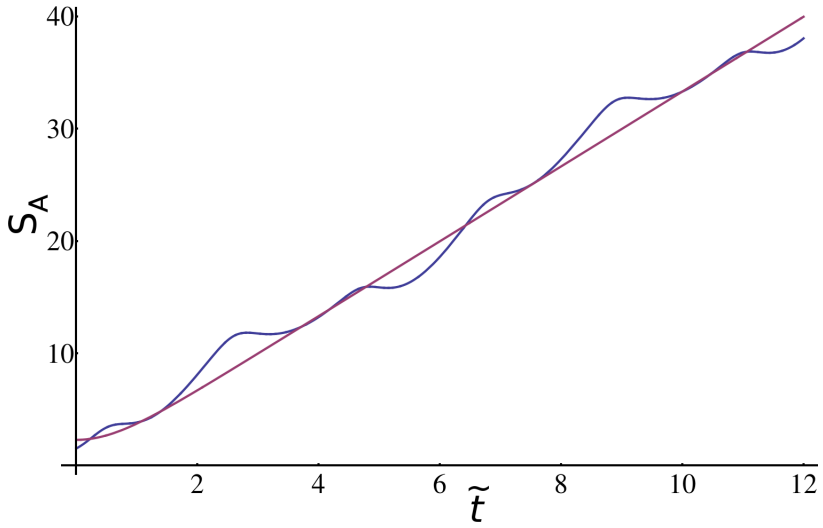

Figure 3.5: Time evolution of HEE. The red-line represents the linear growth of HEE for a region consisting of spatial half-lines of both sides of a constant 2-sided BTZ geometry. The blue-line represents the HEE growth of the region consisting of half-lines of both sides of the SGD transformed geometry, for $G(\tilde{t}) = \tilde{t} + \frac{1}{6}\cos(3\tilde{t})$ and $H_1(\tilde{t}) = \tilde{t} + \frac{3}{5}\sin(\tilde{t})$. The undulating curve can be explained in terms of the quasiparticle picture of [59]; the entanglement entropy departs from its usual linear behaviour as the quasiparticle pairs locally go out and back in to the entangling region as the region is subjected to a conformal transformation.

3.7 Entropy

As discussed in previous sections, our solutions of Section 3.2.3 are characterized by a smooth, albeit undulating, horizon (see Figure 3.4). This allows us, following [43], to define a holographic entropy current. We will first review the equilibrium situation (static black string), and then describe the calculation for the general, time-dependent solution. We will include a comparison with CFT calculations in both cases.

3.7.1 Equilibrium

Bulk calculation: In case $L = \bar{L} =$ constant, our solutions represent BTZ black strings 3.4 with a horizon at $\lambda = \lambda_0$. The horizon $\mathcal{H}$ is a two-dimensional null surface, described by

the metric

$$ds^2|_{\mathcal{H}} \equiv H_{\mu\nu}dx^\mu dx^\nu = \left(\sqrt{L}dv/2 - \sqrt{\bar{L}}dw/2\right)^2 \tag{3.63}$$

Since the normal to $\mathcal{H}$ at any point, given by $n^M = \partial^M\lambda(M = \{\lambda, v, w\})$, also lies on $\mathcal{H}$, $\mathcal{H}$ possesses a natural coordinate system (τ, α) where α labels the one-parameter family of null geodesics, and τ measures the affine distance along the geodesics. In such a coordinate system, we get, by construction

$$ds^2|_{\mathcal{H}} = gd\alpha^2 \tag{3.64}$$

The area 1-form and the entropy current on the horizon are defined by the equations [43] [22],

$$a \equiv 4G_3\epsilon_{\mu\nu}J^\mu_S dx^\nu = \sqrt{g}d\alpha, \tag{3.65}$$

By inspection, from 3.63 and 3.64, we find the following expressions for the area-form and the entropy current

$$\begin{aligned} a &= \sqrt{L}dv/2 - \sqrt{\bar{L}}dw/2 \\ J^v_s &= \frac{1}{8G_3}\sqrt{\bar{L}},\ J^w_S = \frac{1}{8G_3}\sqrt{L} \end{aligned} \tag{3.66}$$

The holographic entropy current on the boundary $\mathcal{B}$ is obtained by using a map $f : \mathcal{B} \to \mathcal{H}$ and pulling back the area-form (or alternatively the entropy current $J_{S,\mu}$) from the horizon to the boundary. It turns out [23] that the natural pull back retains the form of the area-form or entropy current, namely the expressions 3.66 still hold at the boundary.

To find the entropy density, we define the boundary coordinates $t = (v + w)/2, x = (v - w)/2$ (see Section 3.6), (so that 3.7 has the canonical form $-dt^2 + dx^2$). With this the entropy density becomes

$$s \equiv J^T_S = \frac{1}{8G_3}\left(\sqrt{L} + \sqrt{\bar{L}}\right) \tag{3.67}$$

[22] Our convention for $\epsilon_{\mu\nu}$ is $\epsilon_{vw} = -1$.

[23] The map f is defined by shooting 'radial' null geodesics inwards from the boundary, and is found to be of the form $f : (\lambda_{ir}, v, w) \mapsto (\lambda_{ir}, v + C_1, w + C_2)$.

CFT calculation: The entropy density from the Cardy formula is [24]

$$s = \sqrt{c\pi T_{vv}/3} + \sqrt{c\pi T_{ww}/3} \tag{3.68}$$

Using the identification 5.60 and 3.8, we can easily see that the two expressions 3.67 and 3.68 exactly match.

3.7.2 New metrics: non-equilibrium entropy

Bulk calculation: We will now follow a similar procedure as above, for the general solution in Section 3.2.3. We find that (in coordinate chart EF1)

$$ds^2|_{\mathcal{H}} = \frac{1}{4}d\alpha^2 = \frac{1}{4}(\sqrt{L}G'_+(\tilde{v})d\tilde{v} - \sqrt{\bar{L}}G'_-(\tilde{w})d\tilde{w})^2 \tag{3.69}$$

leading to the following area one form on the horizon

$$a = \frac{1}{2}\sqrt{L}G'_+(\tilde{v})d\tilde{v} - \frac{1}{2}\sqrt{\bar{L}}G'_-(\tilde{w})d\tilde{w} \tag{3.70}$$

Note that this could alternatively be obtained from the area form in 3.66 by a diffeomorphism. The resulting expression for the entropy current, following the steps above, is

$$\tilde{J}^{\tilde{v}}_s = \frac{1}{8G_3}\sqrt{\bar{L}}G'_-(\tilde{w}),\ \tilde{J}^{\tilde{w}}_S = \frac{1}{8G_3}\sqrt{L}G'_+(\tilde{v}) \tag{3.71}$$

Let us define, as before, the spacetime coordinates as $\tilde{x}, \tilde{t}$ with $(\tilde{v}, \tilde{w}) = \tilde{t} \pm \tilde{x}$. The entropy density is then given by

$$\tilde{s} = \tilde{J}^{\tilde{t}}_S = \frac{1}{4G_3}\left(\frac{1}{2}\sqrt{L}G'_+(\tilde{v}) + \frac{1}{2}\sqrt{\bar{L}}G'_-(\tilde{w})\right) \tag{3.72}$$

[24] Recall that both T_{vv}, T_{ww} are constant in this case. The more familiar form of 3.68, for a circular spatial direction of length 2π, is obtained by putting $S = 2\pi s$, $L_0 = 2\pi T_{vv}$, and $\bar{L}_0 = 2\pi T_{ww}$, which gives $S = 2\pi(\sqrt{cL_0/6} + \sqrt{c\bar{L}_0/6})$.

Note that the entropy current is divergenceless

$$\partial_\mu \tilde{J}^\mu_S = \partial_{\tilde{v}} \tilde{J}^{\tilde{v}}_S + \partial_{\tilde{w}} \tilde{J}^{\tilde{w}}_S = 0 \tag{3.73}$$

This has two implications:

1. No dissipation: We have entropy transfers between different regions with no net entropy loss or production (see Figure 3.6).

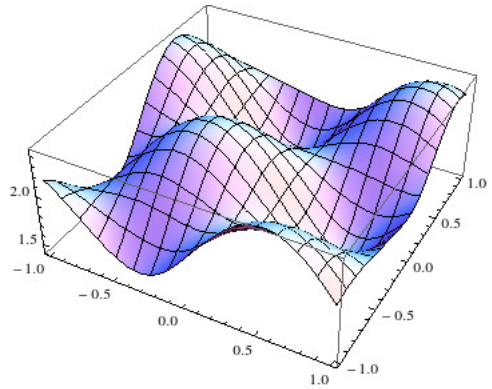

Figure 3.6: The undulating horizon of Figure 3.2 leads to the non-trivial entropy current 3.72. In this figure, we plot the entropy density $\tilde{s}$ as a function of $\tilde{v}, \tilde{w}$ for the right CFT. Note that although the entropy density fluctuates, the entropy flow here is such that there is no net entropy production (or destruction) (see Eq. 3.73).

2. Total entropy is not changed by the conformal transformation: The other implication is that the integrated entropy over a space-like (or null) slice Σ

$$\tilde{S} = \int_\Sigma \epsilon_{\mu\nu} J^\mu_S d\sigma^\nu \tag{3.74}$$

is independent of the choice of the slice. In particular, choosing the slice to be $\Sigma_0 : t = v + w = 0$, we get

$$\tilde{S} = \frac{1}{8G_3} \int_{\Sigma_0} \left(\sqrt{L} G'_+(\tilde{v}) d\tilde{v} - \sqrt{\bar{L}} G'_-(\tilde{w}) d\tilde{w} \right) = \frac{1}{8G_3} \int_{\Sigma_0} \left(\sqrt{L} dv - \sqrt{\bar{L}} dw \right) \tag{3.75}$$

$$= \frac{1}{8G_3} \int dx \left(\sqrt{L} + \sqrt{\bar{L}} \right) = \int dx \; s = S \tag{3.76}$$

Hence although the entropy density is clearly transformed, the total entropy is not changed by the conformal transformation.

CFT calculation:

In a non-equilibrium situation, there is no natural notion of an entropy. However under the adiabatic approximation, the instantaneous eigenstates of a time-dependent Hamiltonian are a fair representation of the actual time-dependent wave functions. The consequent energy level density can thus be used to define an approximate time-dependent entropy. Generalizing this principle to slow time *and* space variations, and applying this to the stress tensor, one expects a space-time dependent version of 3.68, namely

$$\tilde{s} = \sqrt{\frac{\pi c}{3}\tilde{T}_{\tilde{v}\tilde{v}}} + \sqrt{\frac{\pi c}{3}\tilde{T}_{\tilde{w}\tilde{w}}} \tag{3.77}$$

where the stress tensors are given by 3.41. Since we have made the adiabatic approximation, we expect the above formula to be valid only up to the leading order of space and time derivatives. Under this approximation, we have

$$8\pi G_3 T_{\tilde{v}\tilde{v}} = \frac{L}{4} G'_+(\tilde{v})^2, \quad 8\pi G_3 T_{\tilde{w}\tilde{w}} = \frac{\bar{L}}{4} G'_-(\tilde{w})^2 \tag{3.78}$$

which exactly agrees with the holographic entropy density in 3.72. [25]

Total entropy for $\mathcal{H}_R$ is unchanged by the conformal transformation:

Under the conformal transformation 3.34, the reduced density matrix ρ_R is changed by a unitary transformation:

$$\rho_R = \mathrm{Tr}_{\mathcal{H}_L}|\psi\rangle\langle\psi| = U_R\,\rho_{0,R}\,U_R^\dagger, \quad \rho_{0,R} = \mathrm{Tr}_{\mathcal{H}_L}|\psi_0\rangle\langle\psi_0| \tag{3.79}$$

[25] Note that throughout this chapter, we have not used the adiabatic approximation anywhere else. Thus, it is unsatisfactory to use this approximation here. It is, in fact, tempting to believe that the entropy density in 3.72, and not that in 3.77, actually gives the CFT entropy in general; however, this requires more investigation.

The total entropy of the system after the transformation is given by the von Neumann entropy $\tilde{S} = -\mathrm{T}r\rho_R \log \rho_R$ which, therefore, is equal to the entropy before; it is unchanged by the unitary transformation.

3.8 Conclusion and open questions

In this chapter we have solved the boundary value problem for 3D gravity (with $\Lambda < 0$) with independent boundary data on two asymptotically AdS_3 exterior geometries. The boundary data, specified in the form of arbitrary holographic stress tensors, yields spacetimes with wormholes, *i.e.* with exterior regions connected across smooth horizons. The explicit metrics are constructed by the technique of solution generating diffeomorphisms (SGD) from the eternal BTZ black string. By using the fact that the SGD's reduce to conformal transformations at both boundaries, we claim that the dual CFT states are specific time-dependent entangled states which are conformal transformations of the standard thermofield double. We compute various correlators and a dynamical entanglement entropy, in the bulk and in the CFT, to provide evidence for the duality. We also arrive at an expression for a non-equilibrium entropy function from the area-form on the horizon of these geometries.

Our work has implications for a number of other issues. We briefly discuss two of them below; a detailed study of these is left to future work.

3.8.1 ER=EPR

As mentioned above, our work constructs an infinite family of AdS-CFT dual pairs in which quantum states entangling two CFTs are holographically dual to spacetimes containing a wormhole region which connects the two exteriors. Both the quantum states and the wormhole geometries are explicitly constructed (see eqns. 3.28 and (3.12,3.20)). Our examples generalize the construction in [67, 138, 177][26] (for other remarks on unitary

[26] See [175, 225, 226]

transformations of the thermofield double and related geometries see [22,27,185,225,226]) and provide an infinite family of examples of the relation ER=EPR, proposed in [175]. Since this relation has been extensively discussed and debated in the literature ([22,27,225,226]), we would like to make some specific points pertaining to some of these discussions.

RR correlators vs RL correlators

It has been argued in [27], [226] and [225] that for typical entangled states connecting two CFTs, $\mathcal{H}_{\mathcal{R}}$ and $\mathcal{H}_{\mathcal{L}}$, correlators involving operators on the left and the right are suppressed relative to those involving operators all on the right. In particular, according to [27], correlators of the form $\langle O_R O_L \rangle$ are of the order $e^{-S}\langle O_R O_R \rangle$, where S is the entropy of the right sided Hilbert space.

In Section 3.5 we have computed general two-point functions, both of the kind $\langle O_R(P) O_R(Q) \rangle$ and $\langle O_R(P) O_L(Q') \rangle$.[27] In case of the eternal BTZ (dual to the standard thermofield double), an inspection of 3.45 and 3.47 suggests that as the boundary point $\mathbf{P}$ goes off to infinity, the cosh and sinh factors tend to be equal, thus $L(\mathbf{P}, \mathbf{Q}) \approx L(\mathbf{P}, \mathbf{Q}')$, thus there is no extra suppression in the two-sided correlator $\langle O_R\, O_L \rangle$. Of course, such a statement, regarding the standard thermofield double, has been regarded as somewhat of a special nature.

We are therefore naturally led to ask: what happens in case of the new solutions found in this chapter? The geodesic lengths $L(\mathbf{P}, \mathbf{Q})$ and $L(\mathbf{P}, \mathbf{Q}')$ are now given by 3.49 and 3.50. Once again, if the point P goes off towards the boundary of the Poincare plane, $\tilde{v} \to \infty$. Hence $G_+(\tilde{v}) \to \infty$ (since G_+ is a monotonically increasing function). Hence, both the geodesic lengths approach each other. Thus, we do not see any peculiar additional suppression, even for our general entangled state, arising when the second point of the correlation function is moved from the right to the left CFT.

[27] We use unprimed labels for operators on the right and primed labels for those on the left.

On the genericity of our family of examples

We start with the following Lemma.

Lemma: Any state $\in \mathcal{H} \otimes \mathcal{H}$,

$$|\Psi\rangle = \sum_{i,j} C_{ij}|i\rangle|j\rangle, \;\; C_{ij} \in \mathbb{C}, \tag{3.80}$$

can be expressed in the form

$$|\Psi\rangle = \sum_{i,j,n} e^{-\lambda_n} U_{L,in} U_{R,jn} |n\rangle|n\rangle \tag{3.81}$$

where U_R, U_L are two unitary operators and $\lambda_n \geq 0$.

Proof: Using the canonical map $\mathcal{H} \otimes \mathcal{H} \to \mathcal{H} \otimes \mathcal{H}^*$, we can regard the above state $|\Psi\rangle$ as an operator $\mathbf{\Psi}$ in $\mathcal{H}$, with matrix elements C_{ij}. Using the singular value decomposition theorem on a general complex matrix, we can write $C = U_L D U_R^\dagger$ where D is a diagonal matrix with real, non-negative entries. By denoting D as diag$[e^{-\lambda_n}]$, we get 3.81.

The state 3.81 can be regarded as a thermofield double with Hamiltonian $H = \sum_n \lambda_n/\beta |n\rangle\langle n|$ transformed by unitary operators U_L on the left and by U_R on the right. Thus, the above Lemma suggests that the most general entangled state 3.80 can be written as a unitary transformation of *some* thermofield double state. Now, note that the state 3.81 is of the same general form as that of 3.28 discussed in this chapter. *Are our states 3.28 the most general entangled states then?*

The answer is no, since the $U_{L,R}$ we use are made of Virasoro generators (see Appendix 3.10.1), and are not the most general unitaries of 3.81. However, in spite of this restriction, it is clear that the states 3.28 do form a fairly general class. Furthermore, if the states 3.81

are states in which only the stress tensor is excited, then indeed these states are all contained in our class of states 3.28. [28]

Weakly entangled states

To assess the genericity of our states, we ask a different question now: do our set of states 3.28, which are *all* explicitly dual to wormholes, include those with a very small entanglement entropy S for a given energy E?[29] The answer to this question turns out to be yes. As we have noted in the remarks around 3.76 and 3.79, the entropy S, which is actually the entanglement entropy of the right Hilbert space, is the same for all our states. However, the same manipulations as in 3.76 shows that the energy of these states are *not* the same; indeed by choosing the derivatives $G'_{\pm}$ to be large, we can make the energy of the transformed state to be much larger than that of the standard thermofield double. Stated in another way, for states of a given energy, our set of states includes states with entanglement entropy much less than that of the thermofield double. This is consistent with the proposal of [175] that even a small entanglement is described by a wormhole geometry.

3.8.2 Generalizations and open questions

It would be interesting to rephrase the results in this chapter in terms of the $SL(2,R) \times SL(2,R)$ Chern-Simons formulation [237] of three-dimensional gravity. By the arguments in [237], all diffeomorphisms (together with appropriate local Lorentz rotations) can be understood as gauge transformations of the Chern-Simons theory. The Chern-Simons formulation has been extended to the gauge group $SL(N,R) \times SL(N,R)$ to describe higher spin theories [30, 66]. It would be interesting to see whether the nontrivial gauge transformations in this chapter generalizes to these higher gauge groups, and hence to higher

[28] If a CFT dual to pure gravity were to exist, then our states 3.28 in such a theory would indeed be the most general state of the form 3.80. However, such a unitary theory is unlikely to exist [118, 178], although chiral gravity theories which are dual to CFTs with only the Virasoro operator have been suggested (see, e.g. [5]). We would like to thank Justin David for illuminating discussions on this point.

[29] This question was suggested to us by Sandip Trivedi.

spin theories. A possible application of our methods in this case would be to compute HEE by the prescriptions in [17] and [93] in the nontrivial higher spin geometries[30]. We hope to come back to this issue shortly.

The solutions presented in this chapter are generated by SGDs which can be regarded as forming a group $(\widetilde{\text{Vir}} \times \widetilde{\text{Vir}})_L \times (\widetilde{\text{Vir}} \times \widetilde{\text{Vir}})_R$. Here the first $\widetilde{\text{Vir}}$ denotes a group of SGDs which is parametrized by the function G_+, and so on. As we emphasized in 3.79, the reduced density matrix on the right ρ_R undergoes a unitary transformation under this group of transformations, leaving the entropy unaltered. The family of pure states 3.28 considered in this chapter can, therefore, be considered as an infinite family of purifications of the class of density matrices ρ_R; it would be interesting to see if these can be regarded as 'micro-states' which can 'explain' the entropy of ρ_R. We hope to return to this issue shortly.

It would also be interesting to use our work to explicitly study various types of holographic quantum quenches involving quantum states entangling two CFTs.[31] It would be of particular interest to study limiting cases of our solutions which correspond to shock-wave geometries.

3.9 Appendix

3.9.1 Coordinate systems for the eternal BTZ geometry

As we explained in the Introduction, the metric 5.57 describes only the region exterior to the black hole horizon 3.3. As is well-known, for constant $(L, \bar{L})$, 5.57 describes a standard BTZ black hole with mass M and angular momentum J given by

$$L = 8G_3(M + J),\ \bar{L} = 8G_3(M - J) \tag{3.82}$$

[30] We thank Rajesh Gopakumar for a discussion on this issue.
[31] For a single CFT, a similar computation was done in, e.g., [218, 234].

In this section we will describe various coordinate systems for this case. In particular, we will describe the five coordinate charts of Figure 3.1 which cover our spacetime.

Eddington-Finkelstein coordinates

EF1 (Right Exterior + Black Hole Interior) For a black hole with constant mass and angular momentum, it is straightforward to find a coordinate transformation from the (z, x_+, x_-) coordinates to a set of Eddington Finkelstein coordinates which we denote by EF1 (λ, v, y)

$$x_+ = v - \frac{1}{2\sqrt{L}} \log\left(\frac{\lambda - \lambda_0}{\lambda + \lambda_0}\right), \quad x_- = y + \sqrt{\frac{L}{\bar{L}}} v - \frac{1}{2\sqrt{\bar{L}}} \log\left(\frac{\lambda^2 - \lambda_0^2}{4\bar{L}}\right) \tag{3.83}$$

$$z = \sqrt{\frac{2}{\lambda_0^2}\left(\lambda - \sqrt{\lambda^2 - \lambda_0^2}\right)} \tag{3.84}$$

Under these transformations, we obtain the following metric

$$ds^2 = -\frac{2}{\bar{L}}\lambda_0(\lambda - \lambda_0)dv^2 + \frac{1}{\sqrt{\bar{L}}} dv d\lambda + \frac{\bar{L}}{4} dy^2 - (\lambda - \lambda_0) dv dy \tag{3.85}$$

The horizon 3.3 of the metric 5.57 is now located at $\lambda_0 = \sqrt{L\bar{L}}/2$. The metric is obviously smooth and describes the black hole interior.[32] To achieve a symmetry between the boundary coordinates, we find it convenient to make one further coordinate transformation from y to w

$$y = w - \sqrt{\frac{L}{\bar{L}}} v + \frac{1}{\sqrt{\bar{L}}} \log\left(\frac{\lambda + \lambda_0}{2\sqrt{\bar{L}}}\right) \tag{3.86}$$

In these new coordinates (λ, v, w), the metric becomes

$$ds^2 = \frac{d\lambda^2}{4(\lambda + \lambda_0)^2} + \frac{L}{4} dv^2 + \frac{\bar{L}}{4} dw^2 - \lambda dv dw + \frac{\sqrt{L}}{2(\lambda + \lambda_0)} dv d\lambda + \frac{\sqrt{\bar{L}}}{2(\lambda + \lambda_0)} dw d\lambda, \tag{3.87}$$

[32] It develops a coordinate singularity at the inner horizon $\lambda = -\lambda_0$; we do not discuss interpolation beyond the inner horizon in this chapter, although it can be easily done. In any case, there are strong reasons to believe that generically, the inner horizon and the associated exotic feature of infinitely repeating universes are unstable against even infinitesimal perturbations.

which is clearly symmetric between the 'boundary coordinates' v and w.

EF2 (Left Exterior + Black Hole Interior)

We can invent a second set of coordinate transformations starting from the metric in the (z, x_+, x_-) coordinates which would describe the left exterior region of the black hole along with the interior. This transformation is the following

$$x_+ = u + \frac{1}{2\sqrt{\bar{L}}} \log\left(\frac{\lambda_1 - \lambda_0}{\lambda_1 + \lambda_0}\right), \;\; x_- = y_1 + \sqrt{\frac{L}{\bar{L}}} u + \frac{1}{2\sqrt{\bar{L}}} \log\left(\frac{\lambda_1^2 - \lambda_0^2}{4\bar{L}}\right) \tag{3.88}$$

$$z = \sqrt{\frac{2}{\lambda_0^2}\left(\lambda_1 - \sqrt{\lambda_1^2 - \lambda_0^2}\right)} \tag{3.89}$$

The Eddington-Finkelstein metric obtained via this transformation is

$$ds^2 = -\frac{2}{\bar{L}}\lambda_0(\lambda_1 - \lambda_0)du^2 - \frac{1}{\sqrt{\bar{L}}} du d\lambda_1 + \frac{\bar{L}}{4} dy_1^2 - (\lambda_1 - \lambda_0) du dy_1 \tag{3.90}$$

As before, we make a further coordinate transformation y_1 to ω

$$y_1 = \omega - \sqrt{\frac{L}{\bar{L}}} u - \frac{1}{\sqrt{\bar{L}}} \log\left(\frac{\lambda_1 + \lambda_0}{2\sqrt{\bar{L}}}\right) \tag{3.91}$$

to obtain the following metric in the (λ_1, u, ω) coordinates

$$ds^2 = \frac{d\lambda_1^2}{4(\lambda_1 + \lambda_0)^2} + \frac{L}{4} du^2 + \frac{\bar{L}}{4} d\omega^2 - \lambda_1 du d\omega - \frac{\sqrt{\bar{L}}}{2(\lambda_1 + \lambda_0)} d\omega d\lambda_1 - \frac{\sqrt{L}}{2(\lambda_1 + \lambda_0)} du d\lambda_1 \tag{3.92}$$

EF3 (Left Exterior + White Hole Interior)

Starting from (z, x_+, x_-) coordinates, we do the following transformations

$$x_+ = v_1 - \frac{1}{2\sqrt{L}} \log\left(\frac{\lambda_1 - \lambda_0}{\lambda_1 + \lambda_0}\right), \;\; x_- = w_1 - \frac{1}{2\sqrt{\bar{L}}} \log\left(\frac{\lambda_1 - \lambda_0}{\lambda_1 + \lambda_0}\right) \tag{3.93}$$

$$z = \sqrt{\frac{2}{\lambda_0^2}\left(\lambda_1 - \sqrt{\lambda_1^2 - \lambda_0^2}\right)} \tag{3.94}$$

The metric obtained is

$$ds^2 = \frac{d\lambda_1^2}{4(\lambda_1 + \lambda_0)^2} + \frac{L}{4} dv_1^2 + \frac{\bar{L}}{4} dw_1^2 - \lambda_1 dv_1 dw_1 + \frac{\sqrt{L}}{2(\lambda_1 + \lambda_0)} dv_1 d\lambda_1 + \frac{\sqrt{\bar{L}}}{2(\lambda_1 + \lambda_0)} dw_1 d\lambda_1 \tag{3.95}$$

This metric covers the left exterior and the white hole interior.

EF4(Right Exterior + White Hole Interior)

Starting from (z, x_+, x_-) coordinates, we do the following transformations

$$x_+ = u_1 + \frac{1}{2\sqrt{L}} \log\left(\frac{\lambda - \lambda_0}{\lambda + \lambda_0}\right), \;\; x_- = \omega_1 + \frac{1}{2\sqrt{\bar{L}}} \log\left(\frac{\lambda - \lambda_0}{\lambda + \lambda_0}\right) \tag{3.96}$$

$$z = \sqrt{\frac{2}{\lambda_0^2}\left(\lambda - \sqrt{\lambda^2 - \lambda_0^2}\right)} \tag{3.97}$$

The metric obtained is

$$ds^2 = \frac{d\lambda^2}{4(\lambda + \lambda_0)^2} + \frac{L}{4} du_1^2 + \frac{\bar{L}}{4} d\omega_1^2 - \lambda du_1 d\omega_1 - \frac{\sqrt{L}}{2(\lambda + \lambda_0)} du_1 d\lambda - \frac{\sqrt{\bar{L}}}{2(\lambda + \lambda_0)} d\omega_1 d\lambda \tag{3.98}$$

This metric covers the right exterior and the white hole interior.

Regions of Overlap

Right Exterior The 'Right Exterior' region is described by both the EF1 (λ, v, w) and EF4 (λ, u_1, ω_1) coordinates. These are related by the following smooth coordinate transformations

$$v = u_1 + \frac{1}{\sqrt{L}} \log\left(\frac{\lambda - \lambda_0}{\lambda + \lambda_0}\right) \qquad w = \omega_1 + \frac{1}{\sqrt{L}} \log\left(\frac{\lambda - \lambda_0}{\lambda + \lambda_0}\right) \tag{3.99}$$

Black Hole Interior The 'Black Hole Interior' region is described by both the EF1 (λ, v, w) and EF2 (λ_1, u, ω) coordinates, which are related by the following smooth coordinate transformations

$$v = u + \frac{1}{\sqrt{L}} \log\left(\frac{\lambda_0 - \lambda_1}{\lambda_0 + \lambda_1}\right), \qquad w = \omega + \frac{1}{\sqrt{L}} \log\left(\frac{\lambda_0 - \lambda_1}{\lambda_0 + \lambda_1}\right), \quad \lambda_1 = \lambda \tag{3.100}$$

Left Exterior The 'Left Exterior' region is described by both the EF2 (λ_1, u, ω) and EF3 $(\lambda_1, v_1, \omega_1)$ coordinates, which are related by the following smooth coordinate transformations:

$$v_1 = u + \frac{1}{\sqrt{L}} \log\left(\frac{\lambda_1 - \lambda_0}{\lambda_1 + \lambda_0}\right) \qquad w_1 = \omega + \frac{1}{\sqrt{L}} \log\left(\frac{\lambda_1 - \lambda_0}{\lambda_1 + \lambda_0}\right) \tag{3.101}$$

White Hole Interior The 'White Hole Interior' finds a description in both the EF3 $(\lambda_1, v_1, \omega_1)$ and EF4 (λ, u_1, ω_1) coordinates, which are related by the following smooth coordinate transformations:

$$v_1 = u_1 + \frac{1}{\sqrt{L}} \log\left(\frac{\lambda_0 - \lambda}{\lambda_0 + \lambda}\right), \qquad w_1 = \omega_1 + \frac{1}{\sqrt{L}} \log\left(\frac{\lambda_0 - \lambda_1}{\lambda_0 + \lambda_1}\right), \quad \lambda = \lambda_1 \tag{3.102}$$

Kruskal coordinates

The union of all the above coordinate patches, together with a neighbourhood (indicated by K5 in Fig 3.1) of the bifurcation surface (the meeting point of the past and future horizons in the Penrose diagram) can be described by a set of Kruskal coordinates, in which the metric

reads

$$ds^2 = -\frac{1}{2\lambda_0} dU dV + \frac{1}{\sqrt{L}} U dV dy + \frac{\bar{L}}{4} dy^2 \tag{3.103}$$

The coordinate transformation between various EF coordinates and the Kruskal coordinates are given below.

1. Right exterior + Black Hole Interior : EF1 to Kruskal

The transformation from EF1 to the (U, V, y) coordinates is

$$U = -\exp(-\sqrt{L}v)(\lambda - \lambda_0), \;\; V = \exp(\sqrt{L}v), \;\; y = w - \sqrt{\frac{L}{\bar{L}}} v + \frac{1}{\sqrt{\bar{L}}} \log\left(\frac{\lambda + \lambda_0}{2\sqrt{\bar{L}}}\right) \tag{3.104}$$

In the 'Right Exterior' region, $\lambda > \lambda_0$, while in the 'Black Hole Interior', $\lambda < \lambda_0$. The above transformations give us the metric 3.103 in both the regions.

2. Left Exterior + Black Hole Interior : EF2 to Kruskal

The transformation from EF2 to (U, V, y) coordinates is

$$U = \exp(-\sqrt{L}u)(\lambda_1 + \lambda_0), \;\; V = -\exp(\sqrt{L}u)\frac{\lambda_1 - \lambda_0}{\lambda_1 + \lambda_0}, \;\; y = \omega - \sqrt{\frac{L}{\bar{L}}} u + \frac{1}{\sqrt{\bar{L}}} \log(\lambda_1 + \lambda_0) \tag{3.105}$$

with,

$$y_1 = y - \frac{2}{\sqrt{\bar{L}}} \log\left(\frac{\lambda_1 + \lambda_0}{2\sqrt{\bar{L}}}\right) \tag{3.106}$$

In the 'Black Hole Interior' $\lambda_1 < \lambda_0$, while in the 'Left Exterior' region $\lambda_1 > \lambda_0$. These coordinate transformations give us the metric 3.103 in both the regions.

3. Left Exterior + White Hole Interior : EF3 to Kruskal

The transformations from EF3 to the (U, V, y) coordinates is

$$U = \exp(-\sqrt{L}v_1)(\lambda_1 - \lambda_0), \;\; V = -\exp(\sqrt{L}v_1), \;\; y = w_1 - \sqrt{\frac{L}{\bar{L}}} v_1 + \frac{1}{\sqrt{\bar{L}}} \log\left(\frac{\lambda_1 + \lambda_0}{2\sqrt{\bar{L}}}\right) \tag{3.107}$$

In the 'Left Exterior' region $\lambda_1 > \lambda_0$, while in the 'White Hole Interior', $\lambda_1 < \lambda_0$. These transformations give us the metric 3.103 in both the regions.

4. Right Exterior + White Hole Interior : EF4 to Kruskal

The transformation from EF4 to the (U, V, y) coordinates is

$$U = -\exp(-\sqrt{L}u_1)(\lambda + \lambda_0), \;\; V = \exp(\sqrt{L}u_1)\frac{\lambda - \lambda_0}{\lambda + \lambda_0}, \;\; y = \omega_1 - \sqrt{\frac{L}{\bar{L}}}u_1 + \frac{1}{\sqrt{\bar{L}}}\log(\lambda + \lambda_0) \tag{3.108}$$

with,

$$y_1 = y - \frac{2}{\sqrt{\bar{L}}}\log\left(\frac{\lambda_1 + \lambda_0}{2\sqrt{\bar{L}}}\right) \tag{3.109}$$

In the 'White Hole Interior' $\lambda < \lambda_0$, while in the 'Right Exterior' region $\lambda > \lambda_0$. The above transformations give us the metric 3.103 in both the regions.

Poincare

In this section we show how the EF1, EF2 coordinates can, in fact, be obtained from Poincare coordinates $\zeta, X_\pm = X_0 \pm X_1$, in terms of which the metric is written as

$$ds^2 = \frac{1}{\zeta^2}(d\zeta^2 - dX_+ dX_-) \tag{3.110}$$

We will choose $L = \bar{L}$ for simplicity, so $\lambda_0 = L/2$.

The coordinate transformation from $X_\pm, \zeta$ to the EF1 coordinates is given by

$$v = \frac{\log(X_+)}{\sqrt{L}}, \; w = -\frac{1}{\sqrt{L}}\log\left(\frac{-X_+X_- + \zeta^2}{X_+}\right), \; \frac{\lambda}{\lambda_0} = \frac{-2X_+X_- + \zeta^2}{\zeta^2} \tag{3.111}$$

whereas the coordinate transformation from $X_\pm, \zeta$ to the EF2 coordinates is given by

$$u = \frac{1}{\sqrt{L}}\log\left(\frac{-X_+X_- + \zeta^2}{X_-}\right), \; \omega = -\frac{\log(X_-)}{\sqrt{L}}, \; \frac{\lambda_1}{\lambda_0} = \frac{-2X_+X_- + \zeta^2}{\zeta^2} \tag{3.112}$$

There are similar coordinate transformations between the other charts EF3/4 and Poincare.[33]

3.9.2 The new metrics in the charts EF3 and EF4

$$\text{EF3:}\quad ds^2 = \frac{1}{B^2}\Big[d\tilde{\lambda}_1^2 + A_+^2 d\tilde{v}_1^2 + A_-^2 d\tilde{w}_1^2 + 2A_+ d\tilde{u}_1 d\tilde{\lambda}_1 + 2A_- d\tilde{w}_1 d\tilde{\lambda}_1 \\ - \tilde{\lambda}_1\Big(B^2 + 2\Big(A_+\frac{H_-''(\tilde{w}_1)}{H_-'(\tilde{w}_1)} + A_-\frac{H_+''(\tilde{v}_1)}{H_+'(\tilde{v}_1)} + \tilde{\lambda}\frac{H_+''(\tilde{v}_1)H_-''(\tilde{w}_1)}{H_+'(\tilde{v}_1)H_-'(\tilde{w}_1)}\Big)\Big)d\tilde{w}_1 d\tilde{v}_1\Big] \quad (3.113)$$

where

$$A_+ = \sqrt{L}H_+'(\tilde{v}_1)(\tilde{\lambda}_1 + \tilde{\lambda}_{10}) - \tilde{\lambda}_1\frac{H_+''(\tilde{v}_1)}{H_+'(\tilde{v}_1)},\ A_- = \sqrt{\bar{L}}H_-'(\tilde{w}_1)(\tilde{\lambda}_1 + \tilde{\lambda}_{10}) - \tilde{\lambda}_1\frac{H_-''(\tilde{w}_1)}{H_-'(\tilde{w}_1)},\ B = 2(\tilde{\lambda}_1 + \tilde{\lambda}_{10})$$

$$\text{EF4}: \quad ds^2 = \frac{1}{B^2}\Big[d\tilde{\lambda}^2 + A_+^2 d\tilde{u}_1^2 + A_-^2 d\tilde{\omega}_1^2 - 2A_+ d\tilde{u}_1 d\tilde{\lambda} - 2A_- d\tilde{\omega}_1 d\tilde{\lambda} \\ - \tilde{\lambda}\Big(B^2 - 2\Big(A_+\frac{G_-''(\tilde{\omega}_1)}{G_-'(\tilde{\omega}_1)} + A_-\frac{G_+''(\tilde{u}_1)}{G_+'(\tilde{u}_1)} - \tilde{\lambda}\frac{G_+''(\tilde{u}_1)G_-''(\tilde{\omega}_1)}{G_+'(\tilde{u}_1)G_-'(\tilde{\omega}_1)}\Big)\Big)d\tilde{\omega}_1 d\tilde{u}_1\Big] \quad (3.114)$$

where

$$A_+ = \sqrt{L}G_+'(\tilde{u}_1)(\tilde{\lambda} + \tilde{\lambda}_0) + \tilde{\lambda}\frac{G_+''(\tilde{u}_1)}{G_+'(\tilde{u}_1)},\ A_- = \sqrt{\bar{L}}G_-'(\tilde{\omega}_1)(\tilde{\lambda} + \tilde{\lambda}_0) + \tilde{\lambda}\frac{G_-''(\tilde{\omega}_1)}{G_-'(\tilde{\omega}_1)},\ B = 2(\tilde{\lambda} + \tilde{\lambda}_0)$$

3.9.3 UV/IR cutoffs in EF coordinates

From AdS/CFT it is well-known that in a Fefferman-Graham coordinate system such as in 5.57, an IR cutoff surface $z = \epsilon$ in the asymptotically AdS spacetime corresponds to a UV cutoff ϵ in the CFT. We wish to express the IR cutoff in the geometry in terms of the EF

[33] As explained in [138] , it is possible to describe the BTZ black string in terms of a single Poincare chart. The BTZ black *hole* is a quotient of AdS_3, which in appropriate coordinates [29] corresponds to the periodic identification of the spatial direction; the BTZ string discussed in this chapter is obtained by decompactifying the spatial circle, which gives back AdS_3.

coordinates. By using the relation

$$z = \sqrt{\frac{2}{\lambda_0^2}\left(\lambda - \sqrt{\lambda^2 - \lambda_0^2}\right)} \tag{3.115}$$

we clearly see that $z = \epsilon$ for ϵ small, corresponds to $\lambda = 1/\epsilon^2$.

3.10 An alternative to Banados' metric

In a beautiful paper [218], Roberts showed that the Banados metric 5.57 can be obtained from the Poincare metric 5.54 by a Brown-Henneaux type diffeomorphism (an 'SGD' in the language of this chapter), given by

$$\begin{aligned} X_\pm &= f_\pm(x_\pm) + \frac{2z^2 f'_\pm(x_\pm)^2 f''_\mp(x_\mp)}{8f'_\pm(x_\pm)f'_\mp(x_\mp) - z^2 f''_\pm(x_\pm)f''_\mp(x_\mp)} \\ \zeta &= z\,\frac{\left(4f'_+(x_+)f'_-(x_-)\right)^{\frac{3}{2}}}{8f'_+(x_+)f'_-(x_-) - z^2 f''_+(x_+)f''_-(x_-)} \end{aligned} \tag{3.116}$$

It was shown in [218] that the above diffeomorphism reduces to a *conformal transformation* on the boundary, with the the following asymptotic form (as z→0)

$$\begin{aligned} X_\pm &= f_\pm(x_\pm) + O(z^2) \\ \zeta &= z\sqrt{f'_+(x_+)f'_-(x_-)} + O(z^3) \end{aligned} \tag{3.117}$$

It was also shown in this chapter that $L(x_+), \bar{L}(x_-)$ appearing in 5.57 can be obtained from the zero stress tensor through the conformal transformation $f_\pm$.

A different choice of gauge: The SGD 3.116 used by Roberts seems fairly involved compared to the ones we use in this chapter, e.g. 3.11. Can we obtain the metric 5.57 by a simpler SGD similar to ours, which nevertheless has the same conformal asymptotic form 3.117? The answer turns out to be yes. Indeed the simplest way of inventing such a

transformation is to take the asymptotic form 3.117 and gauge fix all the higher order terms in z to 0. We then have a new, exact transformation of the form

$$X_\pm = f_\pm(x_\pm), \qquad \zeta = z\sqrt{f'_+(x_+)f'_-(x_-)} \tag{3.118}$$

Note the similarity with our SGDs, say 3.11 (recall that $z \sim 1/\sqrt{\lambda}$ near the boundary). 3.118 transforms the Poincare metric to

$$\begin{aligned} ds^2 =& \frac{dz^2}{z^2} + \frac{f''_+(x_+)}{zf'_+(x_+)}dx_+dz + \frac{f''_-(x_-)}{zf'_-(x_-)}dx_-dz + \frac{1}{4}\left(\frac{f''_+(x_+)^2}{f'_+(x_+)^2}dx_+^2 + \frac{f''_-(x_-)^2}{f'_-(x_-)^2}dx_-^2\right) \\ & - \left(\frac{2}{z^2} - \frac{f''_+(x_+)f''_-(x_-)}{2f'_+(x_+)f'_-(x_-)}\right)dx_+dx_- \end{aligned} \tag{3.119}$$

A priori this is a new metric different from 5.57. However, the holographic stress tensor [28] obtained from this metric is the same as obtained from 5.57 given by 3.41. As discussed in Section 3.2.5 and 3.2.5, the above metric and 5.57 differ only by a trivial diffeomorphism, and are hence essentially identical.[34] Note that this example shows the enormous gauge ambiguity in the choice of a metric in AdS_3 (whose physical content is manifested in the boundary behaviour). Indeed, by the same token even the SGD's employed in this chapter are ambiguous; the solutions presented in Section 3.2 are one of a gauge equivalent class of metrics.

3.10.1 Unitary realization of conformal transformation

Under a finite, non-trivial, holomorphic coordinate transformation, $w \to w' = f(w)$, the stress tensor of a 2D CFT transforms as

$$\tilde{T}(w') = \left(\frac{\partial w'}{\partial w}\right)^{-2}[T(w) - \frac{c}{12}S(w', w)] \tag{3.120}$$

[34]Note that in this new metric 3.119, the position of the horizon is at $z = \infty$. Of course, it can be brought to a finite value by an additional coordinate transformation involving the radial coordinate.

with the Schwarzian derivative $\mathrm{S}(w', w)$ given by

$$S(w', w) = \left(\frac{\partial^3 w'}{\partial w^3}\right)\left(\frac{\partial w'}{\partial w}\right)^{-1} - \frac{3}{2}\left(\frac{\partial^2 w'}{\partial w^2}\right)^2\left(\frac{\partial w'}{\partial w}\right)^{-2} \tag{3.121}$$

For an infinitesimal transformation $w \to w' = f(w) = w + \epsilon(w)$, the Schwarzian derivative turns out to be

$$S(w', w) = \epsilon'''(w) + \mathcal{O}(\epsilon^2) \tag{3.122}$$

The change in the stress tensor, under such a transformation, becomes

$$\delta T(w) \approx -\epsilon(w)T'(w) - 2\epsilon'(w)T(w) - \frac{c}{12}\epsilon'''(w) + \mathcal{O}(\epsilon^2) \tag{3.123}$$

Now, the Laurent expansion of $T(w)$ and $\epsilon(w)$ is

$$T(w) = \sum_{m=-\infty}^{\infty} \frac{L_m}{w^{m+2}} \qquad\qquad \epsilon(w) = \sum_{m=-\infty}^{\infty} \epsilon_m w^{-m+1} \tag{3.124}$$

where $L_n^\dagger = L_{-n}$, $\epsilon_n^\dagger = -\epsilon_{-n}$ and the L_n's satisfy the Virasoro algebra

$$[L_m, L_n] = (m-n)L_{m+n} + \frac{c}{12}m(m^2-1)\delta_{m+n,0} \tag{3.125}$$

Plugging 3.124 into 3.123, we get

$$\delta L_m = \sum_{n=-\infty}^{\infty} \left\{(m+n)L_{m-n}\epsilon_n + \frac{c}{12}n(n^2-1)\epsilon_n\delta_{m-n,0}\right\} \tag{3.126}$$

We wish to construct a unitary operator $U = U(\epsilon)$ which implements the above conformal transformations, namely that it satisfies

$$U(\epsilon)^\dagger L_m U(\epsilon) - L_m = \delta L_m + O(\epsilon^2) \tag{3.127}$$

The required unitary operator, in fact, is

$$U(\epsilon) = \exp(\sum_{n=-\infty}^{\infty} \epsilon_n L_{-n}) \tag{3.128}$$

The proof is straightforward. Note that the LHS of 3.127 becomes

$$(1 - \sum_n \epsilon_{-n} L_n) L_m (1 + \sum_n \epsilon_n L_{-n}) - L_m = -\sum_{n=-\infty}^{\infty} \epsilon_{-n}(L_n L_m) + \sum_{n=-\infty}^{\infty} \epsilon_n (L_m L_{-n}) + \mathcal{O}(\epsilon^2)$$

After flipping the sign of n in the first sum, this becomes

$$\epsilon_n [L_m, L_{-n}]$$

which reduces to the expression 3.126 upon using the Virasoro algebra 3.125.

Thus, we have explicitly constructed a unitary operator U such that $U^\dagger T(w) U - T(w)$ is given by 3.123.

Chapter 4

Thermalization with chemical potentials and Higher Spin Black Holes[1]

4.1 Introduction and Summary

In this chapter, we will focus on two-dimensional conformal field theories (CFTs) on an infinite line $\sigma \in \mathbb{R}$. We will consider the system at $t = 0$ to be in a "quenched state"

$$|\psi_0\rangle = \exp[-\epsilon_2 H - \sum_{n=3}^{\infty} \epsilon_n W_n]|Bd\rangle \tag{4.1}$$

with $|Bd\rangle$ being the conformal boundary state (as discussed in the introduction). The exponential factors cut off the UV modes to make the state normalizable. W_n denote

[1]The contents of this chapter have partial overlap with the thesis work of Sorokhaibam Nilakash Singh. The conclusions arrived at are results of joint effort.

the additional conserved charges in the theory.[2] This choice of the quenched state is a generalization of that in [59] for which $\epsilon_n = 0$, for $n > 3$.

The wavefunction for $t > 0$ is given by

$$|\psi(t)\rangle = \exp[-iHt]|\psi_0\rangle \tag{4.2}$$

The questions we will explore, and answer, are: what is the long time behaviour of various observables in $|\psi(t)\rangle$? In particular, does the expectation value of an operator (or a string of operators) approach a constant? In other words, do they equilibrate? If so, (i) is the constant value characterized by a thermodynamic equilibrium, and (ii) what is the rate of approach to the constant value? More generally, we would also address, and partially answer, the questions: how does the existence and rate of thermalization depend on the initial state and the choice of observables?

Thermalization We find in this chapter that the expectation values of local observables (supported on a finite interval $A : \sigma \in [-l/2, l/2]$) asymptotically approach (see 4.12 for the precise statement) their values in an equilibrium ensemble,

$$\rho_{eqm} = \frac{1}{Z}\exp[-\beta H - \sum_n \mu_n W_n], \quad Z = \mathrm{Tr}\exp[-\beta H - \sum_n \mu_n W_n] \tag{4.3}$$

whose temperature and chemical potentials are related to the cutoff scales in 5.1 as follows

$$\beta = 4\epsilon_2, \quad \mu_n = 4\epsilon_n, \quad n = 3, 4, ... \tag{4.4}$$

The relations 4.4 are uniquely dictated by the requirement that the expectation values of the conserved charges $H, W_3, W_4, ...$ in the initial state match those in the mixed state 4.3

[2] For the purposes of this chapter, we will identify them with W_n-charges of 2D CFT, $n = 3, 4, ...$ (with $W_2 \equiv H$), although much of what we say will go through independent of this specific choice as long as these charges mutually commute and are defined from currents which are quasiprimary fields of the conformal algebra.

(see 4.52). In the absence of the extra parameters $\epsilon_n, n = 3, 4, ...$ this result is derived by the elegant method of conformal transformations [59]. In the presence of these parameters, this method is not available. In this chapter, we deal with the extra exponential factors in terms of an infinite series and do a resummation.

We emphasize that the thermalization we found above persists even when we have an integrable model with an infinite number of conserved charges. Relaxation in integrable systems has been found in recent years in the context of, e.g., (a) one-dimensional hardcore bosons [216], (b) transverse field Ising model [56], and (c) matrix quantum mechanics models [179]. The equilibrium ensembles in this context have been called a generalized Gibbs ensemble (GGE). Our present result on integrable conformal field theories adds to the list of these examples. Interestingly, the thermalization we find works even for free conformal field theories, e.g. a free scalar field theory.[3]

With the above identification of parameters, we will rewrite the initial quenched state 4.1 henceforth as

$$|\psi_0\rangle = \exp[-(\beta H - \sum_{n=3}^{\infty} \mu_n W_n)/4]|Bd\rangle \tag{4.5}$$

We find the following specific results:

1. Thermalization time scale for single local observables: We find that at large times

$$\langle\psi(t)|\phi_k(\sigma)|\psi(t)\rangle = \mathrm{Tr}\,(\phi_k(0)\rho_{eqm}(\beta,\mu_i)) + a_k\, e^{-\gamma_k t} + ... \tag{4.6}$$

where $\phi_k(\sigma)$ is an arbitrary quasiprimary field (labelled by an index k). Below we compute the thermalization exponent γ_k in a perturbation in the chemical potentials and to linear

[3]This happens essentially due to the fact that we consider here thermalization of local observables and that local field modes are mutually coupled even in a free field theory. Thermalization happens at times greater than the scale of localization, as we will see below.

order it is given by

$$\gamma_k = \frac{2\pi}{\beta}\left[\Delta_k + \sum_n \tilde{\mu}_n Q_{n,k} + O(\tilde{\mu}^2)\right], \ \tilde{\mu}_n \equiv \frac{\mu_n}{\beta^{n-1}}, \tag{4.7}$$

Here $\Delta_k = h_k + \bar{h}_k$ is the scaling dimension and $Q_{n,k}$ are the (shifted) W_n-charges (see 4.37 for the full definition) of the field ϕ_k (in case of primary fields) or of the minimum-dimension field which appears in the conformal transformation of ϕ_k. To obtain this result, we perform the infinite resummation mentioned below 4.4. At large times, the perturbation series for the one-point function in the chemical potentials exponentiates (see 4.37), to give the corrected exponent in the above equation. *In various related contexts, finite orders of perturbation terms in chemical potentials have been computed before [34, 89, 121]. Our finding in this chapter is that at large times, there is a regularity among the various orders leading to an exponential function as in 4.6 (see Section 4.2.2 for details).*

Universality: In the case of zero chemical potentials, it has been noted in [60], that although the relaxation time $\tau_k = \pi\epsilon_2/(2\Delta_k) = 2\pi\beta/(\Delta_k)$ is non-universal (in the sense that it depends on the specific initial state 4.1), the ratio of relaxation times for two different fields, namely, $\tau_{k_1}/\tau_{k_2} = \Delta_{k_2}/\Delta_{k_1}$ is universal (it depends only on the CFT data and not on the initial state and is hence expected to be valid for a general class of initial states). In the presence of the additional cut-off parameters $\epsilon_i, i = 3, ...$ in the initial state 4.1, the ratio $\tau_{k_1}/\tau_{k_2} = \gamma_{k_2}/\gamma_{k_1} = (\Delta_{k_2} + \sum_n \tilde{\mu}_n Q_{n,k_2})/(\Delta_{k_1} + \sum_n \tilde{\mu}_n Q_{n,k_1})$ is, however, not independent of the initial state.

However, as we will briefly discuss in Section 4.6, for a large class of quench states (e.g. where the energy density is uniform outside of a domain of compact support) the β-dependence of τ_k, in the absence of chemical potentials, can be understood as the dependence on the uniform energy density (see a related discussion in [129]). The time scales τ_k, therefore, do have a limited form of universality in the sense that it depends on a rather robust feature of the initial state. Our calculations in this chapter leads us to believe that this feature will continue in the presence of chemical potentials, in the sense that the additional dependence of

the time scales $1/\gamma_k$ on the μ_n is fixed by the charge densities corresponding to the additional conserved charges.

2. Multiple local observables, reduced density matrix: Besides the one-point functions discussed above, it turns out that we can demonstrate thermalization of *all operators in an interval A of length l*. It is convenient to define a 'thermalization function' $I_A(t)$ [71] as

$$I_A(t) = \mathrm{T}r(\hat{\rho}_{dyn,A}(t)\hat{\rho}_{eqm,A}(\beta,\mu_n)) = \frac{\mathrm{T}r(\rho_{dyn,A}(t)\rho_{eqm,A}(\beta,\mu_n))}{[\mathrm{T}r(\rho_{dyn,A}(t)^2)\mathrm{T}r(\rho_{eqm,A}(\beta,\mu_i)^2)]^{1/2}}$$
$$\rho_{dyn,A}(t) = \mathrm{T}r_{\bar{A}}\ |\psi(t)\rangle\langle\psi(t)|,\ \rho_{eqm,A}(\beta,\mu_n) = \mathrm{T}r_{\bar{A}}\ \rho_{eqm}(\beta,\mu_i) \tag{4.8}$$

Here $\hat{\rho} = \rho/\sqrt{\mathrm{T}r\rho^2}$ denotes a 'square-normalized' density matrix.[4][5] We show below that at large times the thermalization function has the form

$$I_A(t) = 1 - \alpha(\tilde{l})\ e^{-2\gamma_m t} + ...,\ \tilde{l} \equiv l/\beta \tag{4.9}$$

where γ_m refers to the exponent 4.7 for the operator ϕ_m with minimum scaling dimension.[6] $\alpha(\tilde{l})$ is computed as a power series in $\tilde{l}$ which we find using the short interval expansion, valid for $\tilde{l} \ll 1$, i.e. $l \ll \beta$.

Two immediate consequences of 4.9 are

(i) Thermalization of an arbitrary string of operators: Note, from 4.9, that

$$I_A(t) \xrightarrow{t\to\infty} 1, \tag{4.10}$$

[4]Note that operators in a Hilbert space H can themselves be regarded as vectors in $\mathsf{H}\times\mathsf{H}^*$; under this interpretation $\mathrm{T}r(A\ B)$ defines a positive definite scalar product. With this understanding, we will regard the hatted density matrices as unit vectors.

[5]Throughout this chapter, we will consider field theories with an infinite spatial extent. The entire Hilbert space is assumed to be of the form $\mathsf{H}_A \otimes \mathsf{H}_{\bar{A}}$. $\mathrm{T}r_{\bar{A}}$ implies tracing over $\mathsf{H}_{\bar{A}}$.

[6]We will assume here that the spectrum of such Δ's is bounded below by a finite positive number. In case of a free scalar field theory, we can achieve this by considering a compactified target space.

Since the square-normalized density matrices can be regarded as unit vectors (in the sense of footnote 4), and $I_A(t)$ can be regarded as the scalar product $\hat{\rho}_{dyn,A}(t)\cdot\hat{\rho}_{eqm,A}$, 4.10 clearly implies

$$\hat{\rho}_{dyn,A}(t) \xrightarrow{t\to\infty} \hat{\rho}_{eqm,A} \tag{4.11}$$

This implies the following statement of thermalization for an arbitrary string of local operators (with $\sigma_1, \sigma_2, ... \in A$)

$$\begin{aligned}\langle\psi(t)|O(\sigma_1,t_1)O(\sigma_2,t_2)...|\psi(t)\rangle = \mathrm{Tr}(\hat{\rho}_{dyn,A}(t)O(\sigma_1,t_1)O(\sigma_2,t_2)...)\\ \xrightarrow{t\to\infty} \mathrm{Tr}(\hat{\rho}_{eqm,A}O(\sigma_1,t_1)O(\sigma_2,t_2)...).\end{aligned} \tag{4.12}$$

(ii) Long time behaviour of reduced density matrix:

Carrying on with the interpretation of $I_A(t)$ as a scalar product, we can infer following asymptotic behaviour of $\hat{\rho}_{dyn}(t)$ from 4.9:

$$\hat{\rho}_{dyn,A}(t) = \hat{\rho}_{eqm,A}(\beta,\mu_i)\left(1-\alpha\, e^{-2\gamma_m t}+...\right) + \hat{Q}\left(\sqrt{2\alpha}\, e^{-\gamma_m t}+...\right) \tag{4.13}$$

where $\mathrm{Tr}(\hat{Q}^2) = 1, \quad \mathrm{Tr}(\hat{\rho}_{eqm,A}(\beta,\mu_i)\hat{Q}) = 0$. We will specify further properties of $\hat{Q}$ later on.

Importance of local observables: In case of a free massless scalar field, it is easy to show that quantities like $\langle\psi(t)|\alpha_1^2\alpha_1^\dagger|\psi(t)\rangle$ perpetually oscillate and never reach a constant (see a related calculation in [179]). The modes α_n represent Fourier modes and are non-local. Indeed, as [60,65,71] showed, in the absence of chemical potentials, the exponential term in 4.9 is $e^{-2\gamma_m(t-l/2)}$ and the thermalization sets in only after t exceeds $l/2$. Thus, for $l=\infty$, there is no thermalization, which is consistent with the above observation about perpetual oscillations. We expect the form $e^{-2\gamma_m(t-l/2)}$ to

continue to hold in the presence of chemical potentials[7], since the effect of the chemical potentials on the exponent γ_k can be viewed as a shift of the anomalous dimension $\delta\Delta_k = \sum_n \tilde{\mu}_n Q_{n,k} + O(\tilde{\mu}^2)$ (see, e.g. 4.64). This shows that, as in the case of zero chemical potentials, equilibration sets in only after t exceeds $l/2$. We will see a similar phenomena next in the context of a decay of perturbations to a thermal state.

3. Decay of perturbations to a thermal state: We compute (see Section 4.4 for details) the time-dependent two-point Green's function $G_+(t, l; \beta, \mu)$ for two points spatially separated by a distance l. We find that for $t, l, t-l \gg \beta$, the time-dependence is exponential, with the same exponent as in 4.6:

$$G_+(t, l; \beta, \mu) \equiv \frac{1}{Z} \mathrm{Tr}\left(\phi_k(l, t)\phi_k(0, 0)e^{-\beta H - \sum_n \mu_n W_n}\right) = \text{const } e^{-\gamma_k t} \tag{4.14}$$

Note that the above thermalization sets in for $t > l$. For $t < l$, the two-point function has an exponential decay in the spatial separation (see Section 4.4 and Figure 4.3).

The computation of the above relaxation times in the presence of an arbitrary number of chemical potentials uses the technique, described above, of summing over an infinite number of Feynman diagrams, and is one of the main results of this chapter.

4. Collapse to higher spin black holes: In [138, 177] the bulk dual to the time-dependent state 5.2 corresponding to initial condition 5.1, for large central charges, has been constructed in the case of zero chemical potentials. The dual geometry corresponds to one half of the eternal BTZ (black string) geometry, whose boundary represents an end-of-the-world brane. In [67] the result has been extended to the case of non-zero angular momentum and a Chern-Simons charge. In case of an infinite number of chemical potentials, a bulk dual to the equilibrium ensemble 4.3 has been identified, in the context of the

[7] Although, in the short-interval expansion employed in this chapter to derive 4.9, which uses $t \gg \beta \gg l$, such an l-dependence in the exponent cannot be easily seen from the pre-factor $\alpha(l)$ unless one sums over an infinite orders in $\tilde{l}$.

Gaberdiel-Gopakumar hs(λ) theory [119], as a higher spin black hole with those chemical potentials [131, 162]. It is natural to conjecture [67, 179] that the time-development 5.2 should be dual to a collapse to this higher spin black hole. At late times, therefore, the thermalization exponent found above should correspond to the quasinormal frequency of the higher spin black hole. We find that (see Section 4.5) this is indeed borne out in a specific example.

The plan of this chapter is as follows. The results 1, 2, 3 and 4 above are described in Sections 5.2.2, 4.3, 4.4 and 4.5, respectively. The resummation of an infinite number of Feynman diagrams (corresponding to insertions of arbitrary number of chemical potential terms) is discussed in Section 4.2.2, which uses results in Appendix 5.7.3. The calculation of the overlap of reduced density matrices in Section 4.3 needs the use of the short-interval expansion, which is described in Appendix 4.7.2. In Section 4.6 we present our conclusions and make some remarks on inhomogeneous quenches.

4.2 One-point functions

In this section we will consider the behaviour of the following one-point functions of a quasiprimary field $\phi_k(\sigma)$

$$\begin{aligned} \langle \phi_k(\sigma,t)\rangle_{dyn} &\equiv \langle \psi(t)|\phi_k(\sigma)|\psi(t)\rangle, \\ \langle \phi_k(\sigma)\rangle_{eqm} &\equiv \mathrm{Tr}\left(\phi_k(\sigma)\rho_{eqm}(\beta,\mu_n)\right) \end{aligned} \tag{4.15}$$

We will briefly recall how these are computed in the absence of the chemical potentials [59, 96]. The first expectation value corresponds to the one-point function on a strip geometry, with complex coordinate $w = \sigma + i\tau$, $\sigma \in (-\infty, \infty)$, $\tau \in (-\beta/4, \beta/4)$ where τ is eventually to be analytically continued to $\tau = it$. This can be conformally transformed to an upper half

plane by using the map

$$z = ie^{(2\pi/\beta)w} \tag{4.16}$$

For a primary field with $h_k = \bar{h}_k$ (of the form $\phi_k(w,\bar{w}) = \varphi_k(w)\varphi_k(\bar{w})$), this procedure gives [8](for other primary fields, the one-point function vanishes)

$$\begin{aligned}\langle\phi_k(\sigma,t)\rangle_{dyn} &= \langle\phi_k(w,\bar{w})\rangle_{str} = \left(\frac{\partial z}{\partial w}\right)^{h_k}\left(\frac{\partial \bar{z}}{\partial \bar{w}}\right)^{\bar{h}_k}\langle\phi_k(z,\bar{z})\rangle_{UHP} \\ &= a_k\left(e^{2\pi t/\beta}+e^{-2\pi t/\beta}\right)^{-2h_k} \sim a_k e^{-\gamma_k^{(0)}t}+..., \;\; \gamma_k^{(0)} = 2\pi\Delta_k/\beta = 4\pi h_k/\beta \end{aligned} \tag{4.17}$$

We have used the following result for the one-point function on the UHP:

$$\langle\phi_k(z,\bar{z})\rangle_{UHP} = A_k\langle\varphi_k(z)\varphi_k^*(z')\rangle_{UHP} = A_k(z-z')^{-2h_k}, \;\; h_k = \bar{h}_k, \;\; z' = \bar{z} \tag{4.18}$$

which follows by using the method of images where the antiholomorphic factor of $\phi_k(z,\bar{z})$ on the upper half plane at the point $(z,\bar{z})$ is mapped (up to a constant) to the holomorphic φ_k^* [9] on the lower half plane at the image point $(z',\bar{z}')$ with $z' = \bar{z}, \bar{z}' = z$ [74, 96]. In the above a_k, A_k are known numerical constants. Note that

$$z = ie^{2\pi(\sigma+i\tau)/\beta} = ie^{2\pi(\sigma-t)/\beta}, \;\; z' = \bar{z} = -ie^{2\pi(\sigma-i\tau)/\beta} = -ie^{2\pi(\sigma+t)/\beta} \tag{4.19}$$

so that in the large time limit we have

$$t \to \infty \Rightarrow z \to 0, \bar{z} \to -i\infty. \tag{4.20}$$

The second, thermal, expectation value in 4.15, for $\mu_n = 0$, corresponds to a cylindrical geometry in the w-plane, with $\tau = 0$ identified with $\tau = \beta$. By using the same conformal

[8]The subscripts *str, cyl* will denote a 'strip' and a 'cylinder', respectively.
[9]We distinguish φ_k^* from φ_k to allow for charge conjugation.

map 4.16 this can be transformed to a one-point function on the plane. For a primary field the latter vanishes. Hence 4.6 is trivially satisfied.

For a quasiprimary field ϕ_k, its conformal transformation generates additional terms, including possibly a c-number term c_k (e.g. the Schwarzian derivative term for $\phi_k = T_{ww}$) and generically lower order operators. The c-number term does not distinguish between a plane and an UHP. This leads to the following overall result (for $\mu_n = 0$):

$$\begin{aligned} &\langle \phi_k(\sigma) \rangle_{eqm} = \langle \phi_k(w, \bar{w}) \rangle_{cyl} = c_k, \\ &\langle \phi_k(\sigma, t) \rangle_{dyn} = \langle \phi_k(w, \bar{w}) \rangle_{str} = c_k + a_k e^{-\gamma_k^{(0)} t} + ..., \ \ \gamma_k^{(0)} = 2\pi \Delta_k / \beta, \end{aligned} \tag{4.21}$$

where Δ_k now is the scaling dimension of the minimum-dimension operator in a $T(z_1)\phi_k(z)$ OPE. This is clearly of the general form 4.6 for $\mu_n = 0$.

We now turn to a discussion of these expectation values 4.15 in the presence of chemical potentials $\mu_n, n = 3, 4, ...$, as in 5.1 and 4.3. We will denote the new conserved currents as $\mathcal{W}_n(w)$ and $\bar{\mathcal{W}}_n(\bar{w})$, $n = 3, 4, ...$ The conserved charge, W_n, is defined as

$$W_n = \frac{1}{2\pi} \int_\Gamma W_{\tau\tau...\tau} d\sigma = \frac{1}{2\pi} \int_\Gamma \left(i^n dw_1 \, \mathcal{W}_n(w_1) + (-i)^n d\bar{w}_1 \, \bar{\mathcal{W}}_n(\bar{w}_1) \right) \tag{4.22}$$

Here the contour Γ is taken to be a $\tau =$ constant line along which $dw_1 = d\bar{w}_1 = d\sigma$. Under the conformal transformation 4.16 to the plane/UHP, the holomorphic part of the contour integral becomes

$$W_n|_{hol} = \frac{i^n}{2\pi} \left(\frac{2\pi}{\beta} \right)^{n-1} \int_{\Gamma_1} dz_1 \left[z_1^{n-1} \mathcal{W}_n(z_1) + \sum_{m=1}^{[n/2]} a_{n,n-2m} z_1^{n-2m-1} \mathcal{W}_{n-2m}(z_1) \right] \tag{4.23}$$

where the $a_{n,n-2m}$ denote the mixing of $\mathcal{W}_n(z_1)$ with lower order W-currents under conformal transformations [47, 210]. The contour Γ_1 is an image of the contour Γ onto the plane. The expression for the antiholomorphic part $W_n|_{antihol}$ is similar.

As mentioned before, in this chapter we will regard the W_n as conserved charges of a W-algebra, although the results we derive will be equally valid as long as these charges, together with H, form a mutually commuting set, and the currents $(\mathcal{W}_n(w), \bar{\mathcal{W}}_n(\bar{w}))$ are quasiprimary fields.

4.2.1 One-point function on the cylinder with chemical potentials

For simplicity we first consider the equilibrium expectation value in 4.15. Unfortunately, unlike the thermal factor above, the factor $e^{-\sum_n \mu_n W_n}$ in 4.3 cannot be dealt with in terms of a conformal map. We will, therefore, treat this factor as an operator insertion, and write

$$\langle \phi_k(\sigma)\rangle_{eqm} \equiv \mathrm{T}r\left(\phi_k(w,\bar{w})\rho_{eqm}(\beta,\mu_n)\right) = \frac{\langle e^{-\sum_n \mu_n W_n}\phi_k(w,\bar{w})\rangle_{cyl}}{\langle e^{-\sum_n \mu_n W_n}\rangle_{cyl}} \equiv \langle \phi_k(w,\bar{w})\rangle^{\mu}_{cyl} \tag{4.24}$$

We will now illustrate how to compute this for a single chemical potential, say μ_3, using perturbation theory Feynman diagrams:[10]

$$\langle \phi_k(w,\bar{w})\rangle^{\mu}_{cyl} = \langle \phi_k(w,\bar{w})\rangle_{cyl} - \mu_3\langle W_3\phi_k(w,\bar{w})\rangle^{conn}_{cyl} + \frac{\mu_3^2}{2!}\langle\, W_3W_3\phi_k(w,\bar{w})\rangle^{conn}_{cyl} + \mathcal{O}(\mu_3^3) \tag{4.25}$$

The first term in the above expression is the constant c_k that we already encountered in 4.21. For a holomorphic primary field ϕ_k, the second, $O(\mu_3)$, term, transformed on to the plane, gives

$$\langle W_3\phi_k(w)\rangle^{conn}_{cyl} = \frac{2\pi}{\beta^2}z^{h_k}\left[i^3\int_{\Gamma_1} dz_1\; z_1^2\langle \mathcal{W}_3(z_1)\phi_k(z)\rangle^{conn}_{\mathbb{C}} + (-i)^3\int_{\Gamma_1} d\bar{z}_1\; \bar{z}_1^2\langle \bar{\mathcal{W}}_3(\bar{z}_1)\phi_k(z)\rangle^{conn}_{\mathbb{C}}\right] \tag{4.26}$$

Here we have used the contour representations 4.22 and 4.23. The correlator inside the second integral obviously vanishes (it factorizes into a holomorphic and an antiholomorphic

[10] The superscript *conn* denotes 'connected'.

one-point functions, leading to a vanishing connected part). The first integral vanishes unless $\phi_k = \mathcal{W}_3$ (this uses the orthogonality of the basis of quasiprimary fields). In the latter case, using

$$\langle \mathcal{W}_3(z_1)\mathcal{W}_3(z)\rangle_{\mathbb{C}} = \frac{c/3}{(z_1 - z)^6}$$

the integral evaluates to $c/(90z^3)$; combining with the factor of z^3 outside ($h_k = 3$ in this case) we get a z-independent constant, as we must, because of translational invariance on the plane. With an antiholomorphic primary field ϕ_k, the calculation is isomorphic. For a primary field with nonvanishing $h_k, \bar{h}_k$ the result vanishes. For quasiprimary ϕ_k, as well as for other W_n charges, the conformal transformation to the plane additionally generates lower order operators (see, e.g. 4.23)), each of which can be dealt with as in 4.26. The result is a finite constant which we will denote as

$$\langle W_n \phi_k(w, \bar{w})\rangle = c_{n,k}$$

(this will be non-vanishing only for special choices of ϕ_k, e.g. $\phi_k = \mathcal{W}_n$). As explained above, for $n = 3$ and $\phi_k(w, \bar{w}) = \mathcal{W}_3(w)$, $c_{n,k} = -2\pi c/(90\beta^2)$.

In a similar fashion, the $O(\mu_3^2)$ term in 4.25 can be transformed to the plane. Again, we present the explicit expression for the simple case of a holomorphic primary field ϕ_k.

$$\begin{aligned}\langle W_3 W_3 \phi_k(w)\rangle_{cyl}^{conn} = \Big(\frac{2\pi}{\beta^2}\Big)^2 z^{h_k} \Big[i^6 \int_{\Gamma_1} dz_1 \int_{\Gamma_2} dz_2 \langle \mathcal{W}_3(z_1)\mathcal{W}_3(z_2)\phi_k(z)\rangle_{\mathbb{C}}^{conn}\ z_1^2 z_2^2 \\ + (-i)^6 \int_{\Gamma_1} d\bar{z}_1 \int_{\Gamma_2} d\bar{z}_2 \langle \bar{\mathcal{W}}_3(\bar{z}_1)\bar{\mathcal{W}}_3(\bar{z}_2)\phi_k(z)\rangle_{\mathbb{C}}^{conn}\ \bar{z}_1^2 \bar{z}_2^2 + \int_{\Gamma_1} dz_1 \int_{\Gamma_2} d\bar{z}_2 \langle \mathcal{W}_3(z_1)\bar{\mathcal{W}}_3(\bar{z}_2)\phi_k(z)\rangle_{\mathbb{C}}^{conn}\ z_1^2 \bar{z}_2^2 \\ + \int_{\Gamma_1} d\bar{z}_1 \int_{\Gamma_2} dz_2 \langle \bar{\mathcal{W}}_3(\bar{z}_1)\mathcal{W}_3(z_2)\phi_k(z)\rangle_{\mathbb{C}}^{conn}\ \bar{z}_1^2 z_2^2 \Big] \end{aligned} \tag{4.27}$$

For holomorphic quasiprimary ϕ_k, additional, similar, terms appear due to the generation of lower order operators under conformal transformation to the plane. Only the holomorphic correlator survives (as in the O(μ_3) calculation). Thus, e.g. if $\phi_k = T(z)$, the stress tensor,

we have

$$\langle \mathcal{W}_3(z_1)\mathcal{W}_3(z_2)T(z)\rangle_{\mathbb{C}} = \frac{c}{(z_1-z_2)^4(z_1-z)^2(z_2-z)^2}$$

Again, after performing the integration over z_1 and z_2, we obtain a z-independent constant, as we must. The analysis of more general fields ϕ_k and two arbitrary W-charges is straightforwardly generalizable. The result is a finite constant (can be zero for a particular ϕ_k) which we denote as

$$\langle W_m W_n \phi_k(w,\bar{w})\rangle = c_{mn,k}$$

Note that in 4.27 the result does not depend on the location of the contours Γ_1, Γ_2 on the plane, since the W-currents are conserved.

Summarizing, we get

$$\langle \phi_k(w,\bar{w})\rangle^{\mu}_{cyl} = c_k - \sum_n \mu_n \; c_{n,k} + \frac{1}{2!}\sum_{m,n} \mu_m\mu_n \; c_{mn,k} + O(\mu^3) \tag{4.28}$$

4.2.2 One-point function on the strip with chemical potentials

Similarly to the previous subsection, we will treat the μ-deformations in 5.1 as operator insertions:

$$\langle \phi_k(\sigma,t)\rangle_{dyn} \equiv \langle \psi(t)|\phi_k(\sigma)|\psi(t)\rangle = \frac{\langle e^{-\sum_n \mu_n W_n/4}\, \phi_k(w,\bar{w})\, e^{-\sum_n \mu_n W_n/4}\rangle_{str}}{\langle e^{-\sum_n \mu_n W_n/2}\rangle_{str}} \equiv \langle \phi_k(w,\bar{w})\rangle^{\mu}_{str} \tag{4.29}$$

As before, we begin by illustrating the calculation of this quantity with the simplest case of a single chemical potential μ_3, using perturbation theory Feynman diagrams:

$$\begin{aligned}\langle \phi_k(w,\bar{w})\rangle^{\mu}_{str} &= \langle \phi_k(w,\bar{w})\rangle_{str} - \frac{\mu_3}{4}\langle\{W_3, \phi_k(w,\bar{w})\}\rangle^{conn}_{str} \\ &+ \left(\frac{\mu_3}{4}\right)^2 \frac{1}{2!}(\langle\{W_3W_3, \phi_k(w,\bar{w})\}\rangle^{conn}_{str} + 2\langle W_3\phi_k(w,\bar{w})W_3\rangle^{conn}_{str}) + \mathcal{O}(\mu_n^3)\end{aligned} \tag{4.30}$$

The $\{\ ,\}$ denotes an anticommutator. The operator ordering implies the following: when W_3 appears on the left of $\phi_k(w,\bar{w})$, e.g., in $\langle W_3\phi_k(w,\bar{w})\rangle$, the integration contour 4.22 for W_3 on the strip lies above the point $(w,\bar{w})$; similarly when W_3 appears on the right of $\phi_k(w,\bar{w})$, e.g. in $\langle\phi_k(w,\bar{w})W_3\rangle$, the contour for W_3 is below the point $(w,\bar{w})$.

The first, μ-independent, term in the above expansion is already calculated in 4.21.

$\mathcal{O}(\mu_n)$ Calculation

As before, we find it convenient to use the conformal transformation 4.16. The correlator on the strip then reduces to that on the UHP, as in the $\mu = 0$ case before. For a holomorphic primary field ϕ_k, this gives

$$\langle W_3\phi_k(w)\rangle^{conn}_{str} = \frac{2\pi}{\beta^2}z^{h_k}\left[i^3\int_{\Gamma_1}dz_1\ z_1^2\langle\mathcal{W}_3(z_1)\phi_k(z)\rangle^{conn}_{\text{UHP}} + (-i)^3\int_{\Gamma_1}d\bar{z}_1\ \bar{z}_1^2\langle\bar{\mathcal{W}}_3(\bar{z}_1)\phi_k(z)\rangle^{conn}_{\text{UHP}}\right] \tag{4.31}$$

where the operator ordering explained above implies that the contour Γ_1 lies to the left of the point $(z,\bar{z})$ on the UHP. Now, in the analogous calculation 4.26, the second connected correlator on the complex plane vanished because of factorization into one-point functions. Correlators on the UHP are, however, related to those on the plane by the method of images (an example of which we saw in 4.18). In particular, $\bar{\mathcal{W}}_3$ at the point $(z_1,\bar{z}_1)$ on the UHP becomes the holomorphic operator $\mathcal{W}_3^* = -\mathcal{W}_3$ on the LHP at the point $(z_1',\bar{z}_1')$ with $z_1' = \bar{z}_1$ [74, 96]. The contour Γ_1 gets mapped to its mirror image Γ_1' on the lower half plane. With this, we get

$$\langle W_3\phi_k(w)\rangle^{conn}_{str} = \frac{2\pi}{\beta^2}z^{h_k}\left[i^3\int_{\Gamma_1+\Gamma_1'}dz_1\ z_1^2\langle\mathcal{W}_3(z_1)\phi_k(z)\rangle^{conn}_{\mathbb{C}}\right] \tag{4.32}$$

On the complex plane, the contour Γ_1 on the UHP can be deformed to Γ_1' on the LHP, hence the two contours simply yield a factor of 2. In fact, combining with the other ordering, and applying a similar reasoning, we get an overall factor of 4. Thus, combining with results

from Section 4.2.1, we get, for holomorphic primary fields

$$-\frac{\mu_3}{4}\langle\{W_3,\phi_k(w)\}\rangle_{str}^{conn}=-\mu_3\langle W_3\phi_k(w)\rangle_{cyl}^{conn} \tag{4.33}$$

A similar statement is true for an antiholomorphic primary field.

Let us turn now to primary fields $\phi_k(w,\bar{w})$ with $h_k,\bar{h}_k\neq 0$ (of the form $\phi_k(w,\bar{w})=\varphi_k(w)\varphi_k(\bar{w})$, as discussed before in the context of 4.18). In the cylinder calculation in Section 4.2.1 the μ-corrections for these vanished. In the present case, they are non-zero for operators of the form $\phi_k(w,\bar{w})=\varphi_k(w)\bar{\varphi}_k(\bar{w})$, with $h_k=\bar{h}_k$ (as in 4.17). After conformally transforming to the UHP, we regard $\bar{\varphi}_k$ on the UHP as φ_k^* at the image point on the LHP (up to a constant). Combining with the arguments used for the holomorphic operators, we eventually get

$$\begin{aligned}&\frac{\langle\{W_3,\phi_k(w,\bar{w})\}\rangle_{str}^{conn}}{\langle\phi_k(w,\bar{w})\rangle_{str}}=i^3\frac{2\pi}{\beta^2}(z\bar{z})^h I_3(z,z'),\\ &I_3(z,z')\equiv\int_{\Gamma_1+\Gamma_1'+\tilde{\Gamma}_1+\tilde{\Gamma}_1'}dz_1\ z_1^2\langle\mathcal{W}_3(z_1)\varphi_k(z)\varphi_k^*(z')\rangle_{\mathbb{C}}^{conn}/\langle\varphi_k(z)\varphi_k^*(z')\rangle_{\mathbb{C}}^{conn}\end{aligned} \tag{4.34}$$

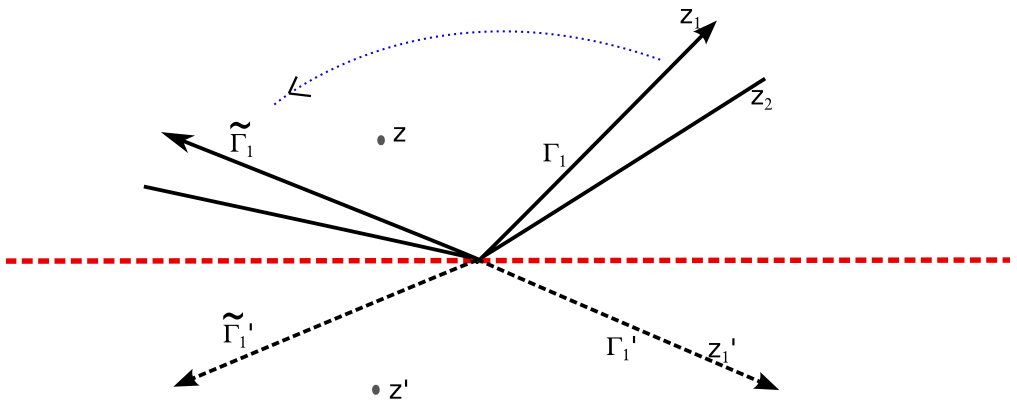

Figure 4.1: Various contours needed to compute the W_n insertions in 4.30. At late times, the insertion of each contour, irrespective of the position of the contour, amounts to insertion of a given factor linear in t. This allows to resum arbitrary orders of arbitrary W_n-charge insertions, leading to the exponential time-dependence as in 4.6. See Figure 4.2 for more.

The ratio of correlators inside the integral is given by

$$\langle \mathcal{W}_3(z_1)\varphi_k(z)\varphi_k^*(z')\rangle_{\mathbb{C}}^{conn} / \langle \varphi_k(z)\varphi_k^*(z')\rangle_{\mathbb{C}}^{conn} = q_3 \frac{(z-z')^3}{(z_1-z)^3(z_1-z')^3} \tag{4.35}$$

where q_3 is the $\mathcal{W}_3$-charge of the field ϕ_k. Integrals of the kind 4.34 are discussed in detail in Appendix 4.7.1. The final result (see 4.71) is that the $O(\mu_3)$ correction, in the long time limit 4.20, is given by (using that all four contours $\Gamma_1, \tilde{\Gamma}_1, \Gamma_1', \tilde{\Gamma}_1'$ contribute equally, cancelling the $1/4$ in $-\mu_3/4$)

$$\begin{aligned} &\langle \phi_k(\sigma,t)\rangle_{dyn} = a_k e^{-2\pi\Delta_k t/\beta}\left(1 - Q_{3,k}\tilde{\mu}_3\,(\frac{2\pi t}{\beta} + \text{constant}) + O(\mu_3^2)\right) + ..., \\ &Q_{3,k} = i^3 2 q_{3,k}(2\pi),\ \tilde{\mu}_3 = \frac{\mu_3}{\beta^2},\ \Delta_k = 2h_k \end{aligned} \tag{4.36}$$

Up to $O(\mu_3)$, it agrees with 4.7.

In case of a quasiprimary field $\phi_k(w,\bar{w})$, it mixes, under conformal transformation to the plane, with lower dimension operators. The most relevant operator among these, which is of the form $\varphi_k(z)\varphi_k(\bar{z})$, is then to be used in 4.34 for obtaining the dominant time-dependence; in that case $\Delta_k, Q_{3,k}$ refer to this operator (rather than to the original ϕ_k).

For higher W_n charges, the currents $\mathcal{W}_n(w)$ are typically quasiprimary, and hence they mix with lower order $\mathcal{W}_m(z)$ under conformal transformation to the UHP. Thus the $O(\mu_n)$ correction to the dynamical one-point function $\langle\phi_k\rangle_{dyn}$ is a linear combination of terms of the form 4.68 (weighted by a set of coefficients $a_{n,m}$, as in 4.37 below). Collecting all this,

the $O(\mu)$ correction with all chemical potentials is given by

$$\begin{aligned}
\langle\phi_k(\sigma,t)\rangle_{dyn} &= a_k e^{-2\pi\Delta_k t/\beta}\left(1-\sum_{n=3}Q_{n,k}\tilde{\mu}_n\,(\frac{2\pi t}{\beta}+\text{constant})+O(\mu^2)\right)+...,\\
\tilde{\mu}_n &= \frac{\mu_n}{\beta^{n-1}},\ \Delta_k = h_k+\bar{h}_k = 2h_k\\
Q_{n,k} &= 2\sum_{m=0}^{[n/2-1]}a_{n,m}i^{n-2m}(2\pi)^{n-2m-2}q_{n-2m,k}\\
&= i^n(2\pi)^{n-2}2q_{n,k}+i^{n-2}(2\pi)^{n-4}a_{n,2}\,2q_{n-2,k}+...,
\end{aligned}\tag{4.37}$$

Note that for W_3 deformations, the expression for Q_3 as in 4.36 corresponds only to the first term in the above series expression for Q_n. This is because the $\mathcal{W}_3$ current is a primary field and does not mix with any lower $\mathcal{W}$ current under a conformal transformation. From $n=4$ onwards, the additional terms in $Q_{n,k}$'s represent the mixing of $\mathcal{W}_n$ currents with $\mathcal{W}_{n-2m}$ under conformal transformations.

Higher order μ-corrections

Let us first consider that $O(\mu_n^2)$ correction:

$$\langle\phi_k(w,\bar{w})\rangle_{str}^{conn}|_2^{\mu_n} \equiv \frac{(\mu_n/4)^2}{2!}(\langle\{W_nW_n,\phi_k(w,\bar{w})\}\rangle_{str}^{conn}+2\langle W_n\phi_k(w,\bar{w})W_n\rangle_{str}^{conn})\tag{4.38}$$

Again, for holomorphic (or antiholomorphic) primary fields $\phi_k(w)$, it is straightforward to generalize 4.33 to this order.

$$\langle\phi_k(w)\rangle_{str}^{conn}|_2^{\mu_n} = \frac{\mu_n^2}{2!}\langle W_nW_n\phi_k(w)\rangle_{cyl}^{conn}\tag{4.39}$$

For a primary field of the form $\phi_k(w,\bar{w}) = \varphi_k(w)\varphi_k(\bar{w})$, proceeding as in the previous subsection, we get

$$\langle\phi_k(w)\rangle_{str}^{conn}|_2^{\mu_n} = \frac{1}{2!}\left(Q_{n,k}\tilde{\mu}_n t\,\frac{2\pi}{\beta}\right)^2 + \mu_n^2(\text{constant}\times t + \text{constant}) + ... \tag{4.40}$$

The essential ingredient in this calculation is

$$\begin{aligned} I_{nm}(z,z'|\Gamma_1,\Gamma_2) &\equiv \int_{\Gamma_1} dz_1\ z_1^{n-1}\int_{\Gamma_2} dz_2\ z_2^{m-1} f_{nm}(z_1,z_2,z,z'),\\ f_{nm}(z_1,z_2,z,z') &= \frac{\langle\mathcal{W}_n(z_1)\mathcal{W}_m(z_2)\varphi_k(z)\varphi_k^*(z')\rangle_{\mathbb{C}}^{conn}}{\langle\varphi_k(z)\varphi_k^*(z')\rangle_{\mathbb{C}}^{conn}} \end{aligned} \tag{4.41}$$

By repeating the strategy of 4.75, we get

$$\begin{aligned} &\text{Coefficient of } [\log(-z')-\log(-z)]^2 \text{ in } I_{nm}(z,z'|\Gamma_1,\Gamma_2)\\ &= \text{Residue}_{z_1=z}\left[\text{Residue}_{z_2=z}\left(\frac{\langle\mathcal{W}_n(z_1)\mathcal{W}_m(z_2)\varphi_k(z)\varphi_k^*(z')\rangle_{\mathbb{C}}^{conn}}{\langle\varphi_k(z)\varphi_k^*(z')\rangle_{\mathbb{C}}^{conn}}\right)\right] = q_{n,k}\,q_{m,k} \end{aligned} \tag{4.42}$$

where we have first used the $\mathcal{W}_m(z_2)\varphi_k(z)$ OPE, and then the $\mathcal{W}_n(z_1)\varphi_k(z)$ OPE. In a manner similar to that in Appendix 4.7.1, we conclude the following structure of $I_{nm}(z,z')$:

$$I_{nm}(z,z'|\Gamma_1,\Gamma_2) = q_{n,k}\,q_{m,k}([\log(-z')-\log(-z)]+\text{constant})\times([\log(-z')-\log(-z)]+\text{constant}) \tag{4.43}$$

Note that at late times $t \gg \beta$, $([\log(-z')-\log(-z)] \to 2(2\pi t)/\beta$ and dominates over the constant term (the precise sense is that of 4.48). Similar to Appendix 4.7.1, the $4\times 4 = 16$ locations of the contour-pairs (Γ_1,Γ_2),(Γ_1,Γ_2'), $(\Gamma_1,\tilde{\Gamma}_2)$,$(\Gamma_1,\tilde{\Gamma}_2')$, ..., all contribute equally, therefore converting $(\mu_n/4)(\mu_m/4)\to\mu_n\mu_m$. Combining all these, we get 4.40. The charges q_n that are defined by the $\mathcal{W}_n\varphi$ OPE and appear in 4.42, get multiplied by some constants [11] and shifted by lower $\mathcal{W}_{n-2k}$ charges to give the Q_n in 4.42, as in 4.37.

[11] Each $\mathcal{W}_n$ current comes with a factor of $\frac{i^n}{2\pi}\left(\frac{2\pi}{\beta}\right)^{n-1}$, as in 4.23.

Arbitrary orders and Exponentiation:

It is straightforward to generalize the above $O(\tilde{\mu}^2)$ calculation to higher orders in the perturbation in chemical potentials. Thus, at the order $\prod_{i=1}^{r}\mu_{n_i}$, there are r insertions of $\mathcal{W}$-currents, leading to integrals of the form

$$I_{n_1n_2...n_r}(z,z'|\Gamma_1,\Gamma_2,...,\Gamma_r) \equiv \int_{\Gamma_1} dz_1\ z_1^{n_1-1}\int_{\Gamma_2} dz_2\ z_2^{n_2-1}...\int_{\Gamma_r} dz_2\ z_r^{n_r-1} f_{n_1n_2...n_r}(z_1,z_2,...,z_r;z,z'),$$
$$f_{n_1n_2...n_r}(z_1,z_2,...,z_r;z,z') = \frac{\langle \mathcal{W}_{n_1}(z_1)\mathcal{W}_{n_2}(z_2)...\mathcal{W}_{n_r}(z_r)\varphi_k(z)\varphi_k^*(z')\rangle_{\mathbb{C}}^{conn}}{\langle \varphi_k(z)\varphi_k^*(z')\rangle_{\mathbb{C}}^{conn}} \tag{4.44}$$

Again, repeating the strategy of 4.75, we get the following leading (*viz.* $(\log)^r$) contribution (see 4.48 for the definition of the leading-log contribution)

$$\begin{aligned}
&\text{Coefficient of } [\log(-z')-\log(-z)]^r \text{ in } I_{n_1n_2...n_r}(z,z'|\Gamma_1,\Gamma_2,...,\Gamma_r)\\
&= \text{Residue}_{z_1=z}\left[...\text{Residue}_{z_{r-1}=z}\left\{\text{Residue}_{z_r=z}\left(\frac{\langle \mathcal{W}_{n_1}(z_1)...\mathcal{W}_{n_{r-1}}(z_{r-1})\mathcal{W}_{n_r}(z_r)\varphi_k(z)\varphi_k^*(z')\rangle_{\mathbb{C}}^{conn}}{\langle \varphi_k(z)\varphi_k^*(z')\rangle_{\mathbb{C}}^{conn}}\right)\right\}\right]\\
&= q_{n_1,k}...q_{n_{r-1},k}\,q_{n_r,k}
\end{aligned} \tag{4.45}$$

where we have first used the $\mathcal{W}_{n_r}(z_r)\varphi_k(z)$ OPE, then $\mathcal{W}_{n_{r-1}}(z_{r-1})\varphi_k(z)$ OPE, etc. As in the $O(\mu^2)$ calculation above, we obtain the following behaviour at late times

$$\begin{aligned}
&I_{n_1n_2...n_r}(z,z'|\Gamma_1,\Gamma_2,...,\Gamma_r)\\
&= q_{n_1,k}...q_{n_{r-1},k}\,q_{n_r,k}\underbrace{([\log(-z')-\log(-z)]+\text{constant})\times...\times([\log(-z')-\log(-z)]+\text{constant})}_{r\text{ terms}}
\end{aligned} \tag{4.46}$$

The two equations above show that the leading log contribution to 4.44 from every contour integral of the $\mathcal{W}_{n_i}$ current contributes the factor $q_{n_i}[\log(-z')-\log(-z)]$. This is the first basic ingredient for the exponentiation we are going to find. Furthermore, it is easy to see that the leading log contribution is the same irrespective of where each contour Γ_i is placed (out of 4 possible choices, e.g. $\Gamma_1,\Gamma_1',\tilde{\Gamma}_1,\tilde{\Gamma}_1'$ in Figure 4.1). As before we must combine the contribution of all positions of the contours, which, therefore, amounts to multiplying the result for 4.44 by 4^r which converts the original coefficients coming from $\exp[-\sum_n \mu_n W_n/4]$

as follows

$$\frac{\prod_{i=1}^{r}\mu_i/4}{r!} \to \frac{\prod_{i=1}^{r}\mu_i}{r!}.$$

This is the second basic factor leading to the exponentiation. Combining all these, and incorporating some additional constants (see footnote 11) we get the following, leading, order $(\mu_{n_1}...\mu_{n_r})$ contribution

$$\langle\phi_k(w)\rangle_{str}^{conn}|_{r}^{\mu_{n_1}\cdots\mu_{n_r}} = \frac{1}{r!}\prod_{i=1}^{r}\left(Q_{n_i,k}\tilde{\mu}_{n_i}\ \frac{2\pi}{\beta}\right) + O(\mu^r t^{r-l}) \tag{4.47}$$

Once again, the constants Q_n are related to the q_n as in 4.37) in a manner similar to the $O(\tilde{\mu})$ and the $O(\tilde{\mu}^2)$ calculation above. We note that the leading log contribution used in this chapter can be isolated by considering a scaling

$$\tilde{\mu}_n \to 0, \tilde{t} \equiv \frac{t}{\beta} \to \infty, \text{ such that } \tilde{\mu}_n\tilde{t} = \text{constant}. \tag{4.48}$$

The second term in 4.47, or for that matter, in 4.40, is subleading at large times in the sense of this scaling.

Using the above results, we now have, for primary fields of the form $\phi_k(w,\bar{w}) = \varphi_k(w)\varphi_k(\bar{w})$

$$\begin{aligned}\langle\phi_k(w,\bar{w})\rangle_{str} = a_k e^{-\frac{2\pi\Delta_k t}{\beta}}\Bigg[&1 - \sum_n \tilde{\mu}_n\ Q_{n,k}(\frac{2\pi t}{\beta} + \text{const}) \\ &+\frac{1}{2!}\sum_{n,m}\tilde{\mu}_n\tilde{\mu}_m\ Q_{n,k}(\frac{2\pi t}{\beta} + \text{const})\ Q_{m,k}(\frac{2\pi t}{\beta} + \text{const}) + ... \\ &+\frac{1}{r!}\sum_{\{n_i\}}\prod_{i=1}^{r}\tilde{\mu}_{n_i}Q_{n_i,k}\left(\underbrace{(\frac{2\pi t}{\beta} + \text{const})...(\frac{2\pi t}{\beta} + \text{const})}_{r\text{ terms}}\right) + ...\Bigg] \\ &= a_k e^{-2\pi t/\beta\left(\Delta_k + \sum_n \tilde{\mu}_n Q_{n,k} + O(\tilde{\mu}^2)\right)} = a_k e^{-\gamma_k t}\end{aligned} \tag{4.49}$$

where we have absorbed some constant factors in a_k. γ_k is given by 4.7; $Q_{n,k}$ are the shifted W_n charges of ϕ_k as defined in 4.37. The proof of the above equation for general quasiprimary operators $\phi_k(w, \bar{w})$ works out much the same way as in case of the $O(\mu)$ terms, as discussed in Section 4.2.2. *We emphasize that it is only the leading contributions at large times which we have proved here to exponentiate.* Thus, we do not claim that the constant terms marked "const" in the above equation are all the same. As we have remarked before, the leading contributions can be isolated using the scaling mentioned in 4.48.

The schematics of the above calculation is explained in the Figure 4.2.

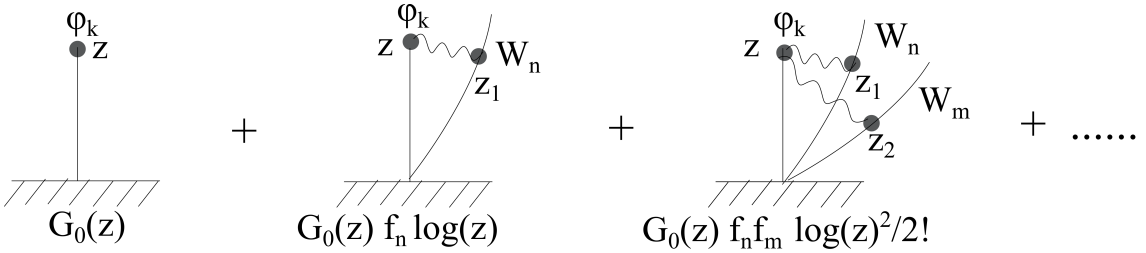

Figure 4.2: The schematics of the calculation of the one-point function. The first term represents the zero-order boundary Green's function 4.17 without chemical potentials (the shading indicates the boundary of the upper half plane). The second term represents the $O(\mu_n)$ correction, which involves one insertion of a W_n-charge (which is an integral over the z_1-contour. As explained in the text, at long times, this insertion amounts to multiplying the zero order term by a term of the form $f_n \log(z)$, where f_n is described in 4.37. The third term represents insertion of two such W-charges; as we explained in the text (see 4.40 and below), each insertion again amounts to multiplying by the factor mentioned above, along with a factor of $\frac{1}{2!}$. The pattern continues, to ensure an exponentiation to $G_0(z)\, z^{\sum_n f_n}$, as in 4.49. Since at long times $G_0(z) \sim e^{-\gamma_k^{(0)} t}$ (see 4.17), and $z \sim e^{-2\pi t/\beta}$, adding the chemical potentials amount to a shift of the exponent $\gamma_k^{(0)} \to \gamma_k$ as in 4.6.

4.3 Calculation of $I(t)$

Let us rewrite the expression for the thermalization function $I(t)$ 4.8 in the form

$$
\begin{aligned}
&I(t) = Z_{sc}/\sqrt{Z_{ss}Z_{cc}} = \hat{Z}_{sc}/\sqrt{\hat{Z}_{ss}\hat{Z}_{cc}},\\
&Z_{sc} \equiv \mathrm{Tr}(\rho_{dyn,A}(t)\rho_{eqm,A}(\beta,\mu)),\ \hat{Z}_{sc} = Z_{sc}/(Z_s Z_c)\\
&Z_{ss} \equiv \mathrm{Tr}(\rho_{dyn,A}(t)\rho_{dyn,A}(t)),\ \hat{Z}_{ss} = Z_{ss}/Z_s^2,\\
&Z_{cc} \equiv \mathrm{Tr}(\rho_{eqm,A}(\beta,\mu)\rho_{eqm,A}(\beta,\mu)),\ \hat{Z}_{cc} = Z_{cc}/Z_c^2,\\
&Z_s = \mathrm{Tr}(\rho_{dyn}(t)) = \langle\psi_0|\psi_0\rangle,\ Z_c = \mathrm{Tr}(\rho_{\beta,\mu})
\end{aligned}
\tag{4.50}
$$

In Appendix 4.7.2 we explain how to compute $I(t)$ using the short interval expansion, valid when the length of the interval l is small compared with the other time scales β and t in the problem. We reproduce the main formula 4.79 for our purpose, where we explicitly denote the dependencies on the length l of the interval, the inverse temperature β and the chemical potentials μ (the dependence on β on the RHS is implicit; the one-point functions depend on both β and μ— see Section 5.2.2).

$$
\begin{aligned}
\hat{Z}_{sc}(l,\beta,\mu) &= \sum_{k_1,k_2} C_{k_1,k_2}(l)\langle\phi_{k_1}(w_1,\bar{w}_1)\rangle^{\mu}_{str}\langle\phi_{k_2}(w_2,\bar{w}_2)\rangle^{\mu}_{cyl},\\
\hat{Z}_{ss}(l,\beta,\mu) &= \sum_{k_1,k_2} C_{k_1,k_2}(l)\langle\phi_{k_1}(w_1,\bar{w}_1)\rangle^{\mu}_{str}\langle\phi_{k_2}(w_2,\bar{w}_2)\rangle^{\mu}_{str},\\
\hat{Z}_{cc}(l,\beta,\mu) &= \sum_{k_1,k_2} C_{k_1,k_2}(l)\langle\phi_{k_1}(w_1,\bar{w}_1)\rangle^{\mu}_{cyl}\langle\phi_{k_2}(w_2,\bar{w}_2)\rangle^{\mu}_{cyl}
\end{aligned}
\tag{4.51}
$$

It is understood, for the logic of the short interval expansion to go through, that all contours which represent insertion of the W-charges (see Fig 4.1) are drawn outside of the small disc-like region of both sheets of Fig 4.4.

4.3.1 Proof of thermalization

Using the short-interval expansion above, and the long time behaviour of one-point functions from Section 5.2.2), it is easy to prove that the system thermalizes in the sense of 4.10 or 4.11.

To prove this, note that it is only the holomorphic (or antiholomorphic) fields ϕ_k which possibly have non-zero expectation values in the long time limit 4.20. For these fields, the one-point functions on the cylinder and on the strip agree (see 4.21, 4.33, 4.39). By virtue of 4.51, we therefore have in the long time limit $Z_{sc} = Z_{ss} = Z_{cc}$. Hence using the expression 4.50 for the thermalization function we get $I(t \to \infty) = 1$ which proves 4.10 and consequently 4.11.

The above-mentioned equality of one-point functions between the strip and cylinder geometries for holomorphic (or antiholomorphic) fields imply the same for the conserved $\mathcal{W}_n$- (or $\bar{\mathcal{W}}_n$)- currents. This, therefore, proves that

$$\langle\psi(t)|W_n|\psi(t)\rangle = \mathrm{Tr}(W_n\rho_{eqm}) \tag{4.52}$$

Note that in proving this, we have used the correspondence 4.4 between the parameters of the initial state and the putative equilibrium state. The above equation, therefore, proves the correspondence 4.4.

4.3.2 Thermalization rate

To evaluate the rate of approach of $I(t)$ to its asymptotic value 1, we organize the terms in $\hat{Z}_{sc}, \hat{Z}_{ss}, \hat{Z}_{cc}$ as follows

$$\begin{aligned}
&\hat{Z}_{sc} = C_{0,0}(1 + S_1^{sc}),\ S_1^{sc} = \sum_a \hat{C}_{a,0}(\langle\phi_a\rangle_{str}^{\mu} + \langle\phi_a\rangle_{cyl}^{\mu}) + \sum_{ab} \hat{C}_{a,b}\langle\phi_a\rangle_{str}^{\mu}\langle\phi_b\rangle_{cyl}^{\mu} \\
&\hat{Z}_{ss} = C_{0,0}(1 + S_1^{ss} + S_2^{ss}),\ S_1^{ss} = 2\sum_a \hat{C}_{a,0}\langle\phi_a\rangle_{str}^{\mu} + \sum_{ab} \hat{C}_{a,b}\langle\phi_a\rangle_{str}^{\mu}\langle\phi_b\rangle_{str}^{\mu},\ S_2^{ss} = \sum_k \hat{C}_{k,k}(\langle\phi_k\rangle_{str}^{\mu})^2 \\
&\hat{Z}_{cc} = C_{0,0}(1 + S_1^{cc}),\ S_1^{cc} = 2\sum_a \hat{C}_{a,0}\langle\phi_a\rangle_{cyl}^{\mu} + \sum_{ab} \hat{C}_{a,b}\langle\phi_a\rangle_{cyl}^{\mu}\langle\phi_b\rangle_{cyl}^{\mu}
\end{aligned} \tag{4.53}$$

where $a, b, ...$ denote descendents of the identity operator, k labels other primaries (than the identity) and their descendents. $\hat{C} \equiv C/C_{0,0}$.

$\mu = 0$

Let us first consider the case of zero chemical potentials. Using the results in Sections 5.2.2, and Appendices 5.7.3 and 4.7.2, we get

$$\begin{aligned}
S_1^{sc} &= -a_T\tilde{l}^2\left(1 + O(\tilde{l})^2\right) + a_{T\bar{T}}\tilde{l}^4 e^{-8\pi t/\beta}\left(1 + O(\tilde{l})^2\right) + O(e^{-8\pi\tilde{t}}) \\
S_1^{ss} &= -a_T\tilde{l}^2\left(1 + O(\tilde{l})^2\right) + 2a_{T\bar{T}}\tilde{l}^4 e^{-8\pi\tilde{t}}\left(1 + O(\tilde{l})^2\right) + O(e^{-8\pi\tilde{t}}) \\
S_2^{ss} &= \sum_k \left[a_k\tilde{l}^{4h_k} e^{-8\pi h_k t/\beta}\left(1 + O(\tilde{l})^2\right) + O(e^{-12\pi h_k\tilde{t}})\right] \\
S_1^{cc} &= -a_T\tilde{l}^2\left(1 + O(\tilde{l})^2\right) \\
a_T &= \frac{c\pi^2}{24},\ a_{T\bar{T}} = \frac{A_{T\bar{T}}\pi^4}{8c}\ a_k = \frac{A_k^2}{n_k}\left(\frac{\pi}{2}\right)^{4h_k}
\end{aligned} \tag{4.54}$$

To this order, it is easy to see that the contribution to $I(t)$ from descendents of identity, demarcated by $a_T, a_{T\bar{T}}$, vanishes. The leading contribution to $I(t)$, demarcated by a_k, occurs only in $\hat{Z}_{ss}$ and comes from $(\langle\phi_m(z,\bar{z})\rangle_{str})^2$ for which h_k is the minimum ($= h_m$) (this could be a field which appears after a conformal transformation of the original quasiprimary field).

The time-dependence shown of S_2^{ss} comes from 4.17. Using this, we get

$$I(t) = 1 - \alpha \exp[-2\gamma_m^{(0)} t] + ..., \ \gamma_m^{(0)} = 2\pi\Delta_m/\beta \tag{4.55}$$

This is of the form 4.9 for $\mu = 0$, with

$$\alpha \equiv \frac{A_m^2}{n_m} \left(\frac{\pi}{2}\right)^{4h_m} (\tilde{l})^{4h_m} \left(1 + O(\tilde{l})^2\right) \tag{4.56}$$

The discarded terms in 4.55 are faster transients. This proves 4.9 for zero chemical potential. This result has already appeared in [71].[12]

$\mu \neq 0$

The generalization of the above result to the case of non-zero chemical potentials is straightforward. Once again, the dominant time-dependence arises from $(\langle\phi_m(z,\bar{z})\rangle_{str}^{\mu})^2$ in the S_2^{ss} or $\hat{Z}_{ss}$. The time-dependence 4.9 follows by using 4.49 in S_2^{ss}.

4.3.3 Properties of $\hat{Q}$

From the asymptotic behaviour 4.9 of the thermalization function we indicated the asymptotic behaviour 4.13 of the dynamical reduced density matrix $\hat{\rho}_{dyn}(t)$. By using the long time behaviour of the one-point functions 4.6, we can easily deduce the following dominant behaviour of overlaps of $\hat{Q}$ with various quasiprimary fields at late times

$$\mathrm{Tr}(\hat{Q}\phi_k(t)) \propto e^{-(\gamma_k - \gamma_m)t}, \ \mathrm{Tr}(\hat{Q}\phi_m(t)) \to \text{constant}.$$

[12] Our exponent differs from Cardy's value by a factor of 2.

4.4 Decay of perturbations of a thermal state

We found in the previous sections that the long time behaviour of the reduced density matrix $\rho_{dyn,A}(t)$ resembles that of a thermal ensemble plus a small deformation which decays exponentially. We will find in the next section that the thermal ensemble (or more accurately the generalized Gibbs ensemble) corresponds to a (higher spin) black hole geometry in the bulk. The small perturbation of the equilibrium ensemble is thus expected to correspond to a small deformation of the black hole geometry. Consequently, the exponential decay of the deformation in the CFT should correspond to a 'ringing-down' or a quasinormal mode in the bulk.

We will address the above issue in the next section which deals with bulk geometry. However, in order to make the correspondence of the above paragraph more precise, in this section we will directly present a CFT computation of the decay of a perturbation to a thermal state. Note that this computation is, in principle, different from the exponential decay of the one-point function in the quenched state, 4.6. However, what we will find is that the long time behaviour 4.6 of an operator $\phi_k(0,t)$ in the quenched state is the same as that of its two-point function 4.57 in the thermal state 4.3 (with chemical potentials). The latter measures the thermal decay of a perturbation and is more directly related to a black hole quasinormal mode. Throughout this section, we will assume that the conformal dimensions of ϕ_k satisfy $h_k = \bar{h}_k$.

We define the thermal two-point function as [13]

$$G_+(t,0;\beta,\mu) \equiv \frac{1}{Z}\mathrm{Tr}(\phi_k(0,t)\phi_k(0,0)e^{-\beta H-\sum_n \mu_n W_n}) \tag{4.57}$$

[13] We use the same notations as in [108].

By the techniques developed in the earlier sections, a computation of this quantity amounts to calculating the following correlator on the plane

$$\langle \phi_k(z,\bar{z})\phi_k(y,\bar{y})e^{-\sum_n \mu_n W_n}\rangle, \quad z = ie^{-2\pi t/\beta}, \bar{z} = -ie^{2\pi t/\beta}, y = i, \bar{y} = -i \tag{4.58}$$

where the μ_n-deformations are understood as an infinite series of contours as in the previous section.

For $\mu = 0$, the above two-point function is standard. Including the Jacobian of transformation, we get

$$G_+(t,0;\beta,0) = (\frac{2\pi}{\beta})^{4h_k}\left[(ie^{-2\pi t/\beta} - i)(-ie^{2\pi t/\beta} + i)\right]^{-2h_k} \xrightarrow{t\to\infty} \text{const } e^{-2\pi t\Delta_k/\beta}, \tag{4.59}$$

which clearly matches the long time behaviour of the one-point function 4.6 in the quenched state for $\mu = 0$. Here $\Delta_k = 2h_k$.

In the above, we considered the thermal Green's function for two points which are both at the same spatial point $\sigma = 0$. It is easy to compute the Green's function when the two points are spatially separated by a distance l, say with $\sigma_1 = l$ and $\sigma_2 = 0$. We get

$$G_+(t,l;\beta,0) \equiv \frac{1}{Z}\text{Tr}(\phi_k(l,t)\phi_k(0,0)e^{-\beta H}) = \left[\frac{2\pi}{\beta}e^{\pi l/\beta}\right]^{4h_k}\left((ie^{2\pi(l-t)/\beta} - i)(-ie^{2\pi(l+t)/\beta} + i)\right)^{-2h_k}$$
$$\xrightarrow{t,l\gg\beta} \begin{cases} \text{const } e^{-2\pi t\Delta_k/\beta}, & (t-l) \gg \beta \\ \text{const } e^{-2\pi l\Delta_k/\beta}, & (l-t) \gg \beta \end{cases} \tag{4.60}$$

The coordinates of the two points, in the notation of 4.58 are modified here to $z = ie^{2\pi(l-t)/\beta}, \bar{z} = -ie^{2\pi(l+t)/\beta}$, $y = i, \bar{y} = -i$. The prefactor with the square bracket comes from the Jacobian of the transformation from the cylinder to the plane. The behaviour of the Green's function is shown in Figure 4.3. It is important to note that the exponential decay, found in 4.6 shows up only for time scales $t \gg l$.

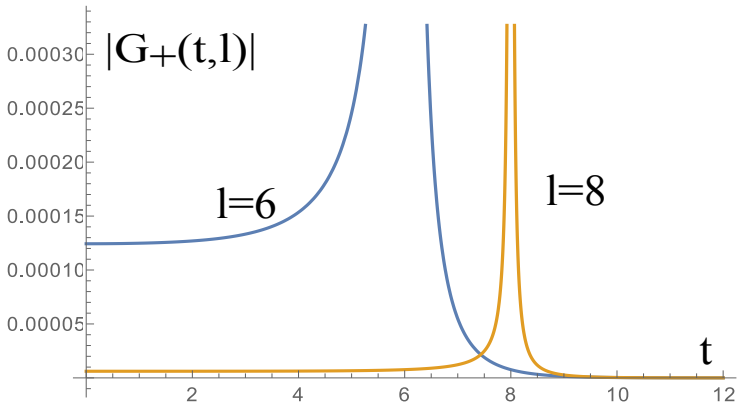

Figure 4.3: Plots of the thermal Green's function $G_+(t, l; \beta, 0)$ for $\beta = 2\pi$, $\Delta_k = 1.5$. The curve on the left (blue) is for $l = 6$, and the curve on the right (orange) is for $l = 8$. Note that the exponential decay in time occurs for times larger than l.

The effect of turning on the chemical potentials can be dealt with as in the previous sections. At $O(\mu_n)$, we will have, as before, a holomorphic contribution and an antiholomorphic contribution. The former is proportional to

$$\langle \phi_k(\bar{z})\phi_k(\bar{y})\rangle \times \int_\Gamma dz_1 z_1^{n-1} \langle \mathcal{W}_n(z_1)\phi_k(z)\phi_k(y)\rangle \tag{4.61}$$

As we see, the structure of the integral is the same as in the previous section. As before, logarithmic terms appear in the above integrals which give the leading, linear, t-dependence. Similar remarks also apply to the antiholomorphic contour. Since the calculations are very similar to those in the previous two sections, we do not provide all details. By resumming the series over the infinite number of contours, we find in a straightforward fashion that

$$G_+(t, 0; \beta, \mu) \xrightarrow{t\to\infty} G_+(0, 0; \beta, 0) b(\mu) e^{-\gamma_k t} \tag{4.62}$$

where $b(\mu)$ is time-independent, and is of the form $b(\mu) = 1 + O(\mu)$. This long time decay is the same as that of the one-point function 4.6 in the quenched state, as claimed above. For points separated by a distance l, the above exponential decay shows up for $t \gg l$, as in 4.60.

In the above, we have discussed the two-point function in real space. It is straightforward to convert the result 4.60 without chemical potentials to Fourier space, which develops poles at

$$\omega_{k,m}|_{\mu=0} = -i\frac{2\pi}{\beta}(\Delta_k + 2m),\ m = 0, 1, 2, ... \tag{4.63}$$

Our results in 4.6 can be interpreted as a shift, caused by the presence of the chemical potentials μ_n, of the dominant

$$\omega_{k,0} = -i\frac{2\pi}{\beta}(\Delta_k + \sum_n \tilde{\mu}_n Q_{n,k}) = -i\gamma_k, \tag{4.64}$$

where the notation is the same as that of 4.6. In this chapter we will not address the question of the shift of the subdominant poles (the current status of these can be found in [34,52,121]).

Two-point functions of the kind 4.57, for a single chemical potential μ_3, and up to order μ_3^2, have appeared earlier in [121] (calculations up to $O(\mu_3^5)$ have appeared in [34]). What we find in this chapter is that at large times, the perturbation series in μ_n, up to all orders in all chemical potentials, can be resummed, to yield the leading correction to the thermalization rate in the presence of chemical potentials.

At a technical level, the one-point function in the quenched state corresponds to a one-point function in a geometry with a boundary, and for operators considered here, these turn into a two-point function on the plane, by virtue of the method of images. The thermal decay naturally involves a two-point function on the plane [14] and agrees with the above two-point function at late times.

[14] Actually the thermal calculation involves a product of two such factors, one holomorphic and the other antiholomorphic, but one of the factors just gives an overall constant and only one factor leads to the important time-dependence.

4.5 Holography and higher spin black holes

Zero chemical potential: As remarked in the Introduction, a global quantum quench described by an initial state of the form 5.1, for large central charges and zero chemical potentials, has been shown in [67, 138, 177] to be dual to one half of the eternal BTZ (black string) geometry, whose boundary represents an end-of-the-world brane.

In an independent development, it was found in [45] that the quasinormal mode of a scalar field $\Phi_k(\sigma, t, z)$ of mass m in a BTZ background (dual to a CFT operator ϕ_k of dimension $\Delta_k \equiv 1 + \sqrt{1+m^2}$) is of the form $\exp[-2\pi\Delta t/\beta]$ at large times. This time-dependence agrees with the CFT exponent in 4.60 exactly. This shows that the exponential decay of a CFT perturbation to a thermal state corresponds to the decay of the corresponding scalar field in the bulk geometry. This result has been extended to higher spin fields in the BTZ background in [88].

Non-zero chemical potentials: In case the CFT has additional conserved charges, in particular if it has a representation of a W_∞ algebra (and consequently the hs(λ) algebra [119]), then the bulk dual corresponding to those conserved charges have been conjectured to be the conserved higher spin charges of higher spin gravity. In particular, [131, 162] have shown that if one interprets the grand canonical ensemble 4.4 (more generally, the GGE) in the framework of an hs(λ) representation, then the bulk dual corresponds to a higher spin black hole.

Thus, we would like to conjecture that the bulk dual of the quantum quench with chemical potentials, would correspond to a gravitational collapse to a higher spin black hole.

As an important consistency check, by analogy with the case with zero potential, in the present case too, the leading quasinormal mode (QNM) of a scalar field $\Phi_k(\sigma, t, z)$ should

have a time-dependence given by 4.62. Following the results in [52] (see also [34, 121]) [15] we find that at late times $t \gg \beta$ the QNM for the hs(λ) scalar field Φ_+ behaves, up to $O(\mu_3)$, as $e^{-i\omega_{k,0}t}$, where

$$\omega_{k,0} = -i\frac{2\pi}{\beta}\left(1+\lambda+\tilde{\mu}_3\frac{1}{3}(1+\lambda)(2+\lambda)\right) \tag{4.65}$$

where the index k here refers to the operator ϕ_k dual to the scalar field Φ_+. Noting that for this operator we have $\Delta_k = 1+\lambda$, and $Q_{3,k} = \frac{1}{3}(1+\lambda)(2+\lambda)$ [34, 121], we see that the QNM frequency $\omega_{k,0}$ agrees, to the relevant order, with the pole 4.64 of the thermal 2-point function which, in turn, is related to the thermalization exponent by the relation $\omega_{k,0} = -i\gamma_k$, with γ_k given in 4.6.

4.6 Discussion

In this chapter, 2D conformal field theories were considered with additional conserved charges besides the energy. We probed non-equilibrium physics starting from global quenches described by conformal boundary states modified by multiple UV cut-off parameters 4.1. It was found that local observables in such a state thermalize to an equilibrium described by a grand canonical ensemble 4.4 with temperature and chemical potentials related to the cut-off parameters. We computed the thermalization rate for various observables, including the reduced density matrix for an interval. It was found that the same rate appears also in the long time decay of two-point functions in equilibrium (see 4.6 and 4.14). In the context where the number of conserved charges is infinite, and they are identified with commuting W_∞ charges, the equilibrium ensemble (a generalized Gibbs ensemble, GGE) corresponds to a higher spin black hole [131, 162]. We found that the thermalization rate found above agrees with the leading quasinormal frequency of the higher spin black hole; this constitutes

[15] We wish to thank Alejandro Cabo-Bizet and Viktor Giraldo-Rivera for informing us that the difference between equation 4.65 above and the corresponding equation (4.2) in a previous version of their paper [52] was due to a typo, which has now been corrected in the new version of their paper.

an additional, dynamical, evidence for the holographic correspondence between the global quenches in this chapter and the evolution into the higher spin black hole.

One of the main technical advances made in this chapter is the resummation of leading-log terms at large times, presented in Section 4.2.2, which leads to exponentiation of the perturbation series, leading to the thermalization rate, presented in 4.6, 4.49, as a function of chemical potentials. This allows us to also compute the effect of chemical potentials on the relaxation times of thermal Green's functions. Another technical advance consists of the computation of the long-time reduced density matrix 4.9, using a short-interval expansion, which allows us to prove thermalization of an arbitrary string of local observables.

One might wonder whether the results presented in this chapter are tied to the use of translationally invariant quenched states such as 4.1, whose energy density and various charge densities are uniform. It turns out that if the initial state has inhomogeneities in a compact domain and has uniform energy densities outside, local observables again thermalize asymptotically with exponents governed by the uniform densities. Other important issues involve local quenches (see, e.g. [55, 201]), and compact spatial dimensions. The issue of thermalization when space is compact is quite subtle. It has been shown in [71] that at large times one can have the phenomenon of revival (observables effectively returning to their initial values). The dynamical entanglement entropy for a quantum quench in a space with boundaries is an interesting, related, issue; which we shall discuss in the next chapter.

NOTE: We would also like to thank Juan Pedraza for drawing our attention to Ref. [53] and Alejandro Cabo-Bizet and Viktor Giraldo-Rivera for a useful correspondence regarding Ref. [52].

4.7 Appendix

4.7.1 Some details on one-point functions

Here we collect some additional helpful material on the one-point functions discussed in this chapter.

A few explicit one-point functions with zero chemical potentials

Case k = descendent of identity: In this case, $\phi_k(w,\bar{w})$ is of the form $T, \bar{T}$, or $:T\bar{T}:$ or some descendents thereof. Under a conformal transformation 4.16, these operators pick up a c-number term in addition to a term proportional to the corresponding operator on the plane/UHP. We will give some examples to illustrate the calculation

1. *cylinder:* In this case

$$\begin{aligned}\langle T(w)\rangle_{cyl} &= \langle\left(-\frac{c\pi^2}{6\beta^2}-\frac{4\pi^2}{\beta^2}z^2T(z)\right)\rangle_{UHP} = -\frac{c\pi^2}{6\beta^2}\\ \langle :T\bar{T}:(w,\bar{w})\rangle_{cyl} &= \langle\left([-\frac{c\pi^2}{6\beta^2}-\frac{4\pi^2}{\beta^2}z^2T(z)][-\frac{c\pi^2}{6\beta^2}-\frac{4\pi^2}{\beta^2}\bar{z}^2\bar{T}(\bar{z})]\right)\rangle_{UHP} = (\frac{c\pi^2}{6\beta^2})^2\end{aligned} \tag{4.66}$$

2. *strip:* In this case

$$\begin{aligned}\langle T(w)\rangle_{str} &= \langle\left(-\frac{c\pi^2}{6\beta^2}-\frac{4\pi^2}{\beta^2}z^2T(z)\right)\rangle_{UHP} = -\frac{c\pi^2}{6\beta^2} = \langle T(w)\rangle_{cyl}\\ \langle :T\bar{T}:(w,\bar{w})\rangle_{str} &= \langle\left([-\frac{c\pi^2}{6\beta^2}-\frac{4\pi^2}{\beta^2}z^2T(z)][-\frac{c\pi^2}{6\beta^2}-\frac{4\pi^2}{\beta^2}\bar{z}^2\bar{T}(\bar{z})]\right)\rangle_{UHP}\\ &= (\frac{c\pi^2}{6\beta^2})^2 + A_{T\bar{T}}(z-\bar{z})^{-4} = (\frac{c\pi^2}{6\beta^2})^2 + a_{T\bar{T}}e^{-8\pi t/\beta}+\ldots\end{aligned} \tag{4.67}$$

where $A_{T\bar{T}}$, $a_{T\bar{T}}$ are constants as in 4.17 and 4.18.

Case k = descendent of other primaries: In this case,

1. *cylinder:* The one-point function vanishes as in the case of primaries.

2. *strip:* The one-point function can be related to one-point function of primaries which is dealt with above.

Some details on $O(\mu_n)$ correction to the one-point function

In this section we will consider the following integrals which arise in connection with $O(\mu_n)$ correction to the one-point function $\langle\phi(\sigma,t)\rangle_{dyn}$:

$$\begin{aligned} I_n(z,z'|\Gamma_1) &\equiv \int_{\Gamma_1} dz_1\ z_1^{n-1} f_n(z_1,z,z'),\quad g_n(z_1,z,z') \equiv \int dz_1\ z_1^{n-1} f_n(z_1,z,z') \\ f_n(z_1,z,z') &= \frac{\langle \mathcal{W}_n(z_1)\varphi_k(z)\varphi_k^*(z')\rangle_{\mathbb{C}}^{conn}}{\langle \varphi_k(z)\varphi_k^*(z')\rangle_{\mathbb{C}}^{conn}} = q_{n,k}\frac{(z-z')^n}{(z_1-z)^n(z_1-z')^n} \end{aligned} \tag{4.68}$$

The second integral on the first line is an indefinite integral. The integrals above can be explicitly computed. E.g.

$$\begin{aligned} g_3(z_1,z,z') &= q_{3,k}[R_3(z,z')(\log(z_1-z)-\log(z_1-z')) - \frac{z^2}{2(z_1-z)^2} + \frac{z'^2}{2(z_1-z')^2} \\ &\qquad + \frac{z'(2z+z')}{(z-z')(z_1-z')} + \frac{z(2z'+z)}{(z-z')(z_1-z)}] \\ I_3(z,z'|\Gamma_1) &= q_{3,k}[R_3(z,z')(-\log(-z)+\log(-z')) + 3\frac{(z+z')}{(z-z')}] \\ R_3(z,z') &\equiv \frac{(z^2+4zz'+z'^2)}{(z-z')^2} \end{aligned} \tag{4.69}$$

Note that I_3 is essentially obtained from the lower limit of the integral, i.e. from $-g(0,z,z')$. The contour Γ_1 in I_3 specifies which branch of the log is to be taken. In particular

$$I_3(z,z'|\Gamma_1) - I_3(z,z'|\tilde{\Gamma}_1) = -2\pi i q_{3,k}\ R_3(z,z') \tag{4.70}$$

In the long time limit 4.20, we get

$$I_3(z,z'|\Gamma_1) = I_3(z,z'|\tilde{\Gamma}_1) = 2q_{3,k}t(2\pi/\beta) + q_{3,k}\times \text{const} + O(e^{-2\pi t/\beta}) \tag{4.71}$$

In this equation we have displayed the principal value of the relevant integrals (the discontinuity 4.70 tells us the coefficient of the log term or the linear t term).

However, we would like to understand the above results more simply, by using the $\mathcal{W}_n(z_1)\varphi_k(z)$ OPE which is of the form:

$$\mathcal{W}_n(z_1)\varphi_k(z) = q_{n,k}\frac{\varphi_k(z)}{(z_1-z)^n} + \sum_{i=1}^{n-1}\alpha_{n,i}\frac{\varphi_{k,i}(z)}{(z_1-z)^{n-i}} + \text{regular terms} \tag{4.72}$$

where $\varphi_{k,i}(z)$ is of dimension h_k+i.[16] Using this, we get an expansion for the connected 3-point function of the form:

$$\frac{\langle \mathcal{W}_n(z_1)\varphi_k(z)\varphi_k^*(z')\rangle_{\mathbb{C}}^{conn}}{\langle \varphi_k(z)\varphi_k^*(z')\rangle_{\mathbb{C}}^{conn}} = \frac{q_{n,k}}{(z_1-z)^n} + \frac{C_{n,1}}{(z_1-z)^{n-1}(z-z')} + O(z-z')^{-2} \tag{4.73}$$

Performing the integral in 4.68,

$$\begin{aligned} g_n(z_1,z,z') = q_{n,k}&\left(\log[z_1-z] - (n-1)\frac{z}{z_1-z} + ...\right) \\ &+ \frac{C_{n,1}}{z-z'}\left(z_1 - z + (n-1)z\log[z_1-z] + ...\right) + ... \end{aligned}$$

The ellipsis in each round bracket represents terms with higher powers of $1/(z_1-z)$ (up to a maximum of $(z_1-z)^{-n}$); successive round brackets themselves are arranged in higher inverse powers of $z-z'$. Using the $\mathcal{W}_n(z_1)\varphi_k^*(z')$ OPE in a similar fashion and using the symmetry property $g_n(z_1,z,z') = (-1)^n g_n(z_1,z',z)$ we can arrive at a general structure

$$g_n(0,z,z') = q_{n,k}(\log[-z] - \log[-z'])R_n(z,z') + ...$$

where $R_n(z,z') = (-1)^{n-1}R_n(z',z)$ is of the form $P_{n-1}(z,z')/(z-z')^{n-1}$ ($P_{n-1}(z,z')$ is a homogeneous symmetric polynomial of degree zero). See the explicit form of R_n for $n=3$ in 4.69. The omitted terms are all ratios of homogeneous polynomials in (z,z') of the same

[16] This is the general form; some of the $\alpha_{n,i}$ coefficients may, of course, vanish.

degree in the numerator and in the denominator. This implies that we have, in the long time limit 4.20

$$I_n(z,z'|\Gamma_1) = I_3(z,z'|\tilde{\Gamma}_1) = 2q_{n,k}(2\pi/\beta)t + q_{n,k} \times \text{const} + O(e^{-2\pi t/\beta}) \tag{4.74}$$

which, of course, agrees with 4.71.

Note that the dominant time-dependence $2q_{n,k}t(2\pi/\beta)$ comes from the long-time limit of the coefficient $R_n(z,z')$ of the log terms, which can be read off from the discontinuity $I_n(z,z'|\Gamma_1) - I_n(z,z'|\tilde{\Gamma}_1)$ (see 4.70). Now, the contour $\int_{\Gamma_1-\tilde{\Gamma}_1} dz_1$ can be deformed to a very small circle $\oint \Gamma_z dz_1$ around the point z; therefore the leading long-time behaviour $R_n^{(0)}(z,z')$ can be derived by using the leading OPE singularity in 4.72 and computing the residue at $z_1 = z$:

$$\begin{aligned} &\text{Coefficient of } [\log(-z') - \log(-z)] \text{ in } I_n(z,z') \\ &= \text{Residue}_{z_1=z} \left(\frac{\langle \mathcal{W}_n(z_1)\varphi_k(z)\varphi_k^*(z')\rangle_{\mathbb{C}}^{conn}}{\langle \varphi_k(z)\varphi_k^*(z')\rangle_{\mathbb{C}}^{conn}} \right) \equiv q_{n,k}R_n^{(0)}(z,z') = q_{n,k} \end{aligned} \tag{4.75}$$

4.7.2 Short interval expansion

In this section we will explain a formalism suitable for computing partition functions of the kind that appear in 4.50. For convenience we will first compute these quantities in Euclidean time $\tau = it$ and later analytically continue back to Lorentzian time. With this, each of the expressions Z_{sc}, Z_{ss}, Z_{cc} is of the form

$$\text{Tr}(\rho_{A,1}\rho_{A,2}) = \int_{\text{geometry 1}} \mathbf{D}\varphi_1 \int_{\text{geometry 2}} \mathbf{D}\varphi_2 \ \delta(F[\varphi_1,\varphi_2]) \exp\left(-S[\varphi_1] - S[\varphi_2]\right) \tag{4.76}$$

where $S[\varphi]$ represents the action for the CFT (with fields φ) and the delta-functional in the measure represents a gluing condition between a geometry '1' and a geometry '2' along a 'cut' which is the location, at a particular time τ, of the spatial interval $A : \sigma \in (-l/2, l/2)$

[17] For Z_{ss}, both geometries are that of a strip of the Euclidean plane described by complex coordinates $(w, \bar{w}) = \sigma \pm i\tau$ defined by boundaries at $\tau = \pm\beta/4$ with boundary conditions determined by the boundary state $|Bd\rangle$ introduced in 5.1. For Z_{cc}, both geometries are that of a cylinder cut of the Euclidean plane with identified boundaries at $\tau = -\beta/4, 3\beta/4$. The geometries for both Z_{ss} and Z_{cc} are familiar from calculations of Entanglement Renyi entropy (of order 2) and can be calculated from appropriate correlation functions of twist fields [64] which exchange two identical geometries. For Z_{sc}, the two glued geometries are different (that of a strip and a cylinder), hence the method of twist operators do not apply in a straightforward fashion. (See Figure 4.4). In this chapter, we will therefore, employ the method of the short interval expansion.

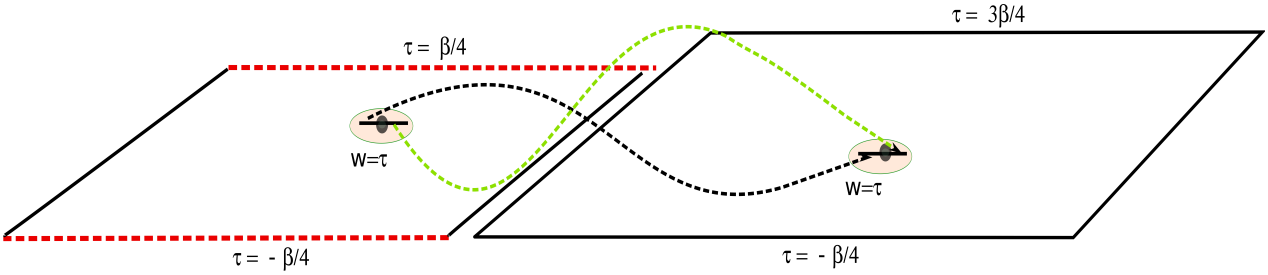

Figure 4.4: Two different geometries, the strip and the cylinder, glued along the cut as described in the text. The method of the short interval expansion allows us to compute the functional integral over this geometry by replacing a small tube enclosing the two glued cuts by a complete basis of operators $\phi_{k_1} \otimes \phi_{k_2}$ where the operators live in the two Hilbert spaces.

The idea of the short interval expansion [63] is as follows. To begin, we express the functional integral 4.76 as an overlap of two wavefunctions in $\mathsf{H}_1 \otimes \mathsf{H}_2$, as follows

$$
\begin{aligned}
Z_{12} = \mathrm{Tr}(\rho_{A,1}\rho_{A,2}) = \langle\psi_{out}|\psi_{in}\rangle = \int_{w_1\in\mathcal{D}_1}\mathbf{D}\overline{\varphi}_1(w_1)\int_{w_2\in\mathcal{D}_2}\mathbf{D}\overline{\varphi}_2(w_2)\ \ \psi_{in}[\overline{\varphi_1},\overline{\varphi_2}]\ \psi^*_{out}[\overline{\varphi_1},\overline{\varphi_2}] \\
\psi_{in}[\overline{\varphi_1},\overline{\varphi_2}] \equiv \int_{w_1\in\mathcal{D}_1}\mathbf{D}\varphi_1(w_1)\int_{w_2\in\mathcal{D}_2}\mathbf{D}\varphi_2(w_2)\delta(\varphi_1|_{\partial\mathcal{D}_1}-\overline{\varphi_1})\delta(\varphi_2|_{\partial\mathcal{D}_2}-\overline{\varphi_2})\delta(F[\varphi_1,\varphi_2])\exp\left(-S[\varphi_1]-S[\varphi_2]\right) \\
\psi_{out}[\overline{\varphi_1},\overline{\varphi_2}] \equiv \int_{w_1\notin\mathcal{D}_1}\mathbf{D}\varphi_1(w_1)\int_{w_2\notin\mathcal{D}_2}\mathbf{D}\varphi_2(w_2)\delta(\varphi_1|_{\partial\mathcal{D}_1}-\overline{\varphi_1})\delta(\varphi_2|_{\partial\mathcal{D}_2}-\overline{\varphi_2})\exp\left(-S[\varphi_1]-S[\varphi_2]\right)
\end{aligned}
\tag{4.77}
$$

[17] To be precise, $\delta[F] = \delta(\varphi_1(A_<) - \varphi_2(A_>))\ \delta(\varphi_1(A_>) - \varphi_2(A_<))$, where $A_<$ ($A_>$) represents the limiting value from below (above) the cut.

Here $\mathcal{D}_1$ (respectively, $\mathcal{D}_2$) is a small disc drawn around the cut in geometry 1 (respectively, geometry 2).

Note that only $|\psi_{in}\rangle$ depends on the gluing condition since the delta functional in the measure does not affect $|\psi_{out}\rangle$. The basic point of the short interval is that in the limit when the length l of the cut is small compared with the characterizing length scale of the geometries (in our case, when $l \ll \beta$), the wavefunction $\psi_{in}[\varphi_1, \varphi_2]$ becomes jointly localized at the centre $(w_1, \bar{w}_1)$ of the disc $\mathcal{D}_1$ *and* at the centre $(w_2, \bar{w}_2)$ of the disc $\mathcal{D}_2$ [18], and hence can be expanded in terms of local operators, as follows

$$|\psi_{in}\rangle = \sum_{k_1,k_2} C_{k_1,k_2}\ \phi_{k_1}(w_1, \bar{w}_1)\, \phi_{k_2}(w_2, \bar{w}_2)|0\rangle_1 \otimes |0\rangle_2 \tag{4.78}$$

Here k_1, k_2 label a complete basis of quasiprimary operators of the CFT Hilbert space. Each term in the sum represents a factorized wavefunction (between geometries 1 and 2), which, therefore, gives [19]

$$\begin{aligned}
\hat{Z}_{sc} &= \sum_{k_1,k_2} C_{k_1,k_2} \langle \phi_{k_1}(w_1, \bar{w}_1)\rangle_{str} \langle \phi_{k_2}(w_2, \bar{w}_2)\rangle_{cyl}, \\
\hat{Z}_{ss} &= \sum_{k_1,k_2} C_{k_1,k_2} \langle \phi_{k_1}(w_1, \bar{w}_1)\rangle_{str} \langle \phi_{k_2}(w_2, \bar{w}_2)\rangle_{str}, \\
\hat{Z}_{cc} &= \sum_{k_1,k_2} C_{k_1,k_2} \langle \phi_{k_1}(w_1, \bar{w}_1)\rangle_{cyl} \langle \phi_{k_2}(w_2, \bar{w}_2)\rangle_{cyl}
\end{aligned} \tag{4.79}$$

Here the subscripts *str* and *cyl* refer to "strip", and "cylinder" respectively. The one-point functions are evaluated on the respective geometries without any cut (see Section 5.2.2 for more details). The glued functional integral 4.76, 4.77 is recovered by summing over k_1, k_2 with the coefficients C_{k_1,k_2}; , as clear from 4.79 these are determined by the gluing condition and depend on the size of the cut [63] (see Section 4.7.2 for more details).

[18] We will take the centre of the disc in each geometry to coincide with the centre of the cut, which has coordinates $w = i\tau, \bar{w} = -i\tau$.

[19] In case geometries 1 and 2 are identical, the superscripts in $w_i, \bar{w}_i, i = 1, 2$ indicate which sheet we are considering.

The coefficients C_{k_1,k_2}

As explained in [63] (see also Section 4.7.2), the coefficients C_{k_1,k_2} are determined by the equation

$$C_{k_1,k_2} = \frac{Z_2}{Z_1^2}(n_{k_1}n_{k_2})^{-\frac{1}{2}} \lim_{z_1\to\infty_1, z_2\to\infty_2} (z_1 z_2)^{2(h_{k_1}+h_{k_2})}(\bar{z}_1\bar{z}_2)^{2(\bar{h}_{k_1}+\bar{h}_{k_2})}\langle\phi_{k_1}(z_1,\bar{z}_1)\phi_{k_2}(z_2,\bar{z}_2)\rangle_{\mathbb{C}_2} \tag{4.80}$$

where $\mathbb{C}_2$ represents two infinite planes glued along a cut A, Z_2 is the functional integral such a glued geometry and Z_1 is the functional integral over a single plane. This equation can be easily proved by inserting quasiprimary a operator at infinity in each plane in an equation like 4.76 or 4.77. The two point function in the glued geometry is to be determined by using the uniformizing map:

$$y = \sqrt{(z+l/2)/(z-l/2)} \tag{4.81}$$

The normalization constants n_k are determined by the following orthogonality condition of the quasiprimary operators

$$\langle\phi_{k_1}(z_1,\bar{z}_1)\phi_{k_2}(z_2,\bar{z}_2)\rangle_{\mathbb{C}} = \frac{n_{k_1}\delta_{k_1,k_2}}{z_{12}^{h_{k_1}+h_{k_2}}\bar{z}_{12}^{\bar{h}_{k_1}+\bar{h}_{k_2}}} \tag{4.82}$$

where n_{k_1} is a normalization constant. Note that $C_{k_1,k_2} = C_{k_2,k_1}$. Below we will use the notation

$$\hat{C}_{k_1,k_2} = C_{k_1,k_2}/C_{0,0} \tag{4.83}$$

Case $(k_1,k_2)=(0,0)$: We will denote the identity operator as $\phi_0 = 1$. It is obvious that

$$C_{0,0} = Z_2/Z_1^2 \tag{4.84}$$

Case $(k_1, k_2) = (k, 0)$: The only case where $C_{k,0} \neq 0$ is when $\phi_k(z, \bar{z})$ is a descendent of the identity operator, e.g. $T(z)$, $\bar{T}(\bar{z})$, $:T(z)\bar{T}(\bar{z}):$, $\Lambda(z)$, $\Lambda(\bar{z})$ etc.[20] E.g.

$$\hat{C}_{T,0} = C_{T,0}/C_{0,0} = \hat{C}_{\bar{T},0} = \frac{l^2}{16}; \hat{C}_{T\bar{T},0} = \frac{l^4}{256}; ... \tag{4.85}$$

All other $C_{k,0}$ vanish as they are proportional to a one-point function of a primary operator on the Riemann surface (and hence to that on the complex plane).

Case $(k_1, k_2) =$ (primary, primary): In case ϕ_{k_1}, ϕ_{k_2} are primary operators, 4.80 gives

$$\hat{C}_{k_1,k_2} = \frac{1}{n_{k_1}} \delta_{k_1,k_2} \left(\frac{l e^{i\pi/2}}{4} \right)^{2(h_{k_1} + \bar{h}_{k_1})} \tag{4.86}$$

Case $(k_1, k_2) =$ (descendent, descendent): In case ϕ_{k_1} is of the form $L_{-n_1} L_{-n_2} ... \bar{L}_{-m_1} \bar{L}_{-m_2} ... \phi_{l_1}$ and ϕ_{k_2} is of the form $L_{-r_1} L_{-r_2} ... \bar{L}_{-s_1} \bar{L}_{-s_2} ... \phi_{l_2}$, we can show that

$$\begin{aligned} &\hat{C}_{k_1,k_2} = \delta_{l_1,l_2} \; \delta_{\sum n, \sum r} \; \delta_{\sum m, \sum s} \, A(n_1, n_2, ..., m_1, m_2, ...; r_1, r_2, ..., s_1, s_2, ...) \, l^{2(h_{k_1} + \bar{h}_{k_1})}, \\ &h_{k_1} = h_{l_1} + \sum n, \quad h_{k_2} = h_{l_2} + \sum m \end{aligned} \tag{4.87}$$

where $A(...)$ is a numerical coefficient.

[20] Here $\Lambda(z) = \; :TT:(z) - \frac{3}{10}\partial_z^2 T$ is the level 4 quasiprimary descendent of the identity.

Chapter 5

Non-Thermalization and Revivals in Cardy-Calabrese States

5.1 Introduction and Summary

In the previous chapter, we understood how one could generalise the CC state to the more general gCC state with a large number of additional conserved charges. In either case, both the correlation functions and reduced density matrices, seemed to thermalise. This implied that these states can be extremely useful in understanding the underlying mechanism via which closed, isolated, out-of-equilibrium quantum systems approached thermal equilibrium. In this chapter, we shall try to understand how such is not always the case. We shall do so by restricting the spatial extent of the 1-D quantum systems to a finite value and trying to understand its effects on thermalization of the system.

In much of the above discussion, the spatial extent of the system is infinite (or much larger than any other length scale in the problem). The effect of a finite spatial extent on thermalization has long been a topic of interest, e.g. in the context of the FPU problem [90, 106, 217]. From the point of view of experimental realizations, in case of 2D CFTs, the spatial boundaries can be thought of as representing impurities in a quantum critical

system. Thermalization, or lack thereof, for global quenches in a finite system of length L has recently been studied in [71], where it has been shown that for rational CFT's, the quenched state returns to itself after a finite period of time which is a multiple of $L/2$. The reason for this 'revival' was roughly that the time-dependence of the wavefunction, for rational highest weights, is a sum of terms with rational periods. Correlation functions and entanglement entropy of subsystems also follow a periodic behaviour. The periodic behaviour of entanglement entropy was explicitly confirmed in the global quench on a circle for free fermions in [233]. In [163], the periodic behaviour observed in [71] is explained by interpreting the quenched state in terms of a Lorentzian-signature conformal transformation of the ground state on the strip. The authors this paper also comment on a corresponding holographic formulation. For other discussions on quenches on the segment, we refer to [82,102,128] and the recent discussion [92]. Revival in higher dimensional field theories has been considered in [73]; holographic entanglement entropy has also been discussed in 2+1 dimensional systems with finite size [3] where a partial revival has been found.

The main focus of this chapter will be to study the effect of finite system size on various time-dependent phenomena. Below we summarize the contents and main results of this chapter:

(i) We study the time evolution of observables in a 2-D CFT starting from a quenched state with a UV cutoff scale $1/\beta$ (as described above) in the presence of finite spatial boundaries (with system size L). The tool used in the CFT computations is a conformal map (the Christoffel-Schwarz transformation), as in [163], which converts a rectangular geometry to an upper half plane (see Section 5.2.1 and Appendix 5.7.1). The map gets simplified in the limits of large L and large β respectively and can be identified with known versions of the map from a cylinder to a plane.

(ii) We show that the spatial boundaries lead to locally thermalized regions (characterized by a *temperature* $1/\beta$) which merge and split periodically at regular time intervals given by the system size. We also quantitatively compute thermalization of certain observables on intermediate time scales prior to the occurrence of the 'revival' phenomena discussed above. We show that in the limit of large L, the relaxation rate agrees with the known results for infinite systems (see Sections 5.2.2, 5.2.3, 5.2.4 and Appendix 5.7.3). Part of the above discussion has already appeared in [102, 163] (see also [92]).

(iii) In Section 5.4 we present a bulk dual of the CFT on a rectangle, following the AdS/CFT proposal for CFT with boundaries [95, 117, 154, 203, 232], coupled with [181, 218, 234] which discuss a *large diffeomorphism* (see Eqn. (5.56)) that reduce to the (analytically continued) conformal map discussed above. The periodicity of various observables mentioned above can be interpreted in terms of the time-periodicity of the above large diffeomorphism, which effects a time-periodic change of the (regulated) AdS boundary and, in turn, causes changes in geometric quantities such as lengths of geodesics tied to the boundary.

(iv) The main results of this chapter, presented in Sections 5.3, 5.4 and 5.5, concern the computation of the entanglement entropy (EE) of a single interval of length l. We use the conformal map described above, and the method of images, to relate the CFT computation of EE to a four-point function of 'twist operators' on the plane. We also compute the EE using holographic methods (Section 5.4.1), developing on earlier work by one of the authors [234]. The holographic result is universal and does not depend on the specific CFT (except on the central charge). The CFT result, on the other hand, involves a four-point function which generically depends on the specific CFT. At large L, the CFT four-point function factorizes, becomes universal, and readily agrees with the holographic result. The analysis for general L/β, however, is much more subtle. We show that (see Section 5.3.4), although the CFT four-point function does not *a priori* factorize, it takes a universal form provided one takes an appropriate large c limit discussed recently [20, 112, 135, 164]. We show that this new universal form then agrees with the result obtained from holography.

(vi) Another novel computation in this chapter (see Section 5.5) is that of the EE by adapting the quasiparticle method [59] to the presence of spatial boundaries. The boundaries lead to hard wall reflection of the quasiparticles, causing periodic entry and exit of EPR partners to and from the interval of interest. We compute the resulting entanglement entropy. The result quantitatively agrees with the large L results discussed in the last paragraph.

(vii) We should remark that in [71], revival was investigated by using the fidelity function $|\langle\psi_0|\exp[-iHt]\psi_0\rangle|^2$ [1]; it was pointed out that no such revival was expected in the presence of a continuum of (or more generally, incommensurate) conformal weights, e.g. in an irrational conformal field theory. The periodicity we find in this chapter in entanglement entropy and other observables is observed, however, in *any* CFT, including large c theories with a holographic dual. This is tied to the fact that these observables are not sufficient to distinguish between rational and irrational theories (see [92] for a recent discussion).

5.2 CFT with finite spatial boundary

In this section, we will describe a quantum quench in the presence of a spatial boundary using conformal field theory methods. We will review some known results [71,163] and some new results for time-dependent one-point functions. We will discuss CFT computation of EE in the next section.

Lewt us consider spatial boundaries at $x = \pm L/2$ and, following [59], an initial state of the form,

$$|\psi_0\rangle = e^{-\beta H/4}|B\rangle. \tag{5.1}$$

where the state $|B\rangle$ is a conformal boundary state (the state $|\psi_0\rangle$ can be regarded as an approximation to a realistic quench state [85,87,180]). The parameter β can be regarded as

[1] This is a simpler version of the so-called Loschmidt echo.

a length scale which cuts off the UV modes to render the state normalizable.[2] Following [59], we will view this wavefunction as the result of a Euclidean time evolution from a boundary state $|B\rangle$ at $\tau = -\beta/4$ to $|\psi_0\rangle$ at $\tau = 0$. Real time evolution of (5.1) is described by continuing τ to complex values:

$$|\psi(t)\rangle = e^{-iHt}|\psi_0\rangle = e^{-\tau H}|B\rangle,\ \tau = \beta/4 + it. \tag{5.2}$$

We would be interested in time-dependent quantities such as (a) the equal-time correlators

$$\langle O_1(x_1,t)...O_n(x_n,t)\rangle \equiv \langle\psi(t)|O_1(x_1)...O_n(x_n)|\psi(t)\rangle. \tag{5.3}$$

or (b) the entanglement entropy $S_{EE}(t)$ of an interval $A = [-l/2, l/2]$ when the system as a whole is described by the wavefunction (5.2). As discussed in [59] (see below), $S_{EE}(t)$ is related to a two-point correlator of the above kind.

As mentioned above, the boundary state $|B\rangle$ implements a certain boundary condition on the time boundary $\tau = -\beta/4$. When the *same* boundary conditions are also imposed at the spatial boundaries $x = \pm L/2$, then the correlators (5.3) can be evaluated by a functional integral over a rectangle (see figure 5.1), with boundary condition relevant to the boundary state $|B\rangle$ imposed on all sides of the rectangle.[3]

5.2.1 Mapping the rectangle to the upper half plane

Functional integrals over a rectangular region are not easy to compute directly. However, since we are dealing with a CFT, and the boundary conditions do not break conformal symmetry, the CFT correlators (5.3) are covariant under conformal transformations. We can

[2] We will find below that for large enough L/β, the energy of this state coincides with the energy of a thermal ensemble characterized by an inverse temperature β (see (2.1)). Hence, from here on we will refer to $1/\beta$ as a 'temperature', although we should remember that we are still dealing with a pure state and the nomenclature is only a formal one.

[3] In case the spatial boundary conditions are different from the temporal boundary conditions, one needs to insert some boundary operators at the corners of the rectangle [74].

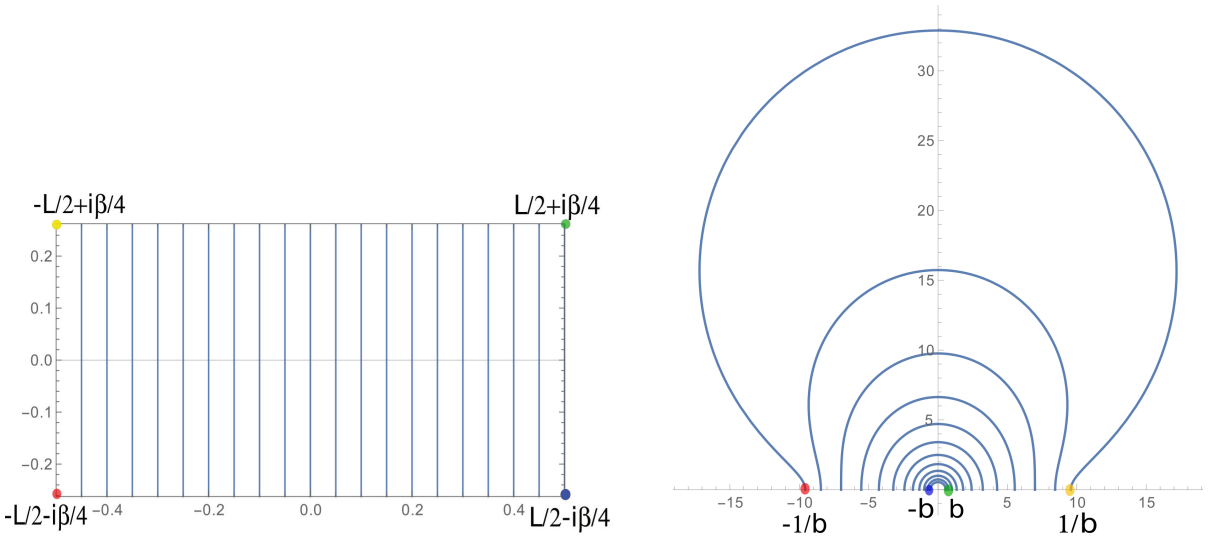

Figure 5.1: Maps between the upper half plane and the rectangle. The colour coding represents the mapping of the corners to the boundary of the UHP. See (5.88) and (5.87). The time evolution contours in the rectangle are mapped to the UHP as shown on the right. We have chosen $L = \beta = 1$.

thus reduce the computation to that on the upper half plane (UHP) by using a conformal map from the rectangle to the UHP. The necessary map for this purpose is a Christoffel-Schwarz transformation[4], defined by

$$w(z) = A \int_0^z \frac{dz}{\sqrt{(z^2 - b^2)(z^2 - \frac{1}{b^2})}} + B, \tag{5.4}$$

Here, z is a complex coordinate on the UHP (defined by the region $\mathrm{Im}(z) \geq 0$ of the plane), whereas $w = x + i\tau$ is a complex coordinate parametrizing the above-mentioned rectangular region (bounded by the lines $|\mathrm{Re}(w)| \leq L/2$, $|\mathrm{Im}(w)| \leq \beta/4$, see figure 5.1). A, B are constants which determine the images of the corners of the rectangle on the boundary of the UHP. Without loss of generality, the four image points can be chosen to have z-coordinates: $(z_1, z_2, z_3, z_4) = (-1/b, -b, b, 1/b)$ with $(0 \leq b \leq 1)$. We will look for a map which sends these points to the following corners of the rectangle respectively:

$$w\left(-\frac{1}{b}\right) = -\frac{L}{2} - i\frac{\beta}{4},\ w(-b) = \frac{L}{2} - i\frac{\beta}{4},\ w(b) = \frac{L}{2} + i\frac{\beta}{4},\ w\left(\frac{1}{b}\right) = -\frac{L}{2} + i\frac{\beta}{4}. \tag{5.5}$$

[4]The transformation we use here is a little different from that found in literature. The reason is that we want to explore both the low and the high values of L/β using this map by simply tuning the parameter b.

The required map is discussed in [163] (see also Appendix 5.7.1). For convenience, we reproduce here the map $z(w)$ (5.88) from the rectangle to the UHP

$$z(w) = b\,\mathrm{sn}\left[\frac{4K(b^4)}{i\beta}\left(w-\frac{L}{2}\right), b^4\right], \quad \bar{z}(\bar{w}) = b\,\mathrm{sn}\left[\frac{4K(b^4)}{-i\beta}\left(\bar{w}-\frac{L}{2}\right), b^4\right]. \tag{5.6}$$

The parameter b determines the aspect ratio of the rectangle:

$$\frac{\beta}{L} = \frac{4K(b^4)}{K(1-b^4)}. \tag{5.7}$$

We show in Appendix 5.7.1 that the map (5.6) can also be regarded as a map from the torus (a product of two circles of sizes $2L, \beta$) owing to the periodicity properties (5.91). The map also has a large L limit (5.96)

$$z(w) = i\exp[-2\pi w/\beta], \tag{5.8}$$

and a low temperature[5] limit (5.97)

$$z(w) = i\cot\left(\frac{\pi}{4}+\frac{\pi w}{2L}\right). \tag{5.9}$$

5.2.2 One Point Function

In this section, we will evaluate a one-point function $\langle O(x,t)\rangle$ as defined in (5.3) (part of the above discussion has already appeared in [102, 163], see also [92]). The evaluation would include calculating the one point function in Euclidean time τ and then analytically continuing to Lorentzian time t. We shall however, first, use the map $z(w)$ (5.6) to relate the one-point function on the rectangle to that on the UHP.

[5] We use the word 'temperature' to refer to $1/\beta$ in the sense of footnote 2.

Primary operators For a primary operator $O(w,\bar{w})$, of dimension $(h,\bar{h})$, the one-point function on the rectangle becomes

$$\langle O(w,\bar{w})\rangle_{\text{rect}} = \left(\frac{\partial z}{\partial w}\right)^{h}\left(\frac{\partial \bar{z}}{\partial \bar{w}}\right)^{\bar{h}}\langle O(z,\bar{z})\rangle_{\text{UHP}}. \tag{5.10}$$

For a holomorphic operator, or an operator with $\bar{h} \neq h$, the above one-point function on the UHP vanishes. However, for a primary operator of the form $O_{h,h}(w,\bar{w}) = \phi_h(w)\phi_h^\dagger(\bar{w})$, (with $\bar{h} = h$) [6] the above one-point function on the UHP is non-zero and is given by the 'method of images' [74]. According to this method, the conformal boundary condition on the UHP amounts to replacing the antiholomorphic operator $\phi_h^\dagger(\bar{z})$ from the point $P = (z,\bar{z})$ by a holomorphic operator $\phi_h(z')$ at the image point $P' = (z',\bar{z}')$ (with $z' = \bar{z}, \bar{z}' = z$). The one-point function is now given by the holomorphic 2-point function on the plane[7]

$$\langle O_{h,h}(P)\rangle_{UHP} = A_b\langle\phi_h(P)\phi_h^\dagger(P')\rangle_{\mathbb{C}} = A_b\langle\phi_h(z)\phi_h^\dagger(z')\rangle_{\mathbb{C}}$$

Hence, the original one-point function, for primary operators $O_{h,h}(w,\bar{w}) \equiv \phi_h(w)\phi_h^\dagger(\bar{w})$ reduces to

$$\langle O_{h,h}(w,\bar{w})\rangle_{\text{rect}} = \left(\frac{\partial z}{\partial w}\right)^{h}\left(\frac{\partial \bar{z}}{\partial \bar{w}}\right)^{h}\langle\phi_h(z)\phi_h^\dagger(z')\rangle_{\mathbb{C}} \tag{5.11}$$

Quasiprimary operators In case the operator $O(w,\bar{w})$ is quasiprimary, it mixes with lower dimension operators under conformal transformations, leading to additional terms in (5.10). For example, for the holomorphic stress tensor $T(w) \equiv T_{ww}(w)$, the conformal transformation to the UHP is given by

$$\langle T(w)\rangle_{\text{rect}} = \left(\frac{\partial z}{\partial w}\right)^{2}\langle T(z)\rangle_{\text{UHP}} - \frac{c}{12}\{z,w\} = -\frac{c}{12}\{z,w\} \tag{5.12}$$

[6] Here we allow for complex operators ϕ; $\phi^\dagger$ denotes the hermitian conjugate.

[7] Up to a constant A_b which depends on the operator O and the boundary state $|B\rangle$. We will assume that $A_b \neq 0$; the precise value of this constant will be unimportant and we will drop it henceforth.

In the second equality we have used the fact that $\langle T(z)\rangle$ on the UHP is the same as that on the plane (since it does not have an antiholomorphic factor), and hence vanishes. The last expression contains the Schwarzian derivative

$$\{z,w\} = \frac{2(\partial_w^3 z)(\partial_w z) - 3(\partial_w^2 z)^2}{2(\partial_w z)^2} \tag{5.13}$$

A similar formula is true for the antiholomorphic stress tensor $\bar{T}(\bar{w})$.

For the operator $O(w,\bar{w}) =: T(w)\bar{T}(\bar{w}) :$, by using a combination of the above techniques, we get a generalization of the formula (5.11):

$$\langle : T(w)\bar{T}(\bar{w}) : \rangle_{\text{rect}} = \left(\frac{\partial z}{\partial w}\right)^2 \left(\frac{\partial \bar{z}}{\partial \bar{w}}\right)^2 \langle T(z)T(z_1)\rangle_{\mathbb{C}} + \left|\frac{c}{12}\{z,w\}\right|^2 \tag{5.14}$$

Analytic continuation to real time correlators

As discussed before, the time-dependent wavefunction (5.2), or equivalently the time-dependent Heisenberg operators $O(x,t)$ can be realized by analytically continuing τ to imaginary values $\tau = it$. Thus, $O(w,\bar{w}) = O(x,\tau)$ can be interpreted as the time-dependent operator $O(x,it)$. In terms of the coordinates on the rectangle, the analytic continuation reads[8]

$$\{w,\bar{w}\} = x \pm i\tau \xrightarrow{\tau = it} x \mp t \equiv x^{\pm} \tag{5.15}$$

This 'Wick rotates' the Euclidean rectangle to the Lorentzian geometry,

$$M_L = \mathbb{I} \times Rx_{\pm} = x \mp t,\ x \in \mathbb{I} = [-L/2, L/2], t \in \mathbb{R} \tag{5.16}$$

Note that such an analytic continuation is possible since the Euclidean observables are separately analytic in $(z,\bar{z})$, and hence in $(w,\bar{w})$. We will use this rule below to explicitly

[8] Note the convention $x^{\pm} \equiv x \mp t$.

compute the time-dependence of one-point functions and later on, the single interval entanglement entropy.

We note here that although for these applications, we do not need to have an analytic continuation of the complex $z, \bar{z}$ plane, we will indeed find an analytic continuation of the Euclidean map (5.6), *viz.* (5.55), from the the above geometry M_L to the Lorentzian $\mathbb{R}^2$. The above map is many-to-one and one can choose a fundamental domain of the map to be a diamond-shaped region $\mathbb{D} : \{x_\pm \in (-L/2, L/2)\} \subset M_L$ in Section 5.4 to build a bulk geometry dual to a CFT on M_L. It has been suggested in [163], and further elaborated in [92], that thermalization appears to happen when one confines to this diamond (which is natural from the viewpoint of the $\mathbb{R}^2$, whereas the actual spacetime is all of M_L, with its built-in recurrence. In Section 5.4, the map (5.55) is crucially used to construct a dual geometry for the CFT state. We will discuss this map in detail in Appendix 5.7.2.

5.2.3 Behavior of the Energy density

In Euclidean CFT, the energy density is given by

$$\mathcal{E}_{Eucl}(w, \bar{w}) = \langle T_{\tau\tau} \rangle = -\left(\langle T(w) \rangle + \langle \bar{T}(\bar{w}) \rangle\right) = \frac{c}{12}\left(\{z, w\} + \{\bar{z}, \bar{w}\}\right) \tag{5.17}$$

where in the last step we have used (5.12) and its antiholomorphic counterpart. In the limits of high and low temperature, (5.8) and (5.9) respectively, the Schwarzian derivative is easy to compute, leading to the constant values

$$\mathcal{E}_{Eucl} = \begin{cases} -c\pi^2/3\beta^2, & \beta \ll L \\ +c\pi^2/12L^2, & \beta \gg L \end{cases} \tag{5.18}$$

Using the methods of Section 5.2.2 and the analytic continuation(5.15), the energy density in the Lorentzian theory is,

$$\mathcal{E}(x,t) = \langle T_{++}(x_+) + T_{--}(x_-)\rangle = \langle T_{tt}\rangle = -\langle T_{\tau\tau}\rangle = -\mathcal{E}_{Eucl}(w = x_+, \bar{w} = x_-) \tag{5.19}$$

Now, the high and low temperature limits are,

$$\mathcal{E}(x,t) = +c\pi^2/3\beta^2, \quad \beta \ll L \tag{5.20}$$

$$= -c\pi^2/12L^2, \quad \beta \gg L. \tag{5.21}$$

which can be identified with the well-known expressions for the thermal energy and Casimir energy respectively.

We note here that some of the results in this subsection have been obtained and discussed in [71, 163]; we include these here for the sake of completeness.

Time-dependence

Away from the above two limits, the energy density (5.19) is both space and time-dependent. We display the behaviour of the 'normalized' dimensionless quantity

$$\widetilde{\mathcal{E}} = \frac{\mathcal{E}L^2}{c} \tag{5.22}$$

in Figures 5.2 and 5.3. In Figure 5.2, one can clearly see two crests getting reflected back and forth periodically at the boundary walls. These correspond to the holomorphic and antiholomorphic stress tensors respectively.

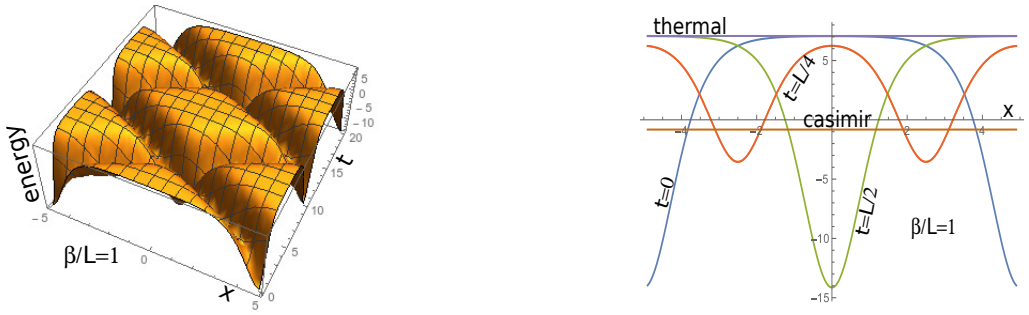

Figure 5.2: The time evolution of the normalized energy density $\widetilde{\mathcal{E}}$ (Eq. (5.22)) in the quench geometry. In both the figures we have chosen $\beta = L = 10$. Left panel: The time range is taken to be $t \in [0, 2L]$. Note that there are two crests, one moving initially to the right (corresponding to $T_{++}(x_+)$ of (5.19)), and the other moving to the left (corresponding to $T_{--}(x_-)$). Both are reflected at the wall at $t = (n+1/2)L, n \in \mathbb{Z}$. Right panel: Here we display, in a 2D plot, some of the features of the 3D plot at $t = 0, L/4, L/2$. At $t = 0$ there is a single local thermal region in the middle. As time progresses, it splits into two separate regions (see the curve for $t = L/4$), reaching the two ends at $t = L/2$. After this time, the two regions turn back and merge at $t = L$, as is clear from the 3D plot on the left.

Space dependence: Localized thermal region

In Figure 5.3, we plot the energy density at a fixed time $t = 0$ as a function of x for various values of the ratio β/L, with temperature increasing from left to right. In the figure, we see that for temperatures $T \lesssim 1/L$, the energy density profile has a localized region in the middle where it agrees with the thermal density. In Section 5.4, we will provide a holographic interpretation of this observation.

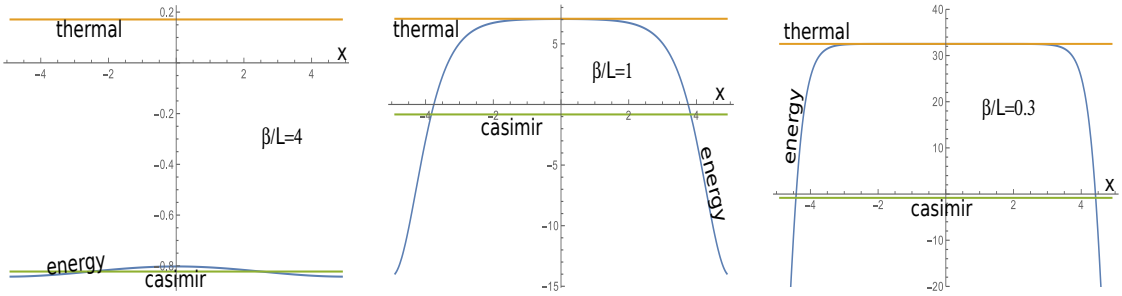

Figure 5.3: Plot of the normalized energy density $\widetilde{\mathcal{E}}(x,t)$ at $t = 0$ for various values of $\frac{\beta}{L} = 4, 2, 0.3$. Left: $\frac{\beta}{L} = 4$. This can be interpreted as low temperature or small 'box size' L. The energy density approaches the uniform limiting value, the Casimir energy density computed in (5.21) in the low temperature limit $\frac{\beta}{L} = \infty$. Middle: $\frac{\beta}{L} = 2$. The energy density approaches the thermal value in a small region near the middle. Right: $\frac{\beta}{L} = \frac{1}{4}$. This can be interpreted as a high temperature or large box size L. The energy density matches in a large region the uniform thermal energy density computed in (2.1) in the limit $\frac{\beta}{L} = 0$. In the first panel, the one-point functions actually have a periodicity with a period $2L$ (see Section 5.4.2).

5.2.4 Thermalization and 'revival' of a local operator

In this section, we discuss some features of time and position dependence of one-point functions, using the formulae derived in Section 5.2.2. We consider primary operators of the form $O_{h,h}(x,t)$ whose one-point functions are given by (5.11) with $\tau = it$. We also consider a particular quasiprimary operator $T\bar{T}(x,t)$, whose one-point function is given by (5.14). The results are presented in Figure 5.4. An important feature of the time-dependence of these operators, for a given x (see the left panel of Figure 5.4), is that there is a time window, $t_1 < t < t_2$, in which all these local operators 'thermalize', i.e., they approach their 'thermal' values:

$$\langle O(x,t)\rangle \to \langle O(x)\rangle_\beta + a\exp[-\gamma(t-t_1)] \tag{5.23}$$

In case of primary operators the thermal average $\langle O(x)\rangle_\beta$ vanishes, whereas for $T\bar{T}$, it is non-zero. It can be seen that the thermalization rate γ is given by

$$\gamma = 2\pi\Delta/\beta,\ \Delta = h + \bar{h} = 2h \tag{5.24}$$

As t exceeds t_2 (which is of order $L/2$ for the operator $T\bar{T}$), the one-point function starts deviating from the thermal value and eventually goes back to its original value at $t = nL$ for some integer n (this is to be compared with the periodic behaviour termed as 'revival' in [71]).

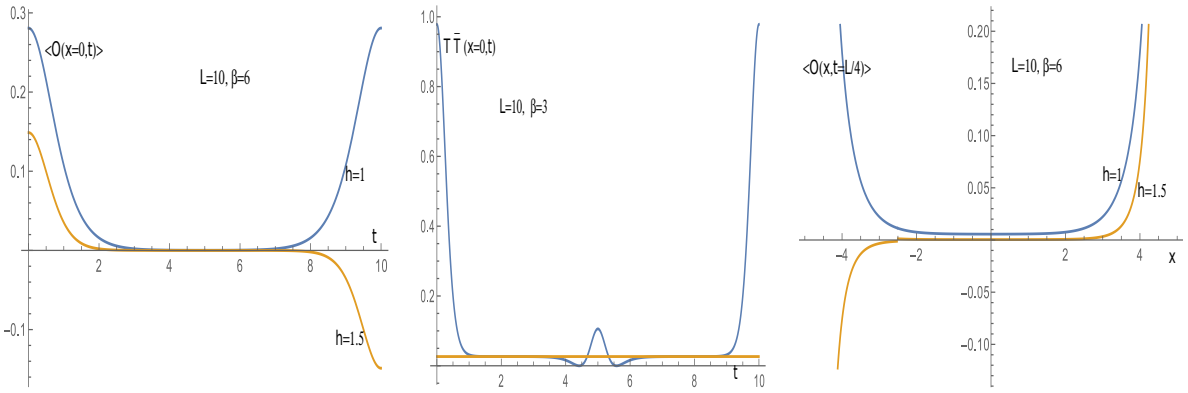

Figure 5.4: Plot of one-point functions as a function of x and t. The left panel shows the time-dependence of one-point functions of two primary fields $\langle O(x,t)\rangle$ with $h=\bar{h}=1$ (blue), and $h=\bar{h}=3/2$ (orange) at a fixed spatial position $x=0$ (see (5.11)). The right panel shows the x-dependence of the same operators at a fixed $t=L/4$, which displays a homogeneous intermediate region. The middle panel shows $\langle :T\bar{T}:(x,t)\rangle$ at $x=0$ as a function of t (see (5.14)). The left and middle panels show the exponential decay at intermediate times to the thermal value and the eventual revival, at $t=L/2$ [71]. In the left panel the thermal value is zero. In the middle panel, the horizontal (orange) line represents the thermal value, which is non-zero since $:T\bar{T}:$ is a quasiprimary operator. More generally, arbitrary one-point functions show a time periodicity of $2L$ (see the derivation in Section 5.4.2).

5.3 Evolution of entanglement entropy following a quench

In this section we would like to compute the time-evolution of entanglement entropy (EE) of a single interval in a CFT with boundaries, following a quantum quench (as described in Section 5.2). We will follow up the CFT calculation in this section by a holographic computation in Section 5.4, and a computation using a quasiparticle picture in Section 5.5.

Let us consider a 2D CFT, defined by the wavefunction (5.1) representing a quantum quench. As explained in Section 5.2, the norm of the wavefunction (5.2), evolved over Euclidean time $\tau=\beta/4$ [9], is given by a functional integral over a Euclidean rectangle Σ. Let us define the reduced density matrix for a spatial interval $A=\{-l/2,l/2\}$ by

$$\rho_A=\frac{1}{\sqrt{Z}}\,\mathrm{Tr}_{A^c}\,|\psi_0\rangle\langle\psi_0|\,,\quad \mathrm{Tr}(\rho_A)=1 \tag{5.25}$$

[9] Quantities depending on real time are obtained by continuing to $\tau=\beta/4+it$.

where Z is a normalization factor. The EE for this interval is then defined as

$$S_A = -\mathrm{Tr}\rho_A \log \rho_A \tag{5.26}$$

A standard procedure to compute this quantity, called the replica trick, is to first calculate the Renyi entropy

$$S_A^{(n)} \equiv \frac{1}{1-n}\mathrm{Tr}(\rho_A^n) \tag{5.27}$$

and then take the limit (after analytically continuing n to real values).

$$S_A = \lim_{n\to 1} S_A^{(n)} = -\frac{\partial}{\partial n}\Big|_{n=1}\mathrm{Tr}\rho_A^n \tag{5.28}$$

Computing (5.27) involves evaluating the partition function on the manifold Σ_n, which is an n-fold cover of the rectangle Σ branched over A. As shown in [64], this amounts to computing a two-point function, on the rectangle, of the so called nth order twist and anti-twist operators, $\sigma_+(w,\bar{w})$ and $\sigma_-(w,\bar{w})$ respectively, each with a conformal dimension $h_n = \bar{h}_n = \frac{1}{2}\Delta_n = \frac{c}{24}(n-\frac{1}{n})$. Thus,

$$\mathrm{Tr}\rho_A^n = \langle \sigma_+(w_1,\bar{w}_1)\,\sigma_-(w_2,\bar{w}_2)\rangle_{\mathrm{rect}}. \tag{5.29}$$

where $(w_i,\bar{w}_i), i=1,2$ are the complex coordinates (5.15) of the end-points of the interval A. Let us choose the position of the end-points of the interval at a Lorentzian time t to be,

$$w_1 = -\frac{l}{2} - t, \quad \bar{w}_1 = -\frac{l}{2} + t, \quad w_2 = \frac{l}{2} - t, \quad \bar{w}_2 = \frac{l}{2} + t \tag{5.30}$$

This 2-point function is obtained by pulling back a corresponding 2-point function on the upper half plane by the conformal maps (5.105), (5.87), in a generalization of Section 5.2.2.

Hence,

$$\mathrm{Tr}\rho_A^n = \prod_{i=1}^{2} \left(\frac{dz_i}{dw_i}\right)^{h_n} \left(\frac{d\bar{z}_i}{d\bar{w}_i}\right)^{\bar{h}_n} \langle \sigma_+(z_1,\bar{z}_1)\sigma_-(z_2,\bar{z}_2)\rangle_{\mathrm{UHP}} \tag{5.31}$$

To evaluate such a 2-point function on the UHP one needs to use the method of images. However, there are subtleties associated with this method which limits its range of validity. We shall point them out in the next section before we proceed to calculate the above 2 point function using the method.

5.3.1 Method of Images

In [74], Cardy showed that an n-point function on the UHP satisfies the same differential equation (corresponding to a Ward Identity) as a $2n$-point function of purely holomorphic operators on the full complex plane $\mathbb{C}$. The two-point function $\langle \sigma_+(z_1,\bar{z}_1)\sigma_-(z_2,\bar{z}_2)\rangle_{\mathrm{UHP}}$ is thus *related*, in this sense, to the 4-point function

$$\langle \sigma_+(z_1)\sigma_-(\bar{z}_1)\sigma_-(z_2)\sigma_+(\bar{z}_2)\rangle_C = \left(\frac{(z_1-\bar{z}_2)(z_2-\bar{z}_1)}{(z_1-z_2)(\bar{z}_1-\bar{z}_2)(z_1-\bar{z}_1)(z_2-\bar{z}_2)}\right)^{\Delta_n} F(\eta), \tag{5.32}$$

where function $F(\eta)$ is a (non-universal) function of the cross ratio

$$\eta = \frac{(z_1-\bar{z}_1)(z_2-\bar{z}_2)}{(z_1-\bar{z}_2)(z_2-\bar{z}_1)} \tag{5.33}$$

The relation mentioned above does not imply, however, that the two-point function on the UHP is always *equal* to the 4-point function on the plane, since, for one thing, the UHP correlator involves information about the boundary condition on the boundary of the UHP whereas the planar correlator does not involve any such information[10].

Having said this, it turns out that there are certain limits where the two correlators are, in fact, essentially[11] equal. One of them is the high temperature limit where both the 2 and the

[10] We thank Justin David and Tadashi Takayanagi for crucial discussions on this issue.

[11] In this subsection, we use the word "essentially" to mean up to an irrelevant proportionality constant.

4-point functions factorize in one way or the other. In such a case, the UHP correlator does turn out to be essentially independent of the boundary state. For intermediate temperatures, however, there is no such factorization and the two-point function on the UHP is different from the 4-point function on $\mathbb{C}$ due to the presence of the boundary.

There is another limit, as we will study, in which the equality holds (in fact, at all temperatures this time). This is the large central charge limit. As we shall see in Section 5.3.4, in this limit, the four point function is easily evaluated and becomes essentially equal to the two-point function on the UHP. Here too the information about the boundary condition is lost in the large c limit.

5.3.2 Large L/β limit

In the limit of large system size L[12], the conformal map is given by (5.8). The computation of EE described above reduces, in this limit, to the analysis of [59, 138]. The complex coordinates (5.30) are mapped to

$$z_1 = ie^{-\frac{2\pi}{\beta}(-\frac{l}{2}-t)},\ \bar{z}_1 = -ie^{-\frac{2\pi}{\beta}(-\frac{l}{2}+t)},\ z_2 = ie^{-\frac{2\pi}{\beta}(\frac{l}{2}-t)},\ \bar{z}_2 = -ie^{-\frac{2\pi}{\beta}(\frac{l}{2}+t)} \tag{5.34}$$

on the upper half plane. Here we have assumed that $t/l \ll L$. Therefore, the cross ratio η in (5.33) becomes

$$\eta = \frac{2\cosh^2\frac{2\pi t}{\beta}}{\cosh\frac{2\pi l}{\beta} + \cosh\frac{4\pi t}{\beta}} \tag{5.35}$$

When $t/\beta, l/\beta \gg 1$, the cross ratio behaves as

$$\eta \simeq \frac{e^{\frac{4\pi t}{\beta}}}{e^{\frac{4\pi t}{\beta}} + e^{\frac{2\pi l}{\beta}}} \tag{5.36}$$

[12]Defined in the sense of the limit (a) of footnote 21.

It is easy to verify that,

$$\eta \to \begin{cases} 0 \text{ for } t < l/2 \\ 1 \text{ for } t > l/2 \end{cases} \tag{5.37}$$

where we have assumed $|t - l/2| \gg \beta$. Both the limits of η correspond to a factorization of the four-point function (5.32) into a product of two-point functions in the two crossed channels, respectively. This leads to a simpler calculation of the EE which gives

$$S_A = \begin{cases} \frac{2c\pi t}{3\beta} \text{ for } t < l/2 \\ \frac{c\pi l}{3\beta} \text{ for } t > l/2 \end{cases} \tag{5.38}$$

where a divergent constant has been subtracted [59].

These results are universal since they depend only on the central charge of the CFT. The behaviour (5.38) represents the linear rise of the EE followed by the saturation to the thermal value (see Figure 5.6, left part of the third panel). By the periodicity properties mentioned in Section 5.4.2, we can also show that CFT results reproduce the right part of the third panel of Figure 5.6. One way to see this is to note that for $L - t, l \ll L$ the map (5.6) reduces to a map similar to (5.34), with $t \to L - t$.

5.3.3 Low temperature (L/β small)

In the low temperature limit[13], the conformal map is given by (5.9). Using this, the w-coordinates (5.30) are mapped to

$$\begin{aligned} z_1 &= i \cot\left(\frac{\pi}{4} + \frac{\pi(-l/2 - t)}{2L}\right), \quad \bar{z}_1 = -i \cot\left(\frac{\pi}{4} + \frac{\pi(-l/2 + t)}{2L}\right) \\ z_2 &= i \cot\left(\frac{\pi}{4} + \frac{\pi(l/2 - t)}{2L}\right), \quad \bar{z}_2 = -i \cot\left(\frac{\pi}{4} + \frac{\pi(l/2 + t)}{2L}\right). \end{aligned} \tag{5.39}$$

[13]Defined in the sense of limit (c) of footnote 21.

The cross-ratio (5.33) now becomes

$$\eta = \cos^2 \frac{\pi l}{2L} \tag{5.40}$$

Thus, unlike in the high temperature limit, the cross ratio does not take a special value. Depending on the size of the interval l, it can lie anywhere between 0 and 1. Consequently, the four-point function (5.32) does not factorize into two-point functions. This implies that the CFT EE remains a non-universal quantity, depending on the particular CFT under consideration.

A puzzle The above remark immediately raises the following puzzle. We will see in Section 5.4.1, the holographic EE, as computed using (5.61) and (5.66), is independent of the details of the dual CFT (except for the dependence on the central charge c which determines the Newton's constant through (5.60)). [14]

The puzzle is that while the holographic EE is universal, the CFT EE certainly does not appear to be so. How does one reconcile this with AdS/CFT? Also, what is the CFT calculation which will agree with the hEE at all temperatures and exhibit universality?

Resolution This puzzle will be resolved in the next subsection, by appealing to the *large central charge* limit.

[14] This is a recurrent theme in AdS/CFT. A similar observation is: many different CFT states appear to evolve into states described by black holes. The emergence of universality in the bulk in that context is related to the universality of thermal physics.

5.3.4 Universality of the Entanglement Entropy at large central charge

At Low Temperature

One way of obtaining universal results for the EE, (as will be shown in the low temperature bulk calculations), from the CFT, is by looking at the large c systematics (similar issues have been addressed in [164]). As has been mentioned, the calculation of $\mathrm{Tr}\rho_A^n$ on the manifold Σ_n, can be mapped to the calculation of the two point correlator of n-th order twist and anti-twist operators on the UHP. Using the method of images, this is equivalent to a four point function of two twist and two anti-twist operators on $\mathbb{C}$. The four point function is then,

$$\mathrm{Tr}\rho_A^n = \prod_{i=1}^{2}\left(\frac{dz_i}{dw_i}\right)^{h_n}\left(\frac{d\bar{z}_i}{d\bar{w}_i}\right)^{\bar{h}_n}\mathcal{G}_4, \quad \mathcal{G}_4 \equiv \langle\sigma_+(z_1)\sigma_-(\bar{z}_1)\sigma_+(\bar{z}_2)\sigma_-(z_2)\rangle_{\mathbb{C}}$$

For convenience, we send the four points $(z_1, \bar{z}_1, z_2, \bar{z}_2)$ to $(\infty, 1, 0, \eta)$, such that

$$\mathcal{G}_4 = (z_{1\bar{2}}z_{\bar{1}2})^{-2h_n}G_n(\eta), \qquad G_n(\eta) = \langle\sigma_+(\infty)\sigma_-(1)\sigma_+(\eta)\sigma_-(0)\rangle_{\mathbb{C}} \tag{5.41}$$

Consider the scaled 4 point function in the $\eta \to 0$ channel. In the large central charge limit, all the conformal blocks exponentiate ([243]). The form of the function is,

$$G_n(\eta) = \sum_p a_p e^{-\frac{nc}{6}f_p(h_n,\eta;nc)} \tag{5.42}$$

Recent results ([135]) suggest that it is only the vacuum block that dominates the above sum over intermediate operators. In that case, the 4-point function is,

$$G_n(\eta) \approx e^{-\frac{nc}{6}f_0(h_n,\eta;nc)} \tag{5.43}$$

Taking the four points $z_{1,2}, \bar{z}_{1,2}$ to be given by (5.39), we get the cross-ratio to be,

$$\eta = \frac{z_{1\bar{1}} z_{2\bar{2}}}{z_{1\bar{2}} z_{2\bar{1}}} = \cos^2 \frac{\pi l}{2L} \tag{5.44}$$

From ([135]), one knows that the result for the vacuum block (in the $\eta \to 0$ channel) is,

$$f_0(h_n, \eta; nc) = 12\alpha \log(\eta) + \mathcal{O}(\alpha^2) \tag{5.45}$$

where $\alpha = \frac{1}{12}(n-1)(= h_n/c)$. Hartman's result tells us that we can extrapolate the result found around $\eta = 0$ up till $\eta = \frac{1}{2}$ owing to monotonicity of the conformal blocks as a function of η for light operator exchanges. A similar statement holds in the other channel around $\eta = 1$. The vacuum block in that case is,

$$f_0(h_n, \eta; nc) = 12\alpha \log(1-\eta) + \mathcal{O}(\alpha^2) \tag{5.46}$$

Here, again, the results can again be extrapolated up to $\eta = \frac{1}{2}$. This enables us to state that the purely holomorphic Euclidean 4-point function is in fact equal to the 2-point function on the UHP. Again, the interesting thing to notice is that the information about the boundary gets completely lost in this equivalence at large c!

The Entanglement Entropy in the s-channel ($\eta \to 0$) is then,

$$S_A = \lim_{n\to 1} \frac{1}{1-n} \log Tr \rho_A^n = \lim_{n\to 1} \left[\frac{4h_n}{1-n} \log(\frac{\pi}{2L}) - \frac{nc}{6} \frac{1}{1-n} 12\alpha \log(\eta) \right] \tag{5.47}$$

where the first term comes from the Jacobian and the prefactor in 5.41. With $\alpha = h_n/c$ and $\eta = \cos^2(\frac{\pi l}{2L})$, we get,

$$S_A = \frac{c}{3} \log \left(\frac{2L}{\pi a} \cos \frac{\pi l}{2L} \right) \tag{5.48}$$

This result is, of course, valid up to $\eta = 1/2$ and hence, for $L/2 \leq l < L$. In the other channel $\eta \to 1$,

$$S_A = \frac{c}{3} \log \left(\frac{2L}{\pi a} \sin \frac{\pi l}{2L} \right) \tag{5.49}$$

This is valid for $0 \leq l \leq L/2$. In both the above cases, we have introduced the UV cut-off a by hand to regulate the answers. As, we will see later, these answers match exactly with the holographic results in the low-temperature limit.

For All Temperatures

The results obtained at low temperatures for large c are much more general. In fact, we would like to show the equivalence of these results with the lengths of the bulk geodesics, which can be calculated for all temperatures. The analysis of the four point function on $\mathbb{C}$ is completely general. The information about the initial nature of the geometry (a rectangle in this case), is contained in the pull-back maps and hence in the Jacobian factors. Only the cross-ratio on the plane knows about the initial geometry through the pull back maps. Let us calculate the entanglement entropy on the plane and use an unspecified conformal transformation to pull it back onto a non-trivial geometry.

On the plane,

$$\mathrm{Tr}\rho_A^n = \prod_{i=1}^{2} \left(\frac{dz_i}{dw_i} \right)^{h_n} \left(\frac{d\bar{z}_i}{d\bar{w}_i} \right)^{\bar{h}_n} \mathcal{G}_4 \tag{5.50}$$

Let us call the Jacobian factors $J = \prod_{i=1}^{2} (\frac{dz_i}{dw_i})(\frac{d\bar{z}_i}{d\bar{w}_i})$ for simplicity. Then (as we saw in the previous section), for the $\eta \to 1$ channel,

$$\begin{aligned} S_A &= \lim_{n\to 1} \frac{1}{1-n} \left[h_n \log \left(\frac{a^4 J}{(z_{1\bar{2}} z_{\bar{1}2})^2} \right) - \frac{nc}{6} 12\alpha \log \eta) \right] \\ &= \lim_{n\to 1} \frac{2h_n}{n-1} \left[\log \left(\frac{z_{1\bar{2}} z_{\bar{1}2}}{a^2 \sqrt{J}} \right) + n \log(\eta) \right] \\ &= \frac{c}{6} \log \left(\frac{\eta}{a^2} \frac{z_{1\bar{2}} z_{\bar{1}2}}{\sqrt{J}} \right) \end{aligned} \tag{5.51}$$

Note, the factor of a^4 in the first line of the expression has been introduced for dimensional reasons and has a length dimension. With the identifications, $c = \frac{3}{2G_3}$ and $\eta = \frac{z_{1\bar{1}} z_{2\bar{2}}}{z_{1\bar{2}} z_{2\bar{1}}}$, the above EE is,

$$S_A = \frac{1}{4G_3} \log\left(\frac{z_{1\bar{1}} z_{\bar{2}2}}{a^2\sqrt{J}}\right) \tag{5.52}$$

This expression for the entanglement entropy exactly coincides the sum of the bulk geodesic lengths between the boundary points $(z_1, \bar{z}_1)$ and $(z_2, \bar{z}_2)$ (with the identifications $z_\pm = f(x_\pm)$), in the geometry corresponding to the pulled back (non-trivial) surface, at all temperatures. This is the 'disconnected' channel in (5.66).

Similarly, when $\eta \to 0$, we shall have to use the conformal block in the other channel. Now, $(1-\eta) = \frac{z_{12} z_{\bar{1}\bar{2}}}{z_{1\bar{2}} z_{\bar{1}2}}$. Using this, the entanglement entropy is,

$$\begin{aligned} S_A &= \lim_{n\to 1} \frac{1}{1-n}\left[h_n \log\left(\frac{a^4 J}{(z_{1\bar{2}} z_{\bar{1}2})^2}\right) - \frac{nc}{6} 12\alpha \log(1-\eta)\right] \\ &= \frac{c}{6}\log\left(\frac{(1-\eta)}{a^2}\frac{z_{1\bar{2}} z_{\bar{1}2}}{\sqrt{J}}\right) \\ &= \frac{1}{4G_3}\log\left(\frac{z_{12} z_{\bar{1}\bar{2}}}{a^2\sqrt{J}}\right) \end{aligned} \tag{5.53}$$

This matches with the bulk entropy in the 'connected' channel in (5.66) with geodesics joining the points (z_1, z_2) and $(\bar{z}_1, \bar{z}_2)$.

5.4 Bulk dual

In this section we discuss a holographic dual to the above two dimensional quenches [234]. It is known that a class of two dimensional CFTs with a large central charge c have an equivalent description in terms of gravity in three dimensional anti de Sitter space (AdS_3). In Poincaré coordinates the metric of AdS_3 is given by

$$ds^2 = \frac{d\zeta^2 + dz_+ dz_-}{\zeta^2}. \tag{5.54}$$

Here $\zeta = 0$ is the conformal boundary of AdS_3. The boundary coordinates $z_\pm = z_1 \mp z_0$ describe the plane where the dual (Lorentzian) CFT lives. We will also consider the Euclidean continuation of the above metric where we will set $z_\pm = \mp i\{z, \bar{z}\}$ (see (5.101), Appendix 5.7.2). The corresponding dual CFT on the complex z-plane will then be Euclidean.

A holographic description of the CFT on a space with boundaries (BCFT) has been proposed in [95, 117, 154, 203, 232]. According to this proposal, the holographic dual of the BCFT on the upper half plane $\{(z_1, z_0)|z_0 > 0\}$ is given by the $z_0 > 0$ region of the Poincare AdS_3. The $z_0 = 0$ plane serves as a boundary of the holographic spacetime[15], with the boundary condition that the extrinsic curvature of the boundary vanishes $K_{\mu\nu} = 0$[16], and ends (at $\zeta = 0$) on the boundary of the UHP. A schematic picture is presented in Figure 5.5.

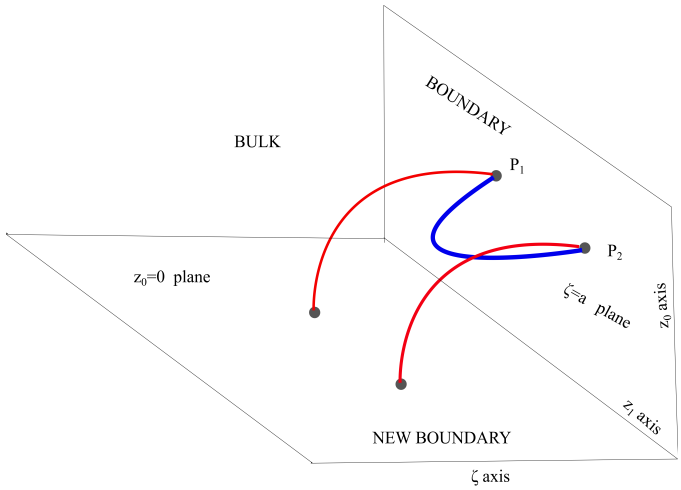

Figure 5.5: Holographic dual to BCFT on the UHP (upper half plane). A one-point function in the UHP is given by an extremal geodesic emanating from the relevant boundary point and ending on the boundary plane (the length of this is half of the geodesic connecting the boundary point and its image). Entanglement entropy of the interval connecting two boundary points P_1 and P_2 is given by the minimum (5.64) of the length of extremal geodesics connecting these points and their images pairwise. We call the 'blue' and 'red' configurations the 'connected' and 'disconnected' channels respectively.

The above description gives the bulk dual of a Lorentzian CFT on the UHP; we would, however, like to obtain the bulk dual for a CFT on a manifold (5.16), M_L = interval $\times\mathbb{R}$.

[15] In a recent proposal [171] a stress-tensor has been ascribed to this plane as in the case of a D-brane.

[16] This boundary condition has a one parameter generalization [117, 232] which corresponds to available boundary conditions in the BCFT.

Now, in Appendix 5.7.2 we will find a map from the manifold M_L to the UHP, given by (5.102):

$$z_\pm = f_\pm(x_\pm), \quad f_+(x) = f_-(x) = f(x) \equiv -b\, \frac{sn\left[\frac{4K(b^4)}{\beta}(x - L/2), 1 - b^4\right]}{cn\left[\frac{4K(b^4)}{\beta}(x - L/2), 1 - b^4\right]} \tag{5.55}$$

Bulk dual through large diffeomorphisms Our strategy to find a bulk dual to the CFT on M_L will be to find a solution to Einstein's equations with a negative cosmological constant whose boundary is M_L. This problem can be solved by the method introduced in [218], where it was shown (building on the works of [50] and [30]) how solutions diffeomorphic to the AdS_3 geometry (5.54) (which are hence solutions to Einstein equations) can be found where the diffeomorphism is non-trivial at the boundary and reduce to the map (5.55). The diffeomorphisms alluded to here are analogous to 'large gauge transformations' [214,236] and are called 'large' diffeomorphisms or 'solution generating diffeomorphisms' [181]. Of course, large diffeomorphisms which reduce to a specific conformal transformation $f_\pm$ are not unique since one can always compose with any local diffeomorphism which reduces to identity at the boundary. This ambiguity can be removed, however, if one demands that the resulting bulk metric is in the Fefferman-Graham gauge. These ideas have been used in the study of quantum quenches in [181, 218, 234]. The quantitative form of 'large' diffeomorphism was found by ([218]) and is given by

$$\zeta = 4z\frac{\left(f'_+ f'_-\right)^{3/2}}{D},\ z_\pm = f_\pm(x_\pm) - \frac{2z^2 {f'_\pm}^2 f''_\mp}{D},\ D = 4f'_+ f'_- + z^2 f''_+ f''_- \tag{5.56}$$

Note, as a check, that as $\zeta \to 0$ (the boundary of the Poincare metric (5.54)), we have $z \to 0$ (assuming that D remains finite), and $z_\pm \to f_\pm(x_\pm)$. It is important to note that for functions $f_\pm(x_\pm)$ which are not one-to-one and have vanishing Jacobians at the boundaries of fundamental domains, one must restrict the above transformation (5.56) to a given choice of fundamental domain.

Applying this large diffeomorphism to the Poincaré metric, we get the following metric [30]

$$ds^2 = \frac{dz^2}{z^2} + \frac{1}{4}\left(L_+ dx_+^2 + L_- dx_-^2\right) + \left(\frac{1}{z^2} + \frac{z^2}{16} L_+ L_-\right) dx_+ dx_-. \tag{5.57}$$

where $L_\pm$ are given in terms of Schwarzian derivatives (5.13) of the boundary conformal map

$$L_\pm = -2\{z_\pm, x_\pm\} = \frac{3f_\pm''^2 - 2f_\pm' f_\pm'''}{f_\pm'^2} \tag{5.58}$$

The metric ((5.57)) is called the Fefferman-Graham metric and has been written in the Fefferman Graham gauge. Note that as $z \to 0$, the leading terms of this metric reduce to that of the Poincaré metric (5.54). The two metrics, however, represent physically different solutions of the theory due to the existence of the subleading terms of the metric (5.57) involving the $L_\pm$ terms which represent nontrivial stress tensors at the boundary [28]. These $L\pm$'s capture the 'surface charges' of [50] characterizing the quantum state. The precise relation ([30], [28]) between $L_\pm$ and the CFT stress tensors is,

$$T_{\pm,\pm}(x_\pm) = \frac{L_\pm}{16G_3} = \frac{c}{24} L_\pm \tag{5.59}$$

where we have used the following relation between the central charge of the CFT and the 3D Newton's constant

$$c = \frac{3}{2G_3}. \tag{5.60}$$

Properties of the metric: The metric (5.57), therefore, provides the promised solution to the Einstein's equations (with $\Lambda < 0$) whose conformal boundary coincides with the manifold M_L. Hence, gravity on this metric provides the geometric dual to the CFT on M_L (which is the CFT of our interest).

We have shown in Appendix 5.7.4 the high temperature limits and low temperature limits of the geometry (5.57) represent the BTZ black hole and the global AdS respectively. We can show that at sufficiently high temperatures the geometry contains a horizon. For the purposes of the rest of the chapter, the important property of the metric (5.56) is that the spatial direction x is compactified with a periodicity L (i.e. equal to the spatial size L). This follows as a consequence of the periodicity properties of the Elliptic functions (see, e.g. (5.91) and similar statements for the Lorentzian map).

The periodicity properties of the CFT observables can be holographically interpreted in terms of the above periodicity property of the bulk metric. Thus, e.g. a two-point function, which can be specified by the geometric properties of a geodesic with end-points at the boundary, are periodic because the geodesic will come back to itself after a time period L. We will find below an explicit example of how this happens in case of the holographic EE.

Other candidate bulk duals It is important to note that in related contexts, somewhat different proposals for bulk dual geometries have appeared. For example, the bulk dual to the large L limit of the CFT studied here, used by [138] is obtained by first dividing the Penrose diagram of an eternal BTZ black string geometry vertically by an end-of-the world brane and then taking the top half of it as the relevant bulk dual geometry. We are currently investigating the relation between our proposal and this geometry. The hEE computed in both geometries turn out to be the same. Some other proposals for bulk geometries dual to quantum quench involve the AdS-Vaidya metric, see, e.g. [26].

5.4.1 Holographic quantum quench and entanglement entropy

As mentioned in Section 5.4, for a class of 2D CFTs with a large central charge c, a holographic description is available in terms of a weakly coupled gravity dual in asymptotically AdS_3 spaces. A computation of the CFT partition function over the branched cover Σ_n maps to a computation of the bulk partition function over a dual geometry whose

conformal boundary coincides with Σ_n [104, 135, 165]. As shown in [165], this observation leads to the well-known Ryu-Takayanagi formula [149, 220] for the holographic entanglement entropy (**hEE**) of an interval A

$$S_{hol,A} = \text{ext}\ \frac{l(\gamma_A)}{4G_3}, \tag{5.61}$$

where γ_A is the extremal curve in the bulk ending at the boundary of the interval A, $l(\gamma_A)$ is the length of this curve, and G_3 is Newton's constant which is related to the central charge c of the dual CFT by (5.60). The extremum is taken among all curves γ_A which are homotopic to the subsystem A.

Let us first compute (5.61) in the bulk dual of the BCFT on the upper half plane. The dual geometry is the upper half of the spacetime (5.54). Suppose that the boundary of the subsystem A consists of two points $P_1 = z_{\mu,1} = (z_{+,1}, z_{-,1})$,$P_2 = z_{\mu,2} = (z_{+,2}, z_{-,2})$, $\mu = +, -$. In this case we have two extremal *geodesics*, as shown in Figure 5.5:

(i) One is a geodesic connecting P_1 and P_2, which we call the connected geodesic, whose length is

$$l(\gamma_A)_c = 2\log\frac{|P_1 - P_2|}{\zeta_{min}} = 2\log\frac{\sqrt{(z_{+,1} - z_{+,2})(z_{-,1} - z_{-,2})}}{\zeta_{min}}, \tag{5.62}$$

where ζ_{min} denotes the UV cut-off in the CFT which, by the rules of AdS/CFT, corresponds to placing the asymptotic boundary at $\zeta = \zeta_{min}$ (this regulates the extremal surface area which will diverge otherwise). $|P_1 - P_2|$ denotes the distance measured in the flat boundary metric $ds^2 = dz_+ dz_-$.

(ii) The presence of the additional spacetime boundary at $z_0 = 0$, leads to the existence of an extra geodesic consisting of two independent geodesic segments, each of which connects P_1 (or P_2) to this new boundary. We will call this the disconnected geodesic; the length of each segment, say the first one, is half of that of a geodesic connecting P_1 to each its 'image

point' P_1' below the boundary (similarly with P_2). Combining the two segments, we get

$$l(\gamma_A)_{dc} = \log \frac{|P_1 - P_1'|}{\zeta_{min}} + \log \frac{|P_2 - P_2'|}{\zeta_{min}} \tag{5.63}$$

The entanglement entropy (5.61) is determined by taking the minimum among these [149].

$$S_{hol,A} = \frac{1}{4G_3} \times \min\{l(\gamma(A))_c, l(\gamma_A)_{dc}\} \equiv \min\{S_c, S_{dc}\} \tag{5.64}$$

Fluctuation of the UV cut-off with a large diffeomorphism The construction here gives the hEE for the bulk dual of a CFT on the UHP, which is (5.54) with an additional boundary. As we found in Section 5.4, the bulk dual to the BCFT on the rectangle, which is of our original interest, is given by the geometry (5.57). Since the latter metric is related to the former by a diffeomorphism (which is non-trivial at the boundary), the extremal geodesics in the latter metric can be obtained by pulling back (5.62), (5.63) into the geometry. This prescription is known to reproduce the time evolution of entanglement entropy in various quantum quenches [228, 234]. The effect of the large diffeomorphism can be represented by a fluctuation of the end-points P_1, P_2 [181, 234], while the inside geometry remains identical. The effect of this is that the point P_1, represented by the coordinates $(\zeta_{min}, z_{\pm,1})$ in the Poincare geometry (5.54) is transformed to $(z_{min}, x_{\pm,1})$ according to (5.56). We define the original CFT to be that on the rectangle, with a lattice cut-off a. In AdS/CFT, this instructs to introduce a UV cut-off surface $z_{min} = a$ in the geometry (5.57). Near the horizon, using the $z \to 0$ limit of (5.56), we have

$$\zeta_{1,min} = a\sqrt{f_+'(x_{+,1}) f_-'(x_{-,1})} \tag{5.65}$$

and similarly for the point P_2. In other words, insisting on a given cut-off in the original CFT leads to a local definition of the UV cut-off, as above. The prescription for generalization of

formulae like (5.62) to take this into account is simple [181, 234]: just replace ζ_{min} in (5.62) by $\sqrt{\zeta_{1,min}\zeta_{2,min}}$.

Expression for the hEE Using these ingredients we get the following formulae for the extremal length of two geodesics in the new bulk geometry (5.57):

$$\begin{aligned} l(\gamma_A)_c &= \log \frac{(f(x_{+,1}) - f(x_{+,2}))(f(x_{-,1}) - f(x_{-,2}))}{a^2\sqrt{f'(x_{+,1})f'(x_{+,2})\, f'(x_{-,1})f'(x_{-,2})}}, \\ l(\gamma_A)_{dc} &= \log \frac{(f(x_{+,1}) - f(x_{-,1}))(f(x_{+,2}) - f(x_{-,2}))}{a^2\sqrt{f'(x_{+,1})f'(x_{-,1})\, f'(x_{+,2})f'(x_{-,2})}} \end{aligned} \tag{5.66}$$

Here $f_+ = f_- = f$ is as defined in (5.55).

The boundary points of interest in this problem are given by the coordinates (which are Lorentzian versions of the points (5.30))

$$x_{\pm,1} = -l/2 \mp t,\ x_{\pm,2} = l/2 \mp t \tag{5.67}$$

These represent the end-points of the entangling interval (region A) at time t.

5.4.2 Evolution of holographic entanglement entropy

In this section, we compute time evolution of holographic entanglement entropy in the global quench with boundaries, using the prescription we mentioned in the previous subsection. We mainly focus on the low temperature limit $\frac{L}{\beta} \to 0$ as well as the high temperature limit $\frac{L}{\beta} \to \infty$. We also compare the result to the naive CFT entanglement entropy derived by neglecting the function $F(z)$ in (5.32) which is the theory dependent part of the four point function (5.32). We find that whereas they do not agree in the low temperature limit, they do agree in the high temperature limit. This suggests that the behavior of the entanglement entropy, as computed from the bulk dual, is universal, which coincides with

the usual universality (coming from the factorization limit) at high temperatures, but it is a *new universality* at low temperatures (see Section 5.3.4).

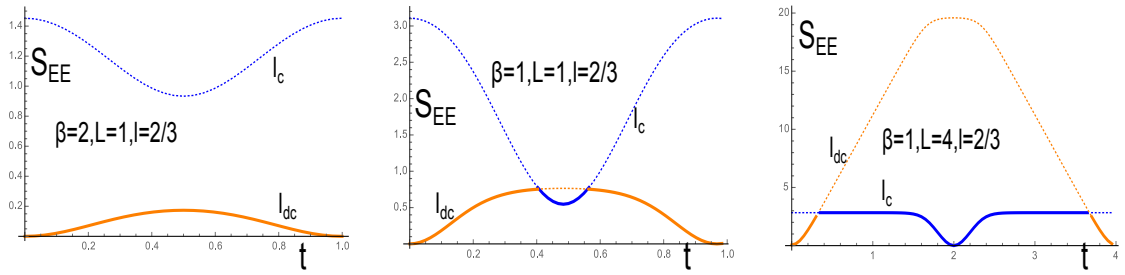

Figure 5.6: Plot of the time evolution of the length of geodesics which determine, via (5.61), (5.64), the entanglement entropy (S_{EE}) of an interval with end-points at $\mp l/2$ (for convenience we have rescaled the geodesic lengths by a factor of $\frac{1}{2}$ and adjusted the height of each curve by choosing the UV cut-off a in (5.66) appropriately). The length of the connected path, l_c (5.62) is shown in blue, and that of the disconnected, l_{dc} (5.63) is shown in red. The left panel corresponds to low temperature with $L/\beta = 1/6$, the middle panel to intermediate temperature with $L/\beta = 1$ and the right panel corresponds to large L (or high temperature[17]) with $L/\beta = 4$. By the minimum prescription of [149], (5.64), S_{EE} is given by the curve segments which lie lower; these are represented by solid lines in the figures. The curve segments lying higher are not relevant in the computation of EE, and are represented by dotted lines. Note the exchange of dominance ('phase transition') for intermediate and high temperatures. The above EE is exactly reproduced by the CFT calculations in the large c limit (see Section 5.3.4). For the rightmost panel, except for the central dip, the EE can be seen to match the CFT result even without the help of large c asymptotics, using factorization into appropriate two-point functions at large L/β.

Time periodicity of two-point functions and the hEE

Note that the map $f(x_\pm)$ appearing in the above expressions satisfies (cf. (5.91)) $f(x_\pm) = f(x_\pm + 2L)$. Since the spatial locations of the boundary points are fixed as in (5.67), the above periodicity implies a periodicity in time $t \equiv t + 2L$ of two-point functions of operators whose AdS representation is in terms of geodesics. The periodicity here can be geometrically understood as follows. The map (5.56) with periodic $f_\pm = f$ effects a quotienting of the Poincare geometry. As time progresses, each end-point of a geodesic climbs along a straight line in the x-t plane; the light-cone coordinates both trace out a periodic path on the cylinder (which is double the manifold M_L (5.16)), leading to the time-periodicity mentioned above.

For the hEE of a centrally located interval (with end-points located at $x = \mp l/2$), the period, in fact, turns out to be L rather $2L$, as in Figure 5.6. This periodicity holds for both

[17]Strictly speaking, we distinguish between $L \to \infty$ and $\beta \to 0$ in the sense of footnote 21.

the connected or the disconnected expression (l_c or l_{dc}) in (5.66). To see this, note that the odd (even) parity of the sn (respectively, cn) functions imply that $f(x_{\pm,1}+L) = -f(x_{\mp,2})$, $f(x_{\pm,2}+L) = -f(x_{\mp,1})$. Here we have used the definitions (5.67). In a similar way we can also show the symmetry $l_c(t) = l_c(L-t)$, $l_{dc}(t) = l_{dc}(L-t)$, which is evident in Figure 5.6.

Low temperature limit $\frac{L}{\beta} \to 0$

In this limit the map $f_\pm$ of (5.55) reduces to the analytic continuation of (5.9), namely

$$z_\pm(x_\pm) = \cot\left(\pi/4 + \pi x_\pm/(2L)\right) \tag{5.68}$$

By using this conformal map, and the formalism described above, we can calculate the contribution of the connected surface to the holographic entanglement entropy S_c, and the contribution of the disconnected surface S_{dc}.

$$S_c = \frac{c}{3}\log\left[\frac{2L}{a\pi}\sin\left(\frac{\pi l}{2L}\right)\right], \qquad S_{dc} = \frac{c}{3}\log\left[\frac{2L}{a\pi}\cos\left(\frac{\pi l}{2L}\right)\right] \tag{5.69}$$

In this case the entanglement entropy does not depend on time, hence we are interested in how this depends on the size of the subsystem A. By taking the minimum between S_c and S_{dc} we get,

$$S_{hEE} = \begin{cases} \frac{c}{3}\log\left[\frac{2L}{a\pi}\sin\left(\frac{\pi l}{2L}\right)\right] & l < \frac{L}{2} \\ \frac{c}{3}\log\left[\frac{2L}{a\pi}\cos\left(\frac{\pi l}{2L}\right)\right] & l > \frac{L}{2} \end{cases} \tag{5.70}$$

When the size of the subsystem is smaller than the half of the subsystem $l < \frac{L}{2}$, the result is the same as that in the vacuum state on a cylinder with circumference $2L$. This is natural because the local physics is the same in both cases. When $l > \frac{L}{2}$, they become different. This is necessary because entanglement entropy has to vanish if we take the subsystem to be the total system.

Nontrivial agreement with CFT Note that the holographic EE obtained above exactly agrees with the CFT EE, discussed in Section 5.3.4 (see (5.51)). As explained before, this is a nontrivial agreement, since in general, including at low temperatures, the CFT EE is, *a priori*, non-universal, being given by a four-point function. However, as we found in Section 5.3.4, in an appropriate limit of large central charge, one recovers a universal result (5.51) which depends only on the central charge and no other feature of the CFT. This then agrees with the hEE obtained above.

Large L limit $\frac{L}{\beta} \to \infty$

If we slightly turn on the temperature, the area of the extremal surfaces starts to depend on time. In the low temperature regime, the area of one extremal surface (the disconnected one) is always smaller than the other one (the connected one) for a fixed subsystem size l (see Figure 5.6). However above some value of the temperature, there are phase transitions. When $0 < t < L/2$, it happens twice. We can check that for sufficiently large $\frac{L}{\beta}$, the area of disconnected surface is smaller at early times, but since S_{dc} linearly grows in time, the connected surface becomes the minimal surface at some critical time. This is the first phase transition. As we will see in the next section, this critical time t_c depends on the size of the subsystem. When $l > \frac{L}{2}$, this is given by $t_c = \frac{L-l}{2}$. When $l < \frac{L}{2}$, this critical time is $t_c = \frac{l}{2}$. This is natural because if we take a small subsystem limit $\frac{l}{L} \ll 1, \frac{L}{\beta} \gg 1$, the result should approach that of the usual global quenches without boundary walls (see Figure 5.6). As is obvious from the periodicity mentioned in Section 5.4.2), we encounter a second phase transition after t crosses $L/2$, when the disconnected surface becomes minimal again. The central dip in this figure cannot be understood from CFT, but in the next section on quasiparticles, we have an accurate understanding of the entire plot of the third panel.

5.5 The quasiparticle picture of the evolution of the entanglement entropy

The evolution of the entanglement entropy at sufficiently high temperatures limit can be interpreted by the free-streaming quasiparticle picture of [59]. In this picture, one models the quenched state as populated by entangled quasiparticles pairs at every point consisting of a left- and a right-moving particle, each moving at the speed of light. The entanglement entropy of an interval A increases by $\frac{\pi c}{6\beta}$ when a quasiparticle goes outside (inside) the interval while its entangled partner is still inside (outside) the interval.

5.5.1 The quasiparticle interpretation for global quench for infinite spatial size

In this subsection we will review the interpretation of the time evolution of the entanglement entropy in the global quench on the non-compact line $\mathbb{R}$. The contribution of the quasi-particle pairs, which are located in $[-(|x|+d|x|), -|x|]$ initially, to the entanglement entropy at a fixed time, depends on the value of $|x|$. If the quasiparticles are located inside the interval, $A = \{|x| < \frac{l}{2}\}$ at the initial time, the contribution to the entanglement entropy $s_A^{(1)}(|x|, t)$ is given by

$$s_A^{(1)}(|x|,t) = \frac{c\pi}{6\beta}\left[\theta\left(t - (-|x| + \frac{l}{2})\right) - \theta\left(t - (|x| + \frac{l}{2})\right)\right] \tag{5.71}$$

This is because, when $t = -|x| + \frac{l}{2}$, the left moving partner of the entangled pair goes outside the interval, and when $t = |x| + \frac{l}{2}$ the right moving partner goes outside the interval.

Similarly, the contribution of the quasi-particles outside the interval A is

$$s_A^{(2)}(|x|,t) = \frac{c\pi}{6\beta}\left[\theta\left(t - (|x| - \frac{l}{2})\right) - \theta\left(t - (|x| + \frac{l}{2})\right)\right] \tag{5.72}$$

The total entanglement entropy $S_A(l,t)$ for the interval A is then given by

$$S_A(l,t) = 2\int_{\frac{l}{2}}^{\infty} s_A^{(2)}(|x|,t)d|x| + 2\int_0^{\frac{l}{2}} s_A^{(1)}(|x|,t)d|x|. \tag{5.73}$$

Here we incorporate the factor 2 to include the contribution of $x > 0$ region. Performing the integral we get

$$S_A(l,t) = \frac{2c\pi t}{3\beta}\theta\left(\frac{l}{2}-t\right) + \frac{c\pi l}{3\beta}\theta\left(t-\frac{l}{2}\right). \tag{5.74}$$

which gives us the result from a CFT calculation [59, 64].

5.5.2 The evolution of entanglement entropy in the presence of boundaries

We would now like to discuss the time evolution of the entanglement entropy in the presence of the boundaries. The new physics in this case comes from the reflection of the quasiparticles off the boundary walls.The entanglement entropy consists of two contributions. One is the contribution from the inside of the interval, and the other is the contribution from the outside of the interval. As we will see below the form of the each contribution is further classified by the ratio $\frac{l}{L}$ of size of the interval l to the size of the total system L.

Let us consider the motion of the left moving and the right moving quasiparticles which are located inside the interval A, say $-|x| \in A$ at the initial time $t = 0$. The left mover goes outside A at $t = \frac{l}{2} - |x|$, then it bounces off the boundary wall at $t = \frac{L}{2} - |x|$, and becomes a right mover. When $t = L - |x| - \frac{l}{2}$, it enters the interval A again. Similarly the right mover goes outside the interval A at $t = \frac{l}{2} + |x|$, bounces off the boundary wall at $\frac{L}{2} + |x|$, and enters the interval again at $t = L + |x| - \frac{l}{2}$.

5.5.3 $\frac{l}{L} > \frac{1}{2}$

Let us consider the contribution of the quasiparticle pairs which are located in $[-(|x| + d|x|), -|x|]$ at the initial time $t = 0$ to the entanglement entropy when $\frac{l}{L} > \frac{1}{2}$. The contribution of those inside the interval depends on the precise value of $|x|$. For $|x| < \frac{L-l}{2}$, since $|x| + \frac{l}{2} < (L - |x| - \frac{l}{2})$,

$$\begin{aligned} s_A^{\text{in}(1)} = & \frac{c\pi}{6\beta}\left[\theta\left(t - (\frac{l}{2} - |x|)\right) - \theta\left(t - (\frac{l}{2} + |x|)\right)\right] \\ & + \frac{c\pi}{6\beta}\left[\theta\left(t - (L - |x| - \frac{l}{2})\right) - \theta\left(t - (L + |x| - \frac{l}{2})\right)\right] \end{aligned} \tag{5.75}$$

When $\frac{L-l}{2} < |x| < \frac{l}{2}$, since $(L - |x| - \frac{l}{2}) < |x| + \frac{l}{2}$

$$\begin{aligned} s_A^{\text{in}(2)} = & \frac{c\pi}{6\beta}\left[\theta\left(t - (\frac{l}{2} - |x|)\right) - \theta\left(t - (L - |x| - \frac{l}{2})\right)\right] \\ & + \frac{c\pi}{6\beta}\left[\theta\left(t - (\frac{l}{2} + |x|)\right) - \theta\left(t - (L + |x| - \frac{l}{2})\right)\right] \end{aligned} \tag{5.76}$$

The contribution of the quasiparticles located outside the interval is

$$\begin{aligned} s_A^{\text{out}} = & \frac{c\pi}{6\beta}\left[\theta\left(t - (|x| - \frac{l}{2})\right) - \theta\left(t - (L - |x| - \frac{l}{2})\right)\right] \\ & + \frac{c\pi}{6\beta}\left[\theta\left(t - (\frac{l}{2} + |x|)\right) - \theta\left(t - (L + |x| - \frac{l}{2})\right)\right] \end{aligned} \tag{5.77}$$

The total entanglement entropy is then given by integrating all contribution of the quasiparticles.

$$S_A(l,t) = 2\int_0^{\frac{L-l}{2}} s_A^{\text{in}(1)} d|x| + \int_{\frac{L-l}{2}}^{\frac{l}{2}} S_A^{\text{in}(2)}(|x|,t) + \int_{\frac{l}{2}}^{\frac{L}{2}} s_A^{\text{out}}(|x|,t) d|x| \tag{5.78}$$

The form of the integral of $s_A^{\text{in}(2)}$ depends on whether $\frac{l}{L} > \frac{3}{4}$ or not. The sum of the remaining two terms also depends on the size of the interval, ie $\frac{l}{L} > \frac{3}{4}$, $\quad \frac{3}{4} > \frac{l}{L} > \frac{2}{3}$ or $\frac{2}{3} > \frac{l}{L} > \frac{1}{2}$. At the end of the day, these different cases give the same net entanglement entropy.

$$S_A(l,t) = \frac{\pi c}{6\beta} \times \begin{cases} 2t, & (0 < t < \frac{L-l}{2}) \quad L-l, \quad (\frac{L-l}{2} < t < \frac{l}{2}) \quad -2t+L, \quad (\frac{l}{2} < t < \frac{L}{2}) \\ 2t-L & (\frac{L}{2} < t < \frac{2L+l}{2}) \quad L-l, (\frac{2L+l}{2} < t < \frac{2L-l}{2}), \quad -2t+2L, (\frac{L+l}{2} < t < L) \end{cases}$$

In figure 5.7, we plot the EE obtained above from the quasiparticle picture and compare it to the holographic result. It is clear that the comparison works rather well.

It is important to note that in this case $l > \frac{L}{2}$, and the entanglement entropy is not thermalized at any time, i.e. it does not become proportional to the interval size l.

5.5.4 $\frac{l}{L} < \frac{1}{2}$

The contribution from inside the interval is now given by

$$\begin{aligned} s_A^{\text{in}} = & \frac{c\pi}{6\beta}\left[\theta\left(t-(\frac{l}{2}-|x|)\right)-\theta\left(t-(\frac{l}{2}+|x|)\right)\right] \\ & + \frac{c\pi}{6\beta}\left[\theta\left(t-(L-|x|-\frac{l}{2})\right)-\theta\left(t-(L+|x|-\frac{l}{2})\right)\right] \end{aligned} \tag{5.79}$$

The contribution of the region $\frac{l}{2} < |x| < \frac{L-l}{2}$ is

$$\begin{aligned} s_A^{\text{out}(1)} = & \frac{c\pi}{6\beta}\left[\theta\left(t-(|x|-\frac{l}{2})\right)-\theta\left(t-(|x|+\frac{l}{2})\right)\right] \\ & + \frac{c\pi}{6\beta}\left[\theta\left(t-(L-|x|+\frac{l}{2})\right)-\theta\left(t-(L+|x|-\frac{l}{2})\right)\right] \end{aligned} \tag{5.80}$$

The contribution of the region is $\frac{L-l}{2} < |x| < \frac{L}{2}$ is

$$\begin{aligned} s_A^{\text{out}(1)} = & \frac{c\pi}{6\beta}\left[\theta\left(t-(|x|-\frac{l}{2})\right)-\theta\left(t-(|x|+\frac{l}{2})\right)\right] \\ & + \frac{c\pi}{6\beta}\left[\theta\left(t-(L-|x|+\frac{l}{2})\right)-\theta\left(t-(L+|x|-\frac{l}{2})\right)\right] \end{aligned} \tag{5.81}$$

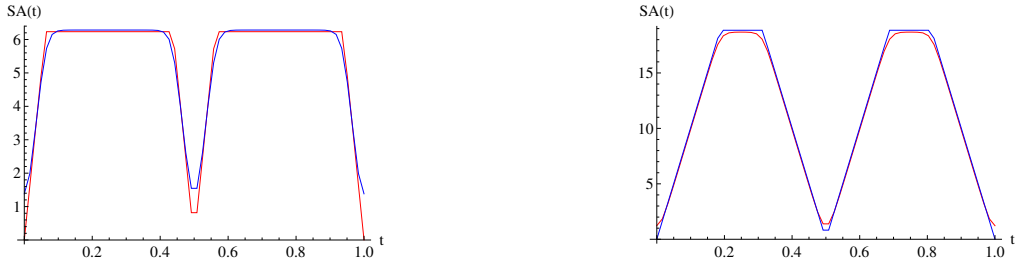

Figure 5.7: Plot of the time evolution of entanglement entropy in the quench in the high temperature regime (blue). We also plot the evolution of the entanglement entropy expected from the quasiparticle picture (red). We take $L = 1, \beta = \frac{1}{8}, l = \frac{1}{8}$ (left panel), $l = \frac{3}{8}$ (right panel).

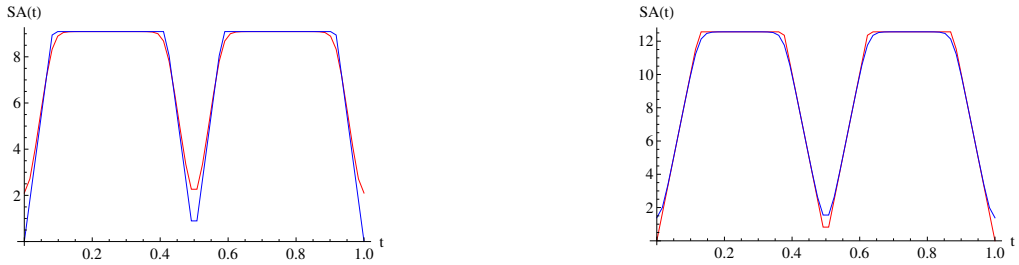

Figure 5.8: Plot of the time evolution of entanglement entropy in the quench in the high temperature regime (blue). We also plot the evolution of the entanglement entropy expected from the quasiparticle picture (red). We take $L = 1, \beta = \frac{1}{8}, l = \frac{5}{6}$ (left panel), $l = \frac{6}{8}$ (right panel).

Combining everything, the total EE is

$$S_A(l,t) = \frac{\pi c}{6\beta} \times \begin{cases} 2t, \quad (0 < t < \frac{l}{2}) \quad l, \quad (\frac{l}{2} < t < \frac{L-l}{2}) \quad -2t + L, \quad (\frac{L-l}{2} < t < \frac{L}{2}) \\ 2t - L \quad (\frac{L}{2} < t < \frac{L+l}{2}) \quad l, (\frac{L+l}{2} < t < \frac{2L-l}{2}), \quad -2t + 2L, (\frac{2L-l}{2} < t < L) \end{cases}$$

As we can see, this behavior of the entanglement entropy is very similar to that of global quenches for infinite spatial size (5.74). This is natural because it takes a while until the reflections off the walls start affecting the entanglement entropy when the size of the subsystem A is small. As a result the entanglement entropy is thermalized when $\frac{l}{2} \leq t \leq \frac{L-l}{2}$. This is expected from the analysis of [71]. When $t \geq \frac{L-l}{2}$, it starts decreasing, leading to the 'revival' behavior discussed in this chapter.

5.6 Conclusion

In this chapter we have explored the properties of single-interval entanglement entropy (EE) in the presence of spatial boundaries. The distinguishing feature arising from such boundaries is the appearance of time-periodicity of the observables, arising from a bulk geometry which is a quotient of the AdS-Poincaré spacetime. The periodicity of the entanglement entropy can be understood in terms of a periodic motion of geodesic end-points. Another feature, for quench states corresponding[18] to high temperatures, is the appearance of thermalization with universal exponents, followed by a revival [71, 163]. For quenches corresponding to intermediate or low temperatures, there is an apparent puzzle: the CFT EE depends on a four-point function which does not factorize and is hence non-universal; the holographic result however does not depend on details of the CFT except for the central charge c. We apply recent large-c techniques to resolve this puzzle. The large c limit of the CFT EE becomes universal and exactly matches the holographic computation at all temperatures. It would be interesting to see, following [111], whether corrections to the leading large c limit are captured by subdominant saddle points in the bulk.

In this chapter, we have particularized to quenches to critical theories and modelled the quenched state by a Calabrese-Cardy (CC) type state [59, 64]. It would be interesting to (a) generalize our results to more general states with higher chemical potentials as discussed in [182], (b) explore realistic quenches with boundaries in the limit of fast ramping speed (some interesting issues have recently been raised in this context in [85, 87]) and (c) relate our results to the study of spatial boundaries in non-conformal theories (see, e.g. [150]). The presence of spatial boundaries can be regarded as a model for impurities or defects in a one-dimensional lattice. It would be interesting to relate some of our results to experimental situations.

[18] In the sense of footnote 2.

An issue which has not been explored in detail in this chapter, and is currently under investigation, is the precise nature of the bulk geometry found here. In particular, we would like to understand the geometrical interpretation of the approximate thermalization of the one-point function and EE and subsequent revival. These issues have been commented upon in [92, 163]. However the explicit bulk metric we have found should shed more light on this issue. It is also interesting to see if the phenomenon of revival has a bearing on the issue of stability of the AdS geometry discussed in, e.g. [46, 51, 97].[19] We hope to return to these issues shortly.

5.7 Appendix

5.7.1 Derivation of conformal maps

In this appendix, we discuss in more detail the conformal map mentioned in Section 5.2.1.

5.7.2 Map from the rectangle to the complex plane (Euclidean)

We consider a rectangle parametrized by

$$w = x + i\tau, \bar{w} = x - i\tau,\ x \in [-\frac{L}{2}, \frac{L}{2}], \tau \in [-\frac{\beta}{4}, \frac{\beta}{4}] \tag{5.82}$$

which we wish to map to the upper half plane

$$z = z_2 + iz_1, \bar{z} = z_2 - iz_1,\ z_1 \geq 0, z_2 \in \mathbb{R} \tag{5.83}$$

[19] We thank Shiraz Minwalla for discussions on this issue.

As mentioned in Section 5.2.1, such a map is given by the Christoffel-Schwarz transformation (5.4)

$$w(z) = A\int_0^z \frac{dz}{\sqrt{(z^2-b^2)(z^2-\frac{1}{b^2})}} + B, \tag{5.84}$$

By definition this map satisfies the following conditions

$$\begin{aligned} w(b) &= \frac{L}{2} + i\frac{\beta}{4}, \qquad & w(-b) &= \frac{L}{2} - i\frac{\beta}{4} \\ w\left(\frac{1}{b}\right) &= -\frac{L}{2} + i\frac{\beta}{4}, \qquad & w\left(-\frac{1}{b}\right) &= -\frac{L}{2} - i\frac{\beta}{4} \end{aligned} \tag{5.85}$$

It is easy to see that β is given by [20]

$$\beta = 2i(w(-b) - w(b) = -2iA\int_{-b}^{b} \frac{dz}{\sqrt{(z^2-b^2)(z^2-\frac{1}{b^2})}} = 4iA\ bK(b^4), \tag{5.86}$$

where $K(m)$ is the Elliptic K function

$$K(m) = \int_0^1 \frac{dx}{\sqrt{(1-x^2)(1-mx^2)}}$$

Similarly

$$L = w(b) - w(1/b) = iA\ bK(1-b^4)$$

The constant B can now be determined from, say, the first of the conditions (5.85). We get $B = L/2$. The map, therefore, is given by

$$w(z) = \frac{i\beta}{4K(b^4)}\ sn^{-1}(\frac{z}{b}, b^4) + \frac{L}{2} \tag{5.87}$$

[20] We have used the convention

$$\frac{1}{\sqrt{(z^2-b^2)(z^2-\frac{1}{b^2})}} = -\frac{1}{\sqrt{(b^2-z^2)(\frac{1}{b^2}-z^2)}}$$

.

where we have used the following result about the Jacobi sn function

$$\int_0^z \frac{dz}{\sqrt{(z^2-b^2)(z^2-\frac{1}{b^2})}} = sn^{-1}(\frac{z}{b}, b^4)$$

The inverse map is

$$z = b\ sn\left[\frac{4K(b^4)}{i\beta}\left(w-\frac{L}{2}\right), b^4\right] \tag{5.88}$$

where we can regard b as determined from

$$\frac{\beta}{L} = \frac{4K(b^4)}{K(1-b^4)} \tag{5.89}$$

The antiholomorphic map reads as

$$\bar{z} = b\ sn\left[-\frac{4K(b^4)}{i\beta}\left(\bar{w}-\frac{L}{2}\right), b^4\right] \tag{5.90}$$

Periodicity properties: Note the periodicity properties

$$z(w) = z(w+2L),\ z(w) = z(w+i\beta) \tag{5.91}$$

and the parity property

$$z(w+i\beta/4) = -z(w-i\beta/4) \tag{5.92}$$

which follow from the following properties of the Jacobi sn function [4]

$$sn(u+2K(m),m) = -sn(u,m) = sn(u-2K(m),m),\ sn(u+2iK(1-m),m) = sn(u,m)$$

Map from $\mathbb{T}^2 \to \mathbb{C}$: The above periodicity properties (5.91) imply that the map $w \to z(w)$ can be viewed from a complex torus to the complex plane:

$$\mathbb{T}^2 w \mapsto z(w) = b\ sn\left(\frac{4K(b^4)}{i\beta}(w - \frac{L}{2}), b^4\right) \in \mathbb{C},$$
$$w \equiv x + i\tau,\ x \in [-\frac{L}{2}, \frac{3L}{2}], \tau \in [-\frac{\beta}{4}, \frac{3\beta}{4}], \quad z = z_2 + iz_1,\ z_1, z_2 \in \mathbb{R} \tag{5.93}$$

Here the torus is represented as a rectangle (whose opposite sides are to be identified). The earlier rectangle (5.82) is the bottom left 'quadrant' of this larger rectangle.

We should note here that the rectangle (5.82) (or rather the Lorentzian continuation of that) is the appropriate geometry for the quench problem, whereas the torus described above is the appropriate geometry for a thermal problem (where we have a periodicity in the imaginary time).

Large L limit: To see this limit, we note the following small m behaviour [4]

$$K(1-m) \approx \frac{1}{2}\log(16/m) + O(m), K(m) = \pi/2 + O(m) \tag{5.94}$$

Thus, the large L limit corresponds to small b, with

$$\frac{\beta}{L} = \frac{4K(b^4)}{K(1-b^4)} \approx \frac{\pi}{\log(2/b)} + O(b^4)$$

Using (5.94) and

$$sn(u,m) = \sin(u) - \frac{1}{4}m(u - \sin u\ \cos u)\cos u + O(m^2),$$
$$\sin(u/i) = -i\sinh(u) \tag{5.95}$$

we get from (5.88)

$$z \approx -ib \sinh\left(\frac{2\pi w}{\beta} - \log(2/b)\right) \approx -ib(-\frac{1}{2}) \exp\left(-\frac{2\pi w}{\beta} + \log(2/b)\right) \approx ie^{-2\pi w/\beta} \quad (5.96)$$

Hence, in this limit, we recover the map (5.8) from the cylinder to the complex plane with periodicity $w \equiv w + i\beta$. This periodicity is consistent with the (5.91) described above, in the limit where the aspect ratio $\beta/L \to 0$, which we can regard as an infinitely wide rectangle with width β whose opposite sides are identified (hence, a cylinder).

Low temperature limit: Using (5.94), and (5.89), we can find the following $b \to 1 - \epsilon$ behaviour

$$\frac{\beta}{L} \approx \frac{4}{\pi} \log\left(\frac{16}{1 - b^4}\right)$$

which shows that $b \to 1 - \epsilon$ corresponds to the low temperature $\beta/L \to \infty$ limit. Using the formula

$$sn(iu, 1 - m) = i \tan(u) + O(m)$$

we can then easily derive the following low temperature limit of (5.88):

$$z(w) = i \cot\left(\frac{\pi}{4} + \frac{\pi w}{2L}\right) \quad (5.97)$$

This shows a periodicity $w \equiv w + 2L$, and is consistent with (5.91). The rectangle representing the torus (5.93) becomes in this limit an infinitely high strip of width L (with opposite sides identified, hence leading to a cylinder).

Lorentzian map

As we saw in the text, the map (5.88) described above helps convert observables computed in the UHP (5.83) to those in the Euclidean rectangle (5.82). As we indicated above, the same map also converts the complex plane to the torus (5.93). As described in Section 5.2.2,

for real-time observables we are interested in a Lorentzian CFT on the manifold (5.16)

$$M_L = \mathbb{I} \times Rx_\pm = x \mp t,\ x \in \mathbb{I} = [-L/2, L/2], t \in \mathbb{R} \tag{5.98}$$

which describes the Wick-rotated rectangle (5.82) (it is an infinite strip of width L). We obtain them by analytically continuing CFT observables on the rectangle according to (5.15):

$$\tau = it, \to w = x + i\tau = x - t \equiv x_+, \bar{w} = x - i\tau = x + t \equiv x_- \tag{5.99}$$

For the holographic calculations described in Section 5.4, we need to *also* analytically continue the Euclidean $z, \bar{z}$ plane to a Lorentzian plane $z_+, z_- \in \mathbb{R}^2$. Thus, we need an analytic continuation of the Euclidean map (5.88), (5.90). To do this, we note the identity [4]

$$sn(x/i, m) = -i\frac{sn(x, 1-m)}{cn(x, 1-m)} \tag{5.100}$$

Since under the analytic continuation (5.99), both $w, \bar{w}$ become real, the above identity implies that both z and $\bar{z}$, become purely imaginary. We, therefore, define the following analytic continuation of the complex z-plane to the real plane

$$\begin{aligned} &z = iz_+,\ \bar{z} = -iz_-, \\ &z_\pm = \begin{cases} -iz \equiv -i(z_2 + iz_1) = z_1 - z_0, \\ +i\bar{z} \equiv +i(z_2 - iz_1) = z_1 + z_0, \end{cases} \qquad z_0 \equiv iz_2 \end{aligned} \tag{5.101}$$

where, $z_\pm$ are given by the following functions (using (5.100))

$$z_\pm = f_\pm(x_\pm),\ f_+(x) = f_-(x) = f(x) \equiv -b\ \frac{sn\left[\frac{4K(b^4)}{\beta}(x - L/2), 1 - b^4\right]}{cn\left[\frac{4K(b^4)}{\beta}(x - L/2), 1 - b^4\right]} \tag{5.102}$$

Note that in this map, $x_\pm = x \mp t$, with $x \in \mathbb{I} = [-L/2, L/2]$, $t \in \mathbb{R}$, whereas $z_\pm = z_1 \mp z_0$, $z_{0,1} \in \mathbb{R}$. Thus the above map is a map from the strip M_L (5.16) to the real plane $\mathbb{R}^2$. The map is clearly conformal, which satisfies the property $dz_+ dz_- = f'(x_+)f'(x_-)dx_+ dx_-$. Note that the Lorentzian version of the high temperature map (5.96) becomes the Rindler map:

$$z_\pm = \exp(-\frac{2\pi x_\pm}{\beta}) \tag{5.103}$$

A different Euclidean map

We note that the map (5.88) is not the unique one that maps the rectangle to the UHP. We may consider, e.g., a different assignment of the corners to the boundary of the UHP:

$$\begin{aligned} w\left(-\frac{1}{b}\right) = \frac{L}{2} - \frac{i\beta}{4}, \quad w\left(\frac{1}{b}\right) = -\frac{L}{2} - \frac{i\beta}{4} \\ w(-b) = \frac{L}{2} + \frac{i\beta}{4}, \quad w(b) = -\frac{L}{2} + \frac{i\beta}{4} \end{aligned} \tag{5.104}$$

By using methods similar to Section 5.7.2, we arrive at the following map

$$z = -b \,\mathrm{sn}\left[\frac{2K(b^4)}{L}(w - \frac{i\beta}{4}), b^4\right] \tag{5.105}$$

where b now is given by

$$\frac{\beta}{L} = \frac{K(1-b^4)}{K(b^4)}.$$

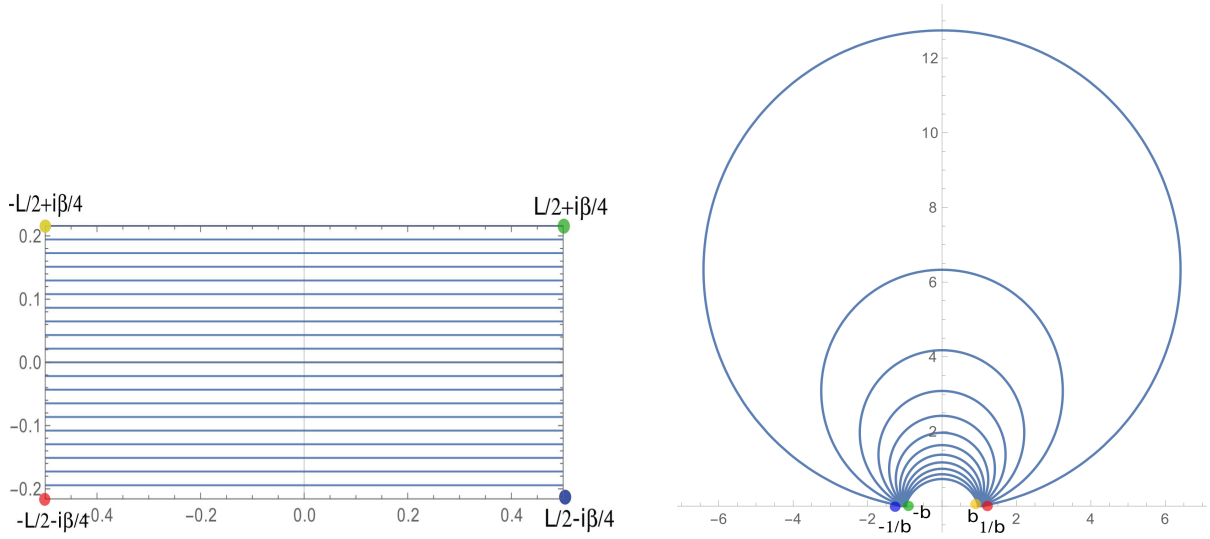

Figure 5.9: The second map between the upper half plane and the rectangle. The colour coding represents the mapping of the corners to the boundary of the UHP. See (5.88) and (5.87). The time evolution contours in the rectangle are mapped to the UHP as shown on the right. We have chosen $L = \beta = 1$. It is clear that this second map is roughly obtained from the first map by exchanging the horizontal and vertical axes of the complex plane.

The periodicity property of this map is the same as in (5.91). This map has the property that its low temperature limit is the standard cylinder map (with periodicity $2L$), as

$$z \approx i \exp(i\frac{\pi w}{L}) \tag{5.106}$$

The Euclidean map (5.105) cannot be analytically continued to a Lorentzian map as in (5.15). Here the continuation is $w = ix_+, \bar{w} = -ix_-$. This means that in the Euclidean theory we need to call $w =: \tau + ix, \bar{w} = \tau - ix$, and then analytically continue $\tau = it$ (here $x_\pm = x \pm t$). The accompanying continuation of the z-plane is $z = iz_+, \bar{z} = -iz_-$. As a simple check, note that (5.106) now becomes a real conformal map

$$z_\pm = \exp(-\frac{\pi x_\pm}{L})$$

Comparing with (5.103), we can see that this second map is indeed related to the first map by an exchange of the horizontal and vertical axes, along with $\beta \leftrightarrow 2L$ (also, compare Figures 5.1 and 5.9).

5.7.3 Decay rate in the high temperature limit

We will consider a one point function at the point $x = 0$ and at time t in the high temperature limit, where $\frac{L}{\beta} \gg \frac{t}{\beta} \gg 1$. Using the high temperature Lorentzian map (5.103), we find that the Lorentzian continuation of the connected correlator $\langle ... \rangle_{\mathbb{C}}$ in (5.11) gives

$$\left(\frac{(z_+ - z_-)}{b}\right)^{-2h} \simeq 2^{2h} \exp(-\frac{2\pi}{\beta}(2h)(t + \frac{L}{2})) \tag{5.107}$$

The Jacobian terms in (5.11) become

$$\left(\frac{z'_+(x_+)z'_-(x_-)}{b}\right)^{h} \simeq (\frac{2\pi}{\beta})^{2h} 2^{-2h} \left(\exp(\frac{4\pi t}{\beta}) + \exp(\frac{2\pi L}{\beta})\right)^{h} \tag{5.108}$$

In the limit $\frac{L}{2\beta} \gg \frac{t}{\beta}$, the second term in the above expression dominates over the first. Combining the above two expressions, we get,

$$\langle \phi(w, \bar{w}) \rangle_{\text{rect}} \simeq \left(\frac{2\pi}{\beta}\right)^{2h} \exp\left(-\frac{4\pi h}{\beta} t\right) \tag{5.109}$$

Thus, the decay rate of the one point function in the limit $\frac{L}{\beta} \gg \frac{t}{\beta} \gg 1$ matches exactly with the decay rate obtained in [71] and [182] in the case of an infinite strip ($L \to \infty$).

5.7.4 The BTZ and the global AdS metric

We will work out the metric (5.57) in case the maps $f_\pm(x_\pm)$ are given by the non-compact limit $L \to \infty$ limit (5.8) and the low temperature $\beta \to \infty$ limits (5.9) of the general transformation (5.6).[21]

[21] We must distinguish between (a) the non-compact limit $L \to \infty$ and (b) the high temperature limit $\beta \to 0$, although in both cases the aspect ratio $L/\beta \to \infty$. The difference is that in (a), ratios such as $\beta/L, x_\pm/L, l/L \to 0$ while ratios such as $x_\pm/\beta, l/\beta$ are not scaled, whereas in (b) ratios such $L/\beta, x_\pm/\beta, l/\beta \to \infty$, while $x_\pm/L, l/L$ are not scaled. In other words, in (a) only $L \to \infty$ and all other length scales are held fixed, while in (b) only $\beta \to 0$ and all other length scales are held fixed. Similarly limits of (c) low temperature $\beta \to \infty$ (where $L, x_\pm, l$ are held fixed) and (d) small system size $L \to 0$ (where $\beta, x_\pm, l$ are held fixed), are different. In this section we consider the limits (a) and (c).

Large L: BTZ Using the map (5.8) we first find that

$$L_+ = L_- \equiv \mathbf{L} = 4\pi^2/\beta^2 \tag{5.110}$$

which is consistent with (5.59) and (2.1). This allows us to write the map (5.8) as

$$z_\pm = f_\pm(x_\pm) = \exp[-\sqrt{\mathbf{L}}x_\pm] \tag{5.111}$$

The denominator D in (5.56) becomes

$$D = \mathbf{L}\left(\mathbf{L}z^2 + 4\right) e^{-2\sqrt{\mathbf{L}}x}, \tag{5.112}$$

The 'large diffeomorphism' (5.56) in this case is, therefore, given by

$$z_+ = f(x_+) \equiv \frac{e^{-\sqrt{\mathbf{L}}x_+}\left(4 - \mathbf{L}z^2\right)}{\mathbf{L}z^2 + 4},\ z_- = f(x_)\,\zeta = \frac{4z\sqrt{\mathbf{L}e^{-\sqrt{\mathbf{L}}(x_- + x_+)}}}{\mathbf{L}z^2 + 4} \tag{5.113}$$

The resulting metric (5.57), turns out to be (see [181, 218, 234] for more details)

$$ds^2 = \frac{dz^2}{z^2} - \frac{\left(\mathbf{L}z^2 - 4\right)^2}{16z^2}dt^2 + \frac{\left(\mathbf{L}z^2 + 4\right)^2}{16z^2}dx^2, \tag{5.114}$$

which represents a BTZ black hole with horizon at

$$z_h = 2/\sqrt{\mathbf{L}} \tag{5.115}$$

In the large L limit the size of the spatial cycle effectively becomes decompactified; thus the above metric represents a BTZ black string. Thus, the BTZ black string is the bulk dual of the CFT on the (analytically continued) cylinder, which, of course, is the Lorentzian equivalent of the statement that the Euclidean black string is the bulk dual of the thermal CFT which is represented by the Euclidean cylinder.

The low temperature limit: Global AdS In the limit $\beta \gg L$, we apply the map (5.9) to the transformation (5.56). Here we find that

$$L_+ = L_- \equiv \mathbf{L} = -\pi^2/L^2 \tag{5.116}$$

which is consistent with (5.59) and (5.21).

By going through similar steps as the above, we find the final form of the metric (5.57) as

$$ds^2 = \frac{dz^2}{z^2} - \frac{(\mathbf{L}z^2+4)^2}{16z^2}dt^2 + \frac{(\mathbf{L}z^2-4)^2}{16z^2}dx^2 \tag{5.117}$$

which represents global AdS, since it is the spatial cycle x which shrinks to zero size at $z = 2/\sqrt{\mathbf{L}}$.

Chapter 6

Higher-point conformal blocks and EE in Heavy States

6.1 Introduction

Much of the power and appeal of holography [176] rests on features of conformal field theories which find natural analogues in gravity. There are several of these features of holographic field theories which are universal and can be captured without reliance to a specific theory. Examples of these include thermodynamic features like the Cardy formula [75] and entanglement entropy [64, 220]. Moreover, it is of substantial interest to identify and explore the 'universality class' of CFTs which admit a holographic description [38, 40, 41, 100, 134, 137, 142, 156].

The evaluation of correlation functions by decomposing into conformal blocks is a minimalistic and powerful approach to extract very general features of CFTs [98, 107, 242, 244]. This direction, recently harnessed by the conformal bootstrap programme, has led to strong results on anomalous dimensions of operators [101, 213, 219] and bounds on central charges [212]. In the AGT correspondence, conformal blocks of Liouville theory (or more

generally Toda theories) are related to the instanton partition functions of 4-dimensional $\mathcal{N} = 2$ SCFTs [8, 241].

Conformal blocks also play an important role in the context of holography since they serve as the CFT detectors of bulk locality and gravitational scattering [100, 113, 142, 143, 152, 173, 207]. Conjunctively, there has also been very strong evidence that conformal blocks are intimately related to geodesics in AdS [10–12, 145–147]. One of the important objects in this context, for a $2d$ CFT, is the correlator of two heavy operators with two light operators [10–12, 113–115, 145–147][1]. As $c \to \infty$, the ratio of the conformal dimension with the central charge remains fixed for heavy operators, whilst that of light operators is much smaller than unity. One can think of these heavy operators being responsible for creating an excited state after a global quench [21, 68]. On the gravity side, this excited state corresponds to the conical defect background [21]. It has been shown that the conformal block of this correlator is precisely reproduced from holography from an appropriate worldline configuration in this bulk geometry [145, 147]. Moreover, the correlation functions in this excited state mimic thermal behaviour if the conformal dimension of the heavy operator exciting the state is greater than $c/24$ [114, 115]. This is an example of a pure microstate (with a sufficiently high energy eigenvalue) behaving effectively like a mixed state being a part of the thermal ensemble.

In this work, we evaluate conformal blocks of two heavy operators and arbitrary number (m) of light operators. We work in the heavy-light approximation and utilize the monodromy method to derive the $(m + 2)$-point conformal block. We expand the correlation function in a basis which involves pairwise fusion of the light operators (see Fig 6.1). In the strict heavy-light limit and at large central charge, we show that, for this class of OPE channels :

[1] See references [77, 110, 141, 166, 189–191, 208] for further interesting aspects of conformal blocks in $2d$ CFTs.

- The conformal block having an even number of light operators and two heavy operators factorizes into a product of 4-point conformal blocks of two heavy and two light operators.

- The conformal block having an odd number of light operators and two heavy operators factorizes into a product of 4-point conformal blocks of two heavy and two light operators and a 3-point function involving one light and two heavy operators.

Our monodromy analysis is developed mostly based on the work [12] which made use of the accessory parameters of the 4-point conformal block as a seed solution in order to obtain those for the 5-point conformal block. Although the factorization we observe is special to the OPE channel configurations we have chosen, the conformal blocks in other bases can be related to ours by performing linear operations. Furthermore, since the correlator itself is a basis independent object, all bases of conformal blocks are on an equal footing. We shall demonstrate this picture by using the correspondence relating CFT correlators to punctured Riemann surfaces.

Our results for conformal blocks from the CFT are reproduced from the bulk by considering suitable generalizations of the worldline configurations considered in [147]. The choice of OPE channels in the CFT are in one-to-one correspondence to geodesic

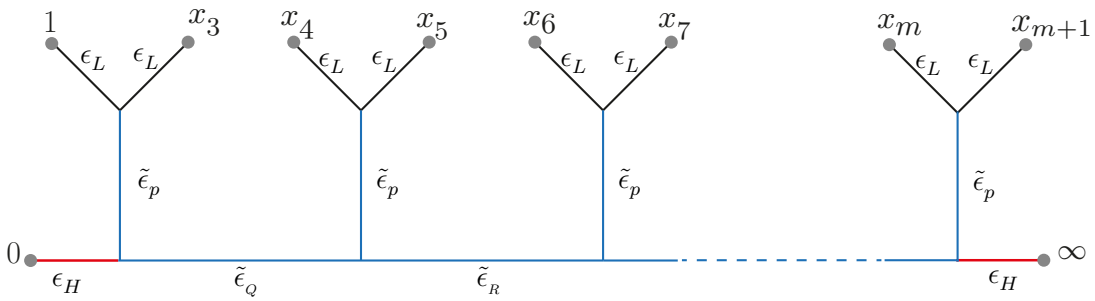

Figure 6.1: The OPE channel which we shall consider here for the conformal block of an even number light operators and two heavy operators. The conformal dimensions are scaled as $\epsilon_i = 6h_i/c$. Note the pairwise fusion of the light operators into operators of conformal dimension $\tilde{h}_p$ which are same in the intermediate channels shown in the figure – this provides a major simplification for the monodromy analysis.

configurations in the bulk. This implies that these higher-point conformal blocks can be fully recast in terms of bulk quantities. This outcome nicely fits within the notion of emergence of locality from a conformal field theory [100] and serves as an explicit demonstration of the same not only for higher-point correlation functions but also for non-vacuum states. It was also shown previously that correlation functions of free theories can be rewritten in terms of closed string amplitudes in AdS [125–127]. Although our correlator is in a very different regime of the parameter space of couplings, it bears in the same spirit the pertinent analogue of admitting an Einstein gravity description instead of the stringy one for free theories.

This circle of ideas finds a natural home in the context of entanglement entropy of heavy states [21]. The light operators then correspond to twist operators, with conformal dimension $c/24\,(n-1/n)$, (which implement the replica trick) in the limit $n \to 1$, where n is the replica index [64]. One can then utilize the higher-point conformal block to obtain the entanglement entropy of an arbitrary number of disjoint intervals. Our choice of monodromy contours, similar to those used in [105, 136], are well-suited to computing entanglement entropy. Furthermore, these results can be straightforwardly used to evaluate the mutual information of two disjoint intervals, $\mathcal{A}$ and $\mathcal{B}$, which is defined as

$$I(\mathcal{A},\mathcal{B}) = S(\mathcal{A}) + S(\mathcal{B}) - S\left(\mathcal{A}\cup\mathcal{B}\right).$$

On the holographic side, the Ryu-Takayanagi prescription [220] instructs us to calculate minimal areas (or geodesics for the case of $3d$ gravity). Our CFT results for entanglement entropy of disjoint intervals agree precisely with that obtained from the bulk using the minimal area prescription. Furthermore, we show that for two or more disjoint intervals, there are multiple geodesic configurations which are possible in the bulk and these are in one-to-one correspondence with various OPE channels or monodromy contours which one chooses to consider in the CFT.

The outline of this chapter is as follows. In Section 6.2, we introduce the correlation function whose conformal block we wish to evaluate and specify the regime of validity of our analysis. The relation of CFT correlators with punctured Riemann surfaces is reviewed in this section. Section 6.3 contains the explicit evaluation of the conformal block. We consider the 5- and 6-point conformal blocks before generalizing the result to arbitrary odd- and even-point blocks. Specializing to the case of light primaries being twist operators, we evaluate the entanglement entropy and mutual information in Section 6.4. In Section 6.5, we consider worldline configurations in the bulk and reproduce the CFT result for odd- and even-point blocks. This section also contains the analysis of the holographic entanglement entropy using the Ryu-Takayanagi formula. We describe the moduli space of the conformal block in Section 6.6. Finally, Section 6.7 has our conclusions along with some future directions.

6.2 On heavy-light correlators and Riemann surfaces

Consider the following p-point correlation function of primary operators $\mathcal{O}_i$, each located at the points $(z_i, \bar{z}_i)$ on a plane. By inserting $(p-3)$ number of complete sets of states equivalent to the identity (Fig 6.1), we can expand in terms of the conformal partial waves as

$$\left\langle \mathcal{O}_1(z_1,\bar{z}_1)\mathcal{O}_2(z_2,\bar{z}_2)\cdots\mathcal{O}_p(z_p,\bar{z}_p)\right\rangle = \sum_{\{\tilde{h}_i\}} d_{\{\tilde{h}_i\}}\mathcal{F}(z_i,h_i,\tilde{h}_i)\bar{\mathcal{F}}(\bar{z}_i,h_i,\tilde{h}_i). \tag{6.1}$$

The complete set of states $\rangle\tilde{h}_i$, running in the $(p-3)$ intermediate channels, is labelled in terms of representations of the Virasoro algebra which includes the primaries as well as their descendants. Here, $d_{\{\tilde{h}_i\}}$ are constructed out of the structure constants c_{ijk} of the algebra of operators in the theory. In what follows, we shall be interested in the following $(m+2)$-point

correlator of two heavy operators and m light operators[2]

$$\langle \mathcal{O}_H(z_1, \bar{z}_1) \prod_{i=2}^{m+1} \mathcal{O}_L(z_i, \bar{z}_i) \; \mathcal{O}_H(z_{m+2}, \bar{z}_{m+2}) \rangle. \tag{6.2}$$

We shall work with CFTs, which in the $c \to \infty$ regime, admit a holographic description in terms of Einstein gravity. We make use of the property that, in this regime, the p-point conformal blocks are expected to exponentiate as [242, 244, 245]

$$\mathcal{F}_{(p)}(z_i, h_i, \tilde{h}_i) = \exp\left[-\frac{c}{6} f_{(p)}(z_i, \epsilon_i, \tilde{\epsilon}_i)\right]. \tag{6.3}$$

Furthermore, the points z_1, z_2 and z_{m+2}, in (6.2), can be sent to ∞, 1 and 0 respectively via the projective transformation

$$x_i = \frac{(z_{m+2} - z_i)(z_2 - z_1)}{(z_{m+2} - z_2)(z_i - z_1)}. \tag{6.4}$$

Upto factors of the Jacobians arising from usual rules of conformal transformations of primary operators, the correlator of interest is now expressed in terms of the cross-ratios, x_i, as

$$\left\langle \mathcal{O}_H(\infty) \left[\mathcal{O}_L(1) \prod_{i=3}^{m+1} \mathcal{O}_L(x_i) \right] \mathcal{O}_H(0) \right\rangle. \tag{6.5}$$

We shall be interested in contributions of Virasoro conformal blocks, $\mathcal{F}_{(p)}(x_i, h_i, \tilde{h}_i)$, to the above correlation function. In addition to the $c \to \infty$ limit, we shall also work in the heavy-light limit, for which the dimensions of the operators scale as

$$\epsilon_H = \frac{6h_H}{c} \sim \mathcal{O}(1) \; , \quad \epsilon_L = \frac{6h_L}{c} \ll 1 \; . \tag{6.6}$$

In words, the ratio of the conformal dimension with central charge of the heavy operators remains fixed and is of order-one in the $c \to \infty$ regime whilst that of the light operators

[2] In this section and the next we move back and forth between using p and m. $p = m + 2$.

much lesser than unity[3]. By referring to this as the 'heavy-light limit', we mean to consider contributions to the conformal block to the leading order in ϵ_L.

The four-point version of the above conformal block was considered in [113] and the five-point in [12]. The conformal block was used to calculate the entanglement entropy of a single interval in heavy states in [21].

It is important to note, that there are several choices of OPE channels along which one can expand a CFT correlation function. Each of these channels correspond to different basis choices of the conformal blocks to rewrite the correlator. The correlation function is a single-valued real analytic function of the coordinates z_i and $\bar{z}_i$. However, this is not true for the conformal blocks themselves (due to presence of branch cuts) and the correlation function is, therefore, independent of the basis of conformal blocks. It can be shown that conformal blocks in different bases are related by the linear operations of braiding, fusion and modular transformation [152, 193–195]. These operations have finite-dimensional representations for rational CFTs but can, nevertheless, be performed on conformal blocks of a generic CFT since these are duality transformations purely arising from associativity of OPEs (crossing-symmetry) and modular invariance[4]. In this chapter, we shall work in a specific basis in which light operators fuse in pairs. As we shall show, this basis admits a generalization to higher point conformal blocks and is geared towards the analysis of entanglement entropy of disjoint intervals [105, 136]. The OPE channel considered for the 5-point function in [12] is different from the one we are about to use but is, however, related to ours by a series of fusion operations[5].

The statements above can be manifestly portrayed if one associates, a Riemann sphere with p punctures, $\sigma_{0,p}$, with a p-point CFT correlation function on the plane [152, 193–195],

[3] In Section 6.4, we specialize to the case of the light operators being twist operators with conformal dimension $c/24\,(n-1/n)$ in the limit $n \to 1$. Here, n is the index for the number of replicas.

[4] See, for example, [152] which explicitly constructs the duality transformations in terms of quantum $6j$-symbols for Liouville theory. Quite intriguingly, the authors also show that the braiding matrix is related to gravitational scattering amplitudes.

[5] See Fig. 18 of [194] to relate the basis used in [12] to the one used here.

248]. Strictly speaking, there is a vector space of conformal blocks $\mathcal{H}(\sigma)$ associated to every Riemann surface σ [116]. The different bases of conformal blocks (or OPE channel choices) are the various ways in which this Riemann surface can be sewn from 3-holed spheres (or as is graphically called 'a pair of pants'). Stated differently, the decomposition of the correlator into conformal blocks is equivalent to the pant-decomposition of the punctured sphere. The intermediate channels in the conformal blocks correspond to the states passing through the sewed holes. The number of intermediate sewings necessary for the p-punctured sphere is $(p-3)$.

Moreover, a p-point CFT correlation function on the plane is related to a moduli space, $\mathcal{M}_{0,p}$, (corresponding to the Riemann surface $\sigma_{0,p}$) [116, 194, 248]. For our correlator (6.5) on the sphere, this is $\mathcal{M}_{0,m+2}$. There are $(m-1)$ complex moduli formed by the cross-ratios $\{x_i\}$. This picture will turn out to be relevant later on in Section 6.6.

6.3 Monodromy problem for conformal blocks

In this section we briefly review the monodromy method to evaluate the Virasoro conformal block. The discussion closely follows [91, 113]. We then proceed to use it for calculating 5- and 6-point conformal blocks and then generalize to blocks with an arbitrary number of light operator insertions.

Let us consider the correlation function we started with, $\left\langle \mathcal{O}_1(z_1)\mathcal{O}_2(z_2)\mathcal{O}_3(z_3)\cdots\mathcal{O}_p(z_p)\right\rangle$. As mentioned before, in order to decompose this p-point correlator into a sum of products of 3 point functions we need to insert $p-3$ resolutions of identity. In terms of these intermediate states, a typical conformal block would read as[6]

$$\mathcal{F}_{(p)}(z_i,h_i,\tilde{h}_i)=\left\langle \mathcal{O}_1(z_1)\mathcal{O}_2(z_2)\rangle\alpha\,\langle\alpha\mathcal{O}_3(z_3)\rangle\beta\,\langle\beta\mathcal{O}_4(z_4)\rangle\gamma\cdots\langle\zeta\mathcal{O}_{p-1}(z_{p-1})\mathcal{O}_p(z_p)\right\rangle. \quad (6.7)$$

[6]Henceforth, we focus attention on the holomorphic part.

Now, one can insert into this conformal block an additional operator, $\hat{\psi}(z)$, whose conformal dimension remains fixed in the $c \to \infty$ limit. This defines the following quantity

$$\Psi(z, z_i) \equiv \left\langle \mathcal{O}_1(z_1)\mathcal{O}_2(z_2)\rangle\alpha \, \langle\alpha\hat{\psi}(z)\mathcal{O}_3(z_3)\rangle\beta \cdots \langle\zeta\mathcal{O}_{p-1}(z_{p-1})\mathcal{O}_p(z_p) \right\rangle.$$

It can then be argued [113] that the insertion of $\hat{\psi}$ changes the leading semi-classical behaviour of the conformal block just by multiplication of a wavefunction

$$\Psi(z, z_i) = \psi(z, z_i)\mathcal{F}_{(p)}(z_i, h_i, \tilde{h}_i). \tag{6.8}$$

We can now choose that the operator $\hat{\psi}$ obeys the null-state condition at level 2.

$$\left[L_{-2} - \frac{3}{2(2h_\psi + 1)}L_{-1}^2\right]\rangle\psi = 0, \qquad \text{with, } h_\psi \overset{c\to\infty}{=} -\frac{1}{2} - \frac{9}{2c}. \tag{6.9}$$

Acting $\Psi(z, z_i)$ by $(L_{-2} - \frac{3}{2(2h_\psi+1)}L_{-1}^2)$, therefore, leads to

$$\left[L_{-2} + \frac{c}{6}L_{-1}^2\right]\Psi(z, z_i) = 0. \tag{6.10}$$

Translating this into a differential equation by using the differential operator realization of Virasoro generators, one arrives at a Fuchsian equation

$$\frac{d^2\psi(z)}{dz^2} + T(z)\psi(z) = 0, \qquad \text{with, } \; T(z) = \sum_{i=1}^{p}\left[\frac{\epsilon_i}{(z - z_i)^2} + \frac{c_i}{z - z_i}\right]. \tag{6.11}$$

Here, $\epsilon_i = 6h_i/c$ and c_i are the accessory parameters related to the conformal block as

$$c_i = -\frac{\partial f_{(p)}(z_i, \epsilon_i, \tilde{\epsilon}_i)}{\partial z_i}. \tag{6.12}$$

The function $f_{(p)}$ is the same as the one appearing in the exponential in equation (6.3) and forms the essential ingredient of the conformal block. Equation (6.12) implies that the

following integrability condition should be satisfied

$$\frac{\partial c_i}{\partial z_j} = \frac{\partial c_j}{\partial z_i}. \tag{6.13}$$

The asymptotic behaviour $T(z) \sim 1/z^4$, at $z \to \infty$, imposes the conditions

$$\sum_{i=1}^{p} c_i = 0, \quad \sum_{i=1}^{p} (c_i z_i + \epsilon_i) = 0, \quad \sum_{i=1}^{p} (c_i z_i^2 + 2\epsilon_i z_i) = 0. \tag{6.14}$$

We shall now work in the coordinate system x_i as defined in (6.4) and also consider two heavy operators at 0 and ∞ and $(p-2)$ light operators at $1, x_3, \cdots, x_{p-1}$. Using the above three relations, we can re-express $c_{1,2,p}$ in terms of other accessory parameters $c_{3,\cdots,p-1}$ and cross-ratios as

$$c_1 = \sum_{i=3}^{p-1} (x_i - 1) c_i + (p-2)\,\epsilon_L, \qquad c_2 = -\sum_{i=3}^{p-1} x_i c_i - (p-2)\,\epsilon_L, \qquad c_p = 0. \tag{6.15}$$

Substituting (6.6) and (6.15) in the expression for $T(z)$ we get

$$T(z) = \frac{\epsilon_H}{z^2} + \frac{\epsilon_L}{(z-1)^2} + \sum_{i=3}^{p-1} \frac{\epsilon_L}{(z-x_i)^2} - \frac{(p-2)\,\epsilon_L}{z(z-1)} + \sum_{i=3}^{p-1} \frac{x_i(1-x_i)}{z(z-1)(z-x_i)} c_i. \tag{6.16}$$

One can solve for the accessory parameters, c_i, by using the monodromy properties of the solution $\psi(z)$ around the singularities of $T(z)$. The main ingredient of the conformal block $f_{(p)}(x_i, \epsilon_i, \tilde{\epsilon}_i)$ can, in turn, be obtained from the accessory parameters upon integrating, $c_i = -\partial f_{(p)}/\partial x_i$. Thinking of the conformal block $\mathcal{F}_{(p)}(x_i, h_i, \tilde{h}_i)$ as a partition function dominated by the saddle-point action $(c/6) f_{(p)}(x_i, \epsilon_i, \tilde{\epsilon}_i)$, the accessory parameters c_i serve as conjugate variables for the cross-ratios x_i[7]. As emphasized in [147], the saddle-point

[7] It was pointed out in [152] that the corresponding Teichmüller space inherits the complex structure (x_i, γ_i) from the punctured Riemann sphere. The authors had also studied quantization arising from the conjugate variables x_i and γ_i. The wavefunction $\Psi(z, z_i)$ in (6.8) can then be thought to be living in the associated Hilbert space.

action dominating the conformal block is closely related to the worldline action in AdS. The accessory parameter can then be identified as the momentum along the geodesic.

We shall now consider two warmup examples of the 5- and 6-point conformal blocks to gain some intuition before analyzing the arbitrary p-point case. Let us reiterate the notation for the number of insertions of operators

$$\begin{aligned}\text{total number of operator insertions} &= p,\\ \text{number of light operator insertions} &= m,\\ \text{number of heavy operator insertions} &= 2.\end{aligned}$$

Therefore, $p = m + 2$. The variable n is reserved for the replica index which will appear in the context of entanglement entropy. Along the way, we also mention the procedure to be used and fix the notation and conventions further.

6.3.1 Warmup examples

Warmup example I : 5-point conformal block

Let us consider the conformal block of the 5-point function

$$\left\langle \mathcal{O}_H(\infty)\mathcal{O}_L(1)\mathcal{O}_L(x_3)\mathcal{O}_L(x_4)\mathcal{O}_H(0) \right\rangle. \tag{6.17}$$

This is the case of $m = 3$ or $p = 5$.

Perturbative expansion of the monodromy equation

We shall solve for the unknown accessory parameters $c_{3,4}$ in perturbation theory in the parameter ϵ_L which is the scaled conformal dimension of the light operator (6.6). We shall be following the procedure used in [12, 113, 147]. However, as mentioned earlier, unlike [12]

which studied the 5-point block in much greater detail, our choice of monodromy contours will be different and we shall be working only up to linear order in ϵ_L which is the light parameter of all our light operators.

The quantities in the monodromy equation (6.11) can be expanded implicitly in powers of the light parameter, ϵ_L, as

$$\begin{aligned}
\psi(z) &= \psi^{(0)}(z) + \psi^{(1)}(z) + \psi^{(2)}(z) + \cdots, \\
T(z) &= T^{(0)}(z) + T^{(1)}(z) + T^{(2)}(z) + \cdots, \\
c_i(z) &= c_i^{(0)}(z) + c_i^{(1)}(z) + c_i^{(2)}(z) + \cdots, \quad \text{for } i = 3, 4, \ldots, m+1.
\end{aligned} \tag{6.18}$$

For the case at hand, $m = 3$. Following [12], we also assume that the expansion of the accessory parameters starts at linear order in ϵ_L and hence $c_i^{(0)} = 0$. The equation (6.11) at the first two orders is

$$\frac{d^2\psi^{(0)}(z)}{dz^2} + T^{(0)}(z)\psi^{(0)}(z) = 0, \tag{6.19}$$

$$\frac{d^2\psi^{(1)}(z)}{dz^2} + T^{(0)}(z)\psi^{(1)}(z) = -T^{(1)}\psi^{(0)}(z). \tag{6.20}$$

From (6.16), the stress-tensor at these orders is

$$T^{(0)}(z) = \frac{\epsilon_H}{z^2}, \tag{6.21}$$

$$\begin{aligned}
T^{(1)}(z) = &\frac{\epsilon_L}{(z-1)^2} + \frac{\epsilon_L}{(z-x_3)^2} + \frac{\epsilon_L}{(z-x_4)^2} - \frac{3\epsilon_L}{z(z-1)} \\
&+ \frac{x_3(1-x_3)}{z(z-1)(z-x_3)}c_3^{(1)} + \frac{x_4(1-x_4)}{z(z-1)(z-x_4)}c_4^{(1)}.
\end{aligned} \tag{6.22}$$

As in [12], we shall also supress the superscript of $c_i^{(1)}$ and simply call it c_i since the accessory parameters at the linear order are sufficient information for the heavy-light limit. In other words, we shall confine our attention to the linear order in ϵ_L which is the extreme heavy-light limit.

The solution to the zeroth order ODE in (6.19) is straightforward

$$\psi_{\pm}^{(0)}(z) = z^{(1\pm\alpha)/2}, \qquad \alpha = \sqrt{1-4\epsilon_H}. \tag{6.23}$$

Let us calculate the monodromy of this first order solution about the points 0 and ∞. It can be easily seen that taking z to $e^{2\pi i}z$, results in

$$\begin{pmatrix} \psi_+^{(0)}(e^{2\pi i}z) \\ \psi_-^{(0)}(e^{2\pi i}z) \end{pmatrix} = - \begin{pmatrix} e^{\pi i\alpha} & 0 \\ 0 & e^{-\pi i\alpha} \end{pmatrix} \begin{pmatrix} \psi_+^{(0)}(z) \\ \psi_-^{(0)}(z) \end{pmatrix}. \tag{6.24}$$

The 2×2 matrix above is therefore the monodromy matrix for a contour containing the point $z=0$. In a similar fashion the monodromy around $z=\infty$ can also be seen by performing the transformation $y = 1/z$

$$\begin{pmatrix} \psi_+^{(0)}(e^{2\pi i}y) \\ \psi_-^{(0)}(e^{2\pi i}y) \end{pmatrix} = - \begin{pmatrix} e^{-\pi i\alpha} & 0 \\ 0 & e^{\pi i\alpha} \end{pmatrix} \begin{pmatrix} \psi_+^{(0)}(y) \\ \psi_-^{(0)}(y) \end{pmatrix}. \tag{6.25}$$

Since $\alpha = \sqrt{1-4\epsilon_H}$, the monodromies above detect the conformal dimensions of the heavy operators inserted at 0 and ∞.

The first order corrections (6.20) can be obtained by the standard method of variation of parameters. The Wronskian is $W(z) = \alpha$. We have

$$\begin{aligned} \psi_+^{(1)}(z) &= \frac{1}{\alpha}\psi_+^{(0)}(z)\int dz\psi_-^{(0)}(z)T^{(1)}(z)\psi_+^{(0)}(z) - \frac{1}{\alpha}\psi_-^{(0)}(z)\int dz\psi_+^{(0)}(z)T^{(1)}(z)\psi_+^{(0)}(z), \\ \psi_-^{(1)}(z) &= \frac{1}{\alpha}\psi_+^{(0)}(z)\int dz\psi_-^{(0)}(z)T^{(1)}(z)\psi_-^{(0)}(z) - \frac{1}{\alpha}\psi_-^{(0)}(z)\int dz\psi_-^{(0)}(z)T^{(1)}(z)\psi_+^{(0)}(z). \end{aligned} \tag{6.26}$$

Monodromy conditions

$T^{(1)}(z)$ has three singular points at 1, x_3 and x_5 i.e. at the location of the light operators. Our choice of contours shall involve one contour enclosing a pair of points and another one enclosing the remaining single point. There are three such possibilities

- $\mathbf{\Omega}_1$: γ_1 enclosing $\{1, x_3\}$ and γ_2 enclosing $\{x_4\}$
- $\mathbf{\Omega}_2$: γ_1 enclosing $\{1, x_4\}$ and γ_2 enclosing $\{x_3\}$
- $\mathbf{\Omega}_3$: γ_1 enclosing $\{x_3, x_4\}$ and γ_2 enclosing $\{1\}$

These contour configurations are in one-to-one correspondence with the OPE channel along which one chooses to expand. For instance, for $\mathbf{\Omega}_1$, we consider the OPE, $\mathcal{O}_L(1)\mathcal{O}_L(x_3)$. We shall elaborate on this further below.

The monodromy matrix upto first order in ϵ_L is

$$\mathbb{M}(\gamma_k) = \mathbb{I} + \begin{pmatrix} I^{(k)}_{++} & I^{(k)}_{+-} \\ I^{(k)}_{-+} & I^{(k)}_{--} \end{pmatrix}, \tag{6.27}$$

where, the $I^{(k)}_{pq}$ are contour integrals

$$\begin{aligned} I^{(k)}_{++} &= \frac{1}{\alpha}\oint_{\gamma_k} dz\, \psi^{(0)}_-(z)T^{(1)}(z)\psi^{(0)}_+(z), \quad I^{(k)}_{+-} = -\frac{1}{\alpha}\oint_{\gamma_k} dz\, \psi^{(0)}_+(z)T^{(1)}(z)\psi^{(0)}_+(z) \\ I^{(k)}_{-+} &= \frac{1}{\alpha}\oint_{\gamma_k} dz\, \psi^{(0)}_-(z)T^{(1)}(z)\psi^{(0)}_-(z), \quad I^{(k)}_{--} = -\frac{1}{\alpha}\oint_{\gamma_k} dz\, \psi^{(0)}_+(z)T^{(1)}(z)\psi^{(0)}_-(z) \end{aligned} \tag{6.28}$$

Note that, $I^{(k)}_{++} = -I^{(k)}_{--}$.

The monodromy conditions we shall impose are [113]

$$\widetilde{\mathbb{M}}(\gamma_k) = -\begin{pmatrix} e^{+\pi i\Lambda} & 0 \\ 0 & e^{-\pi i\Lambda} \end{pmatrix}, \qquad \Lambda = \sqrt{1-4\tilde{\epsilon}_p}\,. \tag{6.29}$$

In words, the above equation means that the monodromy matrix picks up the conformal dimension, $\tilde{h}_p = c\,\tilde{\epsilon}_p/6$, of the operator $\mathcal{O}_p$ which arises upon fusing the operators living inside the contour. The tilde on $\mathbb{M}$ above denotes that this diagonal form of the monodromy matrix is related by similarity transformations to (6.27). Comparing the eigenvalues of (6.27) with that of $\widetilde{\mathbb{M}}(\gamma_k)$ we get the condition

$$\mathcal{X}[\gamma_k] \equiv \left(I^{(k)}_{++}\right)^2 + I^{(k)}_{+-} I^{(k)}_{-+} = -4\pi^2 \tilde{\epsilon}_p^2. \tag{6.30}$$

Here, we have defined $\mathcal{X}[\gamma_k]$ as the monodromy condition for the contour γ_k at the linear order in ϵ_L. We shall now impose this condition for each of the contours in the configurations, $\mathbf{\Omega}_i$. It is worthwhile remarking at this point that, these configurations of monodromy contours are in one-to-one correspondence with the OPE channels. The residues provide information about the singular structure due to the operators residing within the contours.

$\mathbf{\Omega}_1$ channel

The $\mathbf{\Omega}_1$ channel – Fig 6.2 – corresponds to case when we consider the fusion of the light primaries $\mathcal{O}_L(1)$ and $\mathcal{O}_L(x_3)$. The monodromy conditions for this configuration is

$$\begin{aligned}\mathcal{X}[\gamma_1] = -\frac{4\pi^2 x_3^{-\alpha/2}}{\alpha}&[\epsilon_L(\alpha - 1 + (\alpha+1)x_3^\alpha) + (x_3^\alpha - 1)x_3 c_3] \\ &\times [\epsilon_L(\alpha - 2 + (\alpha+2)x_3^\alpha) + (x_3^\alpha - 1)(c_3 x_3 + c_4 x_4)] \;=\; -4\pi^2\tilde{\epsilon}_p^2,\end{aligned} \tag{6.31}$$

and

$$\mathcal{X}[\gamma_2] = -4\pi^2\epsilon_L^2 = -4\pi^2\tilde{\epsilon}_q^2. \tag{6.32}$$

The last equation above is fairly obvious. The residue merely picks up the conformal dimension of the single operator $\mathcal{O}_L(x_4)$ living inside the contour γ_2. Hence, $\tilde{\epsilon}_q = \epsilon_L$, which is consistent with the conformal block diagram shown in Fig 6.2.

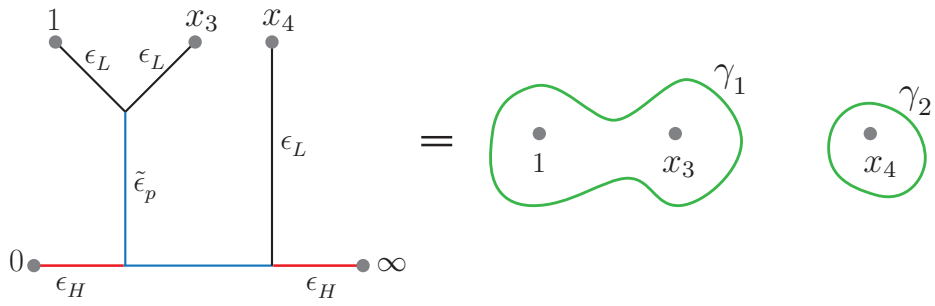

Figure 6.2: OPE channel and monodromy contours for $\mathbf{\Omega}_1$ for the 5-point block.

We are now presented with the task of solving (6.31) for the accessory parameters c_3 and c_4. This is the point where one can utilize the method of seed solutions introduced in [12]. The idea behind this method is that, in order to solve the monodromy problem for the conformal block having m light operators, accessory parameters can be inherited from a lower point conformal block having $(m-1)$ light operators. More precisely, for the block with m light insertions one uses the accessory parameters of the block with $(m-1)$ light insertions as zeroth-order solutions and then deforms these by the light parameter ϵ_L.

Following [12], we choose a seed solution for the accessory parameter c_3 to be the same of that of the 4-point conformal block [113].

$$c_3 = \frac{-\epsilon_L(\alpha - 1 + x_3^{\alpha}(\alpha+1)) + \tilde{\epsilon}_p x_3^{\alpha/2}\alpha}{x_3(x_3^{\alpha}-1)} + \mathcal{O}(\epsilon_L^2). \tag{6.33}$$

(Since, we shall be working the heavy-light limit – i.e. $c_i^{(0)}$ in (6.18) – we shall drop the $\mathcal{O}(\epsilon_L^2)$ from now on for brevity.) Substituting this in (6.31) we get

$$c_4 = -\frac{\epsilon_L}{x_4}. \tag{6.34}$$

The integrability condition (6.13) is trivially satisfied.

It is crucial to note that in [12] an additional expansion was considered in their parameter ϵ_3 corresponding to one of the light operators[8]. In our case, all light parameters have the

[8] See equation (3.5) of [12].

same conformal dimension ϵ_L. One can still consider a correction term of the form $\epsilon_L c_3^{(\text{corr})}$ to c_3 above. However, it can be explicitly seen that $c_3^{(\text{corr})} = 0$ because (6.33) and (6.34) are indeed the solutions to linear order in ϵ_L for the monodromy condition (6.31). Hence, unlike [12], there are no additional corrections to (6.33) and the seed solution for c_3 fully captures the accessory parameter in the heavy-light limit. This simplifying feature is special to the OPE channels or the corresponding monodromy contours we have considered and is also due the fact that all the light operators here have the same conformal dimension.

We can now use (6.12) to obtain the conformal block. Upon integrating the accessory parameters, we get

$$\begin{aligned} f_{(5)}(x_3, x_4; \epsilon_L, \epsilon_H; \epsilon_p) &= \left[\epsilon_L \left((1-\alpha)\log x_3 + 2\log\frac{1-x_3^\alpha}{\alpha}\right) + 2\tilde{\epsilon}_p \log\left[4\alpha\frac{1+x_3^{\alpha/2}}{1-x_3^{\alpha/2}}\right]\right] \\ &\quad + \epsilon_L \log x_4 \\ &= f_{(4)}(1, x_3; \epsilon_L, \epsilon_H; \tilde{\epsilon}_p) + \epsilon_L \log x_4. \end{aligned} \tag{6.35}$$

The integration constants are chosen to be such that $f_{(5)} \sim (2\epsilon_L - \tilde{\epsilon}_p)\log(1-x_3)$ for $x_3 \to 1$ [113, 147][9]. Here, $f_{(4)}$ is the function appearing in the exponential of the conformal block ($\mathcal{F}_{(4)} = \exp(-c f_{(4)}/6)$) of the 4-point function $\left\langle \mathcal{O}_H(\infty)\mathcal{O}_L(x_i)\mathcal{O}_L(x_j)\mathcal{O}_H(0)\right\rangle$ [113].

$$f_{(4)}(x_i, x_j; \epsilon_L, \epsilon_H; \epsilon_p) = \epsilon_L\left((1-\alpha)\log x_i x_j + 2\log\frac{x_i^\alpha - x_j^\alpha}{\alpha}\right) + 2\tilde{\epsilon}_p \log\left[4\alpha\frac{x_j^{\alpha/2} + x_i^{\alpha/2}}{x_j^{\alpha/2} - x_i^{\alpha/2}}\right]. \tag{6.36}$$

[9] This follows from (6.7) and considering the behaviour of the 3-point function $\left\langle \mathcal{O}_L(1)\mathcal{O}_L(x_3)\widetilde{\mathcal{O}}_p(0)\right\rangle$ in the limit $x_3 \to 1$.

We now use the exponentiation of the conformal block (6.3) to obtain

$$\begin{aligned}\mathcal{F}_{(5)}(1,x_3,x_4;\epsilon_L,\epsilon_H;\tilde{\epsilon}_p)_{\mathbf{\Omega}_1} &= \exp\left[-\frac{c}{6}f_{(4)}(1,x_3;\epsilon_L,\epsilon_H;\tilde{\epsilon}_p)\right]\times x_4^{-h_L}\\ &= \mathcal{F}_{(4)}(1,x_3;\epsilon_L,\epsilon_H;\tilde{\epsilon}_p)\times x_4^{-h_L}. \end{aligned} \tag{6.37}$$

The first factor here is the conformal block of the 4-point function $\left\langle \mathcal{O}_H(\infty)\mathcal{O}_L(1)\mathcal{O}_L(x_3)\mathcal{O}_H(0)\right\rangle$. The second factor of $x_4^{-h_L}$ is due to the 3-point function of $\left\langle \mathcal{O}_H(\infty)\mathcal{O}_L(x_4)\mathcal{O}_H(0)\right\rangle$ normalized by $\left\langle \mathcal{O}_H(\infty)\mathcal{O}_H(0)\right\rangle$.

It is worthwhile noting that this factorization shown above is true only at the level of conformal blocks – and not correlators – for a generic $\mathcal{O}_L$. This is because not much is known about precise spectrum at low conformal dimension. In order to make a rigorous statement on the correlation function, one would require information about the structure constants c_{LLa}.

However, for the light operators being twist operators σ_n, $\bar{\sigma}_n$, in the limit $n\to 1$ (relevant for entanglement entropy) the factorization (6.37) shown above can be independently seen (at the level of correlation functions) in terms of the OPE in the regime $x_3\to 1$. This was previously shown in [69]. It is known that twist operators fuse into the identity [64, 170][10]

$$\sigma_n(1)\bar{\sigma}_n(x_3)\sim \mathbb{I}+\mathcal{O}((1-x_3)^r)\ , \qquad r\in\mathbb{Z}^+ \tag{6.38}$$

This means that $\tilde{\epsilon}_p$ is 0 in the intermediate channel after fusion of two light operators. Moreover, the only operators which will arise in the intermediate channel are the identity and its descendants – this includes the stress tensor and operators made of the derivatives and powers of the stress-tensor [21].

[10] We shall be implicitly working in the $n\to 1$ limit to ensure the operators are light.

Let us insert a complete set of states in the 5-point function and make use of the OPE (6.38)

$$\begin{aligned}&\left\langle \mathcal{O}_H(\infty)\sigma_n(1)\bar{\sigma}_n(x_3)\sigma_n(x_4)\mathcal{O}_H(0)\right\rangle_{x_3\to 1}\\&=\sum_{\alpha}\left\langle \mathcal{O}_H(\infty)\sigma_n(1)\bar{\sigma}_n(x_3)\rangle\alpha\langle\alpha\sigma_n(x_4)\mathcal{O}_H(0)\right\rangle.\end{aligned}\tag{6.39}$$

Since the leading term in the OPE (6.38) is the identity operator, the only non-zero contribution will arise from $\rangle\alpha = \rangle\mathcal{O}_H$, due to orthonormality of states. Hence, just a single term in the above sum contributes and we have the factorization

$$\begin{aligned}&\left\langle \mathcal{O}_H(\infty)\sigma_n(1)\bar{\sigma}_n(x_3)\sigma_n(x_4)\mathcal{O}_H(0)\right\rangle_{x_3\to 1}\\&=\left\langle \mathcal{O}_H(\infty)\sigma_n(1)\bar{\sigma}_n(x_3)\mathcal{O}_H(0)\right\rangle\left\langle \mathcal{O}_H(\infty)\sigma_n(x_4)\mathcal{O}_H(0)\right\rangle.\end{aligned}\tag{6.40}$$

The 4-point function above will receive contributions solely from the identity block owing to (6.38).

$\mathbf{\Omega}_2$ channel

The contour configuration for this case is equivalent to that of $\mathbf{\Omega}_1$ upon the replacements $x_3 \leftrightarrow x_4$ and $c_3 \leftrightarrow c_4$. The analysis for this channel is therefore exactly the same as that of $\mathbf{\Omega}_1$ with these exchanges. The final result for the conformal block in this channel is

$$\mathcal{F}_{(5)}(1,x_3,x_4;\epsilon_L,\epsilon_H;\tilde{\epsilon}_p)_{\mathbf{\Omega}_2} = \mathcal{F}(1,x_4;\epsilon_L,\epsilon_H;\tilde{\epsilon}_p)\times x_3^{-h_L}\tag{6.41}$$

$\mathbf{\Omega}_3$ channel

This is the OPE channel which considers fusion of the light primaries $\mathcal{O}_L(x_3)$ and $\mathcal{O}_L(x_4)$. The monodromy contours are shown in Fig. 6.3. The monodromy conditions (6.30) for the

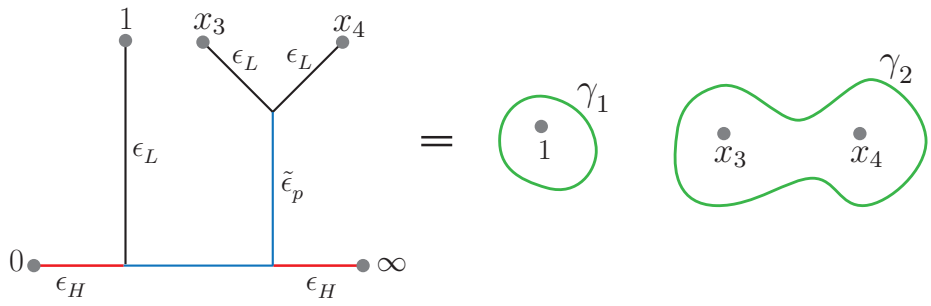

Figure 6.3: OPE channel and monodromy contours for $\mathbf{\Omega}_3$ for the 5-point block.

two contours are

$$\mathcal{X}[\gamma_1] = -4\pi^2\epsilon_L^2 = -4\pi^2\tilde{\epsilon}_p^2 \tag{6.42}$$

and

$$\begin{aligned}\mathcal{X}[\gamma_2] = -\frac{4\pi^2 x_3^{-\alpha/2} x_4^{-\alpha/2}}{\alpha^2}&[\epsilon_L((\alpha-1)x_4^\alpha + (\alpha+1)x_3^\alpha) + (x_3^\alpha - x_4^\alpha)x_3 c_3] \\ &\times [\epsilon_L((\alpha-1)x_3^\alpha + (\alpha+1)x_4^\alpha) + (x_4^\alpha - x_3^\alpha)x_4 c_4] \;=\; -4\pi^2\tilde{\epsilon}_q^2.\end{aligned} \tag{6.43}$$

(6.42) gives $\epsilon_L = \tilde{\epsilon}_q$. Inspired by the accessory parameters of the $\mathbf{\Omega}_1$ and $\mathbf{\Omega}_2$ channels, one can make an educated guess for the seed solution c_3

$$c_3 = \frac{-\epsilon_L(x_4^\alpha(\alpha-1) + x_3^\alpha(\alpha+1) + \tilde{\epsilon}_p x_3^{\alpha/2} x_4^{\alpha/2}}{x_3(x_3^\alpha - x_4^\alpha)}. \tag{6.44}$$

Substituting this in (6.43) we obtain

$$c_4 = \frac{-\epsilon_L(x_3^\alpha(\alpha-1) + x_4^\alpha(\alpha+1) + \tilde{\epsilon}_p x_4^{\alpha/2} x_3^{\alpha/2}}{x_4(x_4^\alpha - x_3^\alpha)}. \tag{6.45}$$

The integrability condition (6.13) is non-trivally satisfied in this case. Integrating the accessory parameters, we obtain

$$f_{(5)}(1,x_3,x_4;\epsilon_L,\epsilon_H;\tilde{\epsilon}_p)=\epsilon_L\left((1-\alpha)\log x_3x_4+2\log\frac{x_3^\alpha-x_4^\alpha}{\alpha}\right)+2\tilde{\epsilon}_p\log\left[\frac{1}{4\alpha}\frac{x_4^{\alpha/2}+x_3^{\alpha/2}}{x_4^{\alpha/2}-x_3^{\alpha/2}}\right]. \tag{6.46}$$

This result can also be written in terms of $f_{(4)}$ appearing in the 4-point conformal block (6.36)

$$f_{(5)}(1,x_3,x_4;\epsilon_L,\epsilon_H;\tilde{\epsilon}_p)=f_{(4)}(1,x_3,x_4;\epsilon_L,\epsilon_H;\tilde{\epsilon}_p)+\epsilon_L\log 1 \tag{6.47}$$

The second term is obviously zero but we have retained it to preserve the structure we found in the previous channels. Exponentiating the above expression using (6.3), we get

$$\mathcal{F}_{(5)}(1,x_3,x_4;\epsilon_L,\epsilon_H;\tilde{\epsilon}_p)_{\mathbf{\Omega}_3}=\mathcal{F}(x_3,x_4;\epsilon_L,\epsilon_H;\tilde{\epsilon}_p)\times(1)^{-h_L}. \tag{6.48}$$

which is the same factorization observed in the channels $\mathbf{\Omega}_1$ and $\mathbf{\Omega}_2$.

Warmup example II : 6-point function

Our second example is the conformal block of the 6-point function

$$\left\langle \mathcal{O}_H(\infty)\mathcal{O}_L(1)\mathcal{O}_L(x_3)\mathcal{O}_L(x_4)\mathcal{O}_L(x_5)\mathcal{O}_H(0)\right\rangle. \tag{6.49}$$

This is the case of $m=4$.

Perturbative expansion of the monodromy equation

Once again, we start with the perturbative expansion in the parameter ϵ_L for $\psi(z)$, $T(z)$ and $c_i(z)$ (6.18). The zeroth and first order equations are the same as that of (6.19) and (6.20).

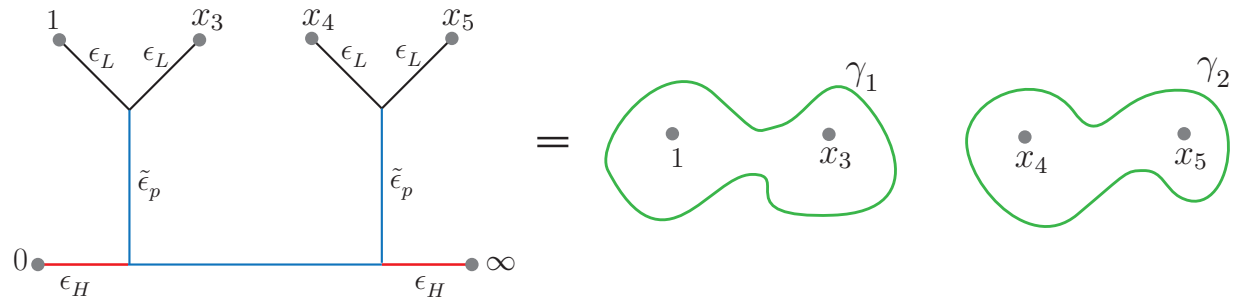

Figure 6.4: The OPE channel and contour configuration of $\mathbf{\Omega}_1$ for the case of the 6-point block.

The stress-tensor at the first two orders is

$$T^{(0)}(z) = \frac{\epsilon_H}{z^2}, \tag{6.50}$$

$$T^{(1)}(z) = \frac{\epsilon_L}{(z-1)^2} + \frac{\epsilon_L}{(z-x_3)^2} + \frac{\epsilon_L}{(z-x_4)^2} + \frac{\epsilon_L}{(z-x_5)^2} - \frac{4\epsilon_L}{z(z-1)} + \frac{x_3(1-x_3)}{z(z-1)(z-x_3)}c_3^{(0)} + \frac{x_4(1-x_4)}{z(z-1)(z-x_4)}c_4^{(0)} + \frac{x_5(1-x_5)}{z(z-1)(z-x_5)}c_5^{(0)}. \tag{6.51}$$

The solution to the zeroth order ODE in (6.19) remains the same

$$\psi_{\pm}^{(0)}(z) = z^{(1\pm\alpha)/2}, \qquad \alpha = \sqrt{1-4\epsilon_H}. \tag{6.52}$$

Similar to the 5-point case, we proceed to study monodromy constraints of the first order solution $\psi^{(1)}(z)$ which in turn is obtained by the method of variation of parameters (6.26).

Monodromy conditions

There are three choices of contours in this case

- $\mathbf{\Omega}_1$: γ_1 enclosing $\{1, x_3\}$ and γ_2 enclosing $\{x_4, x_5\}$
- $\mathbf{\Omega}_2$: γ_1 enclosing $\{1, x_5\}$ and γ_2 enclosing $\{x_3, x_4\}$
- $\mathbf{\Omega}_3$: γ_1 enclosing $\{1, x_4\}$ and γ_2 enclosing $\{x_3, x_5\}$

The above channels are often referred to as s, t and u respectively. The monodromy contour and the corresponding OPE channel for $\mathbf{\Omega}_1$ are shown in the Fig. 6.4.

The monodromy matrix for the contours γ_k above upto first order in ϵ_L has the same form as the one which we encountered in the 5-point block case (6.27) with the elements given by the contour integrals in (6.28). Furthermore, we impose the same monodromy condition $\mathcal{X}[\gamma_i]$ for each of the contours in the configurations above (6.30).

$\mathbf{\Omega}_1$ channel

For the contours of the $\mathbf{\Omega}_1$ channel we have

$$\begin{aligned}\mathcal{X}[\gamma_1] = &-\frac{4\pi^2}{\alpha^2}x_3^{-\alpha}\left[\epsilon_L(\alpha-1+x_3^\alpha(\alpha+1))+c_3x_3(x_3^\alpha-1)\right]\\ &\times\left[\epsilon_L(\alpha-3+x_3^\alpha(\alpha+3)+(x_3^\alpha-1)(c_3x_3+c_4x_4+c_5x_5))\right]=-4\pi^2\tilde{\epsilon}_p^2, \qquad (6.53)\\ \mathcal{X}[\gamma_2] = &-\frac{4\pi^2x_4^{-\alpha}x_5^{-\alpha}}{\alpha^2}\left[\epsilon_L((\alpha-1)x_5^\alpha+(\alpha+1)x_4^\alpha)+x_4(x_4^\alpha-x_5^\alpha)c_4\right]\\ &\times\left[\epsilon_L(\alpha-1)x_4^\alpha+(\alpha+1)x_5^\alpha)-c_5x_5(x_4^\alpha-x_5^\alpha)\right] \;=\; -4\pi^2\tilde{\epsilon}_q^2. \qquad (6.54)\end{aligned}$$

We shall focus on the case when the conformal dimensions of the operators in the channels right after fusion with the light primaries are the same. That is, $\tilde{\epsilon}_p = \tilde{\epsilon}_q$. This is a major simplification, which was also used in [12], to facilitate the analysis. We use the result of the accessory parameter c_3 from the 4-point (or 5-point) conformal block as the seed solution. As we had seen in the previous subsection, this seed solution is

$$c_3 = \frac{-\epsilon_L(\alpha-1+x_3^\alpha(\alpha+1))+x_3^{\alpha/2}\alpha\tilde{\epsilon}_p}{x_3(x_3^\alpha-1)}. \qquad (6.55)$$

Substituting this into the monodromy conditions (6.53) and (6.54) we have two simultaneous equations in c_4 and c_5 which can be solved

$$c_4 = \frac{-\epsilon_L(x_5^\alpha(\alpha-1)+x_4^\alpha(\alpha+1))+x_4^{\alpha/2}x_5^{\alpha/2}\alpha\tilde{\epsilon}_p}{x_4(x_4^\alpha-x_5^\alpha)}, \tag{6.56}$$

$$c_5 = \frac{-\epsilon_L(x_4^\alpha(\alpha-1)+x_5^\alpha(\alpha+1))+x_4^{\alpha/2}x_5^{\alpha/2}\alpha\tilde{\epsilon}_p}{x_5(x_5^\alpha-x_4^\alpha)}. \tag{6.57}$$

It can be verified that the integrability condition (6.13) is satisfied.

We can now use (6.12) to obtain the conformal block.

$$\begin{aligned} &f_{(6)}(x_3,x_4,x_5;\epsilon_L,\epsilon_H;\tilde{\epsilon}_p) \\ &= \left[\epsilon_L\left((1-\alpha)\log x_3+2\log\frac{1-x_3^\alpha}{\alpha}\right)+2\tilde{\epsilon}_p\log\left[4\alpha\frac{1+x_3^{\alpha/2}}{1-x_3^{\alpha/2}}\right]\right] \\ &\quad+\left[\epsilon_L\left((1-\alpha)\log x_4x_5+2\log\frac{x_4^\alpha-x_5^\alpha}{\alpha}\right)+2\tilde{\epsilon}_p\log\left[4\alpha\frac{x_4^{\alpha/2}+x_5^{\alpha/2}}{x_4^{\alpha/2}-x_5^{\alpha/2}}\right]\right]. \end{aligned} \tag{6.58}$$

The structure of each of the terms in square brackets is yet again of the same form as that of 4-point conformal block case (6.36). We now use the exponentiation of the conformal block (6.3), to obtain

$$\begin{aligned} \mathcal{F}_{(6)}(1,x_3,x_4,x_5;\epsilon_L,\epsilon_H;\tilde{\epsilon}_p)_{\mathbf{\Omega}_1} &= \exp\left[-\frac{c}{6}f_{(4)}(1,x_3;\epsilon_L,\epsilon_H;\tilde{\epsilon}_p)\right]\times\exp\left[-\frac{c}{6}f_{(4)}(x_4,x_5;\epsilon_L,\epsilon_H;\tilde{\epsilon}_q)\right] \\ &= \mathcal{F}_{(4)}(1,x_3;\epsilon_L,\epsilon_H;\tilde{\epsilon}_p)\mathcal{F}_{(4)}(x_4,x_5;\epsilon_L,\epsilon_H;\tilde{\epsilon}_q). \end{aligned} \tag{6.59}$$

The 6-point conformal block, therefore, factorizes into a product of two 4-point ones.

Note that this factorization is not due to a decoupling of equations involving accessory parameters and is therefore not a mere doubling of the reduced problem for a single conformal block. In particular, equation (6.53) contains all the accessory parameters and it is not a priori obvious from the monodromy method that this factorization will happen.

Just like the case of the 5-point conformal block this factorization can be anticipated for the special case of twist operators (in the limit $n \to 1$). Inserting a complete set of states in the 6-point function and using the OPE channels (6.38) relevant in the regimes $x_3 \to 1$ or $x_4 \to x_5$ we have

$$\begin{aligned}&\left\langle \mathcal{O}_H(\infty)\sigma_n(1)\bar{\sigma}_n(x_3)\sigma_n(x_4)\bar{\sigma}_n(x_5)\mathcal{O}_H(0)\right\rangle_{x_3\to 1 \text{ and/or } x_4\to x_5}\\ &= \sum_\alpha \left\langle \mathcal{O}_H(\infty)\sigma_n(1)\bar{\sigma}_n(x_3)\rangle\alpha\langle\alpha\sigma_n(x_4)\bar{\sigma}_n(x_5)\mathcal{O}_H(0)\right\rangle. \end{aligned} \tag{6.60}$$

Due to orthonomality of the complete set of states inserted, the only contribution will arise from $\rangle\alpha = \rangle\mathcal{O}_H$, leading to the factorization

$$\begin{aligned}&\left\langle \mathcal{O}_H(\infty)\sigma_n(1)\bar{\sigma}_n(x_3)\sigma_n(x_4)\bar{\sigma}_n(x_5)\mathcal{O}_H(0)\right\rangle_{x_3\to 1 \text{ and/or } x_4\to x_5}\\ &= \left\langle \mathcal{O}_H(\infty)\sigma_n(1)\bar{\sigma}_n(x_3)\mathcal{O}_H(0)\right\rangle\left\langle \mathcal{O}_H(\infty)\sigma_n(x_4)\bar{\sigma}_n(x_5)\mathcal{O}_H(0)\right\rangle. \end{aligned} \tag{6.61}$$

$\mathbf{\Omega}_2$ and $\mathbf{\Omega}_3$ channels

The analysis in the $\mathbf{\Omega}_2$ and $\mathbf{\Omega}_3$ channels proceeds exactly in the same manner as that of the $\mathbf{\Omega}_1$ channel with the replacements $x_3 \leftrightarrow x_4$ and $x_3 \leftrightarrow x_5$ respectively. We obtain the factorizations

$$\mathcal{F}_{(6)}(1, x_3, x_4, x_5; \epsilon_L, \epsilon_H; \tilde{\epsilon}_p)_{\mathbf{\Omega}_2} = \mathcal{F}_{(4)}(1, x_4; \epsilon_L, \epsilon_H; \tilde{\epsilon}_p)\mathcal{F}_{(4)}(x_3, x_5; \epsilon_L, \epsilon_H; \tilde{\epsilon}_q) \tag{6.62}$$

$$\mathcal{F}_{(6)}(1, x_3, x_4, x_5; \epsilon_L, \epsilon_H; \tilde{\epsilon}_p)_{\mathbf{\Omega}_3} = \mathcal{F}_{(4)}(1, x_5; \epsilon_L, \epsilon_H; \tilde{\epsilon}_p)\mathcal{F}_{(4)}(x_4, x_3; \epsilon_L, \epsilon_H; \tilde{\epsilon}_q) \tag{6.63}$$

6.3.2 Conformal block for an arbitrary number of light operator insertions

Equipped with the examples considered above, we now come to the discussion of the correlator

$$\left\langle \mathcal{O}_H(\infty) \left[\mathcal{O}_L(1) \prod_{i=3}^{m+1} \mathcal{O}_L(x_i) \right] \mathcal{O}_H(0) \right\rangle \tag{6.64}$$

which has an arbitrary (even or odd) number of light operator insertions.

Perturbative expansion of the monodromy equation

We are interested in studying the monodromy properties of the ODE (6.11) with $T(z)$ given in (6.16). Just like the warmup examples considered above, we start with the perturbative expansion in the parameter ϵ_L for the quantities $\psi(z)$, $T(z)$ and $c_i(z)$ (6.18). The zeroth and first order equations are the same as that of (6.19) and (6.20). The stress-tensor at the first two orders is

$$T^{(0)}(z) = \frac{\epsilon_H}{z^2} \tag{6.65}$$

$$T^{(1)}(z) = \frac{\epsilon_L}{(z-1)^2} + \sum_{i=3}^{m+1} \frac{\epsilon_L}{(z-x_i)^2} - \frac{m\,\epsilon_L}{z(z-1)} + \sum_{i=3}^{m+1} \frac{x_i(1-x_i)}{z(z-1)(z-x_i)} c_i \tag{6.66}$$

The solution to the zeroth order ODE in (6.19) is

$$\psi_{\pm}^{(0)}(z) = z^{(1\pm\alpha)/2}, \qquad \alpha = \sqrt{1-4\epsilon_H} \tag{6.67}$$

We now consider the monodromy constraints of the first order solution $\psi^{(1)}(z)$ which is obtained by the method of variation of parameters (6.26).

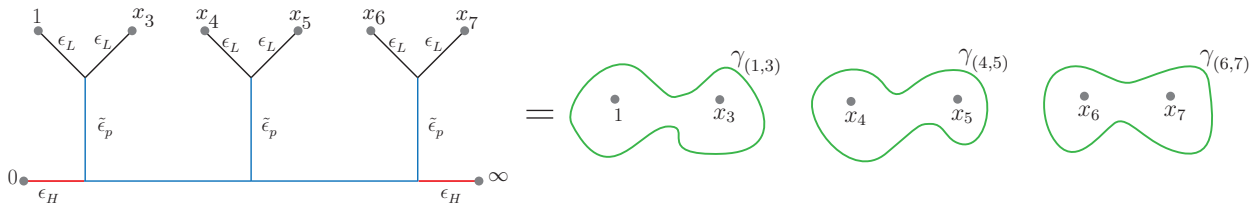

Figure 6.5: OPE channel and monodromy contours for $\mathbf{\Omega}_1$ for the 8-point block.

Contour configurations and their enumerations

The analysis of the 5- and 6-point conformal blocks posits that the choice of contour configurations is slightly different for even or odd m.

For the case of an even number of light operator insertions, we can form contours containing a pair of points each in $\nu_m^{(\text{even})} = m!/(2^{m/2}(m/2)!)$ ways. Each contour contains two light operators located within. The contours fall under two major classes.

- $\gamma_{(1,r)}$: containing the points 1 and x_r with $r \geq 3$.
- $\gamma_{(p,q)}$: containing the points x_p and x_q with $p \neq q$ and $p, q \geq 3$.

We use $\mathbf{\Omega}_i$ as a label for the ith contour configuration which includes information of all the contours $\gamma_k^{(i)}$

$$\mathbf{\Omega}_i = \bigcup_{\{(p,q)\}} \gamma^i_{(p,q)} \ . \tag{6.68}$$

See Fig 6.5 for an example involving 6 light operators and 2 heavy operators.

When an odd number of light operators are present there are $\nu_m^{(\text{odd})} = m!/(2^{(m-1)/2}((m-1)/2)!)$ such contour configurations. For each contour configuration, there is a single contour containing just one light operator. All the other contours enclose a pair of light operators. The classes of contours in this case are four.

- $\gamma_{(1)}$: containing the point 1
- $\gamma_{(s)}$: containing the point x_s with $s \geq 3$

- $\gamma_{(1,r)}$: containing the points 1 and x_r
- $\gamma_{(p,q)}$: containing the points x_p and x_q with $p \neq q$ and $p, q \geq 3$

The set of contour configurations are of two types

$$\mathbf{\Omega}_i^A = \gamma_{(r)} \cup \bigcup_{\{(p,q)\}} \gamma^i_{(p,q)} \quad \text{and} \quad \mathbf{\Omega}_i^B = \gamma_{(1)} \cup \bigcup_{\{(p,q)\}} \gamma^i_{(p,q)} \ . \tag{6.69}$$

An example of the A-type contour configuration is $\mathbf{\Omega}_1$ for the 5-point case shown in Fig 6.2 whereas the $\mathbf{\Omega}_3$ shown in Fig 6.3 is a B-type configuration.

The contour configuration for the odd case ($m = 2j+1$) is equivalent to that of the even case ($m = 2j$) with an additional contour enclosing the extra point. Moreover, it can be seen that $\nu_{2j}^{(\text{even})} = \nu_{2j-1}^{(\text{odd})}$. (This number is 3 for both the 5- and 6-point cases.)

It can be seen that there is a one-to-one mapping between the contour configurations $\mathbf{\Omega}_i$ and the paired fusions of the light operators whose OPEs we consider to calculate the conformal block. We label this set of pairs as $\{(p,q)\}$. Often, we shall denote this map between the contour configurations and the set of fusions as

$$\mathbf{\Omega}_i \mapsto \{(p,q)\} \ .$$

Monodromy conditions

The monodromy conditions are the same as the ones which we had imposed for the 5- and 6-point blocks. The final constraint is $\mathcal{X}[\gamma_i]$ in equation (6.30). We shall now consider the even and odd number of insertions of light operators separately. Additionally, we shall perform the analysis for the specific case of the conformal block in which the resulting intermediate channels from all pairwise fusions of light operators give the operators with the same conformal dimension.

Case I : Even number of light operator insertions

Consider a specific contour configuration $\mathbf{\Omega}_i$. The monodromy condition for a contour enclosing 1 and x_r with $r = 3, 4, 5, \cdots, m$ is

$$\begin{aligned}\mathcal{X}[\gamma_{(1,r)}] = &-\frac{4\pi^2}{\alpha^2} x_r^{-\alpha} \left[\epsilon_L((\alpha-1)+(\alpha+1)x_r^\alpha) + (x_r^\alpha - 1)c_r x_r\right] \\ &\times \left[\epsilon_L((\alpha-m+1)+(\alpha+m-1)x_r^\alpha) + (x_r^\alpha-1)\sum_{i=3}^{m+1} c_i x_i\right] \;=\; -4\pi^2\tilde{\epsilon}_a.\end{aligned} \tag{6.70}$$

and that for a contour enclosing x_p and x_q is

$$\begin{aligned}\mathcal{X}[\gamma_{(p,q)}] = &-\frac{4\pi^2}{\alpha^2} (x_p x_q)^{-\alpha} \left[\epsilon_L((\alpha-1)x_q^\alpha + (\alpha+1)x_p^\alpha) + (x_p^\alpha - x_q^{-\alpha})c_p x_p\right] \\ &\times \left[\epsilon_L((\alpha-1)x_p^\alpha + (\alpha+1)x_q^\alpha) + (x_q^\alpha - x_p^{-\alpha})c_q x_q\right] \;=\; -4\pi^2\tilde{\epsilon}_b.\end{aligned} \tag{6.71}$$

As mentioned above, we shall set $\tilde{\epsilon}_a = \tilde{\epsilon}_b = \tilde{\epsilon}_p$.

Unlike the case of conformal blocks involving only an even number (m) of light operators considered in [136], the system of monodromy conditions with the additional heavy operators does not decouple into $m/2$ independent monodromy problems. It can be seen that the monodromy condition (6.70) involves all the accessory parameters.

The analysis of the 6-point conformal block strongly suggests a guess for the solution of the above coupled equations

$$c_r = \frac{-\epsilon_L(\alpha - 1 + x_r^\alpha(\alpha+1)) + x_r^{\alpha/2}\alpha\tilde{\epsilon}_p}{x_r(x_r^\alpha - 1)}, \tag{6.72}$$

$$c_p = \frac{-\epsilon_L(x_q^\alpha(\alpha-1) + x_p^\alpha(\alpha+1)) + (x_p x_q)^{\alpha/2}\alpha\tilde{\epsilon}_p}{x_p(x_p^\alpha - x_q^\alpha)}, \tag{6.73}$$

$$c_q = \frac{-\epsilon_L(x_p^\alpha(\alpha-1) + x_q^\alpha(\alpha+1)) + (x_q x_p)^{\alpha/2}\alpha\tilde{\epsilon}_p}{x_q(x_q^\alpha - x_p^\alpha)}. \tag{6.74}$$

This obeys the integrability condition $\partial_{x_p} c_q = \partial_{x_q} c_p$. Also, all other integrability conditions get trivially satisfied.

Let us now verify this is indeed a solution to the coupled monodromy constraints (6.70) and (6.71). It can be easily seen that $\mathcal{X}[\gamma_{(p,q)}]$ is obeyed by c_p and c_q above. Consider the monodromy condition $\mathcal{X}[\gamma_{(1,r)}]$ in (6.70) in which one of the contours contain 1 and x_r. This monodromy condition involves all the accessory parameters. Note that, equations (6.73) and (6.74) give

$$c_p x_p + c_q x_q = -2\epsilon_L. \tag{6.75}$$

From (6.75) and (6.72), we have

$$\begin{aligned}\sum_{i=3}^{m+1} c_i x_i &= c_r x_r - (m-2)\epsilon_L \\ &= \frac{-\epsilon_L((\alpha - m + 1) + (\alpha + m - 1)x_r^\alpha) + x_r^{\alpha/2}\alpha\tilde{\epsilon}_p}{(x_r^\alpha - 1)}.\end{aligned} \tag{6.76}$$

The first equality follows from (6.75) and the fact that there are $(m-2)/2$ pairs of contours other than the one containing 1 and x_r. Note that r is fixed and there is no sum over r in the first term $c_r x_r$. It can then be very explicitly checked that substituting (6.76) along with (6.72) in the LHS of equation (6.70) satisfies it giving $-4\pi^2\tilde{\epsilon}_q^2$ (with $\tilde{\epsilon}_a = \tilde{\epsilon}_p$).

We can now use (6.12) to obtain the conformal block by integrating the accessory parameters (6.73), (6.74) and (6.72). The integration constants are fixed in the same manner as the warmup examples, by demanding the expected behaviour $(2\epsilon_L - \tilde{\epsilon}_p)\log(x_p - x_q)$ as $x_p \to x_q$.

$$\begin{aligned}&f(\{x_i\}; \epsilon_L, \epsilon_H; \tilde{\epsilon}_p) \\ &= \sum_{\mathbf{\Omega}_i \mapsto \{(p,q)\}} \left(\epsilon_L(1-\alpha)\log x_p x_q + 2\epsilon_L \log\frac{x_p^\alpha - x_q^\alpha}{\alpha} + 2\tilde{\epsilon}_p \log\left[4\alpha \frac{x_p^{\alpha/2} + x_q^{\alpha/2}}{x_p^{\alpha/2} - x_q^{\alpha/2}}\right]\right) \\ &= \sum_{\mathbf{\Omega}_i \mapsto \{(p,q)\}} f_{(4)}(x_p, x_q; \epsilon_L, \epsilon_H; \tilde{\epsilon}_p).\end{aligned} \tag{6.77}$$

Here the sum is over the set of $m/2$ contours containing a pair of light operators located at x_p and x_q respectively. This set also includes the contour containing 1 and x_r. Equivalently the set $\{(p,q)\}$ is also the OPE channel along which we perform the conformal partial wave expansion.

Equation (6.77) upon exponentiation clearly shows the factorization of the $(m+2)$-point conformal block into $m/2$ 4-point blocks.

$$\begin{aligned}\mathcal{F}_{(m+2)}(\{x_i\};\epsilon_L,\epsilon_H;\tilde{\epsilon}_p) &= \prod_{\mathbf{\Omega}_i\mapsto\{(p,q)\}} \exp\left[-\frac{c}{6}f_{(4)}(x_p,x_q;\epsilon_L,\epsilon_H;\tilde{\epsilon}_p)\right] \\ &= \prod_{\mathbf{\Omega}_i\mapsto\{(p,q)\}} \mathcal{F}_{(4)}(x_p,x_q;\epsilon_L,\epsilon_H;\tilde{\epsilon}_p). \end{aligned} \tag{6.78}$$

This proves that the $(m+2)$-point conformal block, in the specific classes of OPE channels analysed above, factorizes into 4-point conformal blocks. This is a central result of this chapter.

Case II : Odd number of light operator insertions

As noted before, the contour configurations for an odd number of insertions, m, is the sum of the even number contour configurations for $m-1$ light operator insertions plus another contour enclosing a single point.

For the contour configuration of the first kind (6.69), the monodromy conditions are

$$\begin{aligned}\mathcal{X}[\gamma_{(1,r)}] = &-\frac{4\pi^2}{\alpha^2}x_r^{-\alpha}\left[\epsilon_L((\alpha-1)+(\alpha+1)x_r^\alpha)+(x_r^\alpha-1)c_r x_r\right] \\ &\times\left[\epsilon_L((\alpha-m+1)+(\alpha+m-1)x_r^\alpha)+(x_r^\alpha-1)\sum_{i=3}^{m+1}c_i x_i\right] \;=\; -4\pi^2\tilde{\epsilon}_a,\end{aligned} \tag{6.79}$$

and that for a contour enclosing x_p and x_q is

$$\mathcal{X}[\gamma_{(p,q)}] = -\frac{4\pi^2}{\alpha^2}(x_p x_q)^{-\alpha}\left[\epsilon_L((\alpha-1)x_q^\alpha + (\alpha+1)x_p^\alpha) + (x_p^\alpha - x_q^{-\alpha})c_p x_p\right] \tag{6.80}$$
$$\times\left[\epsilon_L((\alpha-1)x_p^\alpha + (\alpha+1)x_q^\alpha) + (x_q^\alpha - x_p^{-\alpha})c_q x_q\right] \;=\; -4\pi^2\tilde{\epsilon}_b.$$

For the contours enclosing the single points, they are

$$\mathcal{X}[\gamma_{(r)}] = -4\pi^2\epsilon_L^2 = -4\pi^2\tilde{\epsilon}_c^2, \tag{6.81}$$

$$\mathcal{X}[\gamma_{(1)}] = -4\pi^2\epsilon_L^2 = -4\pi^2\tilde{\epsilon}_d^2. \tag{6.82}$$

$\mathcal{X}[\gamma_{(s)}]$ and $\mathcal{X}[\gamma_{(1)}]$ imply that the conformal dimension of the operator living within the contour is picked by the residue.

Similar to the previous cases, we shall now set $\tilde{\epsilon}_a = \tilde{\epsilon}_b = \tilde{\epsilon}_p$. For the configuration of the first kind, $\mathbf{\Omega}_i^A$ in (6.69), consisting of the contours $\gamma_{(r)}$, $\gamma_{(p,q)}$ and $\gamma_{(1,r)}$, the solutions for the accessory parameters are

$$c_r = \frac{-\epsilon_L(\alpha - 1 + x_r^\alpha(\alpha+1)) + x_r^{\alpha/2}\alpha\tilde{\epsilon}_p}{x_r(x_r^\alpha - 1)}, \tag{6.83}$$

$$c_p = \frac{-\epsilon_L(x_q^\alpha(\alpha-1) + x_p^\alpha(\alpha+1)) + (x_p x_q)^{\alpha/2}\alpha\tilde{\epsilon}_p}{x_p(x_p^\alpha - x_q^\alpha)}, \tag{6.84}$$

$$c_q = \frac{-\epsilon_L(x_p^\alpha(\alpha-1) + x_q^\alpha(\alpha+1)) + (x_q x_p)^{\alpha/2}\alpha\tilde{\epsilon}_p}{x_q(x_q^\alpha - x_p^\alpha)}, \tag{6.85}$$

$$c_s = -\frac{\epsilon_L}{x_s}. \tag{6.86}$$

The above accessory parameters can be integrated (6.12) to obtain the function appearing in the exponential of the conformal block.

$$
\begin{aligned}
& f(\{x_i\};\epsilon_L,\epsilon_H;\tilde{\epsilon}_p) \\
&= \epsilon_L \log x_s + \sum_{\mathbf{\Omega}_i^A \mapsto \{(p,q)\}} \left(\epsilon_L(1-\alpha)\log x_p x_q + 2\epsilon_L \log \frac{x_p^\alpha - x_q^\alpha}{\alpha} + 2\tilde{\epsilon}_p \log \left[4\alpha \frac{x_p^{\alpha/2}+x_q^{\alpha/2}}{x_p^{\alpha/2}-x_q^{\alpha/2}} \right] \right) \\
&= \epsilon_L \log x_s + \sum_{\mathbf{\Omega}_i^A \mapsto \{(p,q)\}} f_{(4)}(x_p,x_q;\epsilon_L,\epsilon_H;\tilde{\epsilon}_a). \qquad (6.87)
\end{aligned}
$$

This upon exponentiation gives

$$
\begin{aligned}
\mathcal{F}_{(m+2)}(\{x_i\};\epsilon_L,\epsilon_H;\tilde{\epsilon}_p) &= (x_s)^{-\epsilon_L} \prod_{\mathbf{\Omega}_i^A \mapsto \{(p,q)\}} \exp\left[-\frac{c}{6} f_{(4)}(x_p,x_q;\epsilon_L,\epsilon_H;\tilde{\epsilon}_p) \right] \\
&= (x_s)^{-\epsilon_L} \prod_{\mathbf{\Omega}_i^A \mapsto \{(p,q)\}} \mathcal{F}_{(4)}(x_p,x_q;\epsilon_L,\epsilon_H;\tilde{\epsilon}_p). \qquad (6.88)
\end{aligned}
$$

This shows the factorization of the $(m+2)$-point block with odd m into a 3-point function (without the structure constant) and $(m-1)/2$ number of 4-point conformal blocks.

For the second kind of contour configuration, $\mathbf{\Omega}_i^B$ in (6.69), consisting of $\gamma_{(1)}$ and $\gamma_{(p,q)}$ we have

$$
c_p = \frac{-\epsilon_L(x_q^\alpha(\alpha-1)+x_p^\alpha(\alpha+1)) + (x_p x_q)^{\alpha/2}\alpha\tilde{\epsilon}_p}{x_p(x_p^\alpha - x_q^\alpha)}, \qquad (6.89)
$$

$$
c_q = \frac{-\epsilon_L(x_p^\alpha(\alpha-1)+x_q^\alpha(\alpha+1)) + (x_q x_p)^{\alpha/2}\alpha\tilde{\epsilon}_p}{x_q(x_q^\alpha - x_p^\alpha)}. \qquad (6.90)
$$

Integrating these, we obtain (6.12)

$$
\begin{aligned}
& f(\{x_i\};\epsilon_L,\epsilon_H;\tilde{\epsilon}_p) \\
&= \epsilon_L \log 1 + \sum_{\mathbf{\Omega}_i^B \mapsto \{(p,q)\}} \left(\epsilon_L (1-\alpha) \log x_p x_q + 2\epsilon_L \log \frac{x_p^\alpha - x_q^\alpha}{\alpha} + 2\tilde{\epsilon}_p \log \left[4\alpha \frac{x_p^{\alpha/2} + x_q^{\alpha/2}}{x_p^{\alpha/2} - x_q^{\alpha/2}} \right] \right) \\
&= \epsilon_L \log 1 + \sum_{\mathbf{\Omega}_i^B \mapsto \{(p,q)\}} f_{(4)}(x_p, x_q; \epsilon_L, \epsilon_H; \tilde{\epsilon}_a). \qquad (6.91)
\end{aligned}
$$

Exponentiating this to obtain the conformal block using (6.3), we have

$$
\begin{aligned}
\mathcal{F}_{(m+2)}(\{x_i\};\epsilon_L,\epsilon_H;\tilde{\epsilon}_a) &= (1)^{-\epsilon_L} \prod_{\mathbf{\Omega}_i^B \mapsto \{(p,q)\}} \exp\left[-\frac{c}{6} f_{(4)}(x_p, x_q; \epsilon_L, \epsilon_H; \tilde{\epsilon}_a) \right] \\
&= (1)^{-\epsilon_L} \prod_{\mathbf{\Omega}_i^B \mapsto \{(p,q)\}} \mathcal{F}_{(4)}(x_p, x_q; \epsilon_L, \epsilon_H; \tilde{\epsilon}_a). \qquad (6.92)
\end{aligned}
$$

Hence, the factorization is also clear for the contour configuration, $\mathbf{\Omega}_i^B$.

As we had seen the 5- and 6-point examples, the factorization for an arbitrary number of light operator insertions can be expected for the light operators being twist and anti-twist operators. Since, twist operators fuse into the identity (6.38), the correlator with $2N$ number of twist and anti-twist insertions will factorize into N 4-point functions each having two heavy and two twists. This factorization will occur only in specific regimes in the space of $\{x_i\}$ where one can use the OPEs within the correlator.

There is one additional caveat to our monodromy analysis. A curious feature of the above conformal blocks is that they are apparently independent of the conformal dimensions of operators in other intermediate channels — the horizontal channels $\tilde{\epsilon}_{Q,R,\cdots}$ in Fig 6.1 and Fig 6.6. Let us evaluate the conformal dimensions of the operators in these intermediate channels. Consider, $\tilde{\epsilon}_Q$ in Fig 6.6. This can be obtained by evaluating the monodromy around the contour containing $\mathcal{O}_H(0)$, $\mathcal{O}_L(1)$ and $\mathcal{O}_L(x_3)$ — $\gamma_{(0,1,x_3)}$ in Fig 6.6. At the leading order (ϵ_L^0) the only contribution arises from $z = 0$. This is equation (6.24). At

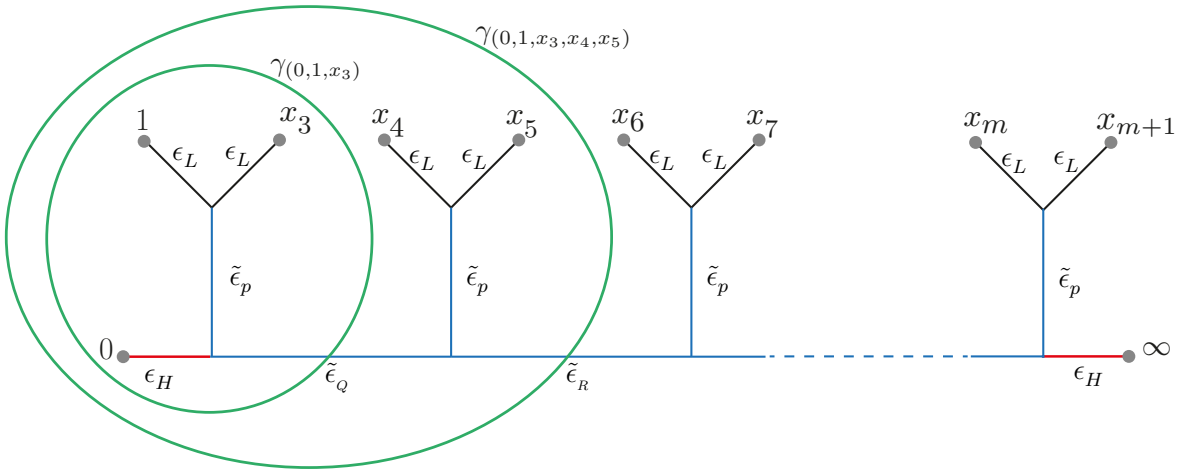

Figure 6.6: Monodromy contours to calculate $\tilde{\epsilon}_Q$ and $\tilde{\epsilon}_R$.

the linear order in ϵ_L, there is a vanishing contribution from the residue at $z = 0$ and the monodromy is effectively the same as that of the contour γ_1 in Fig. 6.2 and leads to equation (6.31). Hence, from (6.24) and (6.27), we have

$$\mathbb{M}(\gamma_{(0,1,x_3)}) = -\begin{pmatrix} e^{\pi i\alpha} & 0 \\ 0 & e^{-\pi i\alpha} \end{pmatrix} + \begin{pmatrix} I^{(k)}_{++}(\gamma_2) & I^{(k)}_{+-}(\gamma_2) \\ I^{(k)}_{-+}(\gamma_2) & I^{(k)}_{--}(\gamma_2) \end{pmatrix}, \qquad \text{with, } \alpha = \sqrt{1-4\epsilon_H}. \quad (6.93)$$

Therefore, comparing (6.93) with (6.29) for the contour $\gamma_{(0,1,x_3)}$ which has $\Lambda = \sqrt{1-4\tilde{\epsilon}_Q}$, results in $\tilde{\epsilon}_Q = \epsilon_H + \mathcal{O}(\tilde{\epsilon}_p)$. Here, the $\mathcal{O}(\tilde{\epsilon}_p)$ term arises from the second term in (6.93) or equivalently from the contour γ_1 in Fig. 6.2 as explained above.

We shall now make our only assumption on the spectrum and OPEs. This is, the intermediate operator ($\tilde{\epsilon}_p$) appearing after fusion of two light operators has $\tilde{\epsilon}_p \ll \epsilon_L$ (and this automatically implies, $\tilde{\epsilon}_p \ll \epsilon_H$). This is a reasonable assumption since the exchanged operators (similar to the identity and stress tensor in the case of twist operators) do not scale as the central charge unlike the light and heavy operators. Hence, the dominant contribution to this monodromy (6.93) comes from the heavy operator at $z = 0$. This shows that in the

heavy-light regime, this intermediate channel $\tilde{\epsilon}_Q$ is dominated by a heavy operator exchange ϵ_H [11].

In order to obtain $\tilde{\epsilon}_R$, one can repeat the above exercise by considering the monodromy of the contour containing 0, 1, x_3, x_4 and x_5 — $\gamma_{(0,1,x_3,x_4,x_5)}$ in Fig 6.6. Once again, the dominant contribution will arise from the heavy operator at $z = 0$, which leads to $\tilde{\epsilon}_R = \epsilon_H$. Continuing in this fashion, it can therefore be seen, that all the horizontal intermediate channels in Fig 6.6 are dominated by heavy operator exchanges in the heavy-light limit[12]. The dependence on the conformal dimension of these channels then enters the conformal block via the relation $\tilde{\epsilon}_Q = \tilde{\epsilon}_R = \cdots = \epsilon_H$. Therefore, the assumption, $\tilde{\epsilon}_p \ll \epsilon_L$ is necessary to have the heavy exchanges in the horizontal channels which results in the factorization of the higher-point block into 4-point blocks.

It is worthwhile mentioning that there are other branches of solutions to the monodromy constraints for the accessory parameters. This point was emphasized in [12]. It was shown in [12] that only one of these branches matches with the one obtained from gravity. In our analysis above, we have restricted our attention solely to the branch which is relevant to make contact with holography in Section 6.5.

6.4 Entanglement entropy and mutual information of heavy states

The results on conformal blocks obtained in the previous section can be utilized to evaluate the entanglement entropy of disjoint intervals in states excited by the heavy operator $\mathcal{O}_H$. The single interval entanglement entropy of heavy states was considered in [21]. Using the

[11] This fact is also supported by $\rangle\alpha = \mathcal{O}_H(0)\rangle 0$ in equations (6.39) and (6.40). We shall also see the bulk counterpart of $\tilde{\epsilon}_p \ll \epsilon_L$ in Section 6.5 which was also previously used in [147].

[12] It is reassuring to observe that this also gives the same spectrum of eigenvalues for $\mathbb{M}(\gamma_{(0,1,x_3,\cdots,x_{m+1})})$ and $\mathbb{M}(\gamma_{(\infty)})$ – as one should expect from the Riemann sphere.

state-operator correspondence, these 'heavy states' can be obtained from the vacuum as[13]

$$\rangle\psi = \mathcal{O}_H(0)\rangle 0 \quad \text{and} \quad \langle\psi = \lim_{z,\bar{z}\to\infty} \bar{z}^{2h_H} z^{2h_H} \langle 0\mathcal{O}_H(z,\bar{z}).$$

We briefly review the definitions of entanglement entropy and the replica trick used to calculate it. The entanglement entropy is defined as the von-Neumann entropy corresponding to the reduced density matrix $\rho_{\mathcal{A}}$

$$S_{\mathcal{A}} \;=\; -\mathrm{Tr}_{\mathcal{A}}\, \rho_{\mathcal{A}} \log \rho_{\mathcal{A}} \tag{6.94}$$

whilst the Rényi entropy is obtained from the moments of $\rho_{\mathcal{A}}$

$$S_{\mathcal{A}}^{(n)} = \frac{1}{1-n} \log\, \mathrm{Tr}_{\mathcal{A}}\, (\rho_{\mathcal{A}})^n. \tag{6.95}$$

The reduced density matrix is, in turn, obtained by tracing out the Hilbert space lying outside $\mathcal{A}$, i.e. $\rho_{\mathcal{A}} = \mathrm{Tr}_{\mathcal{A}'}\rho$. The full density matrix ρ in our case in terms of the excited state is $\rho = \rangle\psi\langle\psi$. The Rényi entropies are a convenient computational tool, as it can be used to obtain the entanglement entropy by the analytic continuation to $n \to 1$. It can be shown via the path integral [64] that the quantity $\mathrm{Tr}_{\mathcal{A}}\, (\rho_{\mathcal{A}})^n$ can be written in terms of the partition function of the n-sheeted Riemann surface (with each copy glued along $\mathcal{A}$) as

$$G_n \equiv \mathrm{Tr}_{\mathcal{A}}\, (\rho_{\mathcal{A}})^n = \frac{Z_n}{Z_1^n}, \tag{6.96}$$

where, we have defined the normalized partition function G_n. The replica trick can be implemented by means of the twist operators, σ_n, $\bar{\sigma}_n$, which impose the required boundary conditions as one moves from one sheet to another. The conformal dimensions of the (anti-

[13] There is a slight abuse of notation here. The ψ or Ψ appearing in this section is neither the same nor related in any way to ψ or Ψ which appeared in Section 6.3.

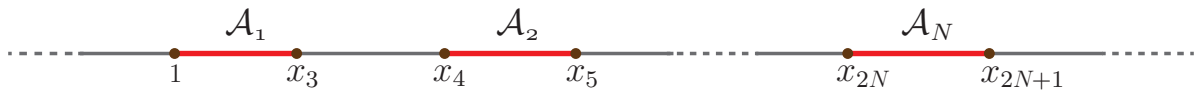

Figure 6.7: Configuration of disjoint intervals on a line.

)twist operators are

$$h_{\sigma_n} = h_{\bar{\sigma}_n} = \frac{c}{24}\left(n - \frac{1}{n}\right). \tag{6.97}$$

Hence, these operators become light in the limit relevant for entanglement entropy, $n \to 1$.

We shall focus on the case in which the sub-system $\mathcal{A}$ is made of N disjoint intervals i.e. $\mathcal{A} = \cup_i \mathcal{A}_i$ [14]. As shown in Fig. 6.7, these intervals are located at $[1, x_3]$, $[x_4, x_5]$, $\ldots [x_{2N}, x_{2N+1}]$. In this setup, $x_i < x_j$ for all $i < j$. This ordering of the locations reduce the number of possible OPE channels. Also, the OPEs are non-vanishing only for a twist with an anti-twist operator and vanishing for a pair of twists (or a pair of anti-twists). The number of allowed OPE channels for N disjoint intervals is actually, given by the Fibonacci number F_{2N-1}. (This is discussed further in Section 6.6.)

For heavy states, the partition function on the n-sheeted Riemann surface is the following correlation function of twist operators

$$G_n(x_i, \bar{x}_i) = \langle \Psi \sigma_n(1)\bar{\sigma}_n(x_3)\sigma_n(x_4)\bar{\sigma}_n(x_5)\sigma_n(x_6)\bar{\sigma}_n(x_7)\ldots\sigma_n(x_{2N})\bar{\sigma}_n(x_{2N+1})\rangle\Psi. \tag{6.98}$$

Here, the state $\rangle\Psi$ is the state in the n-sheeted replica which has insertions of $\mathcal{O}_H$ throughout all its copies. That is,

$$\Psi = \prod_{i=1}^{n}(\mathcal{O}_H)_i, \quad \text{and } h_\Psi = n h_H. \tag{6.99}$$

[14] It might be worth mentioning here, that the replica geometry for N disjoint intervals is a surface of genus $(n-1)(N-1)$ from the Riemann-Hurwitz theorem [105]. However, since we are interested in entanglement entropy (which is the $n \to 1$ limit of the Rényi entropy, $S_{\mathcal{A}}^{(n)}$) this is the limiting case of genus-0 or a sphere. We are therefore allowed use the results for correlation functions on the plane.

The correlator (6.98) can be rewritten as

$$G_n(x_i,\bar{x}_i) = \langle 0\ \Psi(\infty)\ \sigma_n(1)\bar{\sigma}_n(x_3) \prod_{i=4,6,\cdots}^{2N} \sigma_n(x_i)\bar{\sigma}_n(x_{i+1})\ \Psi(0)\ \rangle 0. \tag{6.100}$$

One can evaluate this correlation function by decomposing into conformal blocks. As argued in [21], for a CFT at large central charge with a sparse spectrum of low-dimension operators, the dominant contribution to this correlator will arise from the identity block. We can therefore use the results derived in the previous section for the conformal block with an arbitrary even number of light operator insertions. However, it is important to remember that the number of OPE channels in this case will be reduced for reasons we mentioned earlier. We denote these allowed OPE channels by $\widetilde{\mathbf{\Omega}}_i$ (which is a subset of the channels $\mathbf{\Omega}_i$ in the case of even number of light insertions considered in the previous section). Thus, from equation (6.78), we have, with $\tilde{\epsilon}_p = 0$ for the identity block

$$\begin{aligned} G_n(x_i,\bar{x}_i)|_{n\to 1} &\approx \mathcal{F}_{(2N+2)}(\{x_i\};\epsilon_L,\epsilon_H;0)\bar{\mathcal{F}}_{(2N+2)}(\{\bar{x}_i\};\epsilon_L,\epsilon_H;0) \\ &= \prod_{\widetilde{\mathbf{\Omega}}_i\mapsto\{(p,q)\}} \exp\left[-\frac{nc}{6} f_{(4)}(x_p,x_q;\epsilon_L,\epsilon_H;0)\right] \exp\left[-\frac{nc}{6} f_{(4)}(\bar{x}_p,\bar{x}_q;\epsilon_L,\epsilon_H;0)\right] \\ &= \prod_{\widetilde{\mathbf{\Omega}}_i\mapsto\{(p,q)\}} \mathcal{F}_{(4)}(x_p,x_q;\epsilon_L,\epsilon_H;0)\ \bar{\mathcal{F}}_{(4)}(\bar{x}_p,\bar{x}_q;\epsilon_L,\epsilon_H;0). \end{aligned} \tag{6.101}$$

Note that the central charge above is nc owing to n replicas of the original theory. The essential object here is the function $f_{(4)}$ given by (6.36). For this specific case, we have

$$f_{(4)}(x_i,x_j;\epsilon_L,\epsilon_H;0) = 2\epsilon_L \log \frac{x_i^\alpha - x_j^\alpha}{\alpha(x_i x_j)^{\frac{\alpha-1}{2}}}. \tag{6.102}$$

For the twist operators, $\epsilon_L = \frac{n^2-1}{4n}$, from (6.97). Using the above relations in the limit $n \to 1$, the entanglement entropy is given by

$$S_{\mathcal{A}} = \lim_{n\to 1} S_{\mathcal{A}}^{(n)} = \frac{c}{3} \min_i \left\{ \sum_{\widetilde{\mathbf{\Omega}}_i \mapsto \{(p,q)\}} \log \frac{(x_p^\alpha - x_q^\alpha)}{\alpha (x_p x_q)^{\frac{\alpha-1}{2}}} \right\}. \tag{6.103}$$

This is the final result for the entanglement entropy of N disjoint intervals in the heavy state. The minimal condition above implies that one need to pick the relevant OPE channel ($\widetilde{\mathbf{\Omega}}_i$) depending on the values of the cross-ratios x_i (cf. [136]). The cross-ratios above are taken to be real ($x_i = \bar{x}_i$) since in the Lorentzian picture the intervals are spacelike and one can consider them to be lying on the time slice $t = 0$ without any loss of generality. The above result is the excited state analogue to the one for vacuum derived in [136, 140][15].

For the case of two intervals, the mutual information can be straightforwardly calculated from (6.103). Its definition is

$$I_{\mathcal{A}_i,\mathcal{A}_j} = S_{\mathcal{A}_i} + S_{\mathcal{A}_j} - S_{\mathcal{A}_i \cup \mathcal{A}_j}. \tag{6.104}$$

Without any loss of generality, we can choose the two intervals to be $[1, x_3]$ and $[x_4, x_5]$. From the channels $\mathbf{\Omega}_{1,3}$ for the 6-point block (consisting of 4 twists and 2 heavy operators) considered in subsection 6.3.1, we have

$$I_{\mathcal{A}_1,\mathcal{A}_2} = \begin{cases} 0 & \text{for } s\text{-channel or } \mathbf{\Omega}_1 \\ \frac{c}{3} \log \frac{|1-x_3^\alpha|\,|x_4^\alpha - x_5^\alpha|}{|1-x_5^\alpha|\,|x_3^\alpha - x_4^\alpha|} & \text{for } t\text{-channel or } \mathbf{\Omega}_3 \end{cases} \tag{6.105}$$

[15] This result was independently derived in [114] in the lightcone OPE limit. This requires the light operators $\mathcal{O}_L$ to be far from the heavy operators $\mathcal{O}_H$.

6.5 Conformal blocks and entanglement entropy from holography

In this section, we shall reproduce the conformal blocks considered in Section 6.3 from the gravity dual. This will involve a simple generalization of the bulk picture developed in [147]. As we had noticed before, the heavy operators in the CFT creates an excited state. In the bulk, this state can be thought in terms of a deformation of global AdS_3 into a conical defect geometry. From the conventional holographic dictionary, the primaries in the CFT are dual scalar fields in the bulk. However, since the conformal dimension of these operators scale as the central charge, the mass of the bulk scalar also scales as c ($M = \sqrt{h_L(h_L-1)} \sim c \gg 1$) and can be approximated by worldlines of point-particles. It was shown in [147], that the momenta along these worldlines are equal to the accessory parameters of the conformal block.

We work with asymptotically AdS_3 space in the global co-ordinates in which the dual CFT lives on a cylinder. The metric of the geometry dual to the heavy state is given by [10, 11, 147]

$$ds^2 = \frac{\alpha^2}{\cos^2\rho}\left(-dt^2 + \frac{1}{\alpha^2}d\rho^2 + \sin^2\rho\, d\phi^2\right), \quad \text{with } \alpha = \sqrt{1-24h_H/c}. \tag{6.106}$$

Depending on whether $\alpha^2 > 0$ or $\alpha^2 < 0$ the metric represents a conical defect with the singularity at $\rho = 0$ or a BTZ black hole with the event horizon at $\rho = 0$, respectively. The boundary is at $\rho = \frac{\pi}{2}$. To avoid potential divergences, we use the regularization $\cos\rho|_{\rho\to\frac{\pi}{2}} = \Lambda^{-1}$ (where Λ is the UV cutoff in the dual field theory for momenta or energies). We shall work with a constant time slice of (6.106) which is a disc with radial and angular variables as ρ and ϕ respectively.

The motion of the particle on the background above is described by the worldline action

$$S = M\int_{\lambda_i}^{\lambda_f} d\lambda \sqrt{g_{tt}\dot{t}^2 + g_{\rho\rho}\dot{\rho}^2 + g_{\phi\phi}\dot{\phi}^2}\ . \tag{6.107}$$

We restrict our attention to the constant time slice $\dot{t} = 0$. The required geodesic segments between any two points on the disc can be obtained by extremizing the worldline action (6.107). If we choose the parameter λ as the proper length, the geodesic equation reads [10, 147]

$$\frac{1}{\cos^2\rho}\dot{\rho}^2 + \frac{p_\phi^2}{\alpha^2}\cot^2\rho = 1 \ , \tag{6.108}$$

where, $p_\phi = \alpha^2 \tan^2\rho\,\dot{\phi}$, is the conserved momentum conjugate to ϕ. The solution to the geodesic equation is

$$\cos\rho = \frac{1}{\sqrt{1+p_\phi^2/\alpha^2}}\frac{1}{\cosh\lambda} \ , \tag{6.109}$$

Using these relations one can compute the regularized length of geodesics which will be shown to reproduce the corresponding conformal blocks.

In what follows, we illustrate the worldline configurations corresponding to the 3-point function and the 4-point conformal block in the CFT. Then we shall generalize the bulk picture for conformal blocks with arbitrary number of odd and even operator insertions.

Worldlines corresponding to 3-point function

Let us consider the bulk realization of the 3-point function $\langle \mathcal{O}_H(\infty)\mathcal{O}_L(z)\mathcal{O}_H(0)\rangle$. This is effectively a 1-point function in an excited state. In terms of the cylinder coordinates on the CFT, $(w = -i\log z)$, this is realized in the bulk as a radial geodesic from the point of insertion of the light operator to the singularity (see Fig 6.8). The corresponding conformal block can be computed by determining the regulated length of the geodesic from the position

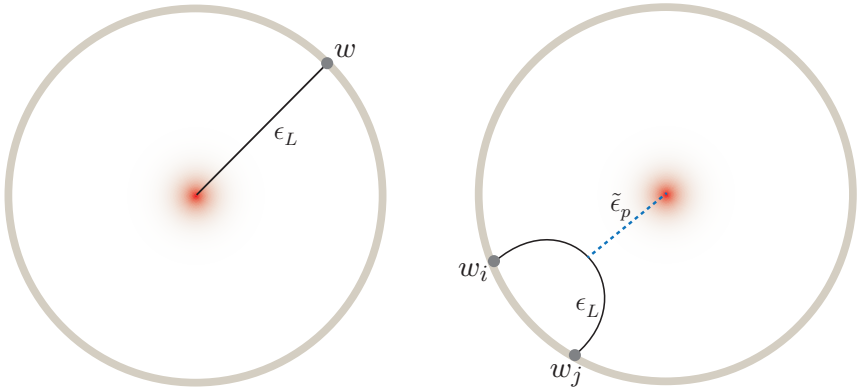

Figure 6.8: Bulk picture of the 3-point function (*left*) and 4-point conformal block (*right*) in CFT. Two of the operators are heavy which deform the background geometry (from the vacuum AdS to the conical defect) and the other light operators are described by geodesics of massive probe particles.

of defect $\rho = 0$ to the boundary i.e, $\cos\rho|_{\rho\to\pi/2} = \Lambda^{-1}$.

$$l_L = \int_0^{\cos\rho=\Lambda^{-1}} \frac{d\rho}{\cos\rho} = \log\left[\frac{\sin\left(\frac{\rho}{2}\right)+\cos\left(\frac{\rho}{2}\right)}{\cos\left(\frac{\rho}{2}\right)-\sin\left(\frac{\rho}{2}\right)}\right]_0^{\cos\rho=\Lambda^{-1}} = \log(2\Lambda)+\mathcal{O}(\Lambda^{-2})\ . \tag{6.110}$$

The contribution to the correlator is given by

$$G(w) = e^{-h_L\, l_L} \approx (2\Lambda)^{-h_L}\ . \tag{6.111}$$

This function is independent of w and just depends on the cut-off Λ. However, this is still a result on the cylinder. To obtain the conformal block on the plane, we use the standard exponential map $z = e^{iw}$ to obtain

$$\mathcal{G}(z) = z^{-h_L} G(w)\big|_{w=-i\,\log z} = (2\Lambda z)^{-h_L} \propto z^{-h_L}\ . \tag{6.112}$$

There are no additional bulk worldlines possible in this case unlike the higher point functions as we shall see below. Equation (6.112) precisely reproduces the z dependence of the normalized 3-point function, $\langle\mathcal{O}_H(\infty)\mathcal{O}_L(z)\mathcal{O}_H(0)\rangle/\langle\mathcal{O}_H(\infty)\mathcal{O}_H(0)\rangle$, which is fixed by conformal invariance.

Worldlines corresponding to 4-point conformal block

The conformal block of the 4-point function $\langle \mathcal{O}_H(\infty)\mathcal{O}_L(x_i)\mathcal{O}_L(x_j)\mathcal{O}_H(0)\rangle$ is described in the bulk by the geodesic configuration shown in Fig.6.8 [147]. The configuration consists of a geodesic anchored at the points of insertion of light operators, namely w_i and w_j on the cylinder[16]. In addition to this, there is another geodesic – which represents exchange of primary operator with conformal dimension $\tilde{h}_p$ – stretched between the singularity ($\rho = 0$) and the former geodesic (see Fig 6.8). The point of intersection of the geodesic segments can be determined by minimizing the worldline action [147]. For the case we are considering, in which the two light operators have same conformal dimensions, the dotted worldline joins the mid-point of the geodesic connecting w_i and w_j (see Fig 6.8). Therefore, the worldline action becomes

$$S = \epsilon_L l_L + \tilde{\epsilon}_p l_p, \tag{6.113}$$

Here, l_L is the length of the geodesic joining the light operators at the boundary whilst l_p is the length of the other geodesic joining the singularity and the mid-point of the former geodesic. We also assume $\tilde{\epsilon}_p \ll \epsilon_L$, such that the radial geodesic does not backreact to the other one [147]. Recall, that in our CFT analysis, $\tilde{\epsilon}_p \ll \epsilon_L$ led to the dominant contribution by heavy operators in the horizontal intermediate channels. For the ϵ_L geodesic (here, $w_{ij} = w_i - w_j$), we have

$$\cos\rho = \frac{\sin\left(\frac{\alpha w_{ij}}{2}\right)}{\cosh\lambda} \tag{6.114}$$

[16]This geodesic is same as the Ryu-Takayanagi one.

The regulated ϵ_L and ϵ_p geodesic lengths are given by

$$l_L(w_{ij}) = 2\lambda\big|_{\cos\rho=\Lambda^{-1}} = 2\,\log\left(\sin\frac{\alpha w_{ij}}{2}\right) + 2\,\log\left(\frac{\Lambda}{2}\right), \tag{6.115}$$

$$l_p(w_{ij}) = \int_0^{\cos\rho=\sin\frac{\alpha w_{ij}}{2}} \frac{d\rho}{\cos\rho} = -\,\log\left(\tan\frac{\alpha w_{ij}}{4}\right). \tag{6.116}$$

The limits of integration for l_p are the ones corresponding to the singularity and the mid-point of the ϵ_L geodesic. The (w_i dependent) contribution to the correlator is given by [147]

$$G(w_i, w_j) = e^{-\frac{c}{6}S(w_i,w_j)} = e^{-h_L\, l_L(w_{ij}) - \tilde{h}_p\, l_p(w_{ij})} = \frac{\left(\tan\frac{\alpha w_{ij}}{4}\right)^{\tilde{h}_p}}{\left(\sin\frac{\alpha w_{ij}}{2}\right)^{2h_L}}. \tag{6.117}$$

Once again, to obtain the conformal block on the plane we need to perform the conformal transformations, $x_i = e^{iw_i}$ and $x_j = e^{iw_j}$

$$\mathcal{F}_{(4)}(x_i, x_j) = x_i^{-h_L} x_j^{-h_L} G(w_i, w_j)\big|_{w_{i,j}=-i\,\log\,x_{i,j}}. \tag{6.118}$$

The extra prefactor comes due to the conformal transformation of the light operator $\mathcal{O}_L(x)$. In terms of the following function

$$\begin{aligned} f(x_i, x_j) &= \left[\epsilon_L \log(x_i x_j) + 2\epsilon_L \log\left(\sin\frac{\alpha w_{ij}}{2}\right) - \tilde{\epsilon}_p \log\left(\tan\frac{\alpha w_{ij}}{4}\right)\right]_{w_{i,j}=-i\log x_{i,j}} \\ &= 2\,\epsilon_L\,\log\frac{x_i^\alpha - x_j^\alpha}{(x_i x_j)^{\frac{\alpha-1}{2}}} + \tilde{\epsilon}_p\,\log\frac{x_i^{\alpha/2} + x_j^{\alpha/2}}{x_i^{\alpha/2} - x_j^{\alpha/2}}\,, \end{aligned} \tag{6.119}$$

the conformal block $\mathcal{F}_{(4)}(x_i, x_j)$ is then given as

$$\mathcal{F}_{(4)}(x_i, x_j) = \exp(-c f(x_i, x_j)/6)\,. \tag{6.120}$$

which indeed agrees with the CFT result (6.36) up to the constant $(\tilde{\epsilon}_p \log 4\alpha - 2\epsilon_L \log\alpha)$.

Worldlines corresponding to higher-point conformal blocks

Largely motivated by the Ryu-Takayanagi proposal for disjoint intervals, the worldline configurations above can be extended to conformal blocks of arbitrary $(m+2)$-point functions of two heavy operators and an arbitrary number (m) of light operators

$$\left\langle \mathcal{O}_H(\infty) \left[\mathcal{O}_L(1) \prod_{i=3}^{m+1} \mathcal{O}_L(x_i) \right] \mathcal{O}_H(0) \right\rangle$$

The basic constituents of the holographic representation of these higher conformal blocks are the worldline configurations for the 3-point function and the 4-point block. One then needs to add up lengths of the geodesic segments in the bulk (l_v), weighted with the corresponding scaled conformal dimensions (ϵ_v), to obtain the worldline action

$$S(w_i) = \sum_v \epsilon_v l_v \tag{6.121}$$

and the conformal block is given by $\exp[-\frac{c}{6}S(w_i)]$. Additionally, we need to perform a conformal transformation to go from the cylinder to the plane. Like the 3- and 4-point examples considered above, we shall mostly concern ourselves with the dependence of conformal block on the cross-ratios (x_i). We now describe the bulk pictures of the two distinct cases.

Odd number of light insertions

Let us consider a $[(2k+1)+2]$-point function in the CFT where two of them are heavy operators whereas an odd number $2k+1$ of them are light $(k \in \mathbb{N})$. Generalizing the previous bulk descriptions, we can see that amongst these $2k+1$ points, $2k$ points of light operator insertions will pairwise form k geodesic segments (see Fig 6.9). These worldlines joining a pair of points in the boundary will also have an additional geodesic segment representing the intermediate exchange of primaries of dimension $\tilde{h}_p$ whose common origin is

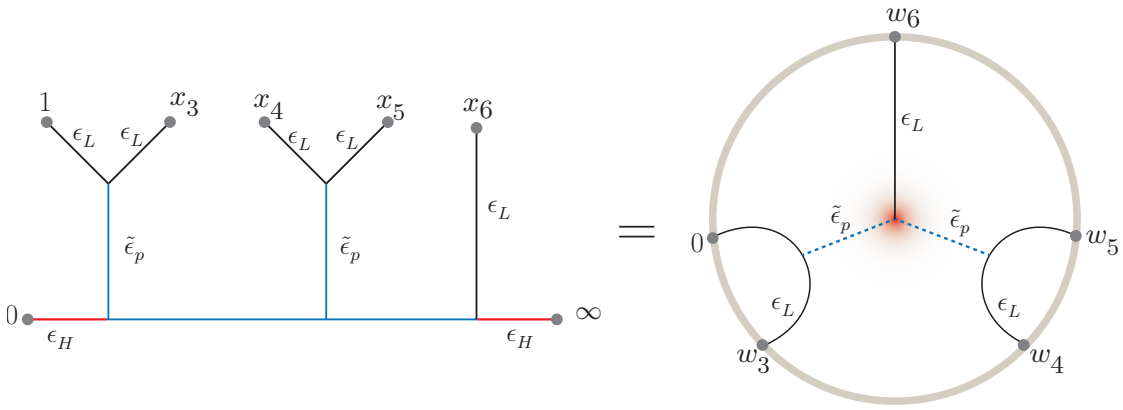

Figure 6.9: Worldline configuration corresponding to $[(2k+1)+2]$-point conformal block (with $k=2$ above). There are k geodesics connecting $2k$ points of light insertions of the CFT whereas one geodesic segment connects the remaining point of insertion to the singularity. Also, there are intermediate exchanges described by the dotted geodesics from the singularity to mid points of the boundary-to-boundary geodesics.

the singularity and each one ends on the mid-points of the boundary-to-boundary geodesic segments. There is another geodesic segment originating from the remaining (or unpaired) light operator insertion will anchor into the singularity at the centre ($\rho = 0$). This is precisely the factorization of $[(2k+1)+2]$ point conformal block into k 4-point blocks and a 3-point function. After summing the geodesic lengths, the net contribution to correlator is (here, $|j| = \prod_{s=3}^{m+1} x_s^{-h_L}$ is the factor arising from the conformal transformation from the cylinder to the plane $x_s = e^{iw_s}$)

$$\begin{aligned}\mathcal{F}_{((2k+1)+2)} &= |j|G(w_i(x_i)) = |j|e^{-\frac{c}{6}S(w_i(x_i))} = |j|e^{-h_L\, l_{L_a}} \prod_{\mathbf{\Omega}_i \mapsto \{(i,j)\}} e^{-h_L\, l_L(w_{ij})} e^{-\tilde{h}_p\, l_p(w_{ij})} \\ &= x_a^{-h_L} \prod_{\mathbf{\Omega}_i \mapsto \{(i,j)\}} \mathcal{F}_{(4)}(x_i, x_j)\ . \end{aligned} \tag{6.122}$$

The prefactor $x_a^{-h_L}$ represents any one of the points of insertion which is left over after connecting the others pairwise by the boundary-to-boundary geodesic segments. The choice of pairings via the geodesics in the bulk is in one-to-one correspondence with OPE channels,

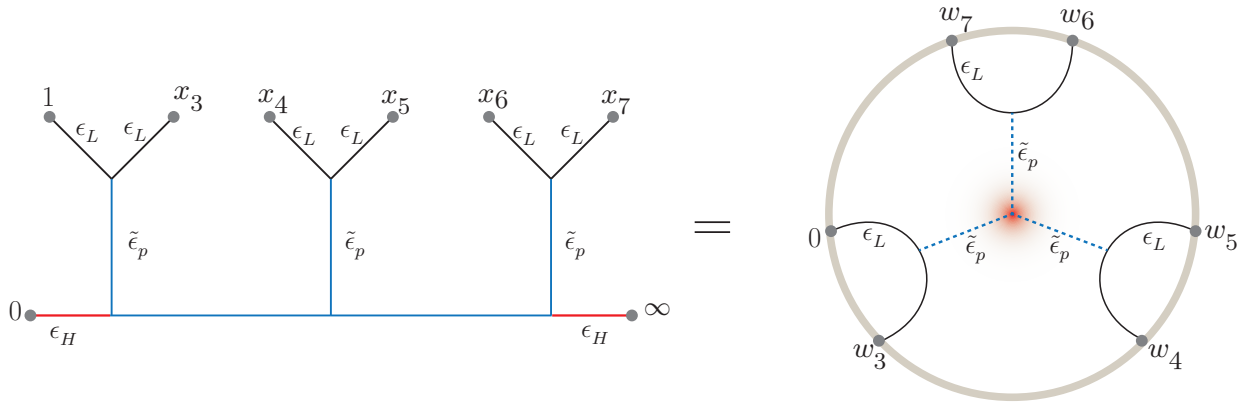

Figure 6.10: Worldline configuration corresponding to $(2k+2)$-point conformal block (with $k = 3$). There are k geodesics connecting $2k$ points of light insertions on the CFT.

$\mathbf{\Omega}_i$, in the CFT[17]. Therefore, the above equation (6.122) precisely matches with the CFT result for odd-point blocks – (6.88) or (6.92).

Even number of light insertions

For an even number $(2k)$ of light operator insertions, we can form k boundary-to-boundary geodesics joining a pair of light operator insertions ($k \in \mathbb{N}$). Again there are additional worldlines starting from the singularity and ending on the mid-point of each boundary-to-boundary geodesic which geometrically describe the intermediate exchanges ($\tilde{h}_p$). This case is, therefore, effectively equivalent to the odd-point block upon removal of the extra geodesic from the unpaired light insertion. The contribution to the correlator is given once again in terms of the worldline action as

$$\begin{aligned}\mathcal{F}_{(2k+2)} = |j|G(w_i(x_i)) = |j|e^{-\frac{c}{6}S(w_i(x_i))} &= |j| \prod_{\mathbf{\Omega}_i \mapsto \{(i,j)\}} e^{-h_L\, l_L(w_{ij})} e^{-\tilde{h}_p\, l_p(w_{ij})} \\ &= \prod_{\mathbf{\Omega}_i \mapsto \{(i,j)\}} \mathcal{F}_{(4)}(x_i, x_j)\ . \end{aligned} \tag{6.123}$$

[17]It may be of potential concern that the worldlines in channels other than the s-channel may intersect each other. Such issues can be avoided by suitably considering infinitesimally separated constant time slices each containing contributions for 4-point block(s) or a 3-point function. In any case, the sum of lengths of geodesics will not change.

(The factor $|j|$ used here, once again, arises from conformal transformations from the cylinder to the plane and is given by $\prod_{s=3}^{m+1} x_s^{-h_L}$.) This agrees with the CFT result for even point blocks obtained in (6.78).

It can therefore be seen that, the conformal blocks in the OPE channels we have considered bears a very natural interpretation in terms of bulk worldline diagrams. Furthermore, the network of geodesics considered here are simpler compared to those in [10, 11] which correspond to other OPE channels. Evidently, the basis, which we have chosen to work with, admits the straightforward generalization to an arbitrary number of light operator insertions.

Holographic entanglement entropy

The Ryu-Takayanagi prescription [220], prescribes that the entanglement entropy is given by the minimal area of a surface in AdS anchored at the endpoints of the interval(s)

$$S_{\mathcal{A}} = \frac{\min[\gamma_{\mathcal{A}}]}{4G_N} \ .$$

For the case of AdS_3, the minimal area surface is equivalent to a geodesic. For the case of multiple intervals, there are several of these geodesic configurations, $\mathbf{G}_i$, which are possible in the bulk, out of which we need to choose the one with the minimal length. Furthermore, G_N is related to the central charge by the Brown-Henneaux relation $c = 3\ell/2G_N$ [49].

For the metric (6.106), the length of the geodesic joining two points in the boundary (CFT on the cylinder) has been calculated in (6.115) – see also [218] and Appendix A of [21]. Considering the CFT on the boundary to be living on a plane, the length of the bulk geodesic joining the points x_i and x_j (both real) is

$$l_{ij} = 2 \log \frac{x_i^\alpha - x_j^\alpha}{\alpha (x_i x_j)^{\frac{\alpha-1}{2}}} \ . \tag{6.124}$$

Hence, summing over all the geodesics and applying the minimal-area condition, the result for holographic entanglement entropy is

$$S_{\mathcal{A}} = \frac{c}{3} \min_i \left\{ \sum_{\mathbf{G}_i \mapsto \{(p,q)\}} \log \frac{x_p^\alpha - x_q^\alpha}{\alpha (x_p x_q)^{\frac{\alpha-1}{2}}} \right\} . \tag{6.125}$$

This agrees exactly with (6.103) – provided the bulk geodesic configurations $\mathbf{G}_i$ are identified with the OPE channels $\widetilde{\mathbf{\Omega}}_i$ in the CFT (cf. [105, 136, 140] for the vacuum case). Hence, depending on the values of the cross-ratios x_i the relevant OPE channel is chosen in the CFT and analogously the geodesic configuration of minimal length is the one that reproduces the corresponding entanglement entropy of the heavy excited state[18].

6.6 Moduli space of the correlation function

As remarked earlier, the correlation function of m light operators and 2 heavy operators on the plane is associated with the Riemann sphere with $(m+2)$ punctures, $\sigma_{0,m+2}$. This can also be seen by thickening the diagrams of the conformal blocks. The expansion in terms of conformal partial waves is, then, the decomposition of this Riemann surface into 3-holed spheres. The moduli space of $\sigma_{0,m+2}$ is $\mathcal{M}_{0,m+2}$ which has $(m-1)$ complex moduli $(x_i, \bar{x}_i)$ [194, 248].

The OPE channels, which involve the pairwise fusion of two light operators, located at $1, x_3, \cdots, x_{m+1}$, describe the moduli space around some specific regions. For instance, the 6-point function in the s-channel, $\mathbf{\Omega}_1$, is restricted to the disjoint regimes around $x_3 \to 1$ and $x_4 \to x_5$. Whereas, the t-channel, $\mathbf{\Omega}_2$, describes the region around $x_5 \to 1$ and $x_3 \to x_4$. The u-channel or $\mathbf{\Omega}_3$ describes the region around $x_4 \to 1$ and $x_3 \to x_5$. The three worldline configurations are the bulk duals equivalently describing these OPE channels. In general, at large central charge, the $(m+2)$-point correlation function switches from regions of one

[18] See [68, 70, 78, 196, 199, 202] for other results on entanglement entropy in excited states.

OPE channel of $\mathcal{M}_{0,m+2}$ to another in the moduli space upon tuning the cross-ratios[19]. Furthermore, the worldline configurations in the bulk also correspond to each of the possible ways of decomposing the punctured Riemann sphere into 3-holed spheres.

In the context of entanglement entropy of N disjoint intervals, the correlator has N twist and N anti-twist operators in addition to two heavy operators. It was shown in [105], that the number of Ryu-Takayanagi geodesic configurations, $\mathcal{N}_N$, is given by the recursive formula

$$\mathcal{N}_N = 3\mathcal{N}_{N-1} - \mathcal{N}_{N-2} \ . \tag{6.126}$$

Interestingly, $\mathcal{N}_N$ above is given by the alternating Fibonacci numbers, F_{2N-1} [1]. As we had seen, the geodesic configurations $\mathbf{G}_i$ are in one-to-one correspondence with the contours considered in the monodromy problem, $\widetilde{\mathbf{\Omega}}_i$. In fact, the contours in the CFT are smoothly shrinkable into the bulk without ever crossing its corresponding geodesic [105]. Therefore, F_{2N-1} also counts the number of possible OPE channels of the conformal blocks (equaling the number of allowed pant-decompositions of the $(2N+2)$-punctured Riemann sphere) in the basis of pairwise fusion of the twist and anti-twist operators. Each of these OPE channels has its regime of validity in N disconnected regions of the moduli space, $x_{2i+1} \to 1$ and $x_{2j} \to x_{2k+1}$[20].

6.7 Conclusions

In this work, we have studied higher-point conformal blocks of two heavy operators and an arbitrary number of light operators in a CFT with large central charge. We focused our

[19] It is worthwhile to note, that this jump is seemingly discrete since we are strictly working in the $c \to \infty$ limit. In fact, it can be explicitly shown that quantum corrections to mutual information smoothen this discrete jump [33]. We are grateful to Arnab Rudra for pointing this possibility.

[20] The twist operators (located at 1 and x_{even}) have non-vanishing OPEs with anti-twist operators (located at x_{odd}). The OPE of (anti-)twist with itself is zero. Moreover, the location of the endpoints of the intervals are $1 < x_3 < x_4 < \cdots < x_{m-1}$. This is the reason why the number of OPE channels gets reduced to F_{2N-1} from $\nu_{2N}^{(\text{even})} = (2N)!/(2^N N!)$.

attention to a specific class of OPE channels in which the light operators fuse in pairs and the conformal dimension of the operator in the intermediate channels (after fusion of two $\mathcal{O}_L$s) are the same. In the heavy-light limit, we have been able to show that these blocks factorize into products of 4-point blocks. This was achieved using the monodromy method and the exponentiation of the block at large central charge. These CFT results could be reproduced from bulk worldline configurations using the methods presented in [147]. We have also applied these results to study the entanglement entropy of an arbitrary number of disjoint intervals for excited states. Hence, this work serves as a twofold generalization of the results of [136, 140] to excited states and that of [21] to multiple intervals. If further information about the spectrum (like structure constants and operator content) of large-c theories is available, these results can be possibly used to know higher-point heavy-light correlation functions in holographic CFTs[21].

It would be interesting to find subleading corrections both in the light parameter ϵ_L as well as in $1/c$ to the higher point conformal block [110]. The $1/c$ corrections would lead to corrections in entanglement entropy as well. One can then try to see whether these can be holographically reproduced by considering one-loop determinants in handlebody geometries obtained from orbifolding the conical defect [33]. Moreover, it can then be seen how $1/c$ effects smoothen the jumps in mutual information.

An immediate application of our results on higher-point conformal blocks is to study time-dependent entanglement entropy of disjoint intervals and mutual information in local quenches. The evolution of entanglement entropy of a single interval in this scenario has been studied in [21] and also the mutual information for joining quenches have been studied in [19].

As we had mentioned in the introduction, there is a fascinating connection between conformal blocks (of a specific pant decomposition) and Nekrasov partition functions arising from the AGT correspondence [8, 197, 241]. This relation was utilized in [10] to derive results

[21] See [137, 156] for some progress along these lines.

for heavy-light blocks. Although, their conformal blocks are in a different basis and explicit results exist only for the 4- and 5-point blocks, it would be interesting to precisely relate the results of [10] to those found here via fusion transformations. Furthermore, it also known that the one-point function of chiral ring elements in the $4d$ gauge theory are related to CFT_2 conformal blocks with insertions of conserved charges [6]. This presents the exciting prospect of utilizing this connection to find the entanglement entropy of heavy states in presence of chemical potentials[22].

Another intriguing direction is to see how the above results for higher-point conformal blocks generalize to theories with additional conserved currents – these include supersymmetric and higher-spin extensions. Our analysis suggests that the factorization could happen for conformal blocks of these theories as well. For the case of CFTs which have higher-spin gravity duals, the bulk Wilson line prescription [91,145] may also suggest such a factorization of the higher-point blocks.

Finally, it would be exciting to see to what extent our analysis of conformal blocks have analogues in higher dimensions. From the holographic side, one can make use of the geodesic Witten diagram prescription of [146]. In a related context, correlation functions of heavy and light operators have also been considered in the context of $\mathcal{N} = 4$ super Yang-Mills and also from the dual string theory [24,79,103,148,246]. The heavy operators correspond to classical string solutions and the typically protected light operators correspond to supergravity modes. The heavy states can be expressed in terms of Bethe states in the spin-chain description of the planar limit. The correlation function is then reduced to finding expectation values of light operators in these states. Although the existing results (involving a sufficiently intricate analysis) are mostly for the structure constant c_{HHL} appearing in the 3-point function, it would be interesting to see a whether a higher point generalization of the same shares any features with its lower dimensional counterpart considered here.

[22] We are grateful to Sujay Ashok for making us aware of this and for related discussions.

Chapter 7

Conclusion

7.1 A Summary

In this thesis, we tried to explore the general idea of how thermalization occurs in pure states describing out-of-equilibrium quantum systems. The motivation for this exploration was many-fold and depended on what kind of states we were considering. Overall, we considered three different types of pure states, namely the thermofield double (TFD) state, the CC (or gCC) state and the heavy primary state. Based on the underlying mechanism for obtaining thermal answers, we can classify the aforesaid states into two separate categories: 1. states that show *sub-system thermalization*, namely the TFD and the CC (or gCC) state; 2. states that display ETH, namely the heavy primary state. In the former class of states, we were interested in studying time dependent scenarios that may help us understand how the sub-system approaches thermal equilibrium. In the TFD state we used the entanglement entropy as a very important tool for the aforesaid purpose. The entanglement entropy behaved in a very characteristic fashion, showing a linear growth followed by a saturation at exactly $t = l/2$, with l being the length of the entangling interval. This behaviour was (previously) shown to be related to how the volume of spacetime grows in the interior of an eternal black hole, starting from a Hartle Hawking state (with the TFD state at its boundary) [138].

In Chapter 2 of this thesis we showed that the time for the saturation of entanglement entropy remains unchanged when we add additional conserved charges to the TFD state, including angular momentum and a $U(1)$ charge. The only difference one could find was in the final thermal value of entanglement entropy which now carried the additional conserved charge and hence, corresponded to a grand canonical ensemble.

In Chapter 3 of this thesis, we wished to investigate exactly how fine-tuned the TFD state was, and whether it could actually accommodate perturbations of any kind without allowing for a firewall to open up near the horizon. To understand that, we acted on the left and right CFTs of the TFD state separately with unitary transformations, made completely out of the Virasoro generators. We found that the bulk geometry could very nicely accommodate these changes by adjusting the position of the horizon (in a given set of co-ordinates). A calculation of the two sided entanglement entropy via the bulk geometry confirmed that the geometry was still smooth, especially the black hole interior. So, besides displaying thermalisation at the level of entanglement entropy, these two chapters also provided more evidence that despite the arguments of AMPS [16], the horizon seems to be a smooth place and the *firewall paradox* definitely needs to be re-visited!

In Chapter 4 of this thesis, we used the method of quantum quenches to drive systems out-of-equilibrium. We then used the ansatz of Cardy-Calabrese (CC) to model the ground state of the gapped Hamiltonian. Using this state, we not only showed the thermalization of the one-point function of quasi-primary operators, but also calculated their rate of decay. Interestingly, this decay rate turned out to be proportional to the quasi-normal mode of a bulk scalar field in a black hole background. This fact might be related to how the rest of the system acts as a bath for a small subsystem where the operator is located. The calculation for the time-dependent EE in these states was performed a long time ago [59,65], and had turned out to display the exact linear growth and saturation as was found in the TFD states, much later. The prime reason for the similarity seems to be how the entanglement structure is encoded in the state of the system. Like in the CC state, one can think of the second system,

in the TFD state, as a bath for the first system. To further probe the thermalisation process, in Chapter 4, we introduce another measure. First suggested by Cardy [71], the measure involves computing directly the overlap of the reduced density matrix (RDM) corresponding to a subsystem being evolved in time, with that of the RDM obtained from a thermal state at inverse temperature β, corresponding to the same subsystem. This is what we also refer to as the *quantum indistinguishability* of states, which tells us about how far away two states are in the Hilbert space. In the context of thermalisation, it is an extremely useful tool, since it provides us with the exact sense in which subsystem thermalisation takes place. Physically, the idea is to look at a small sub-region in a time-evolved system upto the point where the d.o.f. of this local sub-region are so very entangled with the rest of the system, that it is impossible to tell whether the global state of the system is pure, or whether it is thermal! This, of course, happens only when there is a complete overlap between the two RDMs suggesting that the system has thermalised. It is important to understand that thermalisation takes longer and longer to set in with an increase in the size of the subsystem. Thus, in the limit when the subsystem starts approaching the system size, the thermalisation time scale also increases becoming almost infinite, suggesting that thermalisation never takes place in this limit. This is exactly what we expect, since the full system is in a pure state. In the later part of this Chapter, we repeat most of the analysis for the gCC state, which carries an arbitrary number of higher spin conserved charges. The only change is in the decay rate of both the one point function and the RDM, which now get shifted by the charges of the primary operators under the additional $\mathcal{W}_n$ currents. We even match the decay rate with the quasi-normal mode of a scalar in the background of a higher spin three black hole[1].

In Chapter 5, we seriously discuss the question of the effects that spatial boundaries might have on thermalisation, in quench scenarios. In the spirit of the discussion above and still considering CC states, we see that introducing spatial boundaries never lets the system truly thermalise. An earlier analysis [163] had shown this to be the case by analysing the

[1]The quasi-normal mode for black holes with spin greater than 3 have not been calculated. For such cases, our CFT results remain a prediction.

one point function of primary operators and the stress tensor, both of which had shown revivals at times of the order of the system size. In Chapter 5, we additionally calculate the entanglement entropy of a finite size interval and show that it revives in a similar way. The reason for calculating the entanglement entropy is to be able to geometrise it in the form of geodesics in the dual bulk theory. In fact, we are able to reconstruct the entire metric for the oscillating bulk geometry that seems to interpolate between a BTZ black hole and a thermal AdS geometry. This construction therefore seems very intriguing, since it might then help us understand exactly how black holes form and tend to evaporate.

In Chapter 6 of this thesis, we work with the third kind of pure state, namely the heavy primary state. The most intriguing feature of this pure state is that it looks thermal from the low energy point of view. This means that if one computes correlation functions of light operators in this state, they resemble the calculation in a thermal state. Thermalization, in this sense, is more in line with the idea of ETH. The calculation for the one and two point functions in the heavy states were already known. In this chapter, using the monodromy method for evaluating conformal blocks, we show how the higher point correlation functions behave in such states. We find a factorisation of the higher point conformal blocks in terms of the four point conformal blocks. This factorisation boils down to the level of the correlators in case all the external operators have the same scaling dimension. One instance of this is the entanglement entropy where both the twist and anti-twist operators have the same conformal dimension. Thus, the entanglement entropy of a number of finite intervals in such heavy states can be expressed as all possible products of the entanglement entropy of single intervals. The bulk dual of this state is easy to construct and is, in fact, given by a Euclidean black hole geometry. The results for the entanglement entropy of multiple intervals is also easily geometrised. The most interesting part of the result is how the thermal correlators emerge from a seemingly simple vacuum correlation function. This is made possible by suppressing the $1/c$ contributions to the correlators in the large c limit. Including these corrections order by order in c, one should be able to "purify" the thermal correlator. So,

this is yet another way in which we get thermalisation starting from pure states, without any time evolution whatsoever.

To conclude, the pursuit for understanding thermalisation has been a long sought after goal. One of the greatest achievements of modern day physics is having related the problems concerning thermalisation in closed, isolated, quantum systems to that of the problem of black hole formation and evaporation, the understanding for which has remained equally elusive. From the point of view of the AdS/CFT correspondence, solving one problem would be tantamount to solving the other. Another reason why this problem is interesting from the gravity side is because it involves understanding the quantum nature of black holes, in terms of their micro states. A satisfactory solution to the problem in gravity would be a leap ahead towards finding a satisfactory theory of quantum gravity. This makes understanding the tenets of thermalisation all the more important. This thesis has been a small effort towards understanding the very problem of thermalisation better, especially in the light of recent developments.

7.2 Discussions

While the works presented in this thesis were still in progress, a lot of interesting work had begun to appear surrounding the topics presented here. We would like to discuss some that seemed to be the most interesting. One of the earliest developments took place when the paper [226] initiated the study of *shockwave* geometries in AdS gravity to analyse the sensitive dependence on initial conditions in strongly coupled field theories. The calculation involved perturbing a TFD state at very early times and observing how such perturbations grow, such that at exactly the *scrambling time*($t_* \sim \beta \log N^2$) the two-sided correlations in the TFD state get completely destroyed. This growth of mild perturbations at very early times is what [226] attributed to the chaotic nature of black holes. In a follow-up work [225], they sent out multiple shock waves by placing local operators at different times in the CFT

to create longer and longer wormholes without severing the entanglement between the two sides of the TFD state. Putting these works in the context of this thesis, there are two possible things that one could think of. Owing to the work in Chapter 3, one could try to realise such shockwave geometries by acting with our unitary operators on either of the boundaries, to mimic the action of the aforesaid local primaries. From our calculations, it seemed possible to accommodate the action of any unitary by re-defining the stress-tensor dependent terms in the metric. It would be nice to see how the shockwave geometry arises in our context. Another reason why this might be reasonable is because in Chapter 3, we already commented about how to get geometries with very large wormholes without destroying the two-sided correlations. Thus, the ideas in [225] seem to be realisable in the context of unitary transformations alone. Another possible generalisation is to add a spin to the eternal black hole (and hence to the TFD state) in the spirit of the construction in Chapter 2, and try to see how the scrambling time is affected by it.

Owing to the calculation of scrambling time in shockwave geometries, two very interesting papers appeared almost simultaneously. The first paper [69] wanted to calculate the scrambling time from the CFT side of the shockwave geometries. For that, they came up with the idea of calculating mutual information between the two boundaries of the TFD state in the presence of a perturbation. The technical difficulty with this calculation was to obtain the result for a six-point function. They made an assumption on the factorisation of the six point correlation function of twist operators into a product of two four point functions of twist operators in the perturbed geometry, which made the calculation possible. The justification provided for performing the factorisation, however, was not very rigorous mathematically. It just seemed to give the right answer as seen from the bulk shockwave geometry calculation. In Chapter 6, we reasoned via calculations how higher point correlation functions of twist operators in heavy states should factorise in the large c limit, thereby justifying the assumption of [69]. The second paper [172] that appeared, seemed to take a very general stance on how to look at the CFT calculation that

so far, had only been performed for the TFD state. They considered arbitrary large N CFTs with a gap in the spectrum separating the stress tensor from the rest of the levels (basically, the assumptions for a holographic CFT) in a thermal state. They generalised the TFD calculation by considering two heavy and two light operators on the thermal circle while always placing a heavy operator beside a light one, and analytically continuing only the light operators in real time. They called this the out-of-time ordered correlator (OTOC). The TFD state was only one special case of such a correlator. The idea of [172] was to give a very general diagnosis for understanding chaotic systems. They proposed that the decay of the OTOC correlators was enough to render a system chaotic. They went further to provide a bound on the Lyapunov exponent in quantum chaotic systems. Note that this bound was strictly quantum and went all the way to infinity in the classical limit of $h \to 0$. Since this proposal was made, a huge number of papers have appeared in the literature discussing OTOCs in a huge variety of quantum systems. To the best of our knowledge, most of these papers agree on the idea of the OTOCs as a diagnostic for quantum chaos. However, most of these papers consider a quantum system in the thermal state. One very interesting problems that might follow from the calculations in Chapter 6, in this context, is to understand how chaos happens in pure states. The heavy states considered in Chapter 6 are not simple pure states, but rather look thermal from the low energy perspective. It would be very interesting to see how OTOCs of lighter operators display chaotic behaviour, while saturating the Lyapunov bound (since the heavy states are effectively like black holes). However, the more interesting thing to understand would be the $1/c$ corrections to the leading answer that take us away from thermality and hence should correct the Lyapunov exponents in a systematic way. Such a calculation would then tell us one possible way in which the chaotic behaviour emerges in quantum systems.

One of the most intriguing features of the diagnosis of chaos in the context of black holes is that it gives us a new time scale t_*, called scrambling time, much larger that the thermal time scale of a quantum system. In the introduction and various chapters of this thesis, we

studied extensively the phenomenon of thermalization, with an inherent time scale specified by the temperature of the system, $t_d \sim \beta$. However, for systems with a large number of d.o.f., there seems to be another parametrically large time scale present, which is more relevant for the diagnosis of quantum chaos in the system. This implies that much after these systems have settled down or thermalised, there is still an "afterlife" that is invisible from the point of view of the time-ordered correlators, and are only visible to the OTOCs. In case of a black hole, one can imagine a scalar field decaying into it. The relaxation time scale for the black hole is specified by the frequency of the lowest quasi-normal mode (as shown in Chapter 3). However, it seems that there is a lot more that happens to the bits of information that have fallen into the black hole, much after it has thermalised completely from the point of view of an external observer. This could be attributed to the dynamics on the horizon (or perhaps even in the interior of the black hole). One could gather some clue from a much earlier work [224]. Since chaos and thermalization are usually thought of as being closely related, this new definition of quantum chaos seems to open a whole new window for exploring dynamics of thermal systems beyond thermalization.

Having said all the above, quantum chaos is not a new phenomenon. It was discovered a very long time ago and there exists a huge literature on the subject. In the earlier days, quantum chaos was best understood from the point of view of random matrix theories (RMTs) (see [83] for a recent review). In fact, the best definition of chaotic quantum systems is also formulated best in the context of RMTs. According to an earlier definition, a system is said to be quantum chaotic, if the nearest neighbour spacing distribution (NNSD) of its eigenvalues follows the Wigner-Dyson distribution. There is no satisfactory proof of the statement. However, it has been verified in a very large number of quantum systems. The question then is what is the relation between this definition of quantum chaos and the newer definition in terms of the OTOCs. To the best of our knowledge, this still remains an open question. A natural direction to look into would be systems where chaotic behaviour can be diagnosed using both these techniques. Sadly, there are not many systems where such is the

case. One such system is the RMT itself, where one could try to formulate a definition of OTOCs and try to analyse the relation with the NNSD definition. Some attempts have been made in this direction [80,122]. Another system that has been at the centre of attention of the high energy community is the Sachdev-Ye-Kitaev (SYK) model.

The SYK model was proposed a long time ago by Sachdev and Ye in the context of spin glass systems for a wholly different purpose. They first came to light when Kitaev [159] showed that, in a slightly modified version of the model containing Majorana fermions in 0+1 dimensions, the OTOCs of the system not only vanish but rather saturate the Lyapunov bound, rendering the system maximally chaotic. This led to the speculation that they maybe dual to black holes in 2 dimensional AdS spaces. The only trouble was that these models were not conformal to begin with. In [174], it was shown in great gory detail that the model admitted a near conformal limit in the IR and hence could be dual to a near AdS geometry in the bulk. Thereafter, numerous attempts have been made towards constructing the correct bulk dual for the SYK model (see [159] and [221] for a recent review and references therein). In [81], the authors wanted to understand the similarities between the NNSDs of RMTs and the way they become relevant for understanding quantum chaos in black holes. For this, they modelled the black holes with the SYK model and showed a similarity with the NNSDs of the two systems using a tool called the Spectral Form Factor (SFF). This work was however, mostly numerical and a precise analytic calculation to understand the NNSD of the SYK model remains an open question. Nonetheless, the SYK model is a very simple model that perhaps holds the key to a lot of unanswered questions in the context of chaos specifically, and black holes in general.

To conclude the discussion one must mention some other recent advances that have occurred and that might drive future research. One such field is that of the tensor models. The tensor models are truly quantum models, unlike the SYK model, that display the exact same behaviour as the SYK models in the large N limit. By that we mean they have the same form for the Schwinger-Dyson equations. The tensor models may contain bosons or

fermions (complex and real) [130, 160, 239], all of which would contain tensor indices in the fundamental representation of the global symmetry groups. Due to their true quantum nature, and the fact that they allow for a well defined large N limit, these models seem to be very promising. One of the main purposes they serve is to allow for an extension into higher dimensions [39, 211] where the possibility of another AdS/CFT like correspondence can be explored further. One only hopes that these models are able to pave the way for a lot more interesting physics in the future!

Bibliography

[1] *The On-Line Encyclopedia of Integer Sequences, Sequence A001519.* Sloane, N. J. A.

[2] Javier Abajo-Arrastia, João Aparício, and Esperanza López. Holographic evolution of entanglement entropy. *Journal of High Energy Physics*, 2010(11):149, Nov 2010.

[3] Javier Abajo-Arrastia, Emilia da Silva, Esperanza Lopez, Javier Mas, and Alexandre Serantes. Holographic Relaxation of Finite Size Isolated Quantum Systems. *JHEP*, 1405:126, 2014.

[4] M. Abramowitz and I. Stegun. *Handbook of Mathematical Functions.* Dover Publications, 1965.

[5] H. Afshar, A. Bagchi, S. Detournay, D. Grumiller, S. Prohazka, and M. Riegler. *Holographic Chern–Simons Theories*, pages 311–329. Springer International Publishing, Cham, 2015.

[6] Vasyl A. Alba, Vladimir A. Fateev, Alexey V. Litvinov, and Grigory M.ss Tarnopolskiy. On combinatorial expansion of the conformal blocks arising from AGT conjecture. *Lett. Math. Phys.*, 98:33–64, 2011.

[7] Tameem Albash and Clifford V Johnson. Evolution of holographic entanglement entropy after thermal and electromagnetic quenches. *New Journal of Physics*, 13(4):045017, 2011.

[8] Luis F. Alday, Davide Gaiotto, and Yuji Tachikawa. Liouville Correlation Functions from Four-dimensional Gauge Theories. *Lett. Math. Phys.*, 91:167–197, 2010.

[9] Mohsen Alishahiha, Davood Allahbakhshi, and Ali Naseh. Entanglement thermodynamics. *Journal of High Energy Physics*, 2013(8):102, Aug 2013.

[10] K. B. Alkalaev and V. A. Belavin. Classical conformal blocks via AdS/CFT correspondence. *JHEP*, 08:049, 2015.

[11] K. B. Alkalaev and V. A. Belavin. From global to heavy-light: 5-point conformal blocks. 2015.

[12] Konstantin B. Alkalaev and V. A. Belavin. Monodromic vs geodesic computation of Virasoro classical conformal blocks. 2015.

[13] Ahmed Almheiri, Donald Marolf, Joseph Polchinski, Douglas Stanford, and James Sully. An Apologia for Firewalls. *JHEP*, 1309:018, 2013.

[14] Ahmed Almheiri, Donald Marolf, Joseph Polchinski, Douglas Stanford, and James Sully. An apologia for firewalls. *Journal of High Energy Physics*, 2013(9):18, Sep 2013.

[15] Ahmed Almheiri, Donald Marolf, Joseph Polchinski, and James Sully. Black holes: complementarity or firewalls? *Journal of High Energy Physics*, 2013(2):62, Feb 2013.

[16] Ahmed Almheiri, Donald Marolf, Joseph Polchinski, and James Sully. Black Holes: Complementarity or Firewalls? *JHEP*, 1302:062, 2013.

[17] Martin Ammon, Alejandra Castro, and Nabil Iqbal. Wilson Lines and Entanglement Entropy in Higher Spin Gravity. *JHEP*, 1310:110, 2013.

[18] Martin Ammon, Michael Gutperle, Per Kraus, and Eric Perlmutter. Black Holes in Three Dimensional Higher Spin Gravity: A Review. *J.Phys.*, A46:214001, 2013.

[19] Curtis T. Asplund and Alice Bernamonti. Mutual information after a local quench in conformal field theory. *Phys. Rev.*, D89(6):066015, 2014.

[20] Curtis T. Asplund, Alice Bernamonti, Federico Galli, and Thomas Hartman. Holographic Entanglement Entropy from 2d CFT: Heavy States and Local Quenches. *JHEP*, 1502:171, 2015.

[21] Curtis T. Asplund, Alice Bernamonti, Federico Galli, and Thomas Hartman. Holographic Entanglement Entropy from 2d CFT: Heavy States and Local Quenches. *JHEP*, 02:171, 2015.

[22] Steven G. Avery and Borun D. Chowdhury. No Holography for Eternal AdS Black Holes. 2013.

[23] Máximo Bañados, Claudio Teitelboim, and Jorge Zanelli. Black hole in three-dimensional spacetime. *Phys. Rev. Lett.*, 69:1849–1851, Sep 1992.

[24] Zoltan Bajnok, Romuald A. Janik, and Andrzej Wereszczyński. HHL correlators, orbit averaging and form factors. *JHEP*, 09:050, 2014.

[25] V. Balasubramanian, A. Bernamonti, N. Copland, B. Craps, and F. Galli. Thermalization of mutual and tripartite information in strongly coupled two dimensional conformal field theories. *Phys. Rev. D*, 84:105017, Nov 2011.

[26] V. Balasubramanian, A. Bernamonti, J. de Boer, N. Copland, B. Craps, E. Keski-Vakkuri, B. Muller, A. Schafer, M. Shigemori, and W. Staessens. Holographic Thermalization. *Phys. Rev.*, D84:026010, 2011.

[27] Vijay Balasubramanian, Micha Berkooz, Simon F. Ross, and Joan Simon. Black Holes, Entanglement and Random Matrices. 2014.

[28] Vijay Balasubramanian and Per Kraus. A Stress Tensor for Anti-de Sitter Gravity. *Commun.Math.Phys.*, 208:413–428, 1999.

[29] Vijay Balasubramanian, Per Kraus, and Albion E. Lawrence. Bulk versus boundary dynamics in anti-de Sitter space-time. *Phys. Rev.*, D59:046003, 1999.

[30] Maximo Banados. Three-Dimensional Quantum Geometry and Black Holes. pages 147–169, 1998.

[31] Pinaki Banerjee, Shouvik Datta, and Ritam Sinha. Higher-point conformal blocks and entanglement entropy in heavy states. *JHEP*, 05:127, 2016.

[32] J. M. Bardeen, B. Carter, and S. W. Hawking. The four laws of black hole mechanics. *Comm. Math. Phys.*, 31(2):161–170, 1973.

[33] Taylor Barrella, Xi Dong, Sean A. Hartnoll, and Victoria L. Martin. Holographic entanglement beyond classical gravity. *JHEP*, 09:109, 2013.

[34] Matteo Beccaria and Guido Macorini. Resummation of scalar correlator in higher spin black hole background. *JHEP*, 1402:071, 2014.

[35] J. D. Bekenstein. Black holes and the second law. *Lettere al Nuovo Cimento (1971-1985)*, 4(15):737–740, Aug 1972.

[36] Jacob D. Bekenstein. Black holes and entropy. *Phys. Rev. D*, 7:2333–2346, Apr 1973.

[37] Jacob D. Bekenstein. Generalized second law of thermodynamics in black-hole physics. *Phys. Rev. D*, 9:3292–3300, Jun 1974.

[38] Alexandre Belin, Christoph A. Keller, and Alexander Maloney. String Universality for Permutation Orbifolds. *Phys. Rev.*, D91(10):106005, 2015.

[39] Dario Benedetti, Sylvain Carrozza, Razvan Gurau, and Alessandro Sfondrini. Tensorial Gross-Neveu models. *JHEP*, 01:003, 2018.

[40] Nathan Benjamin, Miranda C. N. Cheng, Shamit Kachru, Gregory W. Moore, and Natalie M. Paquette. Elliptic Genera and 3d Gravity. 2015.

[41] Nathan Benjamin, Shamit Kachru, Christoph A. Keller, and Natalie M. Paquette. Emergent space-time and the supersymmetric index. 2015.

[42] Jyotirmoy Bhattacharya, Masahiro Nozaki, Tadashi Takayanagi, and Tomonori Ugajin. Thermodynamical property of entanglement entropy for excited states. *Phys. Rev. Lett.*, 110:091602, Mar 2013.

[43] Sayantani Bhattacharyya, Veronika E. Hubeny, R. Loganayagam, Gautam Mandal, Shiraz Minwalla, et al. Local Fluid Dynamical Entropy from Gravity. *JHEP*, 0806:055, 2008.

[44] Sayantani Bhattacharyya, Veronika E Hubeny, Shiraz Minwalla, and Mukund Rangamani. Nonlinear Fluid Dynamics from Gravity. *JHEP*, 0802:045, 2008.

[45] Danny Birmingham, Ivo Sachs, and Sergey N. Solodukhin. Conformal field theory interpretation of black hole quasinormal modes. *Phys.Rev.Lett.*, 88:151301, 2002.

[46] Piotr Bizon and Andrzej Rostworowski. On weakly turbulent instability of anti-de Sitter space. *Phys.Rev.Lett.*, 107:031102, 2011.

[47] Peter Bouwknegt and Kareljan Schoutens. W symmetry in conformal field theory. *Phys.Rept.*, 223:183–276, 1993.

[48] Samuel L. Braunstein, Stefano Pirandola, and Karol Życzkowski. Better late than never: Information retrieval from black holes. *Phys. Rev. Lett.*, 110:101301, Mar 2013.

[49] J. D. Brown and Marc Henneaux. Central charges in the canonical realization of asymptotic symmetries: an example from three-dimensional gravity. *Comm. Math. Phys.*, 104(2):207–226, 1986.

[50] J. David Brown and M. Henneaux. Central Charges in the Canonical Realization of Asymptotic Symmetries: An Example from Three-Dimensional Gravity. *Commun.Math.Phys.*, 104:207–226, 1986.

[51] Alex Buchel, Steven L. Liebling, and Luis Lehner. Boson stars in AdS spacetime. *Phys.Rev.*, D87(12):123006, 2013.

[52] Alejandro Cabo-Bizet, Edi Gava, V.I. Giraldo-Rivera, and K.S. Narain. Black Holes in the 3D Higher Spin Theory and Their Quasi Normal Modes. *JHEP*, 1411:013, 2014.

[53] Elena Caceres, Arnab Kundu, Juan F. Pedraza, and Di-Lun Yang. Weak Field Collapse in AdS: Introducing a Charge Density. 2014.

[54] Mariano Cadoni and Maurizio Melis. Holographic entanglement entropy of the btz black hole. *Foundations of Physics*, 40(6):638–657, Jun 2010.

[55] P. Calabrese and J. Cardy. Entanglement and correlation functions following a local quench: a conformal field theory approach. *Journal of Statistical Mechanics: Theory and Experiment*, 10:4, October 2007.

[56] P. Calabrese, F. H. L. Essler, and M. Fagotti. Quantum Quench in the Transverse-Field Ising Chain. *Physical Review Letters*, 106(22):227203, June 2011.

[57] P. Calabrese, F. H. L. Essler, and M. Fagotti. Quantum quench in the transverse field Ising chain: I. Time evolution of order parameter correlators. *Journal of Statistical Mechanics: Theory and Experiment*, 7:16, July 2012.

[58] P. Calabrese, F. H. L. Essler, and M. Fagotti. Quantum quenches in the transverse field Ising chain: II. Stationary state properties. *Journal of Statistical Mechanics: Theory and Experiment*, 7:22, July 2012.

[59] Pasquale Calabrese and John Cardy. Evolution of entanglement entropy in one-dimensional systems. *Journal of Statistical Mechanics: Theory and Experiment*, 2005(04):P04010, 2005.

[60] Pasquale Calabrese and John Cardy. Quantum Quenches in Extended Systems. *J. Stat. Mech.*, 0706:P06008, 2007.

[61] Pasquale Calabrese and John Cardy. Entanglement entropy and conformal field theory. *J. Phys.*, A42:504005, 2009.

[62] Pasquale Calabrese, John Cardy, and Benjamin Doyon. Entanglement entropy in extended quantum systems. *Journal of Physics A: Mathematical and Theoretical*, 42(50):500301, 2009.

[63] Pasquale Calabrese, John Cardy, and Erik Tonni. Entanglement Entropy of Two Disjoint Intervals in conformal field theory II. *J.Stat.Mech.*, 1101:P01021, 2011.

[64] Pasquale Calabrese and John L. Cardy. Entanglement entropy and quantum field theory. *J. Stat. Mech.*, 0406:P06002, 2004.

[65] Pasquale Calabrese and John L. Cardy. Time-dependence of correlation functions following a quantum quench. *Phys. Rev. Lett.*, 96:136801, 2006.

[66] Andrea Campoleoni, Stefan Fredenhagen, Stefan Pfenninger, and Stefan Theisen. Asymptotic symmetries of three-dimensional gravity coupled to higher-spin fields. *JHEP*, 1011:007, 2010.

[67] Pawel Caputa, Gautam Mandal, and Ritam Sinha. Dynamical Entanglement Entropy with Angular Momentum and U(1) Charge. *JHEP*, 1311:052, 2013.

[68] Pawel Caputa, Masahiro Nozaki, and Tadashi Takayanagi. Entanglement of local operators in large-N conformal field theories. *PTEP*, 2014:093B06, 2014.

[69] Pawel Caputa, Joan Simón, Andrius Stikonas, Tadashi Takayanagi, and Kento Watanabe. Scrambling time from local perturbations of the eternal BTZ black hole. *JHEP*, 08:011, 2015.

[70] Pawel Caputa and Alvaro Veliz-Osorio. Entanglement constant for conformal families. *Phys. Rev.*, D92(6):065010, 2015.

[71] John Cardy. Thermalization and Revivals after a Quantum Quench in Conformal Field Theory. *Phys.Rev.Lett.*, 112:220401, 2014.

[72] John Cardy. Quantum Quenches to a Critical Point in One Dimension: some further results. 2015.

[73] John Cardy. Quantum Revivals in Conformal Field Theories in Higher Dimensions. 2016.

[74] John L. Cardy. Conformal invariance and surface critical behavior. *Nuclear Physics B*, 240(4):514 – 532, 1984.

[75] John L. Cardy. Operator Content of Two-Dimensional Conformally Invariant Theories. *Nucl.Phys.*, B270:186–204, 1986.

[76] Jean-Sébastien Caux and Fabian H. L. Essler. Time evolution of local observables after quenching to an integrable model. *Phys. Rev. Lett.*, 110:257203, Jun 2013.

[77] Chi-Ming Chang and Ying-Hsuan Lin. Bootstrapping 2D CFTs in the Semiclassical Limit. 2015.

[78] Bin Chen, Wu-Zhong Guo, Song He, and Jie-qiang Wu. Entanglement Entropy for Descendent Local Operators in 2D CFTs. *JHEP*, 10:173, 2015.

[79] Miguel S. Costa, Ricardo Monteiro, Jorge E. Santos, and Dimitrios Zoakos. On three-point correlation functions in the gauge/gravity duality. *JHEP*, 11:141, 2010.

[80] Jordan Cotler, Nicholas Hunter-Jones, Junyu Liu, and Beni Yoshida. Chaos, Complexity, and Random Matrices. *JHEP*, 11:048, 2017.

[81] Jordan S. Cotler, Guy Gur-Ari, Masanori Hanada, Joseph Polchinski, Phil Saad, Stephen H. Shenker, Douglas Stanford, Alexandre Streicher, and Masaki Tezuka. Black Holes and Random Matrices. *JHEP*, 05:118, 2017.

[82] Emilia da Silva, Esperanza Lopez, Javier Mas, and Alexandre Serantes. Collapse and Revival in Holographic Quenches. *JHEP*, 1504:038, 2015.

[83] Luca D'Alessio, Yariv Kafri, Anatoli Polkovnikov, and Marcos Rigol. From quantum chaos and eigenstate thermalization to statistical mechanics and thermodynamics. *Adv. Phys.*, 65(3):239–362, 2016.

[84] Sumit R. Das. Holographic Quantum Quench. *J.Phys.Conf.Ser.*, 343:012027, 2012.

[85] Sumit R. Das, Damian A. Galante, and Robert C. Myers. Universal scaling in fast quantum quenches in conformal field theories. *Phys.Rev.Lett.*, 112:171601, 2014.

[86] Sumit R. Das, Damián A. Galante, and Robert C. Myers. Smooth and fast versus instantaneous quenches in quantum field theory. *JHEP*, 08:073, 2015.

[87] Sumit R. Das, Damián A. Galante, and Robert C. Myers. Universality in fast quantum quenches. *JHEP*, 1502:167, 2015.

[88] Shouvik Datta and Justin R. David. Higher Spin Quasinormal Modes and One-Loop Determinants in the BTZ black Hole. *JHEP*, 1203:079, 2012.

[89] Shouvik Datta, Justin R. David, Michael Ferlaino, and S. Prem Kumar. Universal correction to higher spin entanglement entropy. *Phys.Rev.*, D90(4):041903, 2014.

[90] Thierry Dauxois and Stefano Ruffo. Fermi-Pasta-Ulam nonlinear lattice oscillations. 2008. Scholarpedia article.

[91] Jan de Boer, Alejandra Castro, Eliot Hijano, Juan I. Jottar, and Per Kraus. Higher spin entanglement and $\mathcal{W}_{\rm N}$ conformal blocks. *JHEP*, 07:168, 2015.

[92] Jan de Boer and Dalit Engelhardt. Comments on Thermalization in 2D CFT. 2016.

[93] Jan de Boer and Juan I. Jottar. Entanglement entropy and higher spin holography in ads$_3$. *Journal of High Energy Physics*, 2014(4):89, Apr 2014.

[94] Stanley Deser and R. Jackiw. Three-Dimensional Cosmological Gravity: Dynamics of Constant Curvature. *Annals Phys.*, 153:405–416, 1984.

[95] Oliver DeWolfe, Daniel Z. Freedman, and Hirosi Ooguri. Holography and defect conformal field theories. *Phys.Rev.*, D66:025009, 2002.

[96] P. Di Francesco, P. Mathieu, and D. Senechal. Conformal field theory. 1997. Springer, New York, USA, 890 p, ISBN: 038794785X.

[97] Oscar J.C. Dias, Gary T. Horowitz, and Jorge E. Santos. Gravitational Turbulent Instability of Anti-de Sitter Space. *Class.Quant.Grav.*, 29:194002, 2012.

[98] F. A. Dolan and H. Osborn. Conformal partial waves and the operator product expansion. *Nucl. Phys.*, B678:491–507, 2004.

[99] J. Eisert, M. Cramer, and M. B. Plenio. Colloquium: Area laws for the entanglement entropy. *Rev. Mod. Phys.*, 82:277–306, Feb 2010.

[100] Sheer El-Showk and Kyriakos Papadodimas. Emergent Spacetime and Holographic CFTs. *JHEP*, 10:106, 2012.

[101] Sheer El-Showk, Miguel F. Paulos, David Poland, Slava Rychkov, David Simmons-Duffin, and Alessandro Vichi. Solving the 3D Ising Model with the Conformal Bootstrap. *Phys. Rev.*, D86:025022, 2012.

[102] Dalit Engelhardt. Quench Dynamics in Confined 1+1-Dimensional Systems. 2015.

[103] Jorge Escobedo, Nikolay Gromov, Amit Sever, and Pedro Vieira. Tailoring Three-Point Functions and Integrability II. Weak/strong coupling match. *JHEP*, 09:029, 2011.

[104] Thomas Faulkner. The Entanglement Renyi Entropies of Disjoint Intervals in AdS/CFT. 2013.

[105] Thomas Faulkner. The Entanglement Renyi Entropies of Disjoint Intervals in AdS/CFT. 2013.

[106] Pasta J. Fermi E. and Ulam S. *Studies of nonlinear problems.* University of Chicago Press, 1955. Los Alamos report LA-1940, published later in Collected Papers of Enrico Fermi, E. Segre (Ed.).

[107] S. Ferrara, A. F. Grillo, and R. Gatto. Manifestly conformal covariant operator-product expansion. *Lett. Nuovo Cim.*, 2S2:1363–1369, 1971. [Lett. Nuovo Cim.2,1363(1971)].

[108] Guido Festuccia and Hong Liu. The Arrow of time, black holes, and quantum mixing of large N Yang-Mills theories. *JHEP*, 0712:027, 2007.

[109] R.P Feynman and F.L Vernon. The theory of a general quantum system interacting with a linear dissipative system. *Annals of Physics*, 24:118 – 173, 1963.

[110] A. Liam Fitzpatrick and Jared Kaplan. Conformal Blocks Beyond the Semi-Classical Limit. 2015.

[111] A. Liam Fitzpatrick, Jared Kaplan, Daliang Li, and Junpu Wang. On Information Loss in AdS_3/CFT_2. 2016.

[112] A. Liam Fitzpatrick, Jared Kaplan, and Matthew T. Walters. Universality of Long-Distance AdS Physics from the CFT Bootstrap. *JHEP*, 1408:145, 2014.

[113] A. Liam Fitzpatrick, Jared Kaplan, and Matthew T. Walters. Universality of Long-Distance AdS Physics from the CFT Bootstrap. *JHEP*, 08:145, 2014.

[114] A. Liam Fitzpatrick, Jared Kaplan, and Matthew T. Walters. Virasoro Conformal Blocks and Thermality from Classical Background Fields. *JHEP*, 11:200, 2015.

[115] A. Liam Fitzpatrick, Jared Kaplan, Matthew T. Walters, and Junpu Wang. Hawking from Catalan. 2015.

[116] Daniel Friedan and Stephen H. Shenker. The Analytic Geometry of Two-Dimensional Conformal Field Theory. *Nucl. Phys.*, B281:509, 1987.

[117] Mitsutoshi Fujita, Tadashi Takayanagi, and Erik Tonni. Aspects of AdS/BCFT. *JHEP*, 1111:043, 2011.

[118] Matthias R. Gaberdiel. Constraints on Extremal Self-Dual CFTs. *JHEP*, 0711:087, 2007.

[119] Matthias R. Gaberdiel and Rajesh Gopakumar. An ads_3 dual for minimal model cfts. *Phys. Rev. D*, 83:066007, Mar 2011.

[120] Matthias R. Gaberdiel, Thomas Hartman, and Kewang Jin. Higher spin black holes from cft. *Journal of High Energy Physics*, 2012(4):103, Apr 2012.

[121] Matthias R. Gaberdiel, Kewang Jin, and Eric Perlmutter. Probing higher spin black holes from CFT. *JHEP*, 1310:045, 2013.

[122] Adwait Gaikwad and Ritam Sinha. Spectral Form Factor in Non-Gaussian Random Matrix Theories. 2017.

[123] Jean-Loup Gervais, B. Sakita, and S. Wadia. The Surface Term in Gauge Theories. *Phys.Lett.*, B63:55, 1976.

[124] Christian Gogolin and Jens Eisert. Equilibration, thermalisation, and the emergence of statistical mechanics in closed quantum systems. *Rept. Prog. Phys.*, 79(5):056001, 2016.

[125] Rajesh Gopakumar. From free fields to AdS. *Phys. Rev.*, D70:025009, 2004.

[126] Rajesh Gopakumar. From free fields to AdS. 2. *Phys. Rev.*, D70:025010, 2004.

[127] Rajesh Gopakumar. From free fields to AdS: III. *Phys. Rev.*, D72:066008, 2005.

[128] Wu-Zhong Guo and Song He. Renyi entropy of locally excited states with thermal and boundary effect in 2D CFTs. *JHEP*, 1504:099, 2015.

[129] Rajesh Kumar Gupta and Ayan Mukhopadhyay. On the Universal Hydrodynamics of Strongly Coupled CFTs with Gravity Duals. *JHEP*, 0903:067, 2009.

[130] Razvan Gurau. Colored Group Field Theory. *Commun. Math. Phys.*, 304:69–93, 2011.

[131] Michael Gutperle and Per Kraus. Higher Spin Black Holes. *JHEP*, 1105:022, 2011.

[132] Felix M. Haehl, R. Loganayagam, and Mukund Rangamani. Schwinger-Keldysh formalism. Part I: BRST symmetries and superspace. *JHEP*, 06:069, 2017.

[133] Felix M. Haehl, R. Loganayagam, and Mukund Rangamani. Schwinger-Keldysh formalism. Part II: thermal equivariant cohomology. *JHEP*, 06:070, 2017.

[134] Felix M. Haehl and Mukund Rangamani. Permutation orbifolds and holography. *JHEP*, 03:163, 2015.

[135] Thomas Hartman. Entanglement Entropy at Large Central Charge. 2013.

[136] Thomas Hartman. Entanglement Entropy at Large Central Charge. 2013.

[137] Thomas Hartman, Christoph A. Keller, and Bogdan Stoica. Universal Spectrum of 2d Conformal Field Theory in the Large c Limit. *JHEP*, 09:118, 2014.

[138] Thomas Hartman and Juan Maldacena. Time evolution of entanglement entropy from black hole interiors. *Journal of High Energy Physics*, 2013(5):14, May 2013.

[139] S. W. Hawking. Particle creation by black holes. *Comm. Math. Phys.*, 43(3):199–220, 1975.

[140] Matthew Headrick. Entanglement rényi entropies in holographic theories. *Phys. Rev. D*, 82:126010, Dec 2010.

[141] Matthew Headrick, Alexander Maloney, Eric Perlmutter, and Ida G. Zadeh. Rényi entropies, the analytic bootstrap, and 3D quantum gravity at higher genus. *JHEP*, 07:059, 2015.

[142] Idse Heemskerk, Joao Penedones, Joseph Polchinski, and James Sully. Holography from Conformal Field Theory. *JHEP*, 10:079, 2009.

[143] Idse Heemskerk and James Sully. More Holography from Conformal Field Theory. *JHEP*, 09:099, 2010.

[144] Christopher P. Herzog and Michael Spillane. Tracing through scalar entanglement. *Phys. Rev. D*, 87:025012, Jan 2013.

[145] Eliot Hijano, Per Kraus, Eric Perlmutter, and River Snively. Semiclassical Virasoro Blocks from AdS_3 Gravity. *JHEP*, 12:077, 2015.

[146] Eliot Hijano, Per Kraus, Eric Perlmutter, and River Snively. Witten Diagrams Revisited: The AdS Geometry of Conformal Blocks. 2015.

[147] Eliot Hijano, Per Kraus, and River Snively. Worldline approach to semi-classical conformal blocks. *JHEP*, 07:131, 2015.

[148] Laszlo Hollo, Yunfeng Jiang, and Andrei Petrovskii. Diagonal Form Factors and Heavy-Heavy-Light Three-Point Functions at Weak Coupling. *JHEP*, 09:125, 2015.

[149] Veronika E. Hubeny, Mukund Rangamani, and Tadashi Takayanagi. A covariant holographic entanglement entropy proposal. *Journal of High Energy Physics*, 2007(07):062, 2007.

[150] F. Iglói and Y.-C. Lin. Finite-size scaling of the entanglement entropy of the quantum Ising chain with homogeneous, periodically modulated and random couplings. *Journal of Statistical Mechanics: Theory and Experiment*, 6:4, June 2008.

[151] W. Israel. Thermo-field dynamics of black holes. *Physics Letters A*, 57:107–110, May 1976.

[152] Steven Jackson, Lauren McGough, and Herman Verlinde. Conformal Bootstrap, Universality and Gravitational Scattering. *Nucl. Phys.*, B901:382–429, 2015.

[153] Ted Jacobson, Donald Marolf, and Carlo Rovelli. Black hole entropy: Inside or out? *International Journal of Theoretical Physics*, 44(10):1807–1837, Oct 2005.

[154] Andreas Karch and Lisa Randall. Locally localized gravity. *JHEP*, 0105:008, 2001.

[155] L. V. Keldysh. Diagram technique for nonequilibrium processes. *Zh. Eksp. Teor. Fiz.*, 47:1515–1527, 1964. [Sov. Phys. JETP20,1018(1965)].

[156] Christoph A. Keller and Alexander Maloney. Poincare Series, 3D Gravity and CFT Spectroscopy. *JHEP*, 02:080, 2015.

[157] Esko Keski-Vakkuri. Bulk and boundary dynamics in btz black holes. *Phys. Rev. D*, 59:104001, Mar 1999.

[158] T. W. B. Kibble. Topology of Cosmic Domains and Strings. *J. Phys.*, A9:1387–1398, 1976.

[159] A. Kitaev. In *Hidden Correlations in the Hawking Radiation and Thermal Noise*, Feb 2015.

[160] Igor R. Klebanov and Grigory Tarnopolsky. Uncolored random tensors, melon diagrams, and the Sachdev-Ye-Kitaev models. *Phys. Rev.*, D95(4):046004, 2017.

[161] Per Kraus and Finn Larsen. Partition functions and elliptic genera from supergravity. *Journal of High Energy Physics*, 2007(01):002, 2007.

[162] Per Kraus and Eric Perlmutter. Partition functions of higher spin black holes and their CFT duals. *JHEP*, 1111:061, 2011.

[163] Kevin Kuns and Donald Marolf. Non-Thermal Behavior in Conformal Boundary States. *JHEP*, 1409:082, 2014.

[164] Stefan Leichenauer and Mudassir Moosa. Entanglement Tsunami in (1+1)-Dimensions. *Phys. Rev.*, D92:126004, 2015.

[165] Aitor Lewkowycz and Juan Maldacena. Generalized gravitational entropy. *Journal of High Energy Physics*, 2013(8):90, Aug 2013.

[166] Alexey Litvinov, Sergei Lukyanov, Nikita Nekrasov, and Alexander Zamolodchikov. Classical Conformal Blocks and Painleve VI. *JHEP*, 07:144, 2014.

[167] Hong Liu and Márk Mezei. A refinement of entanglement entropy and the number of degrees of freedom. *Journal of High Energy Physics*, 2013(4):162, Apr 2013.

[168] Hong Liu and S. Josephine Suh. Entanglement Tsunami: Universal Scaling in Holographic Thermalization. *Phys.Rev.Lett.*, 112:011601, 2014.

[169] Jorma Louko, Donald Marolf, and Simon F. Ross. On geodesic propagators and black hole holography. *Phys. Rev.*, D62:044041, 2000.

[170] Oleg Lunin and Samir D. Mathur. Correlation functions for M**N / S(N) orbifolds. *Commun. Math. Phys.*, 219:399–442, 2001.

[171] Javier M. Magan, Dmitry Melnikov, and Madson R. O. Silva. Black Holes in AdS/BCFT and Fluid/Gravity Correspondence. *JHEP*, 11:069, 2014.

[172] Juan Maldacena, Stephen H. Shenker, and Douglas Stanford. A bound on chaos. *JHEP*, 08:106, 2016.

[173] Juan Maldacena, David Simmons-Duffin, and Alexander Zhiboedov. Looking for a bulk point. 2015.

[174] Juan Maldacena and Douglas Stanford. Remarks on the sachdev-ye-kitaev model. *Phys. Rev. D*, 94:106002, Nov 2016.

[175] Juan Maldacena and Leonard Susskind. Cool Horizons for Entangled Black Holes. *Fortsch.Phys.*, 61:781–811, 2013.

[176] Juan Martin Maldacena. The Large N limit of superconformal field theories and supergravity. *Int. J. Theor. Phys.*, 38:1113–1133, 1999. [Adv. Theor. Math. Phys.2,231(1998)].

[177] Juan Martin Maldacena. Eternal Black Holes in Anti-de Sitter. *JHEP*, 0304:021, 2003.

[178] Alexander Maloney and Edward Witten. Quantum Gravity Partition Functions in Three Dimensions. *JHEP*, 1002:029, 2010.

[179] Gautam Mandal and Takeshi Morita. Quantum quench in matrix models: dynamical phase transitions, selective equilibration and the generalized gibbs ensemble. *Journal of High Energy Physics*, 2013(10):197, Oct 2013.

[180] Gautam Mandal, Shruti Paranjape, and Nilakash Sorokhaibam. Thermalization in 2D critical quench and UV/IR mixing. 2015.

[181] Gautam Mandal, Ritam Sinha, and Nilakash Sorokhaibam. The inside outs of AdS(3)/CFT(2): Exact AdS wormholes with entangled CFT duals. *JHEP*, 1501:036, 2014.

[182] Gautam Mandal, Ritam Sinha, and Nilakash Sorokhaibam. Thermalization with chemical potentials, and higher spin black holes. *JHEP*, 08:013, 2015.

[183] Gautam Mandal, Ritam Sinha, and Tomonori Ugajin. Finite size effect on dynamical entanglement entropy: CFT and holography. 2016.

[184] Donald Marolf. The black hole information problem: past, present, and future. *Reports on Progress in Physics*, 80(9):092001, 2017.

[185] Donald Marolf and Joseph Polchinski. Gauge/Gravity Duality and the Black Hole Interior. *Phys.Rev.Lett.*, 111:171301, 2013.

[186] Samir D Mathur. The information paradox: a pedagogical introduction. *Classical and Quantum Gravity*, 26(22):224001, 2009.

[187] Samir D. Mathur. The Information paradox: A Pedagogical introduction. *Class. Quant. Grav.*, 26:224001, 2009.

[188] Samir D. Mathur and Christopher J. Plumberg. Correlations in Hawking radiation and the infall problem. *JHEP*, 09:093, 2011.

[189] Pietro Menotti. Accessory parameters for Liouville theory on the torus. *JHEP*, 12:001, 2012.

[190] Pietro Menotti. On the monodromy problem for the four-punctured sphere. *J. Phys.*, A47(41):415201, 2014.

[191] Pietro Menotti. Classical conformal blocks. 2016.

[192] Sebastian Montes, German Sierra, and Javier Rodriguez-Laguna. Tachyonic quench in a free bosonic field theory. *J. Stat. Mech.*, 1802(2):023102, 2018.

[193] Gregory W. Moore and Nathan Seiberg. Polynomial Equations for Rational Conformal Field Theories. *Phys. Lett.*, B212:451, 1988.

[194] Gregory W. Moore and Nathan Seiberg. Classical and Quantum Conformal Field Theory. *Commun. Math. Phys.*, 123:177, 1989.

[195] Gregory W. Moore and Nathan Seiberg. Lectures on RCFT. In *1989 Banff NATO ASI: Physics, Geometry and Topology Banff, Canada, August 14-25, 1989*, 1989.

[196] Debangshu Mukherjee and K. Narayan. AdS plane waves, entanglement and mutual information. *Phys. Rev.*, D90(2):026003, 2014.

[197] Nikita A. Nekrasov. Seiberg-Witten prepotential from instanton counting. *Adv. Theor. Math. Phys.*, 7(5):831–864, 2003.

[198] Tatsuma Nishioka, Shinsei Ryu, and Tadashi Takayanagi. Holographic Entanglement Entropy: An Overview. *J. Phys.*, A42:504008, 2009.

[199] Masahiro Nozaki. Notes on Quantum Entanglement of Local Operators. *JHEP*, 10:147, 2014.

[200] Masahiro Nozaki, Tokiro Numasawa, Andrea Prudenziati, and Tadashi Takayanagi. Dynamics of entanglement entropy from einstein equation. *Phys. Rev. D*, 88:026012, Jul 2013.

[201] Masahiro Nozaki, Tokiro Numasawa, and Tadashi Takayanagi. Holographic Local Quenches and Entanglement Density. *JHEP*, 1305:080, 2013.

[202] Masahiro Nozaki, Tokiro Numasawa, and Tadashi Takayanagi. Quantum Entanglement of Local Operators in Conformal Field Theories. *Phys. Rev. Lett.*, 112:111602, 2014.

[203] Masahiro Nozaki, Tadashi Takayanagi, and Tomonori Ugajin. Central Charges for BCFTs and Holography. *JHEP*, 1206:066, 2012.

[204] Kyriakos Papadodimas and Suvrat Raju. State-Dependent Bulk-Boundary Maps and Black Hole Complementarity. *Phys.Rev.*, D89:086010, 2014.

[205] Kyriakos Papadodimas and Suvrat Raju. The Black Hole Interior in AdS/CFT and the Information Paradox. *Phys.Rev.Lett.*, 112:051301, 2014.

[206] Shruti Paranjape and Nilakash Sorokhaibam. Exact Growth of Entanglement and Dynamical Phase Transition in Global Fermionic Quench. 2016.

[207] Joao Penedones. Writing CFT correlation functions as AdS scattering amplitudes. *JHEP*, 03:025, 2011.

[208] Eric Perlmutter. Virasoro conformal blocks in closed form. *JHEP*, 08:088, 2015.

[209] Anatoli Polkovnikov, Krishnendu Sengupta, Alessandro Silva, and Mukund Vengalattore. Nonequilibrium dynamics of closed interacting quantum systems. *Rev.Mod.Phys.*, 83:863, 2011.

[210] C.N. Pope. Lectures on W algebras and W gravity. 1991.

[211] Shiroman Prakash and Ritam Sinha. A Complex Fermionic Tensor Model in d Dimensions. *JHEP*, 02:086, 2018.

[212] Riccardo Rattazzi, Slava Rychkov, and Alessandro Vichi. Central Charge Bounds in 4D Conformal Field Theory. *Phys. Rev.*, D83:046011, 2011.

[213] Riccardo Rattazzi, Vyacheslav S. Rychkov, Erik Tonni, and Alessandro Vichi. Bounding scalar operator dimensions in 4D CFT. *JHEP*, 12:031, 2008.

[214] Tullio Regge and Claudio Teitelboim. Role of Surface Integrals in the Hamiltonian Formulation of General Relativity. *Annals Phys.*, 88:286, 1974.

[215] Marcos Rigol. Quantum quenches and thermalization in one-dimensional fermionic systems. *Phys. Rev. A*, 80:053607, Nov 2009.

[216] Marcos Rigol, Vanja Dunjko, Vladimir Yurovsky, and Maxim Olshanii. Relaxation in a completely integrable many-body quantum system: An *Ab Initio* study of the dynamics of the highly excited states of 1d lattice hard-core bosons. *Phys. Rev. Lett.*, 98:050405, Feb 2007.

[217] Bob Rink. Fermi Pasta Ulam systems (FPU): mathematical aspects. 2009. Scholarpedia article.

[218] Matthew M. Roberts. Time Evolution of Entanglement Entropy from a Pulse. *JHEP*, 1212:027, 2012.

[219] Slava Rychkov and Zhong Ming Tan. The ϵ-expansion from conformal field theory. *J. Phys.*, A48(29):29FT01, 2015.

[220] Shinsei Ryu and Tadashi Takayanagi. Holographic derivation of entanglement entropy from ads/cft. *Phys. Rev. Lett.*, 96:181602, May 2006.

[221] Gabor Sarosi. AdS_2 holography and the SYK model. *PoS*, Modave2017:001, 2018.

[222] J. Schwinger. Brownian Motion of a Quantum Oscillator. *Journal of Mathematical Physics*, 2:407–432, May 1961.

[223] Nathan Seiberg. *Notes on Quantum Liouville Theory and Quantum Gravity*, pages 363–395. Springer US, Boston, MA, 1991.

[224] Yasuhiro Sekino and Leonard Susskind. Fast Scramblers. *JHEP*, 10:065, 2008.

[225] Stephen H. Shenker and Douglas Stanford. Multiple Shocks. 2013.

[226] Stephen H. Shenker and Douglas Stanford. Black holes and the Butterfly Effect. *JHEP*, 1403:067, 2014.

[227] Kostas Skenderis and Sergey N. Solodukhin. Quantum Effective Action from the AdS / CFT Correspondence. *Phys.Lett.*, B472:316–322, 2000.

[228] S. Sotiriadis and J. Cardy. Inhomogeneous quantum quenches. *Journal of Statistical Mechanics: Theory and Experiment*, 11:3, November 2008.

[229] Mark Srednicki. Chaos and quantum thermalization. *Phys. Rev. E*, 50:888–901, Aug 1994.

[230] Leonard Susskind, Lárus Thorlacius, and John Uglum. The stretched horizon and black hole complementarity. *Phys. Rev. D*, 48:3743–3761, Oct 1993.

[231] Y. Takahashi and H. Umezawa, (1975).

[232] Tadashi Takayanagi. Holographic Dual of BCFT. *Phys.Rev.Lett.*, 107:101602, 2011.

[233] Tadashi Takayanagi and Tomonori Ugajin. Measuring Black Hole Formations by Entanglement Entropy via Coarse-Graining. *JHEP*, 1011:054, 2010.

[234] Tomonori Ugajin. Two dimensional quantum quenches and holography. 2013.

[235] Mark Van Raamsdonk. Evaporating Firewalls. 2013.

[236] Spenta Wadia. *Canonical Quantization of Non-Abelian Gauge Theory in the Schrodinger Picture: Applications to Monopoles and Instantons*. PhD thesis, 1979.

[237] Edward Witten. (2+1)-Dimensional Gravity as an Exactly Soluble System. *Nucl.Phys.*, B311:46, 1988.

[238] Edward Witten. Anti-de Sitter space and holography. *Adv. Theor. Math. Phys.*, 2:253–291, 1998.

[239] Edward Witten. An SYK-Like Model Without Disorder. 2016.

[240] Gabriel Wong, Israel Klich, Leopoldo A. Pando Zayas, and Diana Vaman. Entanglement temperature and entanglement entropy of excited states. *Journal of High Energy Physics*, 2013(12):20, Dec 2013.

[241] Niclas Wyllard. A(N-1) conformal Toda field theory correlation functions from conformal N = 2 SU(N) quiver gauge theories. *JHEP*, 11:002, 2009.

[242] A. B. Zamolodchikov. Conformal symmetry in two dimensions: an explicit recurrence formula for the conformal partial wave amplitude. *Commun. Math. Phys.*, 96:419–422, 1984.

[243] Al. B. Zamolodchikov. Conformal symmetry in two-dimensional space: Recursion representation of conformal block. *Theor. Math. Phys*, page 1088, 1987.

[244] Al B Zamolodchikov. Conformal symmetry in two-dimensional space: recursion representation of conformal block. *Theoretical and Mathematical Physics*, 73(1):1088–1093, 1987.

[245] Alexander B. Zamolodchikov and Alexei B. Zamolodchikov. Structure constants and conformal bootstrap in Liouville field theory. *Nucl. Phys.*, B477:577–605, 1996.

[246] K. Zarembo. Holographic three-point functions of semiclassical states. *JHEP*, 09:030, 2010.

[247] W. H. Zurek. Cosmological Experiments in Superfluid Helium? *Nature*, 317:505–508, 1985.

[248] Barton Zwiebach. How covariant string theory solves a minimal area problem? *Commun. Math. Phys.*, 136:83–118, 1991.